Advancements in isotopic geolocation tools for insect migration research

Megan Reich

Thesis submitted to the University of Ottawa
in partial fulfillment of the requirements for the
Doctorate in Philosophy degree in Biology

Department of Biology
Faculty of Science
University of Ottawa

“It's a dangerous business, Frodo, going out your door. You step onto the road, and if you don't keep your feet, there's no knowing where you might be swept off to.”

— J.R.R. Tolkien, The Lord of the Rings

Abstract

Migratory insects are vital components of global ecosystems and provide important ecosystem services, yet the migration phenomenon is understudied in insects compared to vertebrates. In this thesis, I aim to deepen our understanding of insect migration, using the monarch butterfly *Danaus plexippus* (L.) and the painted lady butterfly *Vanessa cardui* (L.) as model systems. Studying insect migration is notoriously difficult given the small size, high abundance, and short lifespans of insects. Isotope geolocation has shown promise for overcoming these obstacles. Here, I develop and apply metals and metal isotopes, specifically strontium isotope ratios ($^{87}Sr/^{86}Sr$), to increase the spatial precision of isotope geolocation and demonstrate how isotopic geolocation tools can advance our understanding of insect migration at the population level. In the first chapter, I test the validity of using $^{87}Sr/^{86}Sr$, lead isotopes, and a suite of 23 metals and metalloids to estimate the natal origins of migratory insects, by investigating the pathways of metal incorporation into butterfly wing tissues. Using an 8-week diet-switching experiment, I show that the concentrations of many metals in insect wings can be altered through the adult diet or dust deposition, making them poor candidates for geolocation but potentially interesting tools to study insect physiology, diet, or toxicology. For example, lead was found to accumulate on butterfly wings from external sources, and lead isotopes could potentially be used to quantify the exposure of migratory insects to metal pollution. Some metals, including Ba, Cs, Mg, Na, Rb, Sr, Ti, Tl, and U, are good candidates for developing geolocation tools. I focused on $^{87}Sr/^{86}Sr$ and demonstrated that, despite some caveats, this tool is valid for isotope geolocation. In the second chapter, I outline the steps required to use $^{87}Sr/^{86}Sr$ for the geolocation of insects, including the calibration of a spatial model of isotopic variation (i.e., an isoscape) using random forest regression. I then combine hydrogen isotope values (δ^2H) and $^{87}Sr/^{86}Sr$ into a dual assignment framework to estimate the natal origins of a single generation of monarch butterflies in eastern North America. I demonstrate that combining these two isotopes provides a more spatially constrained estimate of natal origin than using either isotope alone. In the

third chapter, I apply this framework to characterize the migratory patterns and migratory connectivity of an insect species across a geographical barrier, the Sahara. Painted ladies journeying northwards across the Sahara appear to do so in a gradual progression, although spatiotemporal sampling limitations prevented a complete characterization of this movement. In contrast, painted ladies migrating southwards appear to journey in a broad front, parallel migration pattern with little longitudinal movement. Evidence for a leapfrog migration pattern was found in the western region, wherein butterflies of northernmost origin journey farther south than butterflies bred in more southerly regions. This leapfrog migration pattern suggests distinct migratory behaviours within painted lady butterflies wherein some individuals migrate longer distances than others. In the fourth chapter, I apply isotope geolocation to characterize the migration distances of multiple individuals and assess the potential genetic differentiation of butterflies migrating distinct distances. I use $\delta^{2}H$ and $^{87}Sr/^{86}Sr$-based geographic assignment to confirm that some painted ladies migrate up to 4,000 km from Europe to sub-Saharan Africa, while others migrate shorter distances from Europe to the circum-Mediterranean region. Despite these differences in migration distance, genome-wide analysis revealed a lack of adaptive variation between short- and long-distance migrants. Instead, variation in migration distance in painted lady butterflies is likely the result of a plastic response to environmental conditions. Overall, the methodological developments presented in this thesis are a step forward in studying insect migration. The development and application of metals and metal isotopes for insect geolocation opens new avenues to study the migration phenomenon at different scales with widespread relevance for conservation and pest management.

Résumé

Les insectes migrateurs représentent des composantes essentielles des écosystèmes mondiaux et fournissent d'importants services écosystémiques. Cependant, le phénomène migratoire est insuffisamment étudié chez les insectes par rapport aux vertébrés. Dans cette thèse, mon objectif est d' approfondir notre compréhension de la migration des insectes en utilisant le papillon monarque *Danaus plexippus* (L.) et la belle-dame *Vanessa cardui* (L.) comme systèmes modèles. L'étude de la migration des insectes est notoirement complexe en raison de leur petite taille, de leur nombre et de leur courte durée de vie. La géolocalisation isotopique a montré des promesses pour surmonter ces obstacles. Dans ce cadre, je développe et j'applique des outils utilisant les concentrations de métaux et les isotopes de métaux, en particulier les rapports isotopiques du strontium ($^{87}Sr/^{86}Sr$), pour accroître la précision spatiale de la géolocalisation isotopique et démontrer comment ces outils de géolocalisation peuvent faire progresser notre compréhension de la migration des insectes à l'échelle de la population. Dans le premier chapitre, je teste la validité de l'utilisation de $^{87}Sr/^{86}Sr$, des isotopes du plomb et de la concentration d'une série de 23 métaux et métalloïdes pour estimer les origines géographiques des insectes migrateurs en examinant les voies d'incorporation des métaux dans les tissus des ailes de papillon. Grâce à une expérience de changement de régime alimentaire sur 8 semaines, je montre que les concentrations de nombreux métaux dans les ailes des insectes peuvent être modifiées par l'alimentation des adultes ou par le dépôt de poussière, ce qui en fait de mauvais candidats pour la géolocalisation, mais des outils potentiellement intéressants pour étudier la physiologie, l'alimentation ou la toxicologie chez les insectes. Par exemple, le plomb montre une accumulation sur les ailes des papillons à partir de sources externes, et les isotopes du plomb pourraient potentiellement être utilisés pour quantifier l'exposition des insectes migrateurs à la pollution. Certains métaux, dont Ba, Cs, Mg, Na, Rb, Sr, Ti, Tl et U, sont de bons candidats pour le développement d'outils de géolocalisation. Nous nous sommes concentrés sur $^{87}Sr/^{86}Sr$ et avons démontré que, malgré certaines limites, cet outil est valide

pour la géolocalisation isotopique. Dans le deuxième chapitre, j'explicite les étapes requises pour utiliser $^{87}Sr/^{86}Sr$ pour la géolocalisation des insectes, y compris l'étalonnage d'un modèle spatial de variation isotopique (c'est-à-dire un isoscape) à l'aide de la régression de la Forêt d'arbres de décision . J'intègre ensuite les valeurs des isotopes de l'hydrogène (δ^2H) et de $^{87}Sr/^{86}Sr$ dans un cadre d'attribution avec deux isotopes pour estimer les origines natales d'une seule génération de papillons monarques dans l'est de l'Amérique du Nord. Je démontre que la combinaison de ces deux isotopes fournit une estimation plus précise des origines spatiales que l'utilisation de chaque isotope indépendamment. Dans le troisième chapitre, j'applique ce cadre d'attribution pour caractériser les modèles de migration et la connectivité migratoire d'une espèce d'insecte traversant une barrière géographique, le Sahara. Les belle-dames qui migrent vers le nord à travers le Sahara semblent le faire de manière progressive, bien que des limitations d'échantillonnage spatiotemporel aient empêché une caractérisation complète de ce mouvement. En revanche, les belle-dames qui migrent vers le sud semblent suivre un schéma de migration en front large et parallèle, avec peu de déplacement longitudinal. Des preuves d'un schéma de migration en sauts ont été trouvées dans la région occidentale, où les papillons dont les chenilles ont une origine plus septentrionale parcourent des distances plus longues que les papillons dont les chenilles se sont développées dans des régions plus méridionales. Ce schéma de migration en sauts suggère des comportements migratoires distincts chez les belle-dames, où certains individus parcourent des distances plus longues que d'autres. Dans le quatrième chapitre, j'applique la géolocalisation isotopique pour caractériser les distances de migration de plusieurs individus et évaluer la différenciation génétique potentielle des papillons migrant sur des distances différentes. J'utilise une attribution géographique basée sur les isotopes δ^2H et $^{87}Sr/^{86}Sr$ pour confirmer que certaines belle-dames migrent jusqu'à 4 000 km de l'Europe à l'Afrique subsaharienne, tandis que d'autres migrent sur des distances plus courtes de l'Europe à la région circum-méditerranéenne. Malgré ces différences de distance de migration, l'analyse à l'échelle du génome a révélé un manque de variation adaptative entre

les migrateurs à courte et à longue distance. Au contraire, la variation de la distance de migration chez les belle-dames résulte probablement d'une réponse plastique aux conditions environnementales. Dans leur ensemble, les développements méthodologiques présentés dans cette thèse représentent une avancée considérable pour l'étude de la migration des insectes à l'échelle de la population. Le développement et l'application de métaux et d'isotopes métalliques pour la géolocalisation des insectes ouvrent de nouvelles perspectives pour étudier le phénomène de la migration à différentes échelles, avec des implications étendues pour la conservation des insectes migrateurs et la gestion des insectes ravageurs.

Acknowledgments

Thank you to my parents, Cathie and David; my grandparents, Isobel and Doug; my siblings, Sharon and Doug; my extended family, Donna, Jim, Nicole, and Marina; and my dearest friends, Alex and Amanda, for your unconditional love and support. You make me brave.

I am very grateful for my amazing supervisor, Clément Bataille. You e-transferred me two grand in 2018 and told me to fly to Texas and collect milkweed. The adventure never stopped. Your passion for science, candidness, adept sense of humour, and endless optimism make you the best supervisor I could have ever hoped for. Thank you for moulding me into a scientist; I hope to make you proud.

Thank you to everyone at the University of Ottawa who helped me along the way; there are too many people to name. I want to thank the SAiVE lab members, especially Felipe, Julian, Sana, and Eve, for all the laughs and chats about butterflies and isotopes. Thank you to the Kharouba lab for including me in lab meetings and teaching me about butterfly ecology. Thank you to everyone on the BGSA and GSAED councils with me; I hope our efforts made the university a better place. Thank you to Genevieve for always sharing your popcorn.

Graduate school is always difficult, but graduate school during a pandemic was especially stressful. Thank you to my D&D crew, who made me feel safe during the first wave, especially Emma, KJ, Michelle, Chris, and Kevin. Thank you to Mark and Martin for keeping me sane(ish) during the second wave. And thanks to Team Awesome and Dani for our picnic adventures during the third wave.

I also want to thank my international collaborators. Thank you to everybody at SPATIAL and on the ORIGIN project for teaching me about isotopes. I hope our collaboration will develop further in the future. Thank you to Gerard Talavera for sharing his endless curiosity and joy for science and for encouraging me to think big. Thank you to all the iLink members and my friends at IBE and IBB, especially Aurora and Roger. I will never forget our misadventure with the angry lifeguard in Prague. Also, a big thanks to the Backström lab at Uppsala University for hosting me for six months on a Mitacs Globalink Research Award. Thank you, Niclas, for letting me stretch my wings and take over your lab space, and thank you to my labmates for teaching me what a spex is and treating me to weekly fika. Huge thanks to Dasha for cake and her patience as she taught me the basics of population genomics from scratch – you're a rockstar.

I also want to express my gratitude for my little covid-kitty, Milo, who has been my constant companion while writing this thesis. Finally, thank you to the monarchs, painted ladies, and plants used in these studies.

Table of Contents

List of Tables and Figures

General Introduction

Insect migration

Animal migration is often defined at the population scale as the seasonal, round-trip movement of animals between regions (e.g., Ramenofsky & Wingfield, 2007; Greenberg & Marra, 2005; Webster et al., 2002). While this definition may suit the migratory patterns of vertebrates, it fails to capture the multigenerational migratory cycles of insects, wherein successive generations undertake each segment of the annual migration cycle. Individual insects do not typically complete return migrations; instead, their journeys are one-way, causing their movements to be labelled as dispersal rather than migration under this restrictive, population-level definition. Yet, the behavioural characteristics of migration are distinctive across animal taxa, marked by pre-emptive, persistent, directional, non-appetitive, and systematically terminated movement (Dingle & Drake, 2007; Kennedy, 1985). Therefore, in this thesis, I define migration at the behavioural level, in alignment with the literature on insect migration. This perspective considers a suite of traits that enable migratory activity (known as the "migratory syndrome"), including locomotory and orientation ability, responses to environmental cues, endogenous timing, and various behavioural, biochemical, morphological, and physiological adaptations (Dingle, 2014a; Liedvogel & Lundberg, 2014; Dingle & Drake, 2007).

Migration is an innate behaviour in insects; insects are able to migrate at the same time, in the same direction, arriving at similar locations year after year, without any individual ever having completed the entire annual migratory cycle (Merlin & Liedvogel, 2019). Consequently, migratory behaviour is thought to be heritable and under genetic control (Merlin & Liedvogel, 2019; Zhan et al., 2014; Liedvogel et al., 2011; Roff & Fairbairn, 2007). In general, migration is highly labile and has evolved and been lost many times in the tree of life (Dingle, 2014a). For example, within the butterfly genus *Vanessa*, migration is thought to have evolved independently at least six times (Wahlberg & Rubinoff, 2011). This recurrent evolution suggests that the selection pressures and adaptations for migration can

differ between taxa. Regardless, it is widely accepted that the primary driver of migration is to escape from unfavourable environmental conditions, such as winter or dry seasons. In this regard, obligate migration and diapause can be thought of as distinct yet interrelated life history strategies, enabling insects to escape from adverse conditions either through time (by temporarily suspending development and going dormant, i.e., diapause) or through space (by moving to an area with more favourable conditions, i.e., migration) (Rankin & Burchsted, 1992). However, migration comes at a cost to insects in terms of energetic expenditure and an increased risk of mortality during the migratory journey; therefore, to be maintained in the population, migration must offer an advantage over sedentarism (Somveille et al., 2019; Roff & Fairbairn, 2007; Rankin & Burchsted, 1992). The main advantage of migration is the exploitation of seasonal resources, which leads to reproductive benefits, such as higher fecundity and additional generations per year (J. W. Chapman et al., 2015). Migration also benefits organisms by relocating them to regions devoid of predators and parasites (J. W. Chapman et al., 2015). Through migratory culling (the loss of infected migrants during the locomotory period) and migratory escape (the advantages that come from being released from pressure due to parasites), parasitism is thought to be able to maintain migratory behaviour (J. W. Chapman et al., 2015; Altizer et al., 2011).

Thousands of insect species are migratory (Satterfield et al., 2020), including about 600 butterfly species (Chowdhury et al., 2021a). It has been speculated that the number of individual insects migrating every year is in the quadrillions (Satterfield et al., 2020). These insects play a fundamental role in global ecosystems and the provision of ecosystem services. Through their long-distance journeys, migratory insects facilitate the transfer of nutrients, biomass, pollen, and propagules across regions and between continents (Satterfield et al., 2020; Wotton et al., 2019; G. Hu et al., 2016; Landry & Parrott, 2016). They are also important food sources for insectivorous species, including residential and migratory birds and bats (Hawkes et al., 2023; Cohen & Satterfield, 2020). Conversely, migratory insects can pose challenges as agricultural or forestry pests, as exemplified by the devastating crop losses

attributed to the desert locust *Schistocerca gregaria* (Sultana et al., 2021). Furthermore, they can act as vectors of plant and animal diseases (Reynolds et al., 2006). However, despite the importance to ecosystems and agroecosystems, we know relatively little about insect migration (Satterfield et al., 2020).

Our limited understanding of insect migration at the population level poses substantial challenges. It hinders the effective management of conservation initiatives, ecosystem functioning, and biosecurity measures. Migratory connectivity, which refers to the degree of mixing among migratory individuals arriving from different regions, is an important parameter for understanding population genetic structure and formulating strategies to conserve genetic diversity. Globally, the population sizes of many insect species are in decline (Wagner et al., 2021; Warren et al., 2020), but the extent to which such overarching trends affect migratory insect species is largely unknown (Satterfield et al., 2020). An empirical understanding of migratory patterns and connectivity is necessary for recognizing population declines within intricate population dynamics, disentangling the many possible factors contributing to population declines, and creating effective conservation strategies. It is also necessary to understand the transmission pathways of insect-transported materials, such as pollen and spores. The urgency to unravel these intricacies is accentuated by the current backdrop of rapid environmental change due to anthropogenic climate change and widespread habitat degradation. Alterations in insect migratory patterns could have far-reaching consequences for the provision of ecosystem services and for the potential for migratory insects to invade new regions. Similarly, escalating globalization has amplified the movement of goods over land and sea, consequently increasing the incursion rate of exotic migratory insect species (Seebens et al., 2017). In this context, effective biosecurity and pest management relies on a comprehensive understanding of dispersal and migration in agricultural and forestry pests, as well as invasive species.

However, understanding insect migration at the population level also requires an understanding of intraspecific variation in migratory behaviour, known as migratory diversity. Migratory diversity can take many forms, including differences in migratory state (e.g., partial migration), orientation, distance, duration, and timing (A. K. Shaw, 2020). Intraspecific migratory diversity has important conservation implications because it provides a spectrum of behaviours within a population, increasing the likelihood that at least one of these behaviours will confer an advantage in a given context. Migratory diversity has been linked to enhanced resilience to environmental change, an association that is particularly pertinent in the current context of environmental change (Gilroy et al., 2016). Similarly, migratory diversity has also been linked to the ability of a species to colonize new habitats successfully (Snell-Rood & Steck, 2019; Clobert et al., 2009). Species with highly diverse migratory behaviours may have more potential for invasiveness compared to those with limited migratory diversity (A. K. Shaw, 2020; Gilroy et al., 2016). This variation in migratory behaviour can also impact agroecosystems through spatiotemporal variation in the delivery of the costs and benefits of insect migration. For example, variation in migratory behaviour can affect the timing and magnitude of nutrient transport (Satterfield et al., 2020) and pollination services provided to plants (Wotton et al., 2019). Therefore, understanding the mechanisms behind variation in migratory behaviour would improve our ability to predict the extinction risk of species of conservation concern, assess the invasion capacity of species of biosecurity concern, and optimize the provision of ecosystem services.

Tracing the migratory journeys of insects

The greater number of studies on vertebrate animal migration compared to insect migration can be partially attributed to human bias towards birds and mammals in research priorities (Fukano & Soga, 2021). However, a larger component of the disparity can likely be attributed to the innate difficulties in studying insect migration because of the small size, short lifespan, and sheer abundance of insects (Rutz & Hays, 2009). Traditionally, the study of migratory insects depended on the field observations of

committed scientists that remain vital sources of information to this day (e.g. Urquhart & Urquhart, 1976; Williams, 1958; Urquhart, 1941; Williams, 1930). However, these studies were inherently limited by the number of observations that scientists and other interested individuals could collect. More recently, the emergence of community science platforms like iNaturalist, Monarch Watch, and eButterfly (Prudic et al., 2017) has harnessed the considerable observational power of collective effort to amass extensive data on insect presence. These programs have been essential for providing the data required for creating species distribution models, understanding temporal population dynamics, and enabling comparative studies (e.g., van Swaay et al., 2020; Menchetti et al., 2019; Agrawal & Inamine, 2018). Additional work democratizing mark-release-recapture programs has also had tremendous benefits. However, even the large-scale tagging program for the monarch butterfly *Danaus plexippus* (L.) organized by Monarch Watch only sees a 1% annual recovery of tags (James et al., 2018), limiting the ability of this technique to answer specific questions about insect mobility.

In the last few decades, scientists have increasingly deployed various technologies to observe and trace insect migration in the wild (reviewed in Chowdhury et al. (2022) and Reynolds et al. (2006). For example, entomological radar has revealed that quadrillions of individuals from many diverse species of insects conduct high-altitude flights every year (G. Hu et al., 2016; J. W. Chapman et al., 2011). More recently, radio-telemetry has been used on larger insects, like monarch butterflies, death's-head hawkmoths *Acherontia atropos*, and common green darner dragonflies *Anax junius* (Menz et al., 2022; S. M. Knight et al., 2019; Wikelski et al., 2006), to understand migratory behaviour. Radio transmitters are currently too heavy (e.g., up to 50% of the body weight of a monarch butterfly) to be applied on a large scale or to small insects (S. M. Knight et al., 2019), although rapid technological advancements are being made. Genetic data can also be used to relate individuals to geographic areas but requires prior knowledge of spatial population structure (Ruegg et al., 2017; Rundel et al., 2013; Nagoshi et al., 2009). Finally, many geolocation techniques using intrinsic biomarkers have been developed for insects,

including isotopes (Wassenaar & Hobson, 1998), trace element analysis (i.e., “chemoprints”; Holder et al., 2014), and pollen metabarcoding analysis (Suchan et al., 2018).

Of these techniques, isotope-based geographic assignment shows great promise for tracing the natal origin of migratory insects and is becoming a widely used method for geolocation (Wunder, 2012). Isotopes (forms of an element that differ in neutron number) are ubiquitously present in organic materials. Decades of work have given us a basis to predict the spatiotemporal variations of some isotopic systems (including hydrogen, oxygen, and carbon) using empirical or mechanistic approaches to produce isotopic baseline maps (also called “isoscapes”). Local isotopic signatures are incorporated into the larval insect through food and drink and remain relatively unaltered in certain adult tissues (e.g. insect wings; Chapter 1; Lindroos et al., 2023). Therefore, the isotopic signatures of these tissues from migratory individuals can be measured and then compared to isoscapes to provide key insights into insect mobility, a technique known as geographic assignment (Hobson et al., 2010; Figure 0.1).

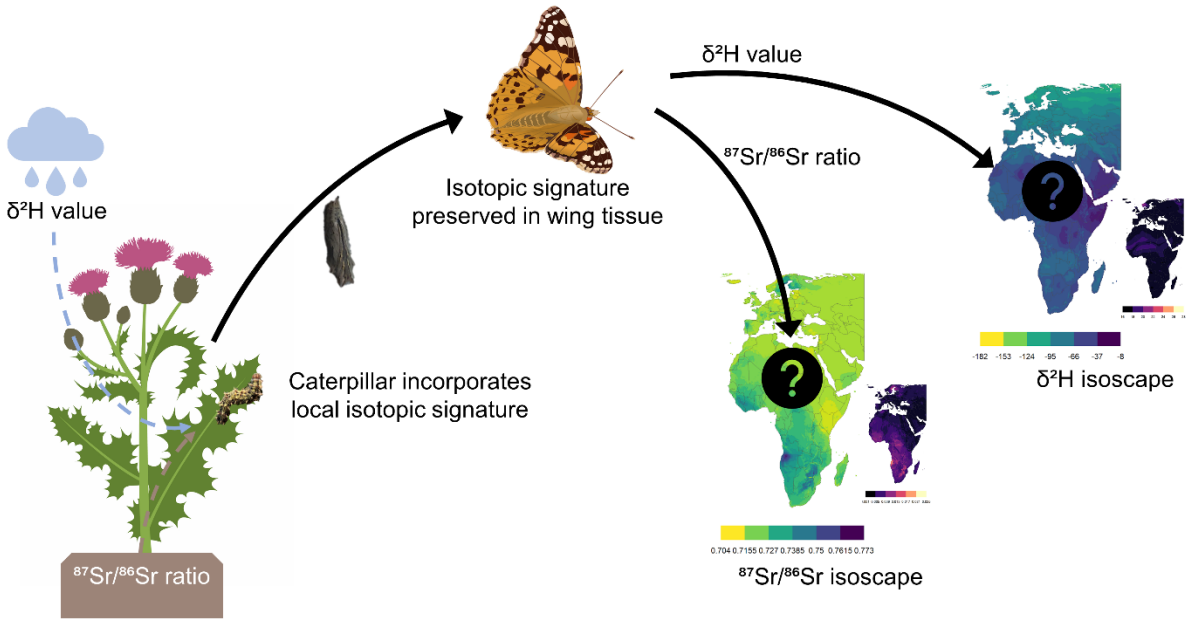

Figure 0.1 Illustration of the process of isotope-based geographic assignment for butterflies using hydrogen isotope values (δ^2H) and strontium isotope ratios ($^{87}Sr/^{86}Sr$). Local isotopic signatures of δ^2H and $^{87}Sr/^{86}Sr$ are incorporated into caterpillar tissues through food and drink (Flockhart et al., 2015; Hobson et al., 1999). After emerging from the chrysalis, this local isotopic signature is largely preserved in the inactive wing tissues of the adult butterfly (Chapter 1; Lindroos et al., 2023). Thus, the isotopic signature of a migratory butterfly's wing can be measured and compared to a spatial model of isotopic variation (i.e., an isoscape) to estimate the butterfly's natal origin.

Unfortunately, the spatial estimate of natal origin provided by a single isotope is often too broad to be of practical use (Hobson, 2023). Combining multiple geolocation techniques is a common tactic to improve the spatial precision of the estimated area of natal origin (Wunder, 2012). For example, isotope-based geographic assignment can be combined with non-isotopic geolocation techniques, including ecological niche modelling (e.g., Ruegg et al., 2017) and wind-trajectory modelling (e.g., Talavera et al., 2018). Multiple isotopes can also be combined, although this technique works best when the drivers of the different geolocation techniques are distinct and uncorrelated. Hydrogen and carbon isotopes have been the most widely used isotopes for the geolocation of insects (e.g., Satterfield et al., 2018; Vander Zanden et al., 2018; Flockhart et al., 2017b). Spatial variability in hydrogen isotopes (δ^2H) is primarily driven by climatic variables, such as precipitation (Bowen et al., 2005), while variability in carbon isotopes is driven by differences in photosynthetic pathways (Still & Powell, 2010). On the other

hand, studies exploring the use of oxygen isotopes for the geolocation of insects have found that, because of the strong correlation between oxygen and hydrogen, oxygen does not strongly improve on geographic assignment performed using δ^2H (Hobson et al., 2019). Recently, sulphur isotopes have been developed for similar use; sulphur isotopes vary across the landscape depending on the distance from the coast, making them an excellent geolocation tool on gradients from coastlines to inland (e.g., Bataille et al., 2021; Heinrich & Collins, 2017). Strontium isotope ratios ($^{87}Sr/^{86}Sr$) also hold promise for insect geolocation (Flockhart et al., 2015). The spatial variation in $^{87}Sr/^{86}Sr$ is primarily influenced by geology, specifically bedrock type and age (Bataille et al., 2020). In this thesis, I contribute to the development of $^{87}Sr/^{86}Sr$ for the study of insect migration.

There are many advantages to using isotopes for tracing the migratory journeys of insects. Unlike in mark-release-recapture studies, the insect only needs to be captured once, at the end of its migratory journey. This is an advantage because recapturing insects is notoriously difficult, and recapture rates are low. Isotope geolocation also benefits from not using marking technology, such as tags or radio transmitters, that can negatively impact migratory behaviour. Additionally, isotopic signatures can be measured on a small quantity of tissue, extending applications to small insects like hoverflies that are too small to be tracked by biologgers and other techniques (e.g., Clem et al., 2023). Another advantage of isotope geolocation is that isotopic analysis can be applied to dead, archived, and preserved specimens. This permits analyses of samples collected in the past, and isotope geolocation can be applied to questions about temporal migratory patterns from archived specimens (e.g., Flockhart et al., 2017b). Therefore, isotope geolocation is an excellent tool with which to study the migratory patterns, ecological impacts, and ecological and evolutionary drivers of insect migration.

Study systems

Butterflies often serve as indicator species for insect diversity and ecosystem health due to the high level of public interest in these charismatic insects, which has led to a wealth of available knowledge about their life history and ecology (Parmesan, 2003). Likewise, butterflies are good candidates as model species for insect migration because they benefit from a good base of taxonomic, ecological, isotopic, and genomic research. Thus, the insights gleaned from the study of butterfly migration have the potential to be applied to the understanding of migration in other insect species.

This thesis focuses broadly on developing and applying isotopic geolocation tools for migratory insects. It encompasses multiple studies conducted across different spatiotemporal scales with the aim of exploring the potential of isotope geolocation to reconstruct the mobility of insects at the population level and refine our understanding of insect migration. The studies use two well-known butterfly species renowned for their long-distance migrations: the monarch butterfly and the painted lady butterfly *Vanessa cardui* (L.). The monarch butterflies in North America are famous for their annual multigenerational migration cycle from Mexico through the U.S.A. to Canada and back (Brower, 1995). These butterflies were long thought to be separated into an eastern and western migratory population, divided by the Rocky Mountains. However, genomic evidence has established that monarch butterflies in North America belong to a single panmictic population (Talla et al., 2020). This thesis concentrates on the monarch butterflies found east of the Rocky Mountains in North America (Chapter 1; Chapter 2). The painted lady butterfly is equally well-known for its extensive distribution, large population sizes, and long-distance migrations. Painted ladies are "virtually cosmopolitan" and can be found on all continents except Antarctica and Australia (Shields, 1992). Although painted ladies are also found in North America, this thesis focuses on the painted ladies found migrating between the Palearctic and Afrotropical regions (Chapter 3; Chapter 4). Painted ladies have long been known to migrate across the Mediterranean Sea

from Europe to North Africa, but recent geolocation using δ^2H showed that they also migrate across the Sahara to sub-Saharan Africa (Talavera et al., 2018; Stefanescu et al., 2016).

The monarch butterfly and painted lady butterfly both belong to the Nymphalidae family; however, the Danainae diverged from the other Nymphalidae subfamilies approximately 71 million years ago (M. Zhang et al., 2008) and these taxa have evolved different life history traits and strategies. Painted ladies are continuously-brooded, obligate migrators that follow a succession of suitable breeding habitats over eight to ten generations per year (Talavera et al., 2023). This migratory strategy resembles that of most other migratory insects (Johnson, 1960), making the painted lady butterfly an ideal species on which to study the underlying drivers of the migratory syndrome because the findings are likely to apply to more insect species (Chapter 4). In contrast, monarch butterflies have a migratory strategy that is unusual among migratory insects. Monarchs proceed through a succession of three to four "summer" generations, followed thereafter by a "super" generation. The super generation, with a lifespan of up to 8 months, enters reproductive diapause before embarking on a return migration. This generation migrates southwards to the oyamel fir forests in Mexico each autumn, where they spend the winter in communal roosts. In the spring, they migrate back northwards to start the next generation (Reppert & de Roode, 2018; Brower, 1995). While the summer generations still migrate northwards, their journeys are unidirectional, and their lives are much shorter (about five weeks), which is reminiscent of the behaviour observed in painted lady butterflies. The super generation also differs morphologically; they typically have larger wings, a trait thought to make them more capable of surviving the longer, more strenuous journeys they undertake (Flockhart et al., 2017a).

Differences in life history strategies between monarchs and painted ladies have rendered the monarch less resilient to disturbances than the painted lady. The population of monarch butterflies in eastern North America is purported to have declined significantly over the last few decades (Brower et al., 2012, but see Meehan & Crossley, 2023). Conversely, the painted lady's risk of extinction is currently

categorized as “least concern” (Walker & Coetzer, 2020). One of the main drivers of the population decline of monarchs is thought to be habitat loss and mortality due to stochastic weather events at the overwintering sites in Mexico (Flores-Martínez et al., 2019). In contrast, painted ladies do not congregate in overwintering sites and thus are not susceptible to environmental changes at a highly specific locality in the same way that monarchs are. Another proposed driver of the monarch population decline is a decrease in hostplant availability on the summer breeding grounds due to changes in farming practices (Pleasants & Oberhauser, 2013). Monarchs are specialist herbivores and rely on milkweed *Asclepias* spp. as their larval host plants. In contrast, painted ladies are highly polyphagous, opportunistic generalists, and larvae can be found feeding on many species of plants across ten plant orders. Although painted ladies have preferred host plants, their host plant flexibility allows them to be found in a broader range of environments than monarchs, promoting their resilience to environmental change (Celorio-Mancera et al., 2016). Other potential drivers of the monarch population decline include climate change (Batalden et al., 2008) and mortality during the southward migration (Inamine et al., 2016). However, the relative importance of these drivers is contentious, and a more thorough understanding of monarch population dynamics is needed to validate the contribution of each driver to the monarch’s population decline (Wilcox et al., 2019).

Thesis objectives

Although migratory insects play vital roles in ecosystems, the study of insect migration is hampered by methodological difficulties. Consequently, this thesis aims to develop methodological solutions to study insect migration at the population scale. This objective is accomplished through a progressive advancement of metals and metal isotopic tools. These tools are applied to the monarch butterfly and painted lady butterfly as model systems to refine our understanding of insect migratory patterns and the ecological and evolutionary basis of the migratory syndrome. I start by exploring the pathways of metal incorporation into insect tissues in a laboratory setting. In this process, I test some of the fundamental assumptions of geolocation using metals and metal isotopes, verifying their applicability for tracking migratory insects and identifying some caveats (Chapter 1). Next, I lay out the steps needed to develop a regional strontium isoscape and use it for the $^{87}Sr/^{86}Sr$-based geographic assignment of insects, using a single generation of monarch butterflies in eastern North America as a case study. I demonstrate that combining $\delta^{2}H$ and $^{87}Sr/^{86}Sr$ into a dual assignment framework can constrain spatial estimates of natal origin, yielding new ecological insights (Chapter 2). This isotopic framework is then extended to painted lady butterflies in the Afro-Palearctic region. I develop a regional strontium isoscape covering Europe and Africa and use $\delta^{2}H$ and $^{87}Sr/^{86}Sr$-based geographic assignment to decipher the migratory patterns and migratory connectivity of multiple generations of painted lady butterflies across the Sahara (Chapter 3). Finally, I combine $\delta^{2}H$ and $^{87}Sr/^{86}Sr$-based geographic assignment with whole-genome resequencing to explore the basis of the migratory syndrome. I demonstrate that isotopes can be applied to characterize migratory behaviour by estimating the migration distances of individual painted lady butterflies. I then investigate the phenotype-genotype associations of migratory behaviour (Chapter 4). The value of these isotopic tools extends beyond advancing our understanding of migration in these two model systems and has the capacity to initiate a transformation in the study of insect migration.

Chapter 1: Metals and metal isotopes incorporation in insect wings: Implications for geolocation and pollution exposure

This chapter is a reproduction of the following published article:

Reich, M. S., Kindra, M., Dargent, F., Hu, L., Flockhart, D. T. T., Norris, D. R., Kharouba, H., Talavera, G., & Bataille, C. P. (2023). Metals and metal isotopes incorporation in insect wings: Implications for geolocation and pollution exposure. *Frontiers in Ecology and Evolution*, 11(1085903).

Contribution

I conceived the idea for the study and led the writing of the manuscript, with input from all coauthors. I led the metals and metal isotopes analysis, with help from CB, MK, FD, and LH. FD, HK, and I designed the insect-rearing component. I led the data analysis with help from MK, FD, and CB. TF and RN collected the wild monarch and milkweed samples.

Abstract

Anthropogenic activities are exposing insects to elevated levels of toxic metals and are altering the bioavailability of essential metals. Metals and metal isotopes have also become promising tools for the geolocation of migratory insects. Understanding the pathways of metal incorporation in insect tissues is thus important for assessing the role of metals in insect physiology and ecology and for the development of metals and metal isotopes as geolocation tools. We conducted a diet-switching experiment on monarch butterflies (*Danaus plexippus* (L.)) with controlled larval and adult diets to evaluate the sources of 23 metals and metalloids, strontium isotopes, and lead isotopes to insect wing tissues over a period of 8 weeks. Concentrations of Ca, Co, Mo, and Sb differed between the sexes or with body mass. Ni and Zn bioaccumulated in the insect wing tissues over time, likely from the adult diet, while increases in Al, Cr, Cd, Cu, Fe, and Pb were, at least partially, from external sources (i.e., dust

aerosols). Bioaccumulation of Pb in the monarch wings was confirmed by Pb isotopes to mainly be sourced from external anthropogenic sources, revealing the potential of Pb isotopes to become an indicator and tracer of metal pollution exposure along migratory paths. Concentrations of Ba, Cs, Mg, Na, Rb, Sr, Ti, Tl, and U appeared to be unaffected by intrinsic factors or additions of metals from adult dietary or external sources, and their potential for geolocation should be further explored. Strontium isotope ratios remained indicative of the larval diet, at least in males, supporting its potential as a geolocation tool. However, the difference in strontium isotope ratios between sexes, as well as the possibility of external contamination by wetting, requires further investigation. Our results demonstrate the complexity of metal incorporation processes in insects and the value of studying metals to develop new tools to quantify pollution exposure, metal toxicity, micronutrient uptake, and insect mobility.

Introduction

Some metals are important micronutrients that sustain life while others have profound implications as toxic metals that reduce survival and fitness. Essential metals are required for metabolic functions such as that the organism cannot survive when the metal is removed from the diet. Essential metals participate in enzyme catalysis, protein structure, cellular signalling, and the creation of electrochemical potentials at membranes (Dow, 2017; Maret, 2016) and it is estimated that up to 30% of proteins are metalloproteins (Aptekmann et al., 2022). Within organisms, these essential metals follow a dose-response curve, in which low doses cause morbidity due to metal deficiency and high doses cause toxicological effects. Conversely, many non-essential metals are toxic even at low doses. However, despite the fundamental importance of metals, little is known about the pathways of metal incorporation into insects in comparison to non-metal macronutrients like C, H, O, and S (Kaspari, 2021; Dow, 2017).

Insects incorporate essential and non-essential metals through their larval and adult diets. When some of these essential metals are limited in the environment, populations of herbivorous insect

species can be strongly affected (Reihart et al., 2021; Kaspari, 2020), whereas abundant essential metals in the environment can boost population sizes (Prather et al., 2018). For example, the community composition and abundance of grasshoppers is influenced by plant concentrations of N, P, Mg, Na and K in grasslands (Joern et al., 2012). Some toxic metals are also bioaccumulated through dietary sources with detrimental effects on insect populations. For example, experiments have demonstrated that *Spodoptera litura* Fabricius moths bioaccumulate Ni from their adult diet with negative impacts on growth rate and fecundity (Sun et al., 2013). However, diet might not be the only source of metal incorporation into insect tissues. Unlike vertebrates, insects respire through a system of tubes called tracheae that form a complex network of gas-filled vessels throughout the body. Many metals, such as Pb and Cd, are concentrated in anthropogenic aerosols and can potentially circulate within the tracheal system (Negri et al., 2015). In addition, chitin, a structural polysaccharide, forms insect exoskeletons and is a powerful metal absorbent (Anastopoulos et al., 2017) that could facilitate metal incorporation in insect tissues through adhesion to the surface of the exoskeleton (Negri et al., 2015). Some elements, such as Sr, Ca, Mg, and Ba, are highly soluble in water and it is possible that they could exchange and diffuse deeper into insect tissues when wetted. Recent controlled studies on metabolically inert keratinous tissues of vertebrates (e.g., feathers: Crowley et al. (2021); hair: Fauberteau et al. (2021)) demonstrated that many metals in keratin are rapidly exchanged and concentrated from external sources (e.g., wet absorption, pollution, dust aerosols; Rodiouchkina et al., 2022; L. Hu et al., 2020b, 2019, 2018). In addition to their incorporation through diet, exogenous bioaccumulation could influence the concentration of metals in chitinous insect tissues.

Understanding the sources and mechanisms of metal incorporation into insect tissues is especially urgent in the context of anthropogenic habitat alteration because human activities have changed the concentrations of toxic and essential metals in the environment. Human activities such as smelting, mining, industrialization, and agriculture are causing insects to be increasingly exposed to toxic

metals at rates above the natural baselines they evolved to tolerate (Monchanin et al., 2021). Even when regulated, these activities can have adverse effects on insects because invertebrates are more susceptible than vertebrates to toxic metals like Cd and Pb and, therefore, often experience adverse effects well below anthropocentric permissible concentration limits (Monchanin et al., 2021; Mogren & Trumble, 2010; Hopkin, 1990). Similarly, activities such as CO_2 enrichment or the application of nitrogen and phosphate fertilizers can alter the availability of essential metals to insects through the nutrient dilution of plants (Nessel et al., 2021; Welti et al., 2020). Limited availability of essential metals can inhibit growth and development and reduce fitness; thus, conservation efforts need to consider both changes to the bioavailability of essential metals to organisms (Filipiak & Filipiak, 2022) and exposure to toxic metals.

Besides these toxicological and micronutrient availability concerns, understanding the mechanisms of metal incorporation into insect tissues is essential to develop new geolocation tools for insect population ecology. The analysis of metal and metal isotopes in insect tissues has become a promising avenue for developing tools aimed at understanding insect migration. Metals (e.g., Tigar & Hursthouse, 2016), metal ratios (e.g., Holder et al., 2014), combined metal composition (i.e., chemoprints, mineral component analysis, chemometrics; e.g., Lin et al., 2019) and metal isotopes (Chapter 2; Holder et al., 2014) have been used to assess long-term patterns of insect dispersal. Insect wings are the primary tissue used to develop these geolocation tools. It has been demonstrated that, for some metal and metal isotopes, the insect wings reflect the chemical signature of the larval diet (e.g., Flockhart et al., 2015). By comparing the chemical signature of the metal or metal isotopes of the insect tissue to metal-specific baseline maps (called “metalscapes” or isoscapes), one can then estimate the location where the tissue formation occurred (i.e., the natal origin). However, making proper geolocation inferences with these metals requires a clear understanding of metal and metal isotope incorporation into insect tissue over time because alteration of the natal signature via, for example, the

uptake of metals through adult feeding, would void any geolocation inferences (Dempster et al., 1986). Insect wings are primarily composed of chitin and proteins, and are not completely inert like vertebrate keratin. They host androconial organs (i.e., pheromone glands), sensory receptors, trachea, nerves, and have hemolymph circulating through their veins (Tsai et al., 2020). Consequently, the circulation of hemolymph could lead to some metal exchange with the rest of the insect body leading to potential modification of metal concentrations during the adult life, as has been observed for hydrogen isotope values (Lindroos et al., 2023). Additionally, exogenous bioaccumulation could contribute to the incorporation of many metals during adult life through aerosol deposition and wetting as has been observed with keratinous tissues (L. Hu et al., 2019, 2018). However, the potential addition of metals to insect wings after tissue formation has not been explicitly investigated.

In this study, we aimed to better characterize the incorporation mechanisms of a suite of metal and metal isotopes in insect wings over time and advance the development of metal-based tools for insect ecology. We conducted a laboratory-based diet-switching experiment to explore the environmental and dietary sources of 23 metals and metalloids, strontium isotopes (measured as $^{87}Sr/^{86}Sr$ ratios), and lead isotopes (measured as $^{208}Pb/^{206}Pb$ and $^{207}Pb/^{206}Pb$ ratios) in insect wings over an 8-week timespan. For each metal, we evaluated the effects of intrinsic factors on metal concentrations and assessed the potential sources of any bioaccumulation. We also assessed the potential for $^{87}Sr/^{86}Sr$ in insect wings to be altered by wetting. Finally, we evaluated the potential of the metal and metal isotopes for providing geolocation or pollution exposure information. By understanding the incorporation of metals and metal isotopes in insect wings over time, we will be better able to test the assumptions of geolocation using metal biomarkers and assess the metal exposure risks of insects.

Materials and Methods

We chose for this study a representative winged insect, the monarch butterfly (*Danaus plexippus* (L.)). The monarch butterfly is an iconic migratory insect famous for its annual, multi-generational, round-trip

migration from the Oyamel fir forests of Central Mexico, through the USA, to Canada, and back. Monarchs are a well-suited species to investigate the incorporation of metal and metal isotope signals. First, they have a large geographic range with known elemental and isotopic variations meaningful for geolocation (Chapter 2; Wieringa et al., 2020). Second, monarch larvae are specialist herbivores dependent on milkweed (*Asclepias* spp.). Plants are known to uptake and regulate metals in a species-specific manner; thus, this relatively high host-specificity will likely minimize potential discrepancies in metal signatures associated with differences in larval host plant species (Tibbett et al., 2021; McLean et al., 1983). Third, metal exposure is of particular concern for monarchs because milkweed is often found in disturbed habitats, such as roadsides, which often correlates with higher pollution exposure (Phillips et al., 2021). As for most insects, the incorporation and toxicology of metals in monarch butterflies are mostly unknown, although Zn has been shown to decrease larval survival under some conditions (e.g., when individuals have low access to macronutrients; Shephard et al., 2022, 2021, 2020).

To explore the incorporation of metal and metal isotopes, we first conducted a diet-switching experiment on monarch butterflies over an 8-week period. We raised larvae from eggs with controlled milkweed dietary inputs and then maintained the adults with a controlled adult diet. We measured the changes in metal concentrations and isotopes in monarch wings at weekly time intervals and compared the metal abundances found in our laboratory experiment to the range of natural metal abundances in the wings of 100 wild-caught monarch butterflies. Next, we explored the incorporation mechanisms of different metals by calculating enrichment factors to the adult diet and a proxy of mineral dust for each metal, analyzing lead isotopes in the monarch wings to assess the source of Pb bioaccumulation, and performing a wetting experiment for Sr. Finally, we measured the concentrations of 12 metals in ashed milkweed samples from across the eastern USA and assessed our ability to use soil and milkweed samples in the construction of metalscapes for monarch butterflies (Appendix A).

Diet-switching experiment

We conducted a diet-switching experiment in the summer of 2019 to assess the sources and preservation of metals and metalloids (hereinafter referred to collectively as metals) and metal isotope signals in monarch wings throughout the life of an adult butterfly. Eggs were collected from a single wild-caught female, allowing us to assume that all the specimens in this experiment are at least half-siblings and control for maternal effects. After collection, eggs were transferred to individual 500 mL glass rearing containers with a mesh lid and placed in a controlled environmental chamber (Biochambers Inc., model LTCB-19) held at a light to dark schedule of 12 h:12 h, light temperature of 28 °C and dark temperature of 26 °C, and humidity of 60%. These conditions reflect optimal conditions for monarch development (Dargent et al., 2021).

Caterpillars were fed wild common milkweed (*Asclepias syriaca* L.) leaves that were collected daily from Aug. 9-22, 2019, from a single 30 m^2 site in Ottawa, Ontario, Canada (45.41°, -75.67°). The collection site is in an urban park next to the Rideau River and is near a light rail station and bike paths. The leaves were cleaned of surface contaminates (e.g., dust) using distilled deionized (DDI) water before being fed ad libitum to the caterpillars. Sub-samples of the cleaned milkweed leaves were collected for analysis to check the assumption that milkweed leaves taken from the same locality will have similar elemental and isotopic signatures over the 2-week period of collection. Frass was removed from the containers daily.

After the monarchs eclosed from the chrysalises (Aug. 29-31, 2019), they were transferred to mesh butterfly cages in an indoor laboratory. Butterflies were kept two per cage, but a cloth divider was installed to minimize wing damage from collisions between individuals. The cages were misted twice a day with DDI water to maintain humidity and were given a light-to-dark schedule of about 12 h:12 h. DDI water was used to avoid additions of metals by water absorption. The temperature in the laboratory was maintained by the building's normal operations and maintenance schedule at approximately 20 °C.

Once per day, the adult butterflies were given a fresh serving of 50% maple syrup solution in a tube with a foam faux-flower perch and allowed to feed *ad libitum*. The adult food was renewed every day to avoid an accumulation of metals from external sources (e.g., dust) in the maple syrup solution to ensure that metals sourced from the diet and exogenous aerosols could be distinguished. Because the butterflies do not always recognize the unnatural food source, individuals were also hand-fed the maple syrup for at least one minute every other day. The first six monarchs were sampled immediately post-eclosion (Day 0; no feeding), and two monarchs were subsequently sampled each week until up to eight weeks post-eclosion (n = 22). Immediately after sampling, monarchs were placed into a freezing chamber at -18 °C. Later, wings were dissected from the body and placed in glassine envelopes until elemental analysis. The time between collection and elemental or isotopic analysis ranged from a few months to 18 months.

Trace element analysis

Elemental analysis of monarch wings, larval diet (i.e., milkweed leaves) and adult diet (i.e., 50% maple syrup solution) was performed in two analytical runs via inductively coupled plasma mass spectrometry (ICP-MS; Agilent 8800 ICP-QQQ, Agilent Technologies Inc., Santa Clara, CA, USA) at the Department of Earth and Environmental Sciences, University of Ottawa. The first analytical run in Feb. 2020 measured 23 metals in monarch wings (n = 18) and maple syrup (n = 4): aluminum (Al), arsenic (As), barium (Ba), calcium (Ca), cadmium (Cd), cobalt (Co), chromium (Cr), copper (Cu), cesium (Cs), iron (Fe), magnesium (Mg), manganese (Mn), molybdenum (Mo), sodium (Na), nickel (Ni), lead (Pb), rubidium (Rb), antimony (Sb), strontium (Sr), titanium (Ti), thallium (Tl), uranium (U), and zinc (Zn). To remove any surface contaminants (e.g. dust), a single forewing from each monarch was cleaned using pressurized nitrogen gas for about 2 min. at 10 psi (Chapter 2). The monarch wings and maple syrup samples were then digested in perfluoroalkoxy alkanes (PFA) vials (Savillex, LLC., Eden Prairie, MN, USA) using 1 mL 16 M HNO_3 (double distilled TraceMetal™ Grade; Fisher Chemical, Mississauga, ON, Canada) and 0.1 mL

ultraclean hydrogen peroxide (for trace analysis Grade; Sigma-Aldrich, Italy) for 12 h at 120 °C. After digestion, the samples were dried on a hot plate at 90 °C and then re-dissolved in 1 mL of 2% v/v HNO_3 (double distilled). A 100 µL aliquot of each solution was extracted, diluted to 2 mL 2% v/v HNO_3, and centrifuged. Calibration standards were prepared using single element certified standards (SCP Science Inc., Montreal, QC, Canada). Detection limits were conservatively estimated as three times the standard deviation of the blanks within each run. For monarch wings, 4 measurements of As, 2 of Tl, and 8 of U were below the detection limit. Concentrations of Cd, Cs, Tl, and U were lower than the calibration range of 1.56 to 100 ppb (~200, ~800, ~900, and ~4600 times lower, respectively). Metal concentrations in maple syrup were comparatively low, with all 4 As and U measures and 1 Fe measure below the detection limit. Additionally, Cd, Tl, and Pb were all well below the calibration range (~600, ~200 and ~200 times lower, respectively). Intra-run relative standard deviation (RSD) of the repeated standard analysis was below 3% except for Cs (RSD = 21%), Sb (RSD = 19%), Rb (RSD = 67%), and Fe (RSD = 38%).

For the second analytical run in May 2021, milkweed samples (n = 3) and analytical replicates of monarchs wings (n = 19) were analyzed for 15 metals: Al, Ba, Ca, Cd, Co, Cr, Cu, Fe, Mg, Mn, Ni, Pb, Sr, Ti, and Zn. Milkweed samples were cleaned with DDI water, an ultrasonic bath (10 min.), and a MilliQ water rinse. Wing samples were dry-cleaned with pressurized nitrogen gas for 2 min. at about 10 psi for a limited, repeated elemental analysis of the monarch wings to assess if there was sample contamination of Pb during storage. For monarch tissues, a single hindwing was used for most samples. However, some samples had too low Pb concentrations and both hindwings (i.e., L2) or both hindwings and the remaining forewings were used (i.e., L11, L16, L17, L21, L5). Samples were then digested in concentrated nitric acid (16 M; distilled TraceMetal™ Grade; Fisher Chemical, Canada) using microwave digestion (Anton Paar Multiwave 7000, Austria): the samples were heated from ambient temperature to 250 °C at a steady rate in 20 min. and then left at 250 °C for 15 min. in a pressurized chamber. An aliquot of 200 µL from each sample was separated and diluted to 2 mL of 2% v/v HNO_3 (double distilled) and run on the

ICP-MS. For monarch wings, 16 measurements of Co and 17 of Cd were below the detection limit; only Cd was lower than the calibration range (~155 times lower). Metal concentrations in milkweed were comparatively high, with Ca and Mg well above the calibration range (~900 and ~200 times higher, respectively). Intra-run RSD of the repeated standard analysis was below 3% except for Mg (RSD = 70%), Ca (RSD = 157%), and Fe (RSD = 143%).

Strontium isotope ratios analyses

The $^{87}Sr/^{86}Sr$ analysis was performed in two runs at the Isotope Geochemistry and Geochronology Research Centre, Carleton University using a ThermoScientific™ Neptune™ high-resolution multi-collector inductively coupled plasma mass spectrometer (MC-ICP-MS; Thermo Fisher Scientific, Bremen, Germany). To prepare for the first run in Feb. 2020, milkweed samples (n = 3) were cleaned using DDI water and an ultrasonic bath (10 min.), then oven-dried at 80 °C before being ashed at 600 °C for 4 h to facilitate digestion. They were then digested in perfluoroalkoxy alkanes (PFA) vials (Savillex, LLC., Eden Prairie, MN, USA) using 1 mL 16 M HNO_3 (double distilled TraceMetal™ Grade; Fisher Chemical, Mississauga, ON, Canada) and 0.1 mL ultraclean hydrogen peroxide (for trace analysis Grade; Sigma-Aldrich, Italy) for 12 h at 120 °C. After digestion, the samples were dried on a hot plate at 90 °C. Dried samples were re-dissolved in 1 mL of 2% v/v HNO_3 (double distilled). A 100 µL aliquot of each solution was extracted, diluted to 2 mL 2% v/v HNO_3, and the concentration of Sr was measured using the ICP-MS in Oct. 2019. The remaining ~900 µL aliquot (90%) of sample digest was dried down and re-dissolved in 0.05 mL 6 M HNO_3. The separation of Sr was processed in 100 µL microcolumn loaded with Sr-spec Resin™ (100–150 µm; Eichrom Technologies, LLC). The matrix was rinsed out using 6 M HNO_3, and Sr was collected with 0.05 M HNO_3. After separation, eluates were dried and re-dissolved in 2 mL 2% v/v HNO_3 for $^{87}Sr/^{86}Sr$ analysis.

For the second analytical run in Sep. 2020, the remaining aliquots (~90%) of the monarch wing (n = 18) and maple syrup (n = 4) samples run on the ICP-MS in Feb. 2020 were used. Samples were dried

down and re-dissolved in 0.5 mL 6 M HNO_3. The separation of Sr was processed in 100 µL microcolumn loaded with Sr-spec Resin™ (100–150 µm; Eichrom Technologies, LLC). The matrix was rinsed out using 6 M HNO_3, and Sr was collected with 0.05 M HNO_3. The microcolumn process was repeated to ensure complete separation. After separation, the eluates were dried, and monarch wing samples were re-dissolved in 200 µL 2% v/v HNO_3 and maple syrup in 2 mL 2% v/v HNO_3 for $^{87}Sr/^{86}Sr$ analysis.

For both analytical runs, sample solutions were introduced to the MC-ICP-MS using a microFAST MC single-loop system (Elemental Scientific Inc., Omaha, NE, USA). The sample introduction flow rate was 30 µL/min, and the loading volume was 200 µL for the milkweed and maple syrup and 100 µL for the monarch wing samples. The solution was introduced using a PFA nebulizer, double-pass quartz spray chamber, quartz torch, and nickel sample and skimmer cones. Isotopes ^{82}Kr, ^{83}Kr, ^{84}Sr, ^{85}Rb, ^{86}Sr, ^{87}Sr, and ^{88}Sr were simultaneously measured in L4, L3, L2, L1, C, H1, and H2 Faraday cups, respectively. Measurements of samples were made using a static multi-collector routine that consisted of one block of either 70 (milkweed and maple syrup) or 30 cycles (monarch wings) with an integration time of 4.194 s/cycle. ^{84}Sr and ^{86}Sr have isobaric interferences from ^{84}Kr and ^{86}Kr, respectively. ^{87}Sr has an isobaric interference from ^{87}Rb. The interferences of ^{84}Sr and ^{86}Sr were corrected by subtracting the amount of ^{84}Kr and ^{86}Kr corresponding to the ^{83}Kr signal. Interference of ^{87}Sr was corrected by subtracting the amount of ^{87}Rb corresponding to the ^{85}Rb signal. Instrumental mass fractionation was corrected by normalizing $^{86}Sr/^{88}Sr$ to 0.1194 using the exponential law (Moore et al., 1982). Strontium isotope compositions are reported as $^{87}Sr/^{86}Sr$ ratios. Procedural blanks were always negligible, with good reproducibility of $^{87}Sr/^{86}Sr$ for NIST SRM987 (0.710251 ± 0.000003 (1 SD), n = 2). Two 100 ng/g pure Sr standards were measured along with the samples as in-house standards (SrSCP: 0.70816 ± 0.00013, n = 11; GSC: 0.70756 ± 0.00002, n = 4). The long-term reproducibility of the SrSCP in-house standard is (0.70822 ± 0.00004, n = 106).

Lead isotope ratios analysis

We analyzed the lead isotope ratios ($^{208}Pb/^{206}Pb$, $^{207}Pb/^{206}Pb$) of monarch wing and milkweed samples to refine the sources of Pb in the monarch wings. The remaining aliquots (~90%) of the microwave-digested milkweed (n = 3) and monarch (n = 19) samples run on the ICP-MS in May 2021 were used. The separation of Pb was processed in polyethylene columns (Bio-Rad, Hercules, California, USA) loaded with 0.6 mL analytical grade anion exchange resin (AG 1-X8, 100-200 mesh, chloride form; Bio-Rad, Hercules, California, USA). Initial rinsing steps used 1 M HBr (OPTIMA™, Fisher Chemical, Canada) followed by the collection of the Pb fraction with ultra-clean 6 M HCl. A second pass through the column was performed to further purify Pb. After separation, the Pb eluates were dried and re-dissolved in 260 µL and 460 µL 2% v/v HNO_3 for monarch and milkweed samples, respectively (TraceMetal™ Grade; Fisher Chemical, Canada). A thallium spike (in a Tl:Pb mass ratio of 1:4) was added to each sample for mass bias correction against $^{203}Tl/^{205}Tl = 0.418922$.

The Pb isotopes analysis was performed at the Isotope Geochemistry and Geochronology Research Centre, Carleton University using a Thermo Scientific™ Neptune™ high-resolution multi-collector inductively coupled plasma mass spectrometer (MC-ICP-MS; Thermo Fisher Scientific, Bremen, Germany). Sample solutions in 2% v/v HNO_3 were aspirated using a PFA nebulizer, double-pass quartz spray chamber, quartz torch, and nickel sample and skimmer cones. Isotopes ^{202}Hg, ^{203}Tl, ^{204}Pb, ^{205}Tl, ^{206}Pb, ^{207}Pb, and ^{208}Pb were simultaneously measured in L3, L2, L1, C, H1, H2 and H3 Faraday cups, respectively. Measurements of samples were made using a static multi-collector routine that consisted of 1 block of 70 cycles for milkweed and 35 - 40 cycles for monarchs with an integration time of 8.389s/cycle. Procedural blanks were negligible (< 50 pg). The reported Pb isotope ratios are corrected for offsets between the analyzed and reported NBS981 (Todt et al., 1996). For a period of 12 months, average ratios and uncertainties (± SD, n = 47) of NBS981 bracketing samples were $^{206}Pb/^{204}Pb = 16.9310$

± 0.0095, $^{207}Pb/^{204}Pb$ = 15.4851 ± 0.0012, $^{208}Pb/^{204}Pb$ = 36.6783 ± 0.0035, $^{208}Pb/^{206}Pb$ = 2.16634 ± 0.00011, and $^{207}Pb/^{206}Pb$ = 0.91460 ± 0.00003.

Statistical analysis

To examine patterns in metal concentrations and isotopes in the monarch wings over time, and to group elements and isotopes with similar characteristics, we used multivariate multiple regression and principal component analysis (PCA). General linear models were constructed with sex, time (days), and body mass (mg) as fixed effects; multiple models were run independently because there were differences in sample size due to exclusions from the quality control process. All models were visually checked for normality, independence, and homoscedasticity of the model residuals. Body mass and sex are strongly associated (point-biserial correlation = -0.70; Figure S1.3), so linear models were re-run without sex as an explanatory variable to test the sensitivity of the results to the confounding variables (Table S1.3). Twenty metals were included in the PCA because of unequal sample size due to As, Tl, and U having measurements below the detection limit. All statistical analyses were performed using R (version 4.1.0; R Core Team, 2021), and a commented R markdown document has been provided (see Data Availability Table).

Mobility index and enrichment factors

To explore the transfer of metals between trophic levels, we calculated the elemental mobility index for each metal between the larval diet (i.e., milkweed) and the monarchs sampled on the day of eclosion (i.e., Day 0). The mobility index was calculated as the ratio between the metal concentration in the monarch wings and the larval diet (Tigar & Hursthouse, 2016). A value greater than one indicates that the monarch wing has a higher metal concentration than its larval food and that the metal is biomagnified, whereas a value of less than one indicates that the monarch wing has lower metal concentrations than its larval food and the metal has been biodiluted.

Enrichment factors (EF) were also calculated between the adult diet and monarch wings (EF_{ms}) and between the upper continental crust (Rudnick & Gao, 2014) and monarch wings (EF_{cc}) to assess the source of metals in butterfly wings. The upper continental crust is used as a proxy for average exogenous contamination from mineral dust, which allows the EF to represent how much of a trace element is sourced endogenously (i.e., from within the organism itself) versus obtained through exogenous contamination (i.e., from the continental crust) (L. Hu et al., 2019). We calculated the EF using calcium concentration as a normalization factor (Kabata-Pendias & Mukherjee, 2007; Equation 1). Ca is one of the major elements in the continental crust and an abundant metal in monarch wings (Table S1.2); normalization to Ca makes the EF calculation less sensitive to variation between samples (L. Hu et al., 2019). An EF of greater than one implies that the metal is enriched in the monarch relative to the source (e.g., diet (EF_{ms}), crust (EF_{cc})), and, therefore, the source has a low potential to contaminate the monarch signal. Conversely, an EF of less than one indicates that this metal in monarch wings is susceptible to contamination from that source.

Eq. 1 $$Enrichment\ Factor_{source} = \frac{[x_{monarch}]/[Ca_{monarch}]}{[x_{source}]/[Ca_{source}]}$$

Wetting experiment

Because $^{87}Sr/^{86}Sr$ are currently the main metal isotopic tool used in insects, we conducted an additional experiment to refine the sources of Sr in wings and assess the potential contamination of Sr due to wetting. Submerging keratin (e.g., hair) in water can result in exogenous contamination of Sr (L. Hu et al., 2020b), but this contamination route is untested for insect chitin. In our diet-switching experiment, the adult monarchs are not wetted, and, therefore, the Sr content and $^{87}Sr/^{86}Sr$ ratios are uncontaminated by wetting. However, in the wild, monarchs might be wetted by rain or other environmental waters, which could possibly lead to exogeneous Sr contamination via exchange, removal, or addition. Since butterfly wings are superhydrophobic (Pass, 2018), we hypothesized that the

Sr in the wings would not be contaminated by submergence in water. We designed a simple wetting experiment to test whether exogeneous Sr could be integrated into the monarch wings when submerged in water. Two beakers of 80 mL 300 ppb Sr certified standard purchased from SCP Science Inc. (Montreal, QC, Canada) were prepared and neutralized with 60 µL 0.5 N NaOH. Two monarch butterfly wings were cleaned of surface dust using pressured nitrogen gas (10 psi for 4 min.). The wings were submerged in the beakers of solution and agitated. At designated time steps, from before the wings were submerged to 28 days after submergence, a 100 µL aliquot of the solution was removed from each beaker, diluted to 3 mL 2% v/v HNO_3 (TraceMetal™ Grade; Fisher Chemical, Canada), and centrifuged. These aliquots were then measured using the ICP-MS to monitor the change in Sr concentration of the beakers over time.

Natural metal concentrations in monarchs

To estimate the natural metal composition of wild monarch butterflies, the wings of 100 monarch butterflies from eastern North America were analyzed for a suite of 12 elements (i.e., Al, Ba, Cd, Co, Cr, Cu, Mg, Mn, Ni, Pb, Sr, Zn). The butterflies were captured in the spring of 2011 from sites in Texas, Oklahoma, and Missouri as part of a previous study (Flockhart et al., 2013). Methodological details can be found in Appendix A.

Results

Metals classified into four categories

The concentrations of Al, As, Ba, Ca, Cd, Co, Cr, Cs, Cu, Fe, Mg, Mn, Mo, Na, Ni, Pb, Rb, Sb, Sr, Ti, Tl, U, and Zn in the wings of the monarch butterflies, the larval diet (i.e., milkweed), and the adult diet (i.e., maple syrup) from the diet-switching experiment are reported in Table S1.2. In the monarch wings, Ca was the most abundant metal (mean ± SD; 640 ± 160 ng/mg, n = 18) followed by Mg (290 ± 180 ng/mg, n = 18) and Fe (87 ± 34 ng/mg, n = 18). Uranium was the least abundant (0.0010 ± 0.0003 ng/mg, n = 10), with many samples falling below the detection limit. In the larval diet, alkaline earth metals Ca, Mg,

and Sr were the most abundant (Ca: 18 ± 2 µg/mg, n = 3; Mg: 4.2 ± 0.3 µg/mg, n = 3; Sr: 190 ± 20 ng/mg, n = 3) and Cd was the least abundant (9.5 ± 2.2 ng/g, n = 3). Similarly, in the adult diet Ca (190 ± 37 ng/mg, n = 4) and Mg (73 ± 5, ng/mg, n = 4) were the most abundant and Cd the least abundant (0.4 ± 0.1 ng/g, n = 4).

Principal component analysis (PCA) was used to help categorize the metals in the monarch wings from the diet-switching experiment. The first principal component (PC1) explained 43.8% of the variation and was driven mainly by Al, Fe, Pb, Cr, and Cs (Figure 1.1A; Figure S1.1A). A linear regression of PC1 with time category (i.e., early, late) and sex (R^2 = 0.80) detected a difference in PC1 between Week 0 and Weeks 1 to 8 (β = 5.5 ± 0.9, 6.3, $p < 0.001$; Figure 1.1B), but not between the sexes ($p = 0.1$). PC2, driven by Cu, Na, Mn, Ca, and Cd (Figure S1.1B), accounted for 16.1% of the variation. A linear regression with day and sex (R^2 = 0.52) found that PC2 trended temporally (β = 0.05 ± 0.02, 3.5, $p = 0.003$) and differed between the sexes (β = 2.3 ± 0.6, 3.7, $p = 0.002$), suggesting that the metals driving PC2 may be influenced by biological variables (Figure 1.1B).

Multivariate multiple regression found that metals in monarch wings showed distinctive associations with the time (days), sex, and body mass (mg; Table 1.1). If metals are accumulated from endogenous or exogenous sources, we would expect a positive correlation between time and metal concentration; such associations were found for Al, Cd, Cu, Fe, Pb, Ni, and Zn. Significant negative correlations with time were found for As and Mn, suggesting that these metals are removed from the butterfly wings over time. Calcium concentrations in male monarch wings were, on average (± SE), 190 ng/mg (± 60) higher than in females (Figure 1.2A). Conversely, on average males had 0.04 ng/mg (± 0.01) less Co and 1.0 ng/mg (± 0.5) less Sb. Body mass was found to have a significant association with Mo (β = -0.0006 ± 0.0002, -2.6, $p < 0.05$).

Enrichment factors and mobility indices calculated for each of the 23 metals showed distinctive patterns in the concentrations between the monarch butterfly wings and the larval diet (i.e., milkweed),

the adult diet (i.e., maple syrup), and a proxy for mineral dust (i.e., continental crust). Chromium was the only metal with a mobility index greater than one indicating that it is biomagnified in monarch wings compared to milkweed (Table 1.1). Nickel and Zn had mobility indices close to one. The remaining elements showed low concentrations in monarch wings compared to milkweed indicating biodilution of these metals. The lowest mobility indices were found among the alkaline earth metals (i.e., Mg (0.13), Ca (0.04), Sr (0.03), and Ba (0.02)). Enrichment factors less than one suggest that the metal was susceptible to contamination from either the adult diet (EF_{ms}) or mineral dust (EF_{cc}). Of the metals that showed an increase in concentration over time, Al and Fe showed particularly low EF_{cc}, indicating that the increase in concentration could be due to additions of Al and Fe from mineral dust. Comparatively low EF_{ms} for Ni and Zn suggest that the bioaccumulation seen in these metals may be due to additions from the adult diet.

Based on the results of the PCAs, multiple multivariate regression, mobility indices, and enrichment factors, metals were separated into four categories: (1) metals affected by intrinsic factors (e.g., sex, body mass), (2) metals showing bioaccumulation likely from external sources, (3) metals showing bioaccumulation likely from dietary sources, and (4) metals without significant effects of intrinsic factors that maintain the initial metal concentration over time (Table 1.1; Figure 1.5). Metals were categorized as Category 1 if sex or mass were associated with metal concentration or there was a decrease in concentration over time. A few of these metals (i.e., Ca, Mn) were the main drivers of PC2 (Figure 1.1A; Figure S1.1B). Metals assigned to Category 1 were As, Ca, Co, Mn, Mo, and Sb. For example, Ca was significantly more abundant in male wings than in female wings (Figure 1.2A), but no effect of time was detected. Category 2 metals had a positive association with time and relatively low EF_{cc}, indicating that their increases in concentration over time were more likely to be sourced from mineral dust rather than from the adult diet. For instance, despite low Al levels in the maple syrup (EF_{ms} = 22), the concentration of Al in the monarch wings increased over time (Table 1.1; Figure 1.2C). As a

terrigenous metal, it is more likely that the accumulated Al is sourced from exogenous mineral dust (EC_{cc} = 0.0072). Some of the Category 2 elements are terrigenous metals, including Al and Fe, but others are associated with anthropogenic pollution (i.e., Cd, Cu, Cr, Pb). Several of the Category 2 metals are essential to living organisms (i.e., Cr, Cu, Fe), but others are toxic to animals even at low concentrations (i.e., Al, Cd, Pb). Category 3 metals (i.e., Ni, Zn) also had a positive association with time, but had high EF_{cc} and relatively low EF_{ms} and are therefore potentially contaminated endogenously through the adult diet. As an illustration, the monarch wings showed a two-fold accumulation of Zn over time from a concentration similar to that of the larval diet (Figure 1.2B). The level of this essential metal was lower in the adult diet than in the larval diet, but the EF_{ms} was relatively low (4.6), suggesting that the increase in Zn may be sourced, at least partially, from the adult diet. Finally, metals were assigned to Category 4 if they showed no significant associations with time, sex, or body mass. These metals were Ba, Cs, Mg, Na, Rb, Sr, Ti, Tl, and U.

Strontium and Strontium isotope ratios

Based on its characteristics, Sr was considered as Category 4 (Table 1.1), a metal that does not bioaccumulate and is not significantly affected by sex or body mass. The mobility index (0.03) indicated that Sr is biodiluted in the monarch wings. These low concentrations did not have significant associations with time, sex, or body mass (Table 1.1), although a non-significant sex-based pattern could be observed (Figure 1.4A).

Multiple regression of monarch wing $^{87}Sr/^{86}Sr$ was performed with predictors time (days), sex, the inverse of Sr (mg/ng), and interactions between time and sex and the inverse of Sr and sex (adj. R^2 = 0.79). As expected, the range of male $^{87}Sr/^{86}Sr$ matched well with the $^{87}Sr/^{86}Sr$ of the larval diet and did not change over time ($p = 0.2$; Figure 1.4B) or with the inverse of Sr ($p = 0.2$; Figure 1.4C). However, on average, the wings of the female monarchs were 0.0014 less radiogenic than the males ($\beta = 0.0014 \pm 0.0004$, 3.6, $p < 0.01$) and the $^{87}Sr/^{86}Sr$ of the female wings increased slowly over time ($\beta = 0.000010 \pm$

0.000004, 2.3, p = 0.03), although the lack of female monarchs sampled at Week 0 may have been biasing this result (Figure 1.4B). If the adult diet is responsible for the increasing $^{87}Sr/^{86}Sr$ of the female monarch wings over time, it seems unlikely that it is through accumulation, as no positive association between Sr and time was detected (p = 0.8; Table 1.1). The $^{87}Sr/^{86}Sr$ of the female monarch wings was associated with the inverse of Sr (β = 0.0037 ± 0.0011, 3.4, p < 0.01), such that females with higher concentrations of Sr had $^{87}Sr/^{86}Sr$ more disparate from those of the males and larval diet (Figure 1.4C). Given that radiogenic strontium isotopes do not fractionate but instead indicate sources of Sr, the principles of mixing models can be used to find missing endmembers (i.e., the $^{87}Sr/^{86}Sr$ of pure sources of Sr to the monarch wings). The intercept of regression indicated a missing endmember for the female monarchs with a less radiogenic $^{87}Sr/^{86}Sr$ of about 0.7073. Females with higher abundances of Sr in their wings tended to be those sampled earlier in the experiment; lower concentrations of Sr in the Week 8 female monarch wings aligned them with the expected $^{87}Sr/^{86}Sr$ of the larval diet (Figure 1.4C). Thus, the female monarchs were likely exposed to the less radiogenic Sr source either as larvae or as young adults (i.e., less than a week old).

The wetting experiment shows that exogenous contamination of Sr in butterfly wings by wetting is possible. After we submerged the monarch wing in the aqueous solution, we detected substantial changes in the Sr concentration of the solution after 100 min. (Figure 1.4D). A new equilibrium was reached after about a week. Since the amount of Sr in the solution decreased over time, it is likely that the Sr accumulated in the wing.

Lead and Lead isotope ratios

Lead was categorized into Category 2 because Pb concentrations in the monarch wings increased over time, likely sourced from mineral dust (Table 1.1; Figure 1.5A). Of all the toxic metals, only Pb levels in the milkweed (0.22 ± 0.06 ng/mg, n = 3) and monarch wings (0.30 ± 0.20 ng/mg, n = 18) were found to exceed the permissible limits of human food (i.e., 0.01 - 1 ng/mg; (Codex Alimentarius: International

Food Standards, 2019), but Pb levels in the maple syrup (1.1 ± 0.6 ng/g, n = 4) were well below health guidelines. Lead isotope ratios showed that the larval diet matched well with regional environmental $^{208}Pb/^{206}Pb$ and $^{207}Pb/^{206}Pb$ signatures measured in snowpack (Simonetti et al., 2000a, 2000b; Figure 1.4B). The early monarchs (i.e., Week 0) also matched with the larval and environmental Pb isotopes, but within a week, the Pb isotopes of the monarch wings deviated to a distinct signature with higher $^{208}Pb/^{206}Pb$ and $^{207}Pb/^{206}Pb$. Although the Pb isotope ratios were measured a year after the Pb levels, repeated measures showed that storage did not significantly change the initial Pb abundances (paired t-test: t = -1.3, df = 16, p = 0.20).

Natural metal concentrations in lab-raised and wild monarchs

In this lab-based study, we controlled the environmental conditions of the monarch caterpillars and adults, minimized conspecific interactions, reduced flight capacity, and fed the adults a non-natural and choice-restricted diet. Thus, the variation in metal concentrations in the laboratory monarch wings is expected to be different from that of wild monarch wings. These differences can clarify important processes. Comparisons with wild monarch wings show that wing concentrations were similar for Cr, Mn, and Ni (Figure S1.5). Conversely, Mg, Al, Co, Cd, Ba, and Pb had higher concentrations in the wild monarch wings and Cu, Zn, and Sr had lower concentrations in the wild monarchs (Figure S1.5).

Discussion

Regulation of metals in insect wings

The 23 metals analyzed in the diet-switching experiment were classified into four categories based on whether they were influenced by intrinsic factors like sex and body mass (Category 1), bioaccumulated metals from external sources (Category 2), bioaccumulated metals from dietary sources (Category 3), or maintained the natal signature (Category 4; Figure 1.3). Metals classified in Category 1, including As, Mn, Mo, and Ca, showed a decreasing concentration in the wings through time or a correlation with the intrinsic characteristics of individuals. These observations suggest that the levels of these metals are

regulated by the insect. Category 1 metals were grouped into two sub-categories based on their distinct trends during the experiment (Table 1.1). The first sub-category included As and Mn, which showed decreasing concentrations in wings throughout the adult life (Table 1.1), suggesting that monarchs may reallocate these metals from the wings to other parts of the body or excrete them (Tibbett et al., 2021). Manganese is an essential co-factor in many enzymes but can impact insect behaviour at low doses and, like all metals, is toxic in excess (Ben-Shahar, 2018). Caterpillars of *Lymantria dispar* and *Cabera pusaria* have been shown to excrete excess Mn through frass and moulting (Martinek et al., 2020; Kula et al., 2014), but adult mechanisms of excretion have not been shown and Mn homeostasis has not been studied in monarchs. Alternatively, As and Mn could be more concentrated in wing scales and decrease through time in the entire wing due to the progressive abrasion of scales as the individual ages.

The second sub-category of Category 1 included several metals (i.e., Ca, Co, Mo, Sb) that showed an influence of sex and/or body mass. However, sex and body mass were strongly correlated, with females being consistently heavier than males, making it challenging to disentangle the direct influence of mass from that of sex (Figure S1.3). Molybdenum showed a negative correlation to body mass (Table 1.1). Molybdenum is an essential metal that acts as a co-factor for many oxidase enzymes (Dow, 2017), some of which relate to wing pigmentation (Feindt et al., 2018) and immune processes (Selvey, 2020). The decrease in Mo concentration in wings with increasing body size might be related to differential regulation of the metal relative to body size, energy reserves, or sex (Orłowski et al., 2020). Alternatively, the decrease in Mo with increasing body size could be driven by differences in surface area-to-mass ratios. Female monarchs have been noted to have thicker wings than males (Davis & Holden, 2015), leading to lower surface area-to-mass ratios in the wings. If Mo is predominantly found at the surface of the wing (e.g., pigmentation), this lower surface area-to-mass ratio could explain the pattern seen in this experiment (Kowalski et al., 1989). Similarly, we found that male monarch wings had significantly more Ca than females (Figure 1.2A). Notwithstanding the confounding effect of body mass,

sex-based differences in Ca have also been detected in whole-body samples of butterflies (Dempster et al., 1986) and damselfly wings (Stuhr et al., 2018), suggesting that sex is the main driver of the observed differences in Ca in wings. Calcium is a known component of insect chorion (Nickles et al., 2002; Studier, 1996) and reproductive organs (Clark, 1958), and Ca has been found to be preferentially allocated to reproductive organs (Mesjasz-Przybyłowicz et al., 2014). This could explain the lower concentrations of Ca found in the wings of female monarchs, as it is possible that Ca is preferentially allocated or reallocated from the wings to reproductive organs for oogenesis. Sex-based differences in metal composition may reflect sexual dimorphism in nutritional demands, which can result in sex-specific nutritional limitations and have ecological consequences (Filipiak et al., 2021; Espeset et al., 2019; Judd et al., 2010). Future studies could investigate the potential for sexual dimorphism in the nutritional demands of monarch butterflies in natural environments and the resultant impacts on population demography, survival, and migratory success (e.g., Snell-Rood et al., 2014).

Little is known about the pathways of metal allocation and regulation in insects. Metallomics, the study of the metal-containing biomolecules that an organism uses, aims to identify and compare metal utilization, function, evolutionary trends, and interactions (Ogra & Hirata, 2017). Of the six metals in Category 1 (Table 1.1), only the regulatory pathways of Ca, Co, and Mo have been well-characterized (Y. Zhang et al., 2019; Dow, 2017), illustrating the large knowledge gap that the newly-developing field of metallomics is seeking to fill. Metal isotopes that fractionate with physiological processes can be particularly useful to advance understanding but have been under-utilized in insects thus far (but see Nitzsche et al., 2022, 2020). For example, in vertebrates, calcium isotopes have been effectively used to investigate sex-specific modifications of Ca homeostasis due to pregnancy, lactation, and egg-laying (Tacail et al., 2020). Analyzing calcium isotope ratios of different insect tissues could shed light on Ca homeostasis in insects, such as the role of calcium-storing spherites (Dow, 2017), and the sources, mechanisms, and ecological consequences of sex-based differences in Ca.

Bioaccumulation of metals in insect wings

We identified a suite of metals, including highly toxic (e.g., Al, Cd, Pb) and essential metals (e.g., Zn, Fe), that accumulated in the wings of the monarch butterflies over time (Categories 2 and 3; Table 1.1). Metals classified in Category 2 (i.e., Al, Cr, Cd, Cu, Fe, and Pb) increased in concentration over time in the monarch wings and had low enrichment factors between the monarch wings and continental crust (Table 1.1). These observations indicate that these metals were sourced, at least partially, from external sources such as mineral dust. For example, Fe and Al are highly concentrated in terrigenous dust, and previous studies on animal hair have shown that these elements were primarily sourced from exogenous sources in keratin tissues (L. Hu et al., 2018; Kempson et al., 2006). Our experiment minimized any accumulation of aerosol dusts in the food by replacing the food daily, thus any additions of metal from aerosols are likely incorporated exogenously. Although the initial deposition of aerosols on insects is likely superficial, the metals could become embedded in an organic matrix (i.e., epicuticular waxes; Negri et al., 2015), or, as has been shown previously for keratin, the metals could slowly penetrate deeper into the tissue when mobilized by high relative humidity or wetting (L. Hu et al., 2018). This pattern of diffusion is evidenced by the gradient of concentrations of these metals in keratinous tissue, from very high concentrations on the surface to low concentrations deeper in the tissue (L. Hu et al., 2018). In insects, high concentrations of Al in the cuticle of honeybees have also been observed, suggesting similar exogenous contamination (J. A. Shaw et al., 2018). However, given that butterfly wings are living tissue and that Fe is an essential element with known regulatory pathways (Slobodian et al., 2021), there are alternate explanations for the increase of Fe in wings through time. First, our experiment examined a single body part and therefore cannot comment on systemic metal homeostasis (Orłowski et al., 2020); iron could be reallocated from different parts of the insect body for sequestration in response to perturbations to systemic homeostasis. Additionally, most of the accumulation of Fe in wings was observed between Week 0 and Week 1 (Figure 1.1B; Table S1.2) and

could be related to sclerotization and maturation processes as the wings finish forming within a few days post-eclosion (Honegger et al., 2008). Finally, Fe in wings could increase due to changes in Fe requirements over time, as has been observed in other insects (Andreani et al., 2021; J. A. Shaw et al., 2018). Finally, metamorphosis is an energetically-costly process, and the teneral butterfly could be Fe-limited, causing a short-term rapid uptake of Fe to reach a regulatory threshold within the first week in an accumulator-regulator dynamic (Tibbett et al., 2021).

Further studies could use natural metal isotopes or isotope tracing to help constrain metal sources in insect tissues, as we exemplify in this study with the use of Pb isotopes (see discussion below). Similar to Al and Fe, Pb accumulated rapidly in the monarch wings with a twentyfold increase over the 8 weeks. In parallel, we observed a temporal shift in Pb isotope ratios of the wings from a composition matching the local environment of the larval diet to a novel isotopic composition (Figure 1.5B). This indicated that the accumulating Pb is likely from external sources of atmospheric deposition and dust present in the laboratory air, such as from lead paint, pipes, or non-local mineral dust from a rock preparation laboratory located in the same building. Our work supports previous studies showing the contamination of insect tissues by exogenous Pb sources (X. Zhou et al., 2018; Negri et al., 2015). The amount of Pb in the wings of the laboratory-reared monarchs exceeded permissible limits for human food, which is between 0.01 and 1 ng/mg (Codex Alimentarius: International Food Standards, 2019). Similarly, Pb in the wings of wild monarchs was also found to be above permissible limits (Table S1.4) to a greater extent than the laboratory monarchs ($F(1, 116) = 24$, $p < 0.001$); our experimental results suggest that the high Pb levels accumulated in wild monarch wings are likely sourced from anthropogenic pollution encountered during their migration. Lead is toxic to insects and can cause mortality and sub-lethal effects such as reduced growth rate, body size, fecundity, and locomotor activity (J. Zhou et al., 2021; Di et al., 2016; Hirsch et al., 2003).

Migratory species could be at an even higher risk of adverse effects from metal exposure than non-migratory species (Seewagen, 2020). Migration is a complex behaviour, and migratory insects can travel hundreds to thousands of kilometres and are potentially exposed to many sources of metal pollution along their migratory routes. However, the potential effects of toxic metals on migratory insect survival and migratory behaviour are virtually unknown. Anthropogenic sources of Pb have unique Pb isotope ratios; thus, Pb and Pb isotope ratios of biological tissues could be used as indicators of environmental contamination sources (K. E. Smith et al., 2021). This principle has been applied to assess the local pollution exposure of non-migrating insects, such as honeybees (K. E. Smith & Weis, 2020; X. Zhou et al., 2018). We argue that Pb and Pb isotope ratios could also be used as bioindicators of pollution exposure for migratory insects. As an individual insect moves along a migratory path, it will accumulate Pb from the different atmospheric pollution sources it encounters along the way. Measuring Pb isotope ratios in migratory butterflies could provide a tool to reconstruct migratory paths and assess the exposure to pollution of individuals going through this route. This tool would be key to relating migratory success and pollution exposure and could also validate migration routes reconstructed through pollen metabarcoding (Suchan et al., 2018) and wind trajectory modelling (Otuka et al., 2005). To quantify how Pb with unique isotope ratios and concentrations are transferred to the wings from pollution sources, new laboratory studies exposing or feeding insects to isotopically-distinct Pb pollution sources having concentrations similar to those in natural systems could be conducted. Ultimately, Pb isotopes in migratory insects could help identify key sources of pollution that are detrimental to specific species.

Metals classified in Category 3 (i.e., Ni and Zn) grouped metals which also bioaccumulated, but unlike Category 2, these metals were characterized by a relatively low enrichment factor between the monarch wings and adult diet (Table 1.1). Nickel is not known to be an essential element to insects. Lepidopterans show variable effects to Ni exposure, from decreased body size and fecundity to no effect

(Kobiela & Snell-rood, 2018; Sun et al., 2013), suggesting that regulation mechanisms are species-specific (Tibbett et al., 2021). Nickel concentrations in the wings of monarchs in the diet-switching experiment did not significantly differ from those of wild monarchs ($p = 0.4$; Figure S1.5), suggesting that concentrations may be below regulatory thresholds and thus increasing due to non-specific uptake of metal from the adult diet. Conversely, Zn was found to be lower in wild monarch wings than in the diet-switching experiment ($F(1, 116) = 40$, $p < 0.001$; Figure S1.5), suggesting that the monarchs in the diet-switching experiment may have excess Zn. The high Zn in the laboratory monarch wings is unlikely to be purely a result of high Zn in the larval diet because the Zn levels in the milkweed provided in the diet-switching experiment (18 ± 4 ng/mg, n = 3; Table S1.2) are low compared to Zn concentrations measured in wild milkweed (10 - 66 ng/mg; Mitchell et al., 2020). Zinc is essential for insect reproduction and immunity (Cardoso-Jaime et al., 2022), and Zn homeostasis is known to be strictly controlled in insects (Slobodian et al., 2021; Xiao & Zhou, 2016). However, excessive Zn can lead to decreased survival, growth rate, body size, and longevity (P. Jin et al., 2020). Although butterfly species are known to have different Zn tolerances, monarchs are sensitive to Zn under certain conditions (Shephard et al., 2022). The accumulation of Zn seen in the diet-switching experiment could reflect an upregulation of Zn metalloproteins due to environmental or physiological conditions, such as increased metabolic processes (Butt et al., 2018). Zinc isotopes have been suggested as a tool to explore the dietary sources of Zn to insects, but applications are currently hampered by the complicated pathways of Zn homeostasis and Zn fractionation in the body (Nitzsche et al., 2020; Wanty et al., 2017; Evans et al., 2017), which are poorly understood in insects compared to humans (e.g., Tanaka & Hirata, 2018).

Geolocation using metals and metal isotopes

Although metals and metal isotopes that bioaccumulate have the potential to impart geographical information, as has been proposed for Pb isotopes, they are unsuitable for provenance studies that aim to estimate the natal origins of insects. Good candidate metals for the geolocation of migratory insects

are those that (1) are unaltered in the tissues of dispersing insects, (2) have predictable spatial patterns, and (3) demonstrate a strong relationship between environmental and biological signatures. Nine metals belonging to Category 4 fit the first requirement and were unaltered over time in the monarch wings: Ba, Cs, Mg, Na, Rb, Sr, Ti, Tl, and U (Table 1.1). For example, the alkaline earth metals Sr and Mg showed consistent concentrations in the monarch wings over time, suggesting that the natal signature is conserved. Continuous-surface geolocation using metal concentrations would require spatial models of metal variation across the landscape (i.e., metalscapes). Mapping Sr and Mg of soil samples across the eastern USA demonstrated that these metals have distinctive spatial patterns, at least in the soil (Figure S1.6). However, correlations between metal concentrations in the soil and the biosphere (i.e., milkweed) were weak and non-significant (Table S1.5). Previous studies have also found similarly weak correlations in both natural (Wieringa et al., 2020) and controlled laboratory conditions (Lin et al., 2021). Exploration of possible predictors of Sr and Mg concentrations in milkweed highlighted land use, milkweed species, month, and year, but not soil concentration (Table S1.5). It is possible that some metal concentrations may vary at too fine a scale to be suitable for geolocation using continuous surfaces (Norris et al., 2007). Before metals can be used as geolocation biomarkers, further studies will need to improve the predictive power of spatial reference models.

Despite the apparent stability of the concentration of these metals from Category 4 through time, caution should be taken in applying these metals for insect geolocation. Of these metals, Mg and Na are essential metals and are thus expected to be regulated. Our results cannot differentiate between metals whose concentrations were unaltered in the monarch wings due to a lack of bioaccumulation and those that were held at a stable concentration through regulation for metal homeostasis. In the case of homeostasis, the metal concentration may be altered under different stressors not experienced in this experiment, such as starvation, disease, different environmental conditions, or increases in metal exposure. These stressors may alter the ability of the organism to maintain homeostasis (Hopkin, 1990)

and thus disrupt the apparent larval signature. Similarly, not all sources of potential exogenous contamination were explored in this study. For example, we showed that Sr in monarch wings is susceptible to contamination or exchange after about 100 min. when submerged in Sr-concentrated aqueous solutions (Figure 1.4D). This supports the finding that Sr is soluble and that exogenous contamination of Sr in keratinous hair readily occurs when hair is submerged in water (L. Hu et al., 2020b, 2018). Monarchs are behaviorally averse to submergence in water and are unlikely to be exposed to these artificial conditions in nature (i.e., full submergence in highly Sr concentrated waters). However, they are likely to be exposed to rain which usually has a low Sr concentration, except near coastal areas, but can have isotopically variable signatures (Nakano et al., 2001). Further studies will need to investigate the effect on Sr concentration and $^{87}Sr/^{86}Sr$ of wetting from rainwater with varied concentrations and isotopic signatures. As evidenced by our wetting experiment, it would take over an hour of full submersion in Sr-concentrated water to exchange Sr in the wing because the superhydrophobic property on the surface of the wings limit the exchange of metals. However, the regular or sudden wetting by rain during storms could potentially alter, accumulate, or exchange some Sr in the wings, particularly in coastal regions where Sr is more concentrated in rainwater. Consequently, future studies should investigate the susceptibility of Sr and other metals to contamination under real-world conditions, including rain, aerosols, and pollution. Raising butterflies in the wild at specific sites with known metal and metal isotope composition could help reinforce the applicability of these tools for geolocation. We have defined a suite of metals suitable for the geolocation of monarch butterflies, but it may be inappropriate to extrapolate these findings to other organisms, including other Lepidoptera. The specialized structures that aid in metal transport can differ between insect taxa, leading to phylogenetic-based differences in metal uptake, transfer, speciation, and segregation (Tibbett et al., 2021). This may be especially important for non-nectarivorous species because nectar contains low concentrations of metals compared to the diets of herbivores or carnivores (e.g., dragonflies). Caution should also be

taken when using whole-body samples rather than a specific insect tissue with relatively low metabolic activity (Orłowski et al., 2020); it can be assumed that whole-body specimens will show greater changes over time than the wings due to greater inputs from the adult diet (Dempster et al., 1986). Even in cases where the adult insect does not feed and, thus, no dietary input is expected (e.g., eastern spruce budworm), metals which may be altered exogenously should be carefully evaluated. Ultimately, many sources of variability in metal composition need to be further explored, including the effects of host plant (Bowden et al., 1984), microbial communities (Consuegra et al., 2020), parasitism (Sures, 2004), type of metamorphosis and life-stage, reproductive status, homeostatic mechanisms, and their interactions (Tibbett et al., 2021).

Strontium isotope ratios have already been applied to the geographic assignment of monarch butterflies and other lepidopteran species and showed great promise for increasing the precision of isotope-based geographic assignment (Chapter 2; Dargent et al., 2023). Here, we confirmed the assumption that the $^{87}Sr/^{86}Sr$ of monarch wings remain the same over time and continue to represent the larval signature despite adult feeding, at least in males (Figure 1.3B). While we showed that the Sr in wings was susceptible to exchange in extreme wetting conditions (Figure 1.3D), we argue that these conditions are unlikely in nature and do not question the applicability of this geolocation tracer. More surprisingly, we also observed sex-based differences in $^{87}Sr/^{86}Sr$, with females having a lower $^{87}Sr/^{86}Sr$ than both the males and their larval diet (Figure 1.3B-C). As $^{87}Sr/^{86}Sr$ trace the mixing of isotopically distinct sources (and not isotopic fractionation), this observation suggests that there is an unidentified source of Sr to the female monarchs. Strontium is chemically similar to Ca and is inadvertently substituted for calcium ions in the body (Capo et al., 1998). Based on our results that Ca and, to a lesser degree, Sr in wings vary by sex (Figure 1.2A; Figure 1.3A), we argue that the difference in $^{87}Sr/^{86}Sr$ is potentially related to the preferential allocation of Ca (and thus Sr) to female reproductive organs for oogenesis, although no eggs were laid during the experiment. In this case, the $^{87}Sr/^{86}Sr$ of the wings

would be determined by the milkweed $^{87}Sr/^{86}Sr$ from a discrete timestep rather than an integration of the entire larval stage. However, previous studies investigating $^{87}Sr/^{86}Sr$ in monarch wings did not detect any differences between males and females (Flockhart et al., 2015), and it is possible that our result reflects the low number of samples. Alternatively, the differences in $^{87}Sr/^{86}Sr$ between the sexes could be due to the high sensitivity of butterfly wings immediately after eclosion. The female monarchs emerged from their chrysalises one day earlier than the males (Figure S1.4). The day that the females eclosed coincided with an observation that paint odours could be smelled in the laboratory where the adult monarchs were kept, although the laboratory itself was not painted. Many indoor paints contain high concentrations of Sr (Van Gorkum & Bouwman, 2005), as do gypsum-based mixtures (Huang, 2020), which are often applied to fill holes and sanded smooth prior to painting. High concentrations of dust from either of these substances present on the day the female monarchs eclosed from their chrysalises could have deposited on the surface of the wings, and since butterfly wings are soft and wet on the day of eclosion, it is possible that external Sr could have mobilized and penetrated the wing tissues. We suggest that future studies explore the link between sex and $^{87}Sr/^{86}Sr$ in monarch wings, and the sensitivity of metals in butterfly wings to environmental conditions on the day of eclosion.

Natural metal concentrations

The metal concentrations measured in the wings of the laboratory monarchs are unlikely to be representative of monarchs in natural environments. All the monarchs in the laboratory experiment were siblings, limiting their genetic diversity and the independence of replicates (Merritt & Bewick, 2017). Comparing the concentrations of metals found in the wings of monarchs in our laboratory study to concentrations of metals in the wings of wild monarchs, we can see that wild monarch wings had significantly higher concentrations of Mg, Al, Co, Cd, Ba, and Pb, but lower concentrations of Cu, Zn, and Sr (Figure S1.5). Differences in the concentration of Category 4 metals (i.e., Mg, Ba, Sr) are likely due to different concentrations of these elements in the larval diets of the wild monarchs. Differences in the

bioaccumulating metals from Categories 2 and 3 (i.e., Al, Cd, Pb, Cu, Zn) are likely due to differences in the metal concentrations of the larval diet, metal concentrations in the adult diet, environmental exposure to metals, and age of the butterflies. Of particular interest is Al, which showed much higher concentrations in the wild monarch wings, likely derived from the higher exposure to mineral dust in natural systems than in laboratory conditions. Comparisons of Zn and Na in the monarch wings with concentrations found in monarch abdomens (Shephard et al., 2021) shows that concentrations in the abdomen are approximately three times higher than in the wings. This large difference is likely due to higher allocations of essential Zn and Na to the abdomen for metabolic processes, but could also be influenced by differences in the metal concentrations of the larval diet, unabsorbed metals contained within the digestive tract of the abdomen, and differences in nutrient requirements between environments. Similar differences have been found in beetles, where abdominal samples had higher concentrations of metals than elytra and only some metals were correlated between the tissues (Orłowski et al., 2020).

Conclusion

This controlled diet-switching experiment demonstrated that the incorporation of metal and metal isotopes within the wings of monarch butterflies has distinct sources. Some elements (e.g., Mn, Mo, Ca) are likely incorporated from the diet but their concentrations are further modulated throughout the adult life by physiological or metabolic processes. Using those metals and their isotopes (e.g., Ca isotopes) could bring new perspectives on the distinct physiological needs and biogeochemistry of adult butterflies. Other elements are bioaccumulated from the larval and adult diet (e.g., Ni, Zn) and their concentrations keep increasing throughout the adult stage. Many heavy metals also have increasing concentrations through time and come, at least in part, from exogenous sources including aerosols (e.g., Al, Fe, Pb). Using those metals or their isotopes (e.g., Pb) could help track the pollution exposure of individuals either locally or through their migratory travels. Finally, a few metals have concentrations

that remain stable in the wing throughout the adult life (e.g., Sr, Mg). Those metals are good candidates for developing geolocation tools in population ecology studies. However, even those metals are not exempt from potential contamination as demonstrated with the rapid exchange of Sr when wings are submerged in water. Despite these caveats, this study supported the use of $^{87}Sr/^{86}Sr$ ratios as a geolocation tool of natal origin and identified other possible geolocation tools. Finally, this study also underlined the complexity of metal incorporation processes and sources in a single insect species' tissue. The accumulation of metals absorbed or exchanged by wetting from atmospheric sources is a major incorporation mechanism for several metals in insect wings. Due to the high body surface area to volume ratio of insects and the absorbent properties of their chitinous exoskeleton, this mechanism might be a prominent contributor of metal incorporation in insect tissues with possible toxicological consequences and roles in controlling insect population dynamics.

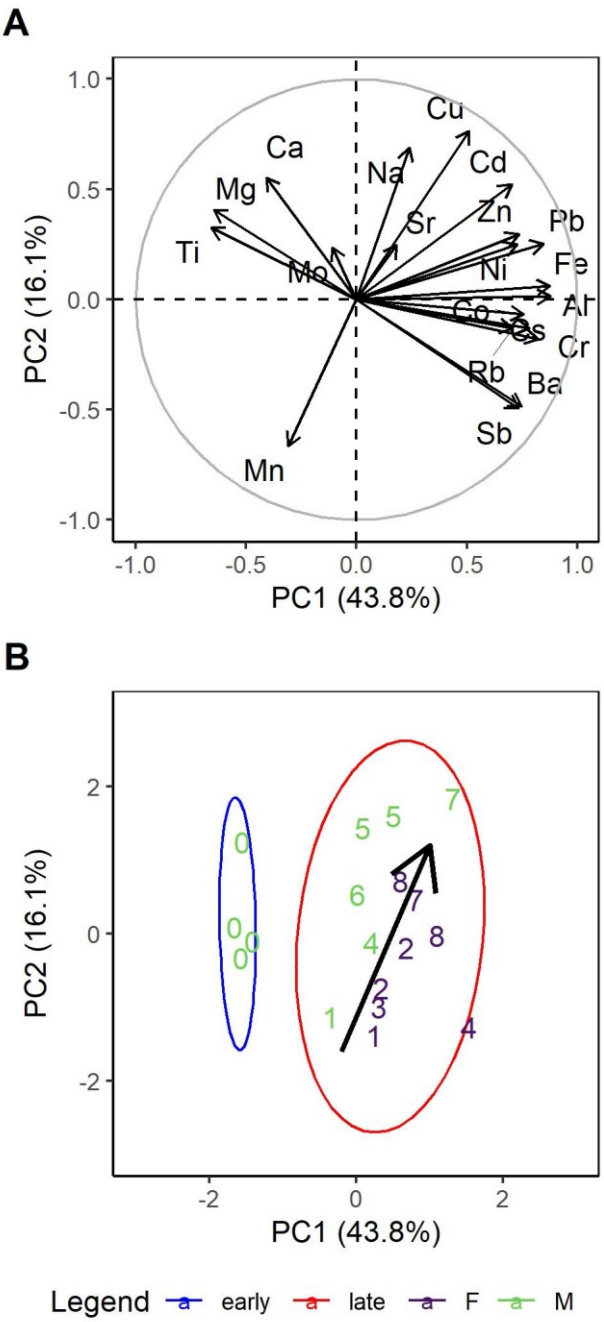

Figure 1.1 Principal components analysis biplots of 20 metals (excluding As, Tl, and U due to measurements below the detection limit) in monarch butterfly wings **(A)** Loading plot of the first two principal components for monarch wings from all weeks explaining 59.9% of the variation. **(B)** PCA score plot of monarch wings from all weeks; numbers depict the week at which the individual was sampled. There is no overlap between the 95% data ellipses of early dates (i.e., Week 0; blue ellipse) and later dates (i.e., Weeks 1 to 8; red ellipse). There is a trend, mainly in PC2, from Week 1 to 8; a red arrow has been superimposed on the biplot to illustrate this trend. There is also grouping between female (purple) and male (green) butterflies.

Table 1.1 Metals are clustered into four categories based on their characteristics in the diet-switching experiment.

Metal	Adj. R^2	Time (days)	Sex	Body mass (mg)	MI	EF_{cc}	EF_{ms}
Category 1: intrinsic factors							
As^{TOX}	**0.60***	**-0.002 ± 0.0006, -3.1***	-0.03 ± 0.03, -1.0	0.0002 ± 0.0002, 1.2	*NA*	0.73	*NA*
Mn^{ESS}	**0.56***	**-0.03 ± 0.008, -3.9***	-0.4 ± 0.4, -0.8	0.004 ± 0.003, 1.3	0.07	0.24	0.79
Ca^{ESS}	**0.74***	0.1 ± 1.0, 0.1	**192 ± 58, 3.3***	-0.7 ± 0.4, -1.9	0.04	*NA*	*NA*
Co^{ESS}	**0.42***	0.0003 ± 0.0003, 1.0	**-0.04 ± 0.02, -2.8***	-0.0001 ± 0.0001, -1.2	0.08	0.11	1.1
Sb	**0.44***	0.004 ± 0.008, 0.5	**-1 ± 0.5, -2.2***	0.001 ± 0.003, 0.4	*NA*	0.0012	86
Mo^{ESS}	0.26	0.0002 ± 0.0006, 0.3	-0.04 ± 0.03, -1.1	**-0.0006 ± 0.0002, -2.6***	*NA*	0.13	28
Category 2: exogenous bioaccumulation							
Al^{TOX}	**0.66***	**0.3 ± 0.06, 4.6***	-2 ± 4, -0.5	0.04 ± 0.02, 1.7	0.08	0.0072	22
Cr	0.29	0.006 ± 0.003, 2.0	-0.2 ± 0.2, -1.1	0.0002 ± 0.0011, 0.15	1.42	0.45	9.2
Cd^{TOX}	**0.45***	**0.0005 ± 0.0001, 3.7***	-0.0005 ± 0.0070, -0.1	-0.00002 ± 0.00005, -0.5	0.32	7.2	12
Cu^{ESS}	**0.47***	**0.04 ± 0.01, 3.9***	0.3 ± 0.6, 0.5	-0.001 ± 0.004, -0.3	0.64	8.2	74
Fe^{ESS}	**0.56***	**1 ± 0.3, 3.2***	-29 ± 17, -1.7	-0.01 ± 0.11, -0.1	0.41	0.091	30
Pb^{TOX}	**0.76***	**0.008 ± 0.001, 6.4***	-0.02 ± 0.07, -0.2	0.0006 ± 0.0005, 1.3	0.13	0.72	85
Category 3: dietary bioaccumulation							
Ni	**0.45***	**0.02 ± 0.007, 3.5***	-0.2 ± 0.4, -0.5	-0.001 ± 0.002, -0.4	1.08	1.7	2.3
Zn^{ESS}	**0.36***	**0.3 ± 0.1, 2.8***	-4 ± 6, -0.6	-0.005 ± 0.037, -0.1	1.02	1.7	4.6
Category 4: geolocation							
Ba	**0.40***	0.02 ± 0.03, 0.8	-2 ± 2, -1.1	0.02 ± 0.01, 1.5	0.02	*NA*	0.20
Cs	0.21	0.00003 ± 0.00002, 1.5	-0.001 ± 0.0009, -1.1	0.0000006 ± 0.000006, 0.1	*NA*	0.033	0.11
Mg^{ESS}	0.16	-3 ± 2, -1.5	21 ± 118, 0.18	-0.8 ± 0.8, -1.1	0.13	0.79	1.2
Na^{ESS}	0.07	0.3 ± .3, 1.2	-5 ± 16, -0.3	-0.1 ± 0.1, -1.2	*NA*	0.11	43
Rb	0.14	0.01 ± 0.007, 2.0	-0.06 ± 0.4, -0.2	0.001 ± 0.003, 0.6	*NA*	0.45	0.048
Sr	-0.08	-0.006 ± 0.028, -0.2	-0.8 ± 1.5, -0.5	-0.01 ± 0.01, -1.2	0.03	0.82	0.51
Ti	0.10	-0.04 ± 0.02, -1.7	-0.08 ± 1.25, -0.07	-0.007 ± 0.008, -0.9	0.70	0.048	24
Tl	-0.006	-0.00003 ± 0.00008, -1.0	0.0006 ± 0.0012, 0.5	-0.000003 ± 0.000008, -0.4	*NA*	1.6	1.1
U^{TOX}	-0.37	0.000004 ± 0.000008, 0.6	0.00009 ± 0.00042, 0.2	0.000001 ± 0.000002, 0.6	*NA*	0.016	*NA*

Results of the multivariate multiple regression examining the contribution of time (days), sex, and body mass (mg) on metal concentrations of monarch wings in the diet-switching experiment are reported. Non-standardized (ng/mg) effect sizes are reported for each predictor (β ± SE, t-value); significant relationships are starred and in bold (α = 0.05). The reference level of sex is female. The sample size is 18 for all metals except As (n = 14), Tl (n = 16), and U (n = 10). The mobility index (MI), enrichment factor between the monarch wings and the continental crust (EF_{cc}), and enrichment factor between the monarch wings and the adult diet (EF_{ms}) are also reported for each metal. Essential metals are denoted with ESS and toxic metals with TOX.

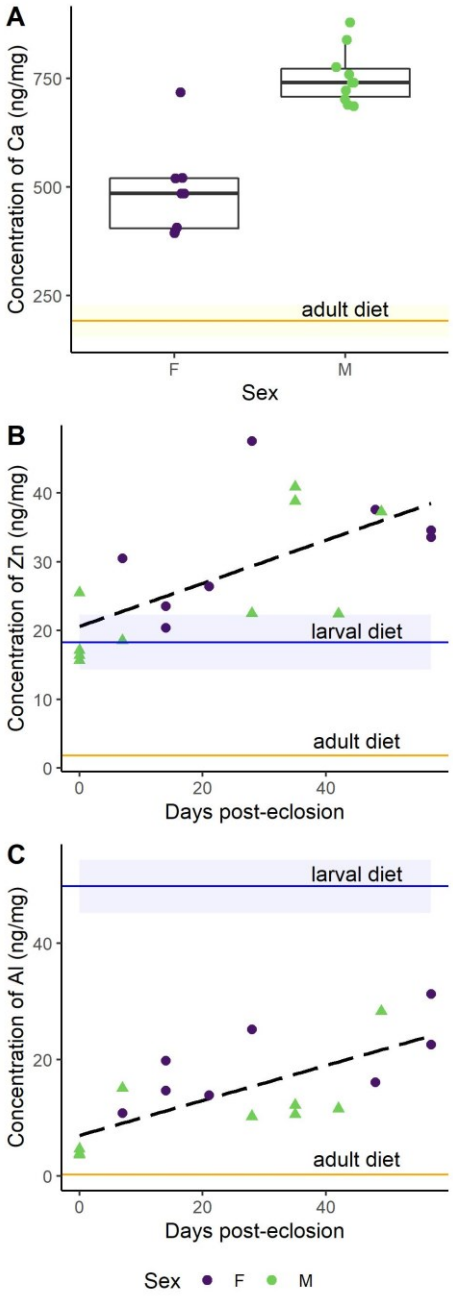

Figure 1.2 Metal concentration in monarch wings (1 ng/mg = 1 ppm) from the diet-switching experiment for representative metals classified in different functional categories. Horizontal blue lines depict the mean concentration (± SD) in the larval diet, milkweed (n = 3), and horizontal orange lines represent the mean concentration (± SD) in the adult diet, maple syrup (n = 4). **(A)** Category 1: Boxplot of Ca concentration (ng/mg) in monarch wings by sex (RSD = 4%). Sex-based differences were detected with males (green) having more Ca than females (purple). The milkweed concentration (18,500 ± 1,800 ng/mg) is not shown as it far exceeds that of the monarch wings. **(B)** Category 2: The concentration of Zn (ng/mg) in monarch wings increased over the 8 weeks (RSD = 1%). **(C)** Category 3: The concentration of Al (ng/mg) in monarch wings increased over the 8 weeks (RSD = 2%).

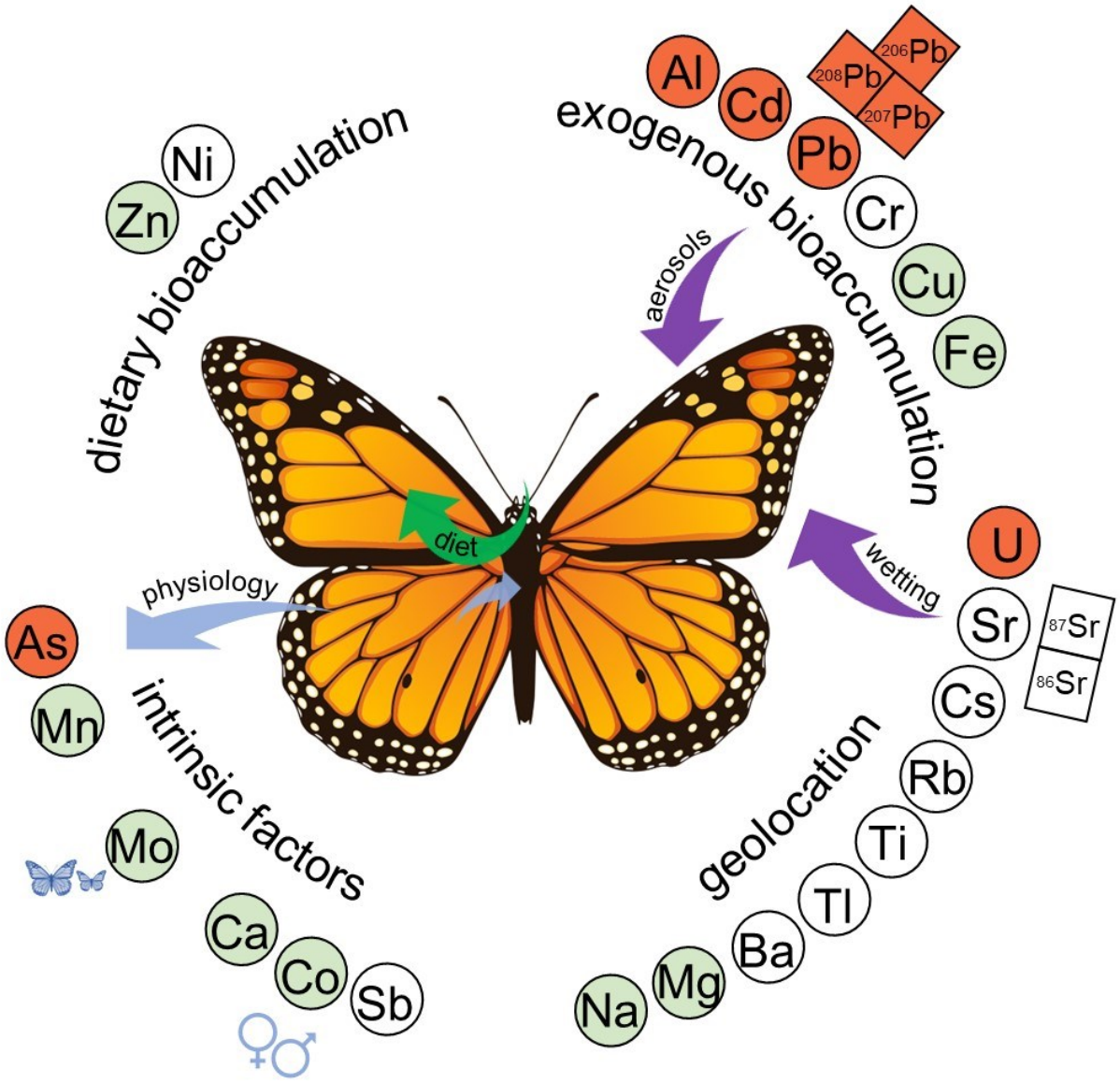

Figure 1.3 Twenty-three metals were classified into four categories based on their characteristics in the diet-switching experiment. Essential metals (green) and highly toxic metals (red) are indicated; metal isotopes are indicated by boxes. Category 1, intrinsic factors (bottom-left), includes two sub-categories: (1) metals (i.e., As, Mn) that decrease in the wing over time through unknown mechanisms (blue arrows), and (2) metals that are influenced by body mass or sex (i.e., Ca, Co, Sb, Mo). Category 2, exogenous bioaccumulation (top-right), includes metals that are, at least partly, accumulated from external sources (purple arrows), such as via aerosol dust (e.g., Pb and Pb isotopes; Figure 1.5) or under wetting conditions (e.g., Sr; Figure 1.4D). Category 3, dietary bioaccumulation (top-left), included metals that are likely accumulated from the adult diet (green arrow). Finally, Category 4, geolocation (bottom-right), includes metals that maintained similar concentrations over the course of the experiment and are good candidates for geolocation studies.

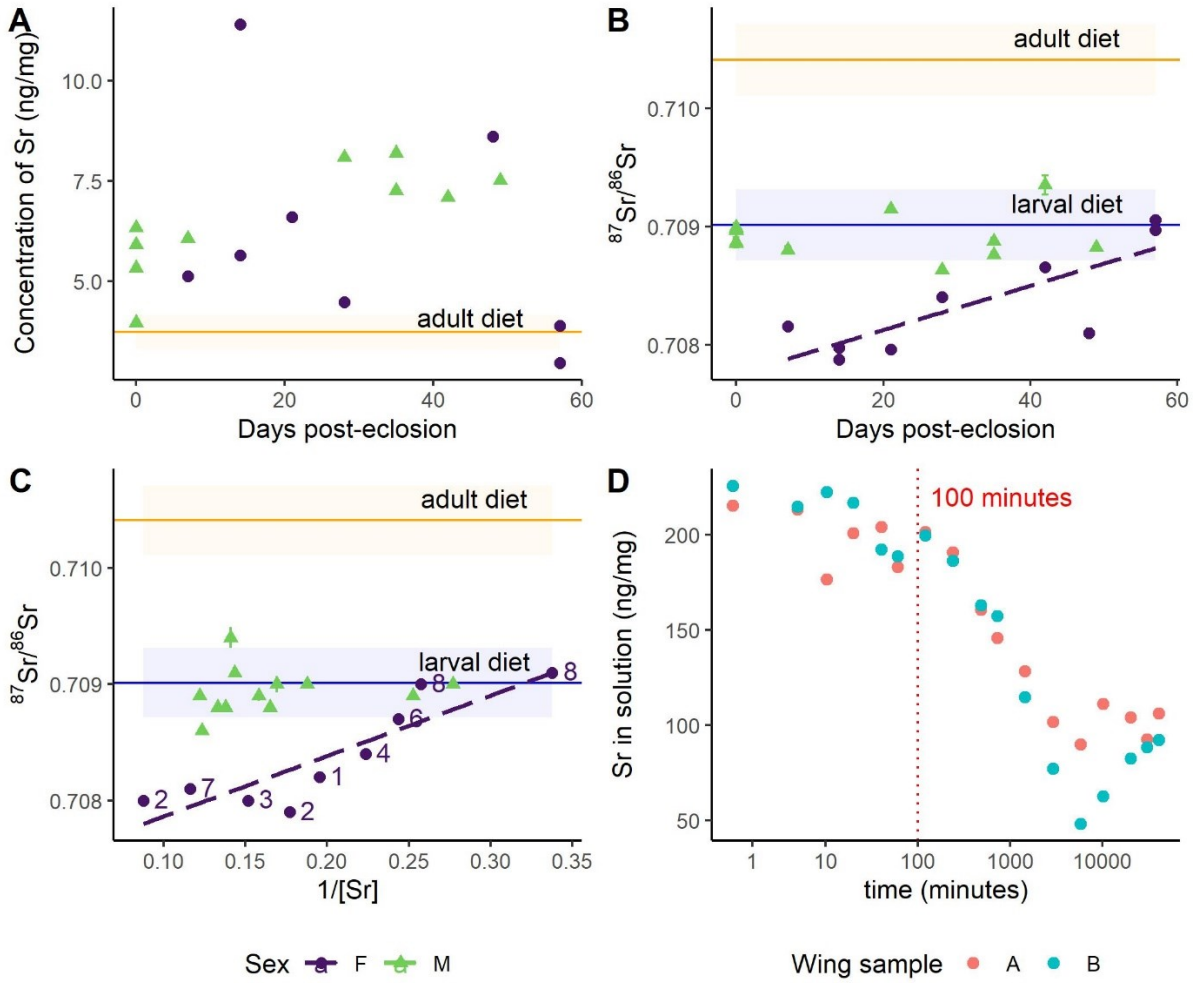

Figure 1.4 Strontium and strontium isotope ratios in monarch wings during the diet-switching and wetting experiments. Horizontal blue lines depict the mean concentration (± SD) in the larval diet, milkweed (n = 3), and horizontal orange lines represent the mean concentration (± SD) in the adult diet, maple syrup (n = 4). **(A)** Concentration of Sr (ng/mg) in monarch wings over 8 weeks (RSD = 1%). The concentration of Sr in the larval diet is not shown as it far exceeds that of the monarchs (189 ± 21 ng/mg). **(B)** Strontium isotope ratios (± SE) in monarch wings over 8 weeks; the $^{87}Sr/^{86}Sr$ ratios of the female monarch wings show a linear relationship with time. **(C)** Strontium isotope ratios (± SE) against the inverse of strontium concentration. The significant linear relationship for females is displayed; numbers depict the weeks post-eclosion that the female monarch was sampled. **(D)** Concentration of Sr (ng/mg) in solution through time during the wing wetting experiment (n = 2).

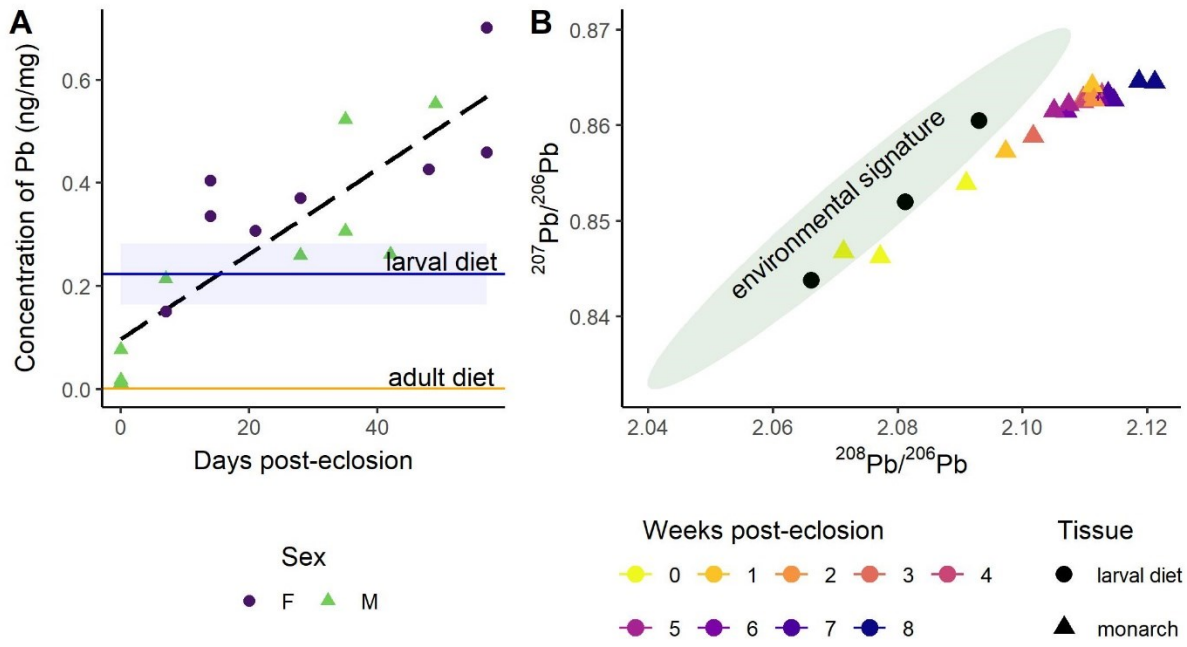

Figure 1.5 Change in lead and lead isotope ratios in monarch wings during the diet-switching experiment **(A)** Concentration of Pb (ng/mg) in monarch wings over 8 weeks (RSD = 1%); the linear relationship (dashed black line) with time is for all samples. The horizontal blue line depicts the mean concentration of Pb (± SD) in the larval diet, milkweed (n = 3), and the horizontal orange line represents the mean concentration of Pb (± SD) in the adult diet, maple syrup (n = 4). **(B)** Biplot of $^{207}Pb/^{206}Pb$ and $^{208}Pb/^{206}Pb$ ratios. Monarch wings are depicted as triangles with colours representing the age of the butterfly in weeks; the standard error is smaller than the symbols. Measurements of the larval diet are depicted as black dots (n = 3). The green 95% data ellipse shows the range of regional lead isotope ratios measured in snowpack (Simonetti et al., 2000a, 2000b).

Chapter 2: Continuous-surface geographic assignment of migratory animals using strontium isotopes: A case study with monarch butterflies

This chapter is a reproduction of the following published article:

Reich, M. S., Flockhart, D. T. T., Norris, D. R., Hu, L., & Bataille, C. P. (2021). Continuous-surface geographic assignment of migratory animals using strontium isotopes: A case study with monarch butterflies. *Methods in Ecology and Evolution*, 00, 1–13. https://doi.org/10.1111/2041-210X.13707

Contribution

CB, TF, and RN conceived the ideas and designed the sampling methodology. I collected most milkweed samples with contributions from TF. I performed the isotopic analysis and data analysis with the help of LH and CB. I led the writing, with large contributions from CB and input from all co-authors.

Abstract

1. Strontium isotope ratios ($^{87}Sr/^{86}Sr$) have shown promise for tracing the geographic origin of animal tissues because they have high-resolution and show discrete spatial patterns independent and complementary to those of light isotopes. In this study, we provide a complete quantitative framework to apply $^{87}Sr/^{86}Sr$ for tracking migratory animals using the eastern North American population of monarch butterflies *Danaus plexippus* as a case study.
2. To enable continuous-surface geographic assignment using $^{87}Sr/^{86}Sr$, we recommend following five key steps: (1) assessing feasibility, (2) sample collection, (3) laboratory analysis, (4) modelling the isoscape and (5) geographic assignment. We provide a detailed outline of these steps and then focus on steps 3–5 for the case study. For monarchs, using an extensive plant $^{87}Sr/^{86}Sr$ dataset (n = 400),

geospatial data and a machine learning approach, we first calibrate a regional, high-resolution $^{87}Sr/^{86}Sr$ isoscape (i.e. a baseline for $^{87}Sr/^{86}Sr$ assignment) over their eastern North American summer breeding range. We then use the $^{87}Sr/^{86}Sr$ isoscape to estimate the posterior probability surface of natal origin for 100 monarchs of unknown origin.

3. Our results demonstrate that $^{87}Sr/^{86}Sr$ can greatly improve the precision of isotope-based geographic assignment. Furthermore, combining δ^2H and $^{87}Sr/^{86}Sr$ into a dual assignment provides the most constrained area of natal origin.
4. We provide a framework for ecologists and palaeoecologists to apply $^{87}Sr/^{86}Sr$-based geographic assignments for animal movement studies using contemporary or archived samples. The addition of the $^{87}Sr/^{86}Sr$ assignment tool will enhance our ability to study migration and dispersal in a wide variety of animals.

Introduction

Animal migration is an understudied and threatened ecological phenomenon found in diverse taxa (Satterfield et al., 2020). Up to 18% of the ~10,000 known bird species (Sekercioglu, 2007) and 3% of the ~20,000 known butterfly species are migratory (Chowdhury et al., 2021a). Despite the prevalence of this life-history strategy, the migratory behaviour of many species is not well documented, especially in insects (J. W. Chapman et al., 2015). This lack of knowledge is problematic because many migratory populations are declining, and the causes of these declines are not always understood (Kauffman et al., 2021; Guo et al., 2020; Brower et al., 2012). In the absence of detailed knowledge of migratory connections and patterns, conservation efforts are likely to be ineffective (Kauffman et al., 2021; C. M. Taylor & Norris, 2010).

One of the reasons that migration is understudied is that tracking animals over long distances is often challenging. Over the last two decades, stable isotopes have become a reliable tool for tracking animal migration (Hobson & Wassenaar, 2019). Stable isotopes are particularly useful for posthumous or

archived samples, such as in palaeoecological studies (Hoppe et al., 1999) and provenance studies of poached animal products (Coutu et al., 2016). Isotopes are also advantageous for insect species because they are small and short-lived, which limits the use of biologging technologies applicable to larger animals (Rutz & Hays, 2009, but see S. M. Knight et al., 2019). Isotopes vary predictably in the environment with biological and physical processes allowing the development of numerical models, called isoscapes, predicting spatial isotopic patterns across the landscape (West et al., 2009). During tissue formation, animals inherit a specific isotopic composition from their food and water that reflects the location of natal origin and is preserved in metabolically inert tissues (Hobson et al., 1999). During the migratory stage, the isotope composition measured from these inert tissues (e.g., insect wings, bird feathers, horn) can be compared to isoscapes to retrace the natal origin (i.e., continuous-surface geographic assignment; Hobson et al., 2019; Talavera et al., 2018; Flockhart et al., 2013; Hobson et al., 1999).

Hydrogen isotope values (δ^2H) are currently the quintessential isotope to infer provenance (e.g., Hobson et al., 2019; Hallworth et al., 2018; Flockhart et al., 2017b, 2013; Wassenaar & Hobson, 1998). Hydrogen isotope composition varies temporally with climate patterns on the landscape and generally produces low resolution latitudinal gradients (Bowen et al., 2005). These latitudinal gradients are often redundant with longitude, limiting the precision of geographic assignments (i.e., the ability of the assignment to restrict the probable area of natal origin) (Hobson et al., 2010).

To enhance the precision and ecological interpretations derived from δ^2H-based geographic assignment of migratory animals, other isotopes are needed. Other isotopes, such as carbon and oxygen isotopes (e.g., Borisov et al., 2020; Satterfield et al., 2018; Dockx et al., 2004), have already been used for geographic assignment in combination with δ^2H, but with limited success due, in part, to their spatial correlation with δ^2H (Hobson et al., 2019). Strontium isotope ratios (i.e., $^{87}Sr/^{86}Sr$) were proposed decades ago as a strong candidate for geographic assignment (Hobson et al., 1999), but have been

limited by analytical hurdles (e.g., low strontium content of organic tissue, reviewed in Bataille et al. (2020). Using $^{87}Sr/^{86}Sr$ is advantageous because they are temporally stable, they show high resolution patterns following geological regimes that are independent from other light isotopes (Bataille et al., 2020) and, unlike light isotopes, they do not show metabolic or trophic-level fractionation (Flockhart et al., 2015). Therefore, $^{87}Sr/^{86}Sr$ have high potential to complement δ^2H in the geographic assignment of migratory animals.

Previous studies, including some on insects (e.g., Flockhart et al., 2015; Holder et al., 2014), have analyzed $^{87}Sr/^{86}Sr$ in animal tissues. However, without independent models predicting $^{87}Sr/^{86}Sr$ variations on the landscape (i.e., a $^{87}Sr/^{86}Sr$ isoscape), $^{87}Sr/^{86}Sr$ from animals can only be compared with each other (e.g., Holder et al., 2014) or to a set of pre-defined locations with known $^{87}Sr/^{86}Sr$ (e.g., Widga et al., 2010; Sellick et al., 2009; Chamberlain et al., 1997), techniques known as the nominal approach (Wunder, 2012). In contrast, continuous-surface geographic assignment compares the measured isotopic composition in animal tissue to an isoscape and produces posterior probability surfaces of origin that are less biased and facilitate visualization of origin (Wunder, 2012). Probability surfaces from multiple isotopes are easily combined within this framework to further constrain geographic origin (Flockhart et al., 2017b). With the recent advances in global $^{87}Sr/^{86}Sr$ isoscapes (Bataille et al., 2020), studies have started to apply $^{87}Sr/^{86}Sr$-based, continuous-surface geographic assignment for ecological applications (e.g., Funck et al., 2021; Kruszynski et al., 2021).

In this study, we provide a systematic framework to apply $^{87}Sr/^{86}Sr$-based, continuous-surface geographic assignment to migratory animals. We then apply this framework to monarch butterflies *Danaus plexippus*, an emblematic insect of conservation concern (Brower et al., 2012), because geographic assignments using light isotopes have been previously used to study monarch migration and provide a basis for comparing the performance of $^{87}Sr/^{86}Sr$ (e.g., Flockhart et al., 2018, 2013; Hobson et al., 1999; Wassenaar & Hobson, 1998). We develop an analytical protocol to rapidly and efficiently clean

and analyze $^{87}Sr/^{86}Sr$ in insect wings. We then analyze the $^{87}Sr/^{86}Sr$ of 100 monarch butterflies that were previously analyzed for δ^2H (Flockhart et al., 2013). To enable continuous-surface geographic assignment of $^{87}Sr/^{86}Sr$, we develop a regional plant $^{87}Sr/^{86}Sr$ isoscape for eastern North America. We use the new regional $^{87}Sr/^{86}Sr$ isoscape to estimate the natal origin of these monarchs and compare the relative performance of $^{87}Sr/^{86}Sr$ and δ^2H geographic assignments. Finally, we combine δ^2H and $^{87}Sr/^{86}Sr$ and into a dual-isotope geographic assignment framework to provide the most precise estimate of natal origin with their associated ecological insights. Throughout this case study, we illustrate the key steps required to apply $^{87}Sr/^{86}Sr$ to animal mobility studies.

Materials and Methods

We detail five key steps to apply $^{87}Sr/^{86}Sr$-based, continuous-surface geographic assignment for animal mobility studies (Figure 2.1): (i) assessing the feasibility of $^{87}Sr/^{86}Sr$ assignment for monarch butterflies, (ii) the collection of known-origin plant samples and unknown-origin monarch butterfly samples, (iii) laboratory $^{87}Sr/^{86}Sr$ analysis, (iv) the development of a regional, accurate, and high-resolution $^{87}Sr/^{86}Sr$ isoscape, and (v) the application of continuous-surface geographic assignment of unknown-origin monarchs using $^{87}Sr/^{86}Sr$ only, δ^2H only and dual δ^2H and $^{87}Sr/^{86}Sr$ assignment. All statistical analyses were performed using R (version 3.6.3; R Core Team, 2013) and a commented R script is provided to guide ecologists through the framework (see Data Availability Table).

In this study, we compare the performance of $^{87}Sr/^{86}Sr$ assignments with δ^2H assignments, the quintessential isotope used in ecological studies. The unknown-origin monarch butterflies used in this study were analyzed for δ^2H and $\delta^{13}C$ as part of a previous study and assigned to their probable natal origins using these isotopes (Flockhart et al., 2013). However, we revised the δ^2H assignments generated in Flockhart et al. (2013) using a recalibrated δ^2H isoscape (Hobson et al., 2019; Figure S2.4).

Step 1: Assessing feasibility

There are multiple factors that need to be considered before starting any isotope-based geographic assignment project, but some considerations are $^{87}Sr/^{86}Sr$-specific (Table S2.1). Here, we develop $^{87}Sr/^{86}Sr$ assignment for monarch butterflies, an ideal species for $^{87}Sr/^{86}Sr$ assignment. The eastern population of monarch butterflies is famous for its annual multi-generational round-trip migration from its overwintering grounds in Central Mexico, through the USA to southern Canada, and back. Monarchs are an ideal species for $^{87}Sr/^{86}Sr$ assignment for multiple reasons. Monarch caterpillars are specialists on milkweed plants and have a very restricted larval range, therefore obtaining Sr from a specific source. The $^{87}Sr/^{86}Sr$ of monarchs is highly correlated with the $^{87}Sr/^{86}Sr$ of milkweed *Asclepias* spp. ($r^2 = 0.88$; Flockhart et al., 2015). The $^{87}Sr/^{86}Sr$ of the milkweed is fixed in inert wing tissues and is not altered by adult feeding (Chapter 1). In addition, sufficient $^{87}Sr/^{86}Sr$ variations exist across North America to allow distinct $^{87}Sr/^{86}Sr$ assignments (Bataille & Bowen, 2012).

Step 2: Sample collection

The monarchs used in this study (n = 100) were collected in the USA between Apr. 13 and May 8, 2011, and were assumed to be individuals returning from the overwintering grounds in Mexico because they were caught early during the northward migration and had high wing condition scores, a proxy for butterfly age (Flockhart et al., 2013; Figure S2.1). We targeted the overwintering generation because they are known to be a mix of individuals originating from across the summer breeding grounds (i.e., east of the Rocky Mountains in the USA and southern Canada) (Flockhart et al., 2017b; Wassenaar & Hobson, 1998) and could thus provide a good test case to compare $^{87}Sr/^{86}Sr$ and δ^2H geographic assignments.

Step 3: $^{87}Sr/^{86}Sr$ analysis of unknown-origin monarch butterflies

We developed a new protocol to prepare and analyze $^{87}Sr/^{86}Sr$ in insect wings. Unlike plants and other organic tissues (e.g., bones and teeth), for which a large amount of material and relatively high Sr

concentration are available, monarch butterfly wings are small (9.3 ± 1.3 mg, n = 99) and have low Sr concentration (3.1 ± 1.8 mg/kg, n = 99). Consequently, the total mass of Sr extracted from a single wing is small for monarchs and insects in general. Such a small Sr mass makes the analysis challenging and the sample sensitive to contamination from exogeneous sources (e.g., dust particles). To prevent potential contamination from solvent-based cleaning methods, we used a dry-cleaning protocol (Holder, 2012; Font et al., 2007) to remove all particles stuck to the butterfly wings by blasting pressurized nitrogen gas (~10 psi) for 2 min. We validated the efficiency of this dry-cleaning protocol for monarch butterflies by comparing butterfly wings before and after cleaning under Scanning Electron Microscopy (Figure S2.7).

Once the cleaning protocol was established, we analyzed the $^{87}Sr/^{86}Sr$ of the very small Sr mass extracted from the single-wing digestion (28.4 ± 16.4 ng, n = 99). The traditional analytical set-up of MC-ICP-MS instrument uses a self-aspiration method which requires large volumes and masses of sample to analyze $^{87}Sr/^{86}Sr$ precisely. However, only a small mass of Sr is available for analysis after insect wing digestion. We used a novel instrument, the microFAST MC (Elemental Scientific, Omaha, NE, USA), to minimize the required volume for $^{87}Sr/^{86}Sr$ analysis and maximize analytical precision. Specifically, the Sr extracted from wings was dissolved in 2% v/v HNO_3 (200 µL, ~100 ppb Sr) and injected at 30 µL/min into the MC-ICP-MS using the microFAST MC. Procedural blanks were negligible (signal-to-noise ratio > 5,000) with excellent reproducibility of $^{87}Sr/^{86}Sr$ for SRM® 987 and an in-house Sr standard across five analytical runs (mean ± sd): 0.71024 (± 0.00002, n = 5) and 0.70815 (± 0.00020, n = 25), respectively. Using this analytical set-up, even smaller masses of Sr could be analyzed (as low as a few ng) which would allow $^{87}Sr/^{86}Sr$ to be applied for provenance of most migratory insect species and other animals.

Step 4: Modelling the regional plant $^{87}Sr/^{86}Sr$ isoscape

We applied the general random forest regression model proposed by Bataille et al. (2018) to calibrate a regional and substrate-specific $^{87}Sr/^{86}Sr$ isoscape for the breeding range of the eastern North American population of monarch butterflies. Strontium isotope ratios are driven largely by bedrock age and

lithology and are therefore expected to change quickly at the discrete boundaries of bedrock units. Random forest regression is a machine learning algorithm that outperforms other traditional spatial statistical approaches (e.g., ordinary kriging) when modelling $^{87}Sr/^{86}Sr$ (Bataille et al., 2018).

Unlike δ^2H, which shows strong isotopic fractionation between insects, host plants, and precipitation and therefore requires calibration (Figure S2.4), the $^{87}Sr/^{86}Sr$ of monarchs and milkweed display a nearly 1:1 relationship (Flockhart et al., 2015). Consequently, we used the $^{87}Sr/^{86}Sr$ of known-origin herbaceous plants as a basis to predict $^{87}Sr/^{86}Sr$ of monarchs. In this study, we analyzed 67 plants from an existing collection (Miller et al., 2011) and 77 newly collected herbaceous plants (Appendix B). After sample collection, the leaves of the 144 new plant samples were used for $^{87}Sr/^{86}Sr$ analysis. To augment this dataset, we searched the literature to compile 256 plant $^{87}Sr/^{86}Sr$ from across eastern North America (Esker et al., 2019; Widga et al., 2017, 2010; Hoppe et al., 1999). This literature search resulted in a calibration dataset of 400 herbaceous plant $^{87}Sr/^{86}Sr$ ratios (144 new plant $^{87}Sr/^{86}Sr$ ratios plus 256 from the literature) for training the random forest regression model (Figure 2.2).

Once the plant $^{87}Sr/^{86}Sr$ calibration dataset was compiled, we collected 29 geospatial data products that represent potential factors influencing $^{87}Sr/^{86}Sr$ variation on the landscape (Bataille et al., 2020, 2018) and used random forest regression to create the regional $^{87}Sr/^{86}Sr$ isoscape. The geospatial data products used here included bedrock geology, tectonostratigraphic terrane age (i.e., a fault-bounded area with a distinctive stratigraphy, structure, and geological history), surficial geology, soil properties, aerosol deposition, topography, climate, and agricultural activity (Table S2.2). We used the sample locations of the georeferenced plant calibration dataset to extract the local pixel values of each of these geospatial data products.

Next, we used the *VSURF* package (Variable Selection Using Random Forest) to select the geospatial variables that were best able to predict the $^{87}Sr/^{86}Sr$ variation (Genuer et al., 2015). We then used random forest regression to integrate the calibration dataset and geospatial data products into a

modelling framework. To optimize and assess the performance of the model, a repeated 10-fold cross-validation was performed using the Root Mean Squared Error (RMSE) and coefficient of determination (R^2) as metrics through the *caret* package (Max, 2008). Using the selected geospatial predictors and the optimized random forest model, we mapped the mean predicted plant $^{87}Sr/^{86}Sr$ across eastern North America, clipping the predictions to the breeding range of monarch butterflies (Flockhart et al., 2017b).

In addition to the mean $^{87}Sr/^{86}Sr$ predictions, $^{87}Sr/^{86}Sr$-based geographic assignment requires a spatially explicit uncertainty layer (Ma et al., 2020). Quantile random forest regression has been proposed to overcome the absence of built-in approaches to assess spatial uncertainty in random forest regression (Fox et al., 2020). However, this approach can overestimate uncertainty, particularly when data have skewed distributions and outliers, as is sometimes seen with $^{87}Sr/^{86}Sr$ (Fox et al., 2020). We calculated spatially explicit uncertainty values by using the logarithmic relationship between absolute residual values and predicted $^{87}Sr/^{86}Sr$ as in Bataille et al. (2020). Although we did not take this step, collecting a known-origin dataset could help further validate the tissue-specific $^{87}Sr/^{86}Sr$ isoscape by using tools available in the *assignR* package (Ma et al., 2020).

Step 5: Geographic assignment

We calculated the continuous-surface geographic assignments of natal origin based on $^{87}Sr/^{86}Sr$ only, δ^2H only, and dual $^{87}Sr/^{86}Sr$-δ^2H. The geographic assignment method depicts the most likely natal origin of each unknown-origin individual as a probability (i.e., a heat-map of probable natal origin). Using the newly developed $^{87}Sr/^{86}Sr$ isoscape and the analyzed $^{87}Sr/^{86}Sr$ of the monarchs, we used the *assignR* package (Ma et al., 2020) to calculate the posterior probability surface (i.e., assignment map) for each individual. The same procedure was followed for δ^2H assignment using the updated δ^2H isoscape (Appendix B) and previously analyzed δ^2H (Flockhart et al., 2013). The *assignR* package does not currently support dual-isotope assignment, so a function developed in a previous study (Wunder, 2010)

and applying multivariate normal probability density was used for the dual $^{87}Sr/^{86}Sr$-$\delta^{2}H$ assignment (Appendix B).

Once assignment maps of monarch natal origin were obtained, we produced a histogram of probability from the assignment map (0 - 100%) in 5% increments. Using this histogram, we calculated the cumulative area represented within each incremental probability bin by dividing the calculated geographic area for each bin by the entire area of the study region. We plotted these cumulative areas for each assignment method to compare the single- and dual-isotope assignments. The precision of geographic assignment is often tested using a known-origin dataset by verifying that probabilities are scaled with the proportion of sites properly assigned (e.g., QA function in *assignR*). In the absence of a monarch known-origin dataset, we defined precision following Rushing et al. (2017) as the ability of the model to restrict the area of natal origin represented by the zone with high probability of natal origin within the study area. We defined high probability using a 2:1 odds ratio (e.g., Flockhart et al., 2013). The 2:1 odds ratio was used to create binary surfaces representing the most probable 33.3% of the probability distribution. These binary surfaces were then used to calculate the area of highly probable natal origin and to assess if the individuals had a local isotopic composition (Appendix B).

To summarize the assignment maps, we applied a k-means cluster analysis to separate individuals into groups of similar natal origin. We also assessed the average probability of origin by summing the probability of all individuals and dividing by the number of individuals; this procedure was also repeated for each cluster. Additionally, to compare summarization techniques with the averaged probability surfaces, the binary surfaces were summed both by cluster and by all individuals and a nominal assignment was performed (Figure S2.9; Figure S2.10).

Results

Unknown-origin monarch butterflies

All monarch $^{87}Sr/^{86}Sr$ fell within the $^{87}Sr/^{86}Sr$ range of the plant samples that were used to construct the plant $^{87}Sr/^{86}Sr$ isoscape. No association between capture date or capture longitude with log-transformed $^{87}Sr/^{86}Sr$ was detected, but associations with capture latitude ($F(1, 93) = 59.8$, $p < 0.001$), sex ($F(1, 93) = 15.7$, $p < 0.001$), and wing condition score ($F(1, 93) = 7.2$, $p < 0.01$) were found. $^{87}Sr/^{86}Sr$ tended to increase with capture latitude ($\beta = 0.00029 \pm 0.00009$, $t = 3.12$, $p = 0.002$), and males tended to have lower $^{87}Sr/^{86}Sr$ than females ($\beta = -0.00058 \pm 0.00016$, $t = -3.56$, $p < 0.001$). These five variables explained 46% of the variance in logged $^{87}Sr/^{86}Sr$ ratios ($F(6, 93) = 15.03$, $p < 0.001$). There was also evidence that sex ($F(1, 93) = 4.6$, $p = 0.03$) influenced δ^2H but no evidence that capture location, capture date, or wing condition score had an effect on δ^2H. Males tended to have lower δ^2H than females ($\beta = -5.4 \pm 2.6$, $t = -2.07$, $p = 0.04$).

Regional plant $^{87}Sr/^{86}Sr$ isoscape

The *VSURF* variable selection procedure identified five geospatial data products to be dominant predictors of $^{87}Sr/^{86}Sr$ in plants across eastern North America, including bedrock model products (Bataille et al., 2018), geological age of rock units (Hartmann & Moosdorf, 2012) and soil pH in H_2O solution (×10) (Hengl et al., 2017; Figure 2.3A; Figure S2.4; Figure S2.5). The resulting model predicted $^{87}Sr/^{86}Sr$ in plants across eastern North America (Figure 2.4C) with an RMSE of 0.0017 ($R^2 = 0.44$) (Figure 2.3B), which represented ~8% of the observed plant $^{87}Sr/^{86}Sr$ range across the dataset (i.e., the normalized RMSE). The random forest regression model produced a high-resolution $^{87}Sr/^{86}Sr$ isoscape that displayed discrete spatial patterns associated with specific geological features, but also variation associated with local environmental conditions (e.g., alkaline soil in the Interior Plains; Figure S2.6). Strontium isotope ratios between 0.709 and 0.711 were predominant in the American Midwest and across the western extremes of the monarch range (Figure 2.4C). Higher $^{87}Sr/^{86}Sr$ (0.711 – 0.715) were

found in the Gulf coast states and north through the Appalachian Mountains. Strontium isotope ratios greater than 0.713 dominated across the northeastern portions of the USA and southern Canada east of Manitoba (Figure 2.4C).

Geographic assignment

We compared the precision of single- and dual-isotope geographic assignments. When averaging across the 100 individuals, $^{87}Sr/^{86}Sr$ assignments showed higher accuracy and precision (Figure S2.8) compared to δ^2H assignment. Dual δ^2H and $^{87}Sr/^{86}Sr$ assignment showed higher precision than single isotope assignment. At high probability (i.e., most probable 33.3%), δ^2H assignment removed on average 89% (± 3) of the study area from the predicted natal origin and $^{87}Sr/^{86}Sr$ assignment removed 93% (± 5) of the area. Dual δ^2H and $^{87}Sr/^{86}Sr$ assignment removed 97% (± 2), a nearly four-fold decrease in the area of estimated origin compared to δ^2H assignment. However, this increase in precision seemed to come with some accuracy trade-offs: single isotope assignments tended to have higher accuracy than dual δ^2H and $^{87}Sr/^{86}Sr$ assignments, as evidenced by the overall higher probability distribution for δ^2H and $^{87}Sr/^{86}Sr$ assignments (Figure S2.8).

To facilitate discussion and visualization, we selected two individuals, MOTF009 and MOTF003, that had distinct and different assignment patterns (Figure 2.5). At the individual level, geographic assignment using δ^2H displayed broad regions of potential origin. Like most of the individuals in this study, both MOTF009 and MOTF003 showed similar δ^2H assignment precision with ~13% of the study area estimated at high probability (Figure 2.5). Conversely, $^{87}Sr/^{86}Sr$ geographic assignment showed more variation in precision between individuals (Figure 2.5C). For 77% of individuals, such as MOTF009, the $^{87}Sr/^{86}Sr$ assignments were restricted to very specific zones and disqualified more of the study area than δ^2H assignment (mean of 5% (± 3.3) of the area estimated; Figure 2.5B). For 23% of individuals, like MOTF003, the area of potential natal origin estimated by $^{87}Sr/^{86}Sr$ assignment exceeded the δ^2H assignment area (mean of 14% (± 3.0) of the area estimated; Figure 2.5A). When combining δ^2H and

$^{87}Sr/^{86}Sr$ for dual assignment, the potential area of origin was more restricted than with δ^2H or $^{87}Sr/^{86}Sr$ alone in 100% of cases (Figure 2.5).

The averaged dual δ^2H and $^{87}Sr/^{86}Sr$ assignment suggested that the highest probability of origin is an area encompassing Texas and northern Mexico (Figure 2.6A). The k-means cluster analysis found three isotopic clusters, predominately driven by differences in δ^2H. When considering the dual δ^2H and $^{87}Sr/^{86}Sr$ assignment maps, monarchs in Cluster 1 (n = 45) displayed natal origin in the southern part of the breeding range in Texas and northern Mexico (Figure 2.6B), Cluster 2 monarchs (n = 32) showed natal origin in a few patches in northern Mexico and the American Midwest (Figure 2.6C) and Cluster 3 monarchs (n = 23) showed natal origin along the Gulf of Mexico in Texas and Florida (Figure 2.6D). These clusters did not differ in their capture location, capture date, proportion of males to females, or wing condition score.

Most individuals showed a probability of origin that was incompatible with their capture site, indicating that they did not originate locally. When looking at δ^2H assignments, only 7% of the individuals had a high probability of natal origin at their capture location (i.e., in the most probable 33.3%). When looking at $^{87}Sr/^{86}Sr$ assignments, 24% of the individual were compatible with local origin. Only 14% of individuals had dual δ^2H and $^{87}Sr/^{86}Sr$ isotopic compositions compatible with their location of capture.

Discussion

Isoscapes

The $^{87}Sr/^{86}Sr$ isoscape showed discrete patterns following the changes in geological units combined with high resolution intra-unit variations associated with soil and atmospheric deposition processes. These patterns were complementary to those of δ^2H which showed broad latitudinal gradients (Figure 2.4). Strontium isotope ratios can therefore constrain area of natal origin within a latitudinal band defined by δ^2H, particularly when the geology in this latitudinal band is heterogenous.

The plant $^{87}Sr/^{86}Sr$ isoscape presented here performed better than other recent, less regional or substrate-specific, $^{87}Sr/^{86}Sr$ isoscapes when comparing model metrics (Bataille et al., 2020, 2018). The overall RMSE of the model was reduced by half in comparison with Bataille et al. (2020, 2018) models. In these previous studies, the $^{87}Sr/^{86}Sr$ isoscape was trained using a dataset mixing samples from different substrates, different sampling strategies, and over geologically unrelated regions. In this study, we only used one specific substrate (i.e., herbaceous plants), we carefully selected our sampling sites, and we trained a model over a region with a common geological history (i.e., eastern North America). All these factors likely contributed to reducing the overall uncertainty of the $^{87}Sr/^{86}Sr$ isoscape.

Performance of the geographic assignments

The potential of $^{87}Sr/^{86}Sr$ assignment to constrain the natal origin of individuals was more variable than for δ^2H assignment (Figure 2.5C). While δ^2H almost always ruled out 89% of the study area, $^{87}Sr/^{86}Sr$ showed either lower or higher influence on the precision of geographic assignment. For some individuals, $^{87}Sr/^{86}Sr$ were not very diagnostic and geographic assignments were similar, or even less precise, than the δ^2H assignment (Figure 2.5A). These individuals tended to have $^{87}Sr/^{86}Sr$ in the range of 0.7085 to 0.711. For other individuals, $^{87}Sr/^{86}Sr$ were much more diagnostic, for example, two individuals with low $^{87}Sr/^{86}Sr$ (i.e., < 0.708) had assignment maps pointing to very restricted areas for natal origin in Texas. This observation supports the findings of Bataille et al. (2020) showing that about 50% of bioavailable $^{87}Sr/^{86}Sr$ of the world fall within a tight range of 0.7085 to 0.711. When individual $^{87}Sr/^{86}Sr$ fell outside this tight range, the potential of $^{87}Sr/^{86}Sr$ assignment to constrain natal origin became increasingly high. Areas that fell outside of this range include geological areas with old or young rock units, including young volcanic regions (e.g., Central Mexico) and older igneous and metamorphic regions (e.g., the Appalachian Mountains and their associated sedimentary basins).

Dual δ^2H and $^{87}Sr/^{86}Sr$ assignment was able to constrain the area of highly probable natal origin nearly four-times better than δ^2H assignment, and twice as well as $^{87}Sr/^{86}Sr$ assignment (Figure S2.8). As

the patterns of $^{87}Sr/^{86}Sr$ and δ^2H are independent on the landscape, the precision improvement of dual-isotope assignments is dependent on the fortuitous complementarity of their isotope patterns. In some cases, dual δ^2H and $^{87}Sr/^{86}Sr$ assignments are highly complementary with their probability surfaces only intersecting on very small areas leading to highly precise dual-isotope assignments (e.g., Figure 2.5B). In other cases, dual δ^2H and $^{87}Sr/^{86}Sr$ assignments cover similar regions on the landscape, leading to only small improvements in precision.

Ecological implications

While our sample size was too small to make inferences at the population scale, the geographic assignment results were generally aligned with previous studies (Flockhart et al., 2017b, 2013; Wassenaar & Hobson, 1998). The American Midwest is often considered to be the most important region contributing to the monarch overwintering population numbers (Flockhart et al., 2017b; Dockx et al., 2004; Wassenaar & Hobson, 1998), and the population decline over the last two decades has been associated with a decrease in host-plant availability in this area (Pleasants & Oberhauser, 2013). In our dataset, we identified a cluster of individuals likely to have originated from a few areas in the American Midwest (Figure 2.6C).

Our analysis also demonstrated that many monarchs had probable natal origins in Texas and northern Mexico (Figure 2.6; Figure S2.9; Figure S2.10). However, it is unclear whether these were individuals hatched in the late summer of the previous year (i.e., a 'fifth generation') that overwintered in Mexico or if they were first-generation individuals hatched in the year they were sampled. Relatively high wing wear scores from this sample suggest that they had flown substantial distances and, therefore, may have been the previous year's fifth generation (Flockhart et al., 2013; Calvert, 1999; Figure S2.1). However, other proxies of monarch age, such as wing shape and size (Altizer & Davis, 2010) and wing pigmentation (Satterfield & Davis, 2014), could confirm that the samples are from the fifth generation. Recent studies have shown that monarchs in Texas can represent a non-negligible

proportion (~5%) of the pre-migratory population (Momeni-Dehaghi et al., 2021) and that up to 18% of migratory monarchs sampled in Texas from Oct. to Dec. are reproductive (i.e., not in diapause, as would be expected if they were migratory; Satterfield et al., 2018). However, the South Central USA is generally not considered a dominant contributing region to the overwintering monarch population, and Texas is well-known as the primary spring breeding area for the first generation (Miller et al., 2012). Furthermore, the spring migration had already progressed further north than the sampling locations during the sampling period (i.e., Apr. 13 to May 8, 2011; Figure S2.2). Thus, we cannot exclude the possibility that some or all of these monarchs might be the first-generation offspring of overwintering monarchs.

A third possible explanation for the prevalence of assignments in Texas is that the $^{87}Sr/^{86}Sr$ of monarchs have experienced exogenous contamination from dust ingestion or through adsorption of Sr from water during the overwintering stage. Caterpillars could ingest dust as they feed on dust-coated leaves. While Sr adsorption from water exists for human hair (L. Hu et al., 2020b), it seems unlikely for monarchs because they behaviourally avoid submergence in water and have superhydrophobic wings (Pass, 2018). These contamination sources might superimpose on the natal origin signal obtained from the milkweed (Flockhart et al., 2015). These hypotheses call for more experimentation to test the role of aerosols from dust and rain in modifying $^{87}Sr/^{86}Sr$ in insects.

Implications and future improvements

We encourage researchers interested in studying animal mobility to consider applying the framework described in this study (Figure 2.1) to combine δ^2H and $^{87}Sr/^{86}Sr$ and enhance the precision of geographic assignment. Geographic assignments derived from isotopes can be combined with other types of ecological data including community science data (Flockhart et al., 2013), trace element analysis (Holder et al., 2014), wind-trajectory modelling (Talavera et al., 2018), genetic data (Ruegg et al., 2017), and ecological niche modelling (Ruegg et al., 2017). Combining these approaches will considerably

enhance our ability to refine the geographic origins and migration pathways of animals. For example, in this study we illustrate how dual-isotope geographic assignments could help understand the productivity of monarchs across the migration cycle over time (Flockhart et al., 2017b). These spatial data are critical to constrain the factors contributing to the monarch population decline and focus habitat restoration efforts.

Conclusion

We provided and tested a novel framework to use $^{87}Sr/^{86}Sr$ for continuous-surface geographic assignment of migratory animals. High-resolution, accurate, regionally calibrated $^{87}Sr/^{86}Sr$ isoscapes can be generated using carefully selected samples, geospatial data, and machine-learning regression. Using appropriate cleaning and analytical procedures, $^{87}Sr/^{86}Sr$ can be precisely analyzed even in tissues with low Sr abundances. We demonstrated that, depending on the underlying geology, $^{87}Sr/^{86}Sr$ can complement δ^2H and substantially constrain geographic origin. The framework, isoscapes, and dataset generated in this study provide a basis to apply dual δ^2H and $^{87}Sr/^{86}Sr$ assignment to contemporary or ancient animals expanding our ability to study the migration phenomenon.

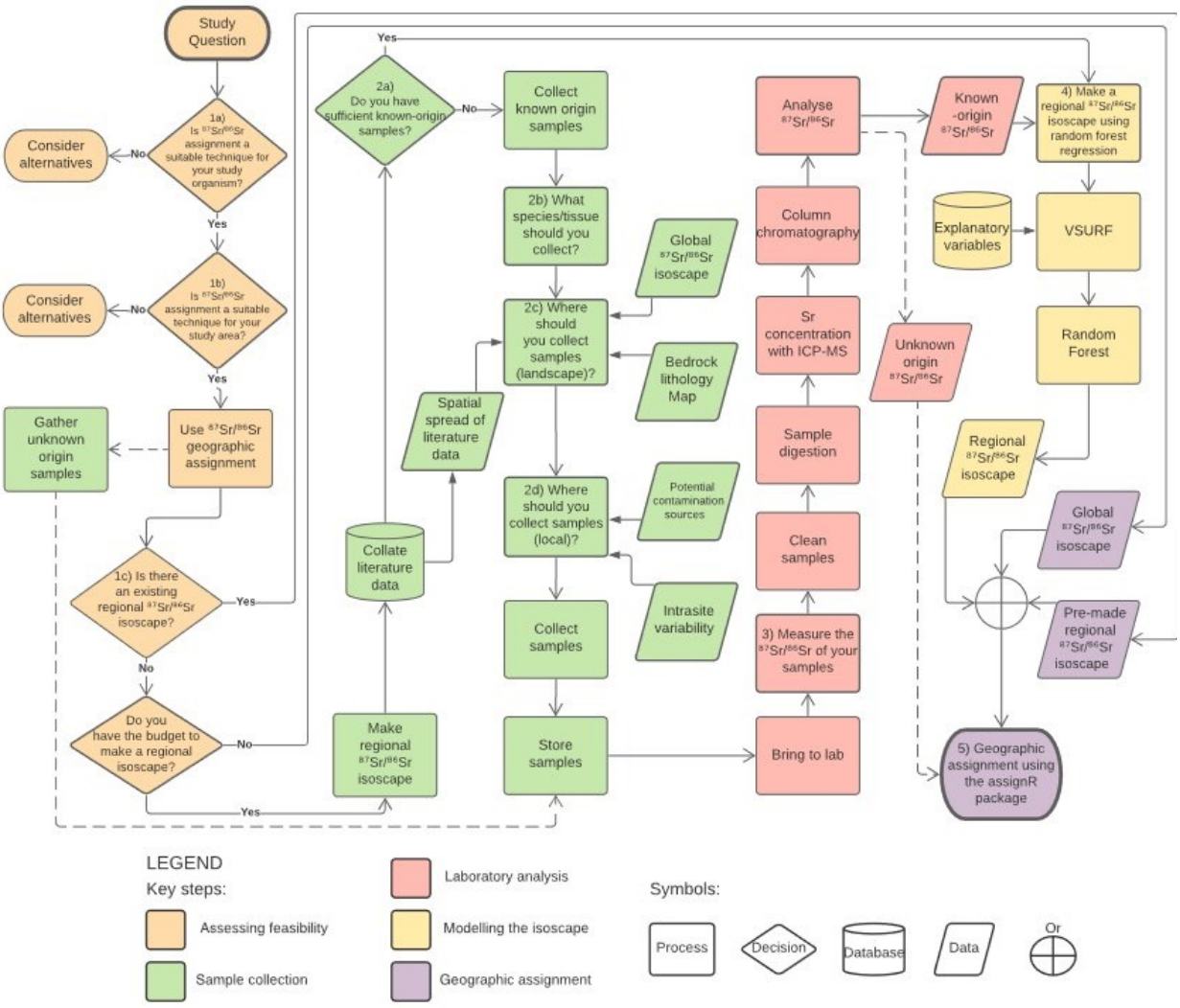

Figure 2.1 Step-by-step guide to using $^{87}Sr/^{86}Sr$-based geographic assignment. A corresponding list of important considerations and literature suggestions can be found in Table S2.1 to help ecologists looking to apply this technique to other systems. The hatched line shows the steps that should be taken with unknown-origin samples. Line arrows show the sequence of steps, and solid arrows indicate data that should inform a process.

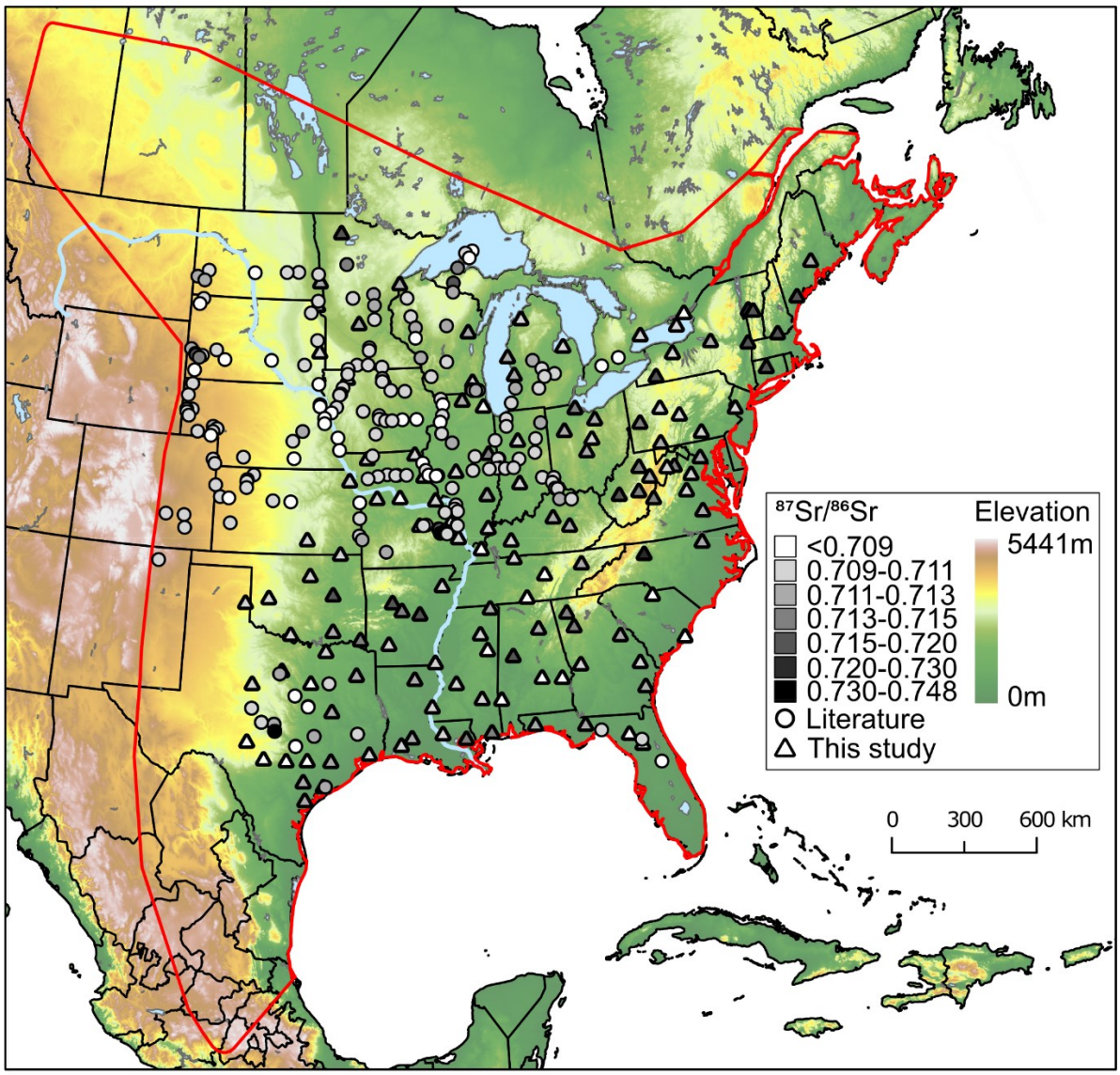

Figure 2.2 Location of plant samples with $^{87}Sr/^{86}Sr$ analyzed in this study or compiled from the literature, and used as training data in the random forest regression. Of these plant $^{87}Sr/^{86}Sr$, 256 are from pre-existing studies (circles), and 144 are presented in this paper (triangles). The base map is a digital elevation model (Commission for Environmental Cooperation, 2007), and the red line represents the breeding distribution of monarch butterflies in eastern North America (Flockhart et al., 2017b).

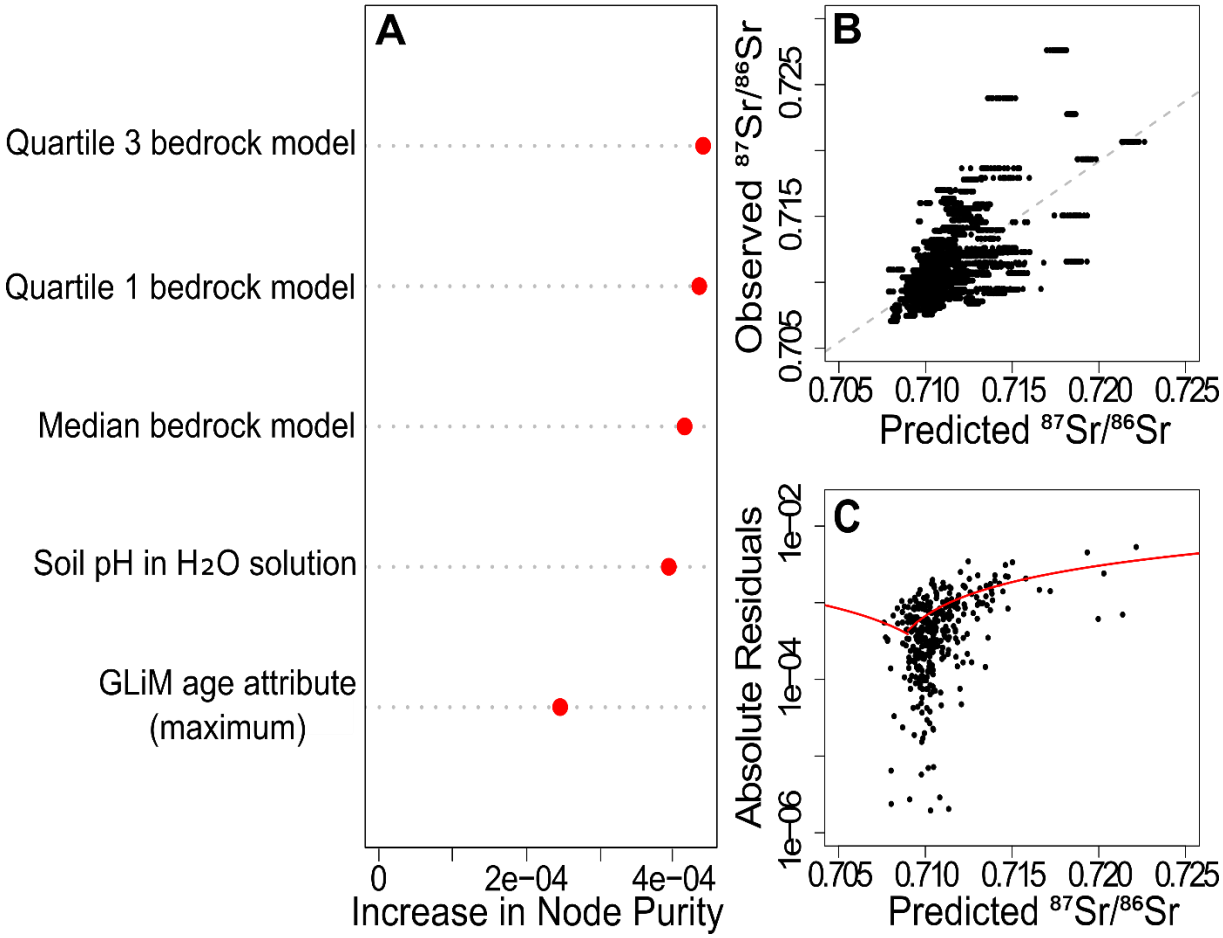

Figure 2.3 Performance of the random forest regression model used to develop the regional $^{87}Sr/^{86}Sr$ isoscape. **(A)** Variable importance plots for the variables selected using *VSURF*. Explanatory variables are listed by the mean increase in node purity, an index of importance to the model. Explanatory variable descriptions can be found in the Supporting Information, Table S2.2; **(B)** Observed versus predicted $^{87}Sr/^{86}Sr$ from the 10-fold cross-validation (RMSE 0.0017, R2 = 0.44, $p < 0.001$). The 1:1 line is marked in grey; **(C)** Absolute residuals at predicted $^{87}Sr/^{86}Sr$. Red lines show the global equation used to calculate the uncertainty raster (Bataille et al., 2020): $x < 0.709$, $y = \log(1.08–0.11x)$, if $x > 0.709$, $y = \log(0.83 + 0.24x)$.

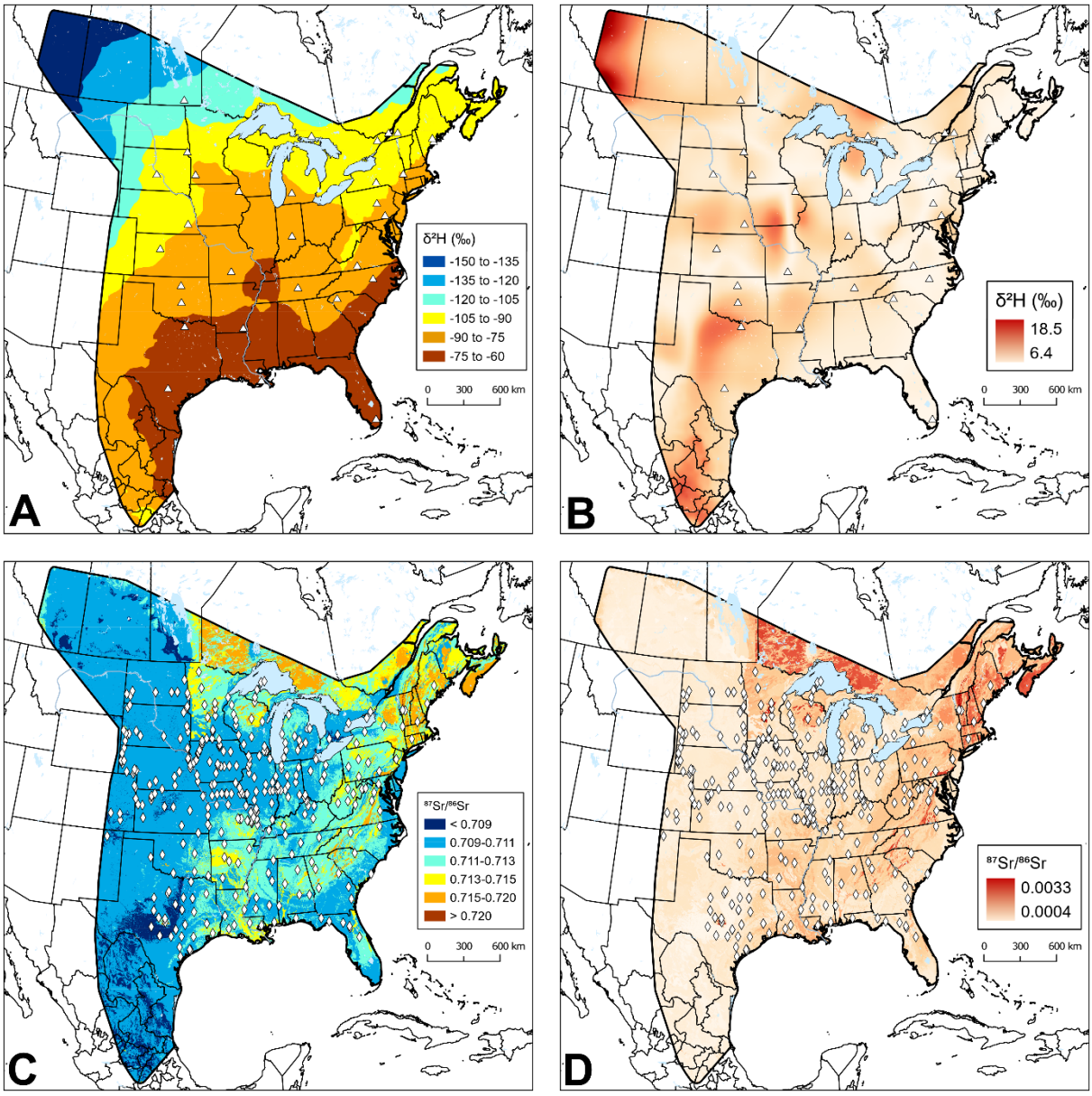

Figure 2.4 Isoscapes and their associated uncertainty. **(A)** Monarch δ^2H isoscape with locations (white triangles) of the known-origin monarch butterflies (Hobson et al., 2019) used to calibrate the isoscape in *assignR* using the growing-season precipitation δ^2H isoscape (Bowen, 2018; IAEA/WMO, 2018; Bowen et al., 2005), **(B)** uncertainty map (±1 SD) for the monarch δ^2H isoscape; dark red areas represent higher uncertainty, **(C)** plant $^{87}Sr/^{86}Sr$ isoscape with locations (white diamonds) of the plant $^{87}Sr/^{86}Sr$ used to train the random forest regression model, **(D)** uncertainty map for the plant $^{87}Sr/^{86}Sr$ isoscape; dark red areas represent higher uncertainty.

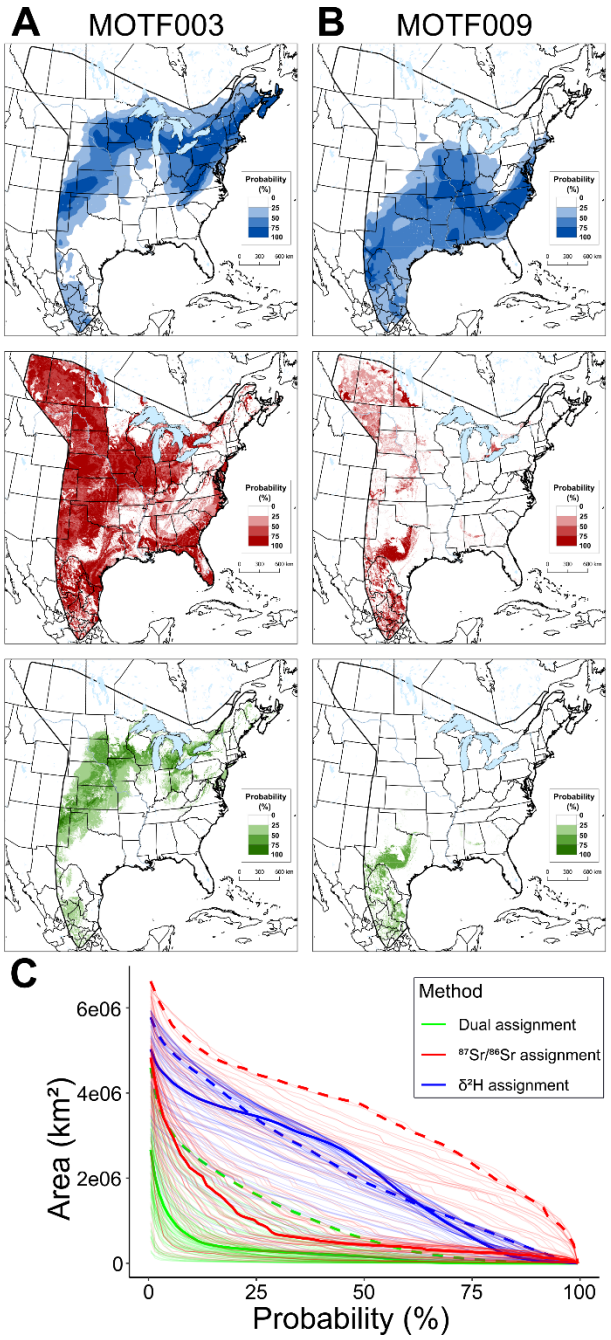

Figure 2.5 Comparison of single- and dual-isotope geographic assignment at the individual level illustrated using two individuals. **(A)** Individual MOTF009 and **(B)** individual MOTF003. For both, the top panel corresponds to the δ^2H-only assignment, middle panel corresponds to the $^{87}Sr/^{86}Sr$-only assignment and the bottom panel corresponds to the dual $^{87}Sr/^{86}Sr$–δ^2H assignment. Dual $^{87}Sr/^{86}Sr$-δ^2H assignment performs better in both cases; **(C)** Comparison of individual assignment precision performance for the 100 individuals. The graph shows the amount of area with an assignment probability greater than or equal to a given assignment probability. Individual MOTF009 is highlighted by a bold solid line and individual MOTF003 by a bold dashed line.

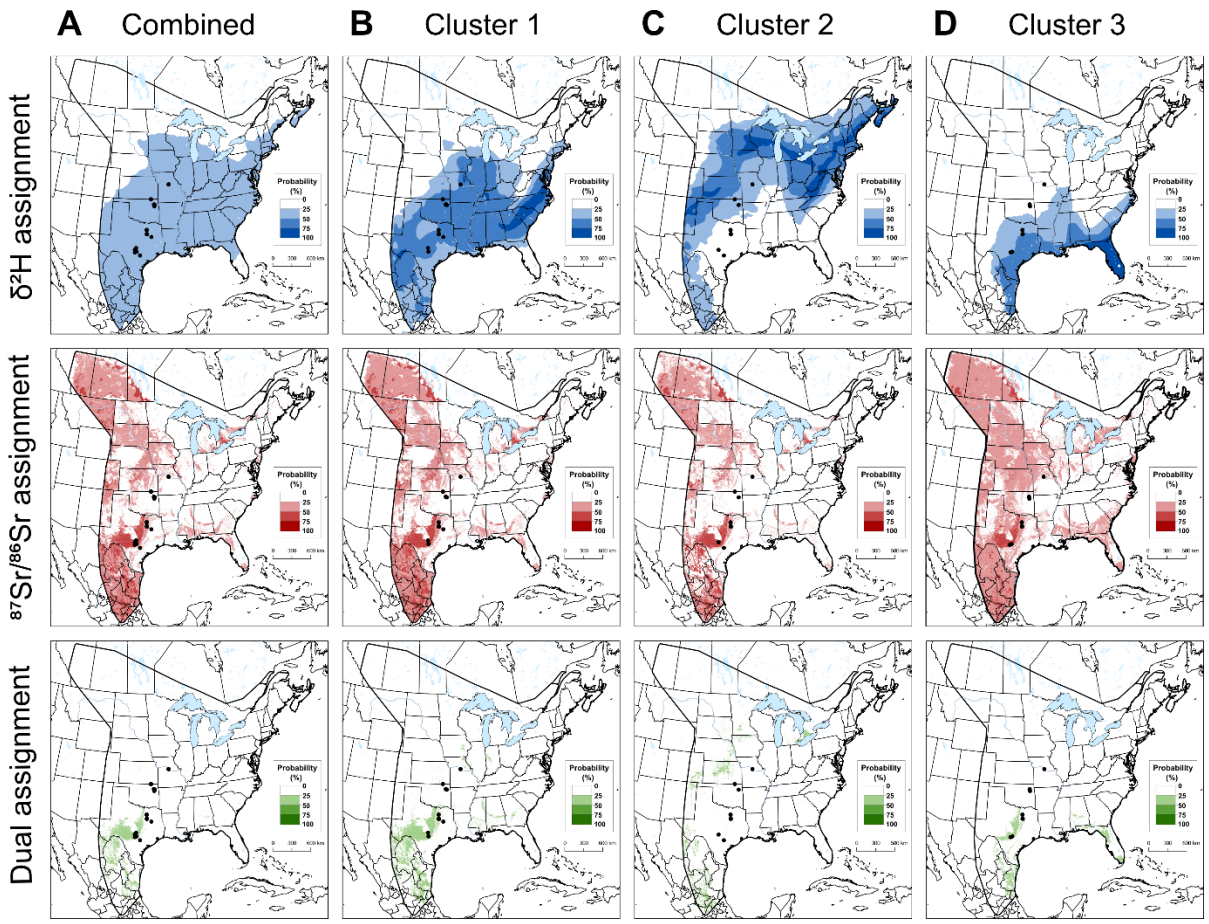

Figure 2.6 Geographic assignment maps of monarch butterflies summarized by group. **(A)** Averaged assignment maps for all monarchs (n = 100), **(B)** averaged assignment map for Cluster 1 (n = 45), **(C)** averaged assignment map for Cluster 2 (n = 32) and **(D)** averaged assignment map for Cluster 3 (n = 23). The black points mark the collection sites of the monarchs.

Chapter 3: Trans-Saharan migratory patterns in *Vanessa cardui* and evidence for a southward leapfrog migration

Megan S. Reich, Sana Ghouri, Samantha Zabudsky, Lihai Hu, Mael Le Corre, Ivy Ng'iru, Dubi Benyamini, Daria Shipilina, Steve C. Collins, Dino J. Martins, Roger Vila, Gerard Talavera, Clément P. Bataille

Note: This manuscript is in preparation for submission and has been formatted accordingly

Contribution

GT and CB conceived of the idea for the study; GT and RV coordinated the sample collection; GT, RV, IN, DB, DM, SC, and I collected the samples; SG, LH, SZ, CB, and I performed the isotopic analyses; SG, CB, and ML modelled the strontium isoscape; I performed the data analysis and geographic assignment; I led the writing of the manuscript with contributions from SG (Methods) and input from all co-authors.

Abstract

Some insects, such as the painted lady butterfly *Vanessa cardui*, exhibit complex annual migratory cycles spanning multiple generations, often **traversing** barriers like seas and deserts. Understanding insect migratory connectivity and patterns across barriers is essential for characterising population dynamics and predicting the impacts of global change on insect-mediated ecosystem services. We develop a bioavailable strontium isoscape for Europe and Africa, and then use isotope geolocation combining hydrogen and strontium isotopes to estimate the natal origins of painted ladies captured north and south of the Sahara during spring and autumn. Our findings reveal moderate migratory connectivity across the Sahara characterised by a broad-front, parallel migration. We also report evidence of a leapfrog migration, wherein early autumn migrants from higher latitudes cover greater distances southward than their late autumn counterparts. This work represents a major advancement in

understanding insect migration patterns, especially in the eastern Sahara, where empirical studies have been scarce.

Introduction

Multi-generational migrations equip insects with the capacity to respond swiftly to seasonal environmental changes, yet this very trait also renders them vulnerable to certain challenges. In contrast to migratory vertebrates, which typically complete round-trip migrations between overwintering and breeding grounds within a single generation, insects, with their shorter lifespans, require several generations to complete their annual migratory cycle, with each generation completing a single segment of the overall cycle (J. W. Chapman et al., 2015). The spatial extent of suitable climatic and biotic conditions, largely determined by host plant availability, can change drastically throughout the year, prompting each generation to embark on migratory journeys in search of suitable habitats (Chowdhury et al., 2021b). However, many individual insects do not survive the journey, while others conclude their journeys in unsuitable habitats that cannot sustain the next generation, potentially leading to local- or regional-scale extirpation and a decline in population size. Fortunately, the range of suitable habitats for migratory insects tends to be broad, with reticular migratory patterns that provide redundancy and compensate for the impact of local bottlenecks (García-Berro et al., 2023). While these reticular patterns are generally thought to enhance the resilience of populations to environmental perturbation (Gao et al., 2020; Gilroy et al., 2016), in the face of large-scale disturbances such as global climate change and habitat degradation, the population dynamics and migratory patterns of some species, are nonetheless, affected. For example, the monarch butterfly *Danaus plexippus* population in North America seems to be declining, with changing spring weather conditions playing an important role in the decline (Zylstra et al., 2021). Similarly, outbreaks of desert locust *Schistocerca gregaria* are influenced by the increasing frequency of extreme weather events (Salih et al., 2020), and changes to monsoon patterns are affecting the migration patterns of the brown planthopper *Nilaparvata lugens*, a devastating agricultural pest (Lv

et al., 2023). Delineating predictable spatiotemporal linkages of insects across their migratory range is an imperative first step for predicting insect population dynamics and understanding how they will respond to global change.

Understanding migratory patterns and connectivity across natural barriers, such as seas and deserts, may be particularly important for insect population dynamics. Migratory journeys across barriers can be especially perilous, and large-scale losses can lead to population bottlenecks (Lok et al., 2015; Klaassen et al., 2014). The Sahara is the world's third-largest desert and, for the migratory animals that traverse it, it constitutes at least a thousand-kilometre journey through unsuitable habitat. The migratory connectivity of many bird species across the Sahara has been well-explored (e.g., Guilherme et al., 2023; Fattorini et al., 2023). These studies gave scientists the baseline information needed to detect that many bird species in the Afro-Palearctic migration system are facing population declines (Sanderson et al., 2006) and propose international conservation action (Marcacci et al., 2023; Vickery et al., 2014), thus illustrating that understanding migratory connectivity across biogeographic barriers and geopolitical borders is important. In general, insect migration remains understudied compared to research on migratory birds and mammals (Satterfield et al., 2020). While there are growing indications that many insect species undertake trans-Saharan journeys, empirical evidence remains limited. The irregular migrations of a well-studied Saharan insect, the desert locust, tend to originate from recessive zones within the Sahara itself, rather than crossing it (Meynard et al., 2017; Pedgley et al., 1995). As a result, the annual migrations of the painted lady butterfly *Vanessa cardui* stand out as the primary example of trans-Saharan insect migration.

Over the past decade, regular seasonal migrations of the painted lady butterfly across the Sahara have been verified using a variety of techniques, including field observations, monitoring stations, isotope geolocation, ecological niche modelling, and pollen metabarcoding analysis (Chapter 4; Gorki et al., *in review.*; Talavera et al., 2023; Menchetti et al., 2019; Talavera et al., 2018; Stefanescu et

al., 2016; Talavera & Vila, 2016). The Afro-Palearctic population of painted lady butterflies undergoes an annual migratory cycle spanning 8 to 10 overlapping generations (Talavera & Vila, 2016). Painted lady adults live for about 3 to 6 weeks, mating multiple times during this period and laying up to over 1,000 eggs that develop into adults over 23 to 45 days, depending on environmental conditions (Stefanescu et al., 2021; Talavera & Vila, 2016; Stefanescu et al., 2013; Hammad et al., 1973). Thus, the offspring of a single female can depart in several migratory waves, intermingling with older generations. Over multiple generations, painted ladies migrate as far north as Scandinavia during the summer, travel south to regions on both sides of the Sahara for the European winter (i.e., North Africa and sub-Saharan Africa), and then return to Europe in the spring (Talavera et al., 2023, 2018; Stefanescu et al., 2016). This recurring migration across the Sahara offers a unique opportunity to study insect migratory connectivity between well-differentiated faunistic regions and across a natural barrier.

There are multiple reasons why insect migration is understudied. For one, the multi-generational migratory cycle adds a layer of complexity to the study of insect migration, demanding investigation of each segment of the annual cycle. Moreover, understanding insect migratory patterns requires addressing both its spatial and temporal dimensions. Thus, large-scale collaborations are essential for investigating the international and intercontinental migrations of insects (e.g., Diffendorfer et al., 2023; Talavera et al., 2023). Another reason why insect migration is understudied is that insects are difficult to track with techniques that are traditionally used to study vertebrates, like biologger technology (e.g., radiotelemetry, light loggers), because insects are small, abundant, and short-lived. Instead, intrinsic biomarkers, such as isotopes, have become quintessential tools for studying insect migration. Local isotopic signatures are incorporated into developing tissues as the larval insect feeds (Flockhart et al., 2015; Hobson et al., 1999) and, after metamorphosis, these local isotopic signatures are largely preserved in the wings (Chapter 1; Lindroos et al., 2023). Thus, the isotopic signature of a migrant butterfly's wing can be measured and compared to a spatial model of isotopic variation to

estimate the individual butterfly's natal origin (i.e., isotope-based geographic assignment). Hydrogen isotope values (δ^2H) have been used for insect geolocation for over twenty years (Hobson et al., 1999; Wassenaar & Hobson, 1998) and, due to global precipitation patterns, often act as a proxy for the latitude of origin (Bowen et al., 2005). However, δ^2H-based geographic assignment rarely provides adequate longitudinal resolution. Strontium isotope ratios ($^{87}Sr/^{86}Sr$) have recently been used for the geolocation of insects and have the potential to provide increased longitudinal resolution (Chapter 2), showing that it is important to further develop technologies to advance our understanding of migratory insect population dynamics and multi-generational migratory connectivity.

Here, we investigate the spatiotemporal trans-Saharan migratory connectivity and patterns of the painted lady butterfly using δ^2H and $^{87}Sr/^{86}Sr$-based geographic assignment. Through a large, international collaboration led by the Painted Lady Migration Network, a global citizen science effort, 118 painted lady samples were opportunistically collected from many sites south and north of the Sahara and the Arabian Desert, an extension of the Sahara, so that the migratory patterns along the length of the geographic barrier could be compared. Applying dual δ^2H and $^{87}Sr/^{86}Sr$ for continuous-surface isotope-based geographic assignment requires a reliable spatial model of isotopic variation across the landscape (i.e., an isoscape). A new hydrogen isoscape was recently calibrated for butterfly wings for the Afro-Palearctic region (Ghouri et al., 2023), but a robust bioavailable strontium isoscape of this region did not exist. We compiled bioavailable $^{87}Sr/^{86}Sr$ data from the literature and completed this database with additional analysis of $^{87}Sr/^{86}Sr$ in plants from 45 sites. We used this database and applied a spatial interpolation ensemble machine-learning framework to develop a strontium isoscape across the study area. Using the isoscapes, we estimated the natal origin of the collected painted lady butterflies, then estimated migration distance and direction of travel. These isotope-based metrics allowed us to discuss the connectivity and migratory patterns of painted ladies across the Sahara and Arabian Desert.

Results and Discussion

Strontium isotope geolocation enables new ecological insights

We developed a regional bioavailable strontium isoscape for the geolocation of painted lady butterflies in the Afro-Palearctic region. This isoscape relies on a compilation of bioavailable $^{87}Sr/^{86}Sr$ data from the literature, the addition of 45 new plant $^{87}Sr/^{86}Sr$ measurements from Africa (n = 1820; Figure S3.1), and 14 spatial predictor variables (Table S3.1; Figure S3.2). Bioavailable strontium isoscapes are typically modelled using a random forest regression (RF) framework (e.g., Chapter 2; Bataille et al., 2020, 2018). However, recent advances have demonstrated that spatial interpolation ensemble machine learning (EML) can outperform this RF framework (Le Corre et al., *in review*). As the EML framework lacks direct interpretability (i.e., does not generate partial dependence plots or report the importance of predictors), we followed Le Corre et al. (*in review*) and selected predictors and assessed bioavailable $^{87}Sr/^{86}Sr$ patterns through the RF framework before using the spatial interpolation EML to produce the most accurate and unbiased strontium isoscape. We found that the spatial interpolation EML had slightly superior performance compared to RF (Figure S3.3). The EML isoscape is largely dominated by RF (highest absolute t-value < 2e-16) but also relies on additional base learners (i.e., gradient boosting (t-value = 0.04), support vector machines (t-value = 0.02) and generalised linear models (t-value = 0.04)). As expected from the dominance of RF in the EML predictions, the EML isoscape showed patterns very similar to the RF-based model with ratios ranging from 0.70366 to 0.77394, with the highest $^{87}Sr/^{86}Sr$ in cratonic areas of Africa and the lowest $^{87}Sr/^{86}Sr$ along the basaltic African rift region (Figure S3.4A; Figure S3.5A). However, as shown by Le Corre et al. (*in review*), the difference between spatial interpolation EML and RF-based modelling was apparent when comparing the spatially explicit uncertainty maps, with the EML isoscape more normally distributed and displaying lower average uncertainty (0.00347 vs. 0.00448) (Figure S3.4B; Figure S3.5B). Overall, the use of multiple learners, spatial dependencies, and an unbiased spatial cross-validation approach led to moderate performance

improvements over RF by enhancing the robustness of the resulting model and the corresponding uncertainty estimates (Le Corre et al., *in review*). This regional bioavailable strontium isoscape provides a ground-breaking tool to investigate the mobility of painted lady butterflies, as well as other terrestrial insects, migratory animals (e.g., migratory megafauna, birds, early hominids; Copeland et al., 2011), archeological and modern human remains (Wang et al., 2023; Degryse et al., 2012; Pye, 2004), and tissues and manufactured substrates across Africa (e.g., drugs, ivory, wood; Van Der Merwe et al., 1990).

As a prerequisite to assessing the migratory patterns of painted lady butterflies migrating northward and southward across the Sahara, we used dual δ^2H and $^{87}Sr/^{86}Sr$-based geographic assignment to estimate the natal origin of each of the collected specimens (n = 118; Table S3.2). Our sampling strategy was crafted to capture migrants from both sides of the Sahara in different seasons (Figure 3.1); however, we were only able to confidently classify 50% of the 118 samples as having migrated (i.e., having travelled > 100 km). The remaining samples had dual isotopic signatures similar enough to their capture location that we could not rule out a local origin (Figure S3.6). It is possible that these individuals are also migrants, but from regions of natal origin with similar isotopic signatures to their capture locations. These putative locals had isotopic signatures that are highly redundant in the Afro-Palearctic region, with $^{87}Sr/^{86}Sr$ ~0.709 ± 0.001 common in most regions with marine sediments (Chapter 2) and δ^2H typical of the warm, wet climates of the Afrotropical region (Ghouri et al., 2023). Alternatively, some of these individuals were collected later in the season and may represent the locally-sourced offspring of migrants. In this study, we are interested in migratory individuals; therefore, we took the most conservative approach and excluded these potentially local individuals from further analyses of migratory connectivity.

Moderate migratory connectivity across the Sahara and Arabian Desert

Migratory connectivity refers to the degree to which individuals from one area of the migratory range migrate exclusively to another area without mixing with other individuals from elsewhere, with strong

connectivity indicating a low amount of mixing (Gao et al., 2020; Marra et al., 2010; Webster et al., 2002). This term is often used to qualify the migratory patterns of birds, which often show strong connectivity and a discrete spatial structure in migratory trajectories across the Afro-Palearctic region (Gao et al., 2020). However, certain bird species exhibit moderate migratory connectivity, which is marked by spatial overlap in the breeding range (e.g., Koleček et al., 2016; Finch et al., 2015). However, insects, due to their multi-generational, reticular migration patterns, typically display weaker migratory connectivity than birds (García-Berro et al., 2023; Gao et al., 2020).

Painted ladies showed moderate migratory connectivity across the Sahara, characterised by a predominantly latitudinal, rather than longitudinal, movement pattern, suggesting parallel migration (Figure 3.2E). Individuals collected in the easternmost regions were estimated to migrate north from East Africa or the southern Arabian Peninsula in the spring (Figure 3.2B) and south from the northern Arabian Peninsula when collected in the autumn (Figure 3.2D). While this migratory pattern has long been suspected, empirical evidence has been absent until now (e.g., Larsen, 1975). For the westernmost butterflies, the most probable regions of origin exhibited less cohesiveness than in their eastern counterparts due to the broader range of sampling locations and times, resulting in a wider range of isotopic signatures. During the autumn, many of the westernmost individuals showed estimates of natal origin in temperate Europe (Figure 3.2C). Conversely, in the spring, individuals from the westernmost regions exhibited broader posterior probability surfaces, suggesting a natal origin ranging from northwestern Africa to as far east as the Arabian Peninsula (Figure 3.2A). Our hypothesis is that the most likely origin for the westernmost spring butterflies sampled in this study lies directly south of their capture locations in the Western Sahara and the Canary Islands (Figure 3.2A). This is supported by the presence of pollen from plants endemic to the Canary Islands present on two of our samples captured in Spain (Sample IDs: 16C413 and 14M265) (Suchan et al., 2018). Furthermore, historical observations, recent ecological niche models, and monitoring data also suggest that the Canary Islands and areas

along the coast of the Western Sahara offer highly suitable breeding conditions for painted ladies from Dec. through to Feb. (Talavera et al., 2023).

Strong migratory connectivity can lead to adaptation and genetic differentiation between populations (Webster et al., 2002). Trans-Saharan migrations in birds often show longitudinal migratory divides, where adaptive populations follow western, eastern and, occasionally, central flyways (e.g., Briedis et al., 2020; Jiguet et al., 2019; Åkesson et al., 2016; Marx et al., 2016). However, the likelihood of discovering an adaptive longitudinal migratory divide among populations of painted ladies in the Afro-Palearctic region is remote, as is shown by the mounting evidence of inter-continental panmixia and shared demographic history (Chapter 4; Suchan et al., *in review*; García-Berro et al., 2023). The migratory connectivity of painted ladies appears to be weaker than that observed in a few other migratory insect species, such as the fall armyworm moth Spodoptera frugiperda and the monarch butterfly (Gao et al., 2020). In these species, well-defined migration routes exist between discrete breeding grounds, separated by a geographic barrier oriented in a north-south direction (i.e., the Appalachian Mountains and Rocky Mountains) (Tessnow et al., 2023). In contrast, painted ladies breed across virtually the entire longitudinal expanse of sub-Saharan Africa, with no significant geographical gaps in suitable habitat, except for tropical forests (Talavera et al., 2023; Menchetti et al., 2019). We anticipate that expanding sampling efforts to include more butterflies in Central Africa and the Central Mediterranean would reveal a continuum of predominantly north-south movement along the Sahara, resulting in a broad-front migration pattern (Figure 3.2E). Instead of indicating adaptation to distinct migratory routes, the moderate migratory connectivity observed across the Sahara may be due to survivorship bias, as butterflies that migrate shorter distances directly across the Sahara likely experience higher survival rates, as is seen in birds (Somveille et al., 2019).

While our data primarily supports the prevalence of latitudinal migratory trajectories, we do not rule out the possibility of some longitudinal movements. A closer examination of the posterior

probability surfaces for individual butterflies reveals that many individuals are probably not following perfectly north-south paths, and there may be variation in origin and migration routes even among individuals collected at the same site (see Data Availability Table). It is likely that environmental conditions along the migration path, such as prevailing wind direction, affect the energetic costs associated with different routes and alter flight trajectories (Fattorini et al., 2023). An example of longitudinal movement is the individual collected in Italy, which displayed natal origins far to the east in the Arabian Peninsula (Figure 3.2B). This specimen was collected in Apr. 2019 (Figure 3.3G), a year marked by an outbreak of painted lady butterflies attributed to anomalous vegetation growth in the Arabian Peninsula (Gorki et al., *in review*; Hawkes et al., 2022; López-Mañas et al., 2022), that likely facilitated the spread of individuals from the hotspot to other parts of the range, extending as far west as Italy. Thus, long-distance longitudinal movements between the westernmost and easternmost parts of our study area can occur but are presumably rare occurrences. The distribution of painted ladies in the Palearctic region extends from Portugal to Japan. The migratory patterns of the easternmost butterflies in our study highlight the role of the Arabian Peninsula as a crucial stepping-stone connecting Europe, Africa, and Asia (Larsen, 1984, 1982; Figure 3.2B; Figure 3.2D). Subsequent research should delineate the migratory patterns of painted lady butterflies across the entire Palearctic and quantify the extent of east-west connections between Europe/Africa and Asia, which could be partially achieved by examining east-west patterns of genetic isolation by geographic distance.

Migratory connectivity has been appraised in only a few insect species but has important conservation implications. In species with weak migratory connectivity and reticular migration patterns, local population bottlenecks can be mitigated through a compensatory demographic model (García-Berro et al., 2023). In contrast, species with stronger migratory connectivity may be more vulnerable to adverse environmental changes in specific sections of their range (Webster et al., 2002). The population of monarch butterflies in North America serves as a good example of this phenomenon. Although

comprised of a single, panmictic population, monarch butterflies show relatively strong migratory connectivity, with monarchs east of the Rocky Mountains remaining largely separate from monarchs to the west (Gao et al., 2020). The monarch butterflies west of the Rockies are at a high risk of local extirpation, likely due to environmental changes in that region (Pelton et al., 2019). However, the strong migratory connectivity of the species largely prevents the larger census size east of the Rockies from bolstering the western numbers (but see Vandenbosch, 2007). Historically, the Afro-Palearctic population of painted ladies has demonstrated demographic stability, albeit with large population fluctuations partially due to outbreak dynamics (García-Berro et al., 2023; López-Mañas et al., 2022). However, in the context of global change, which can influence climate and weather events on a broad scale, even painted lady populations may be impacted. Moderate migratory connectivity across the Sahara may reduce the compensatory abilities of the reticular migration pattern during this part of the annual cycle, leading to increased risk, especially along the eastern and western edges of the geographic range. This is particularly pertinent during Jan. and Feb., when occupancy and spatial extent are at their lowest (Talavera et al., 2023). Future studies quantifying the temporal and spatial migratory connectivity over each segment of the annual migratory cycle are essential for a comprehensive assessment of the compensatory abilities within painted lady migration patterns and how they may be influenced by anthropogenic climate change and habitat degradation.

Northward progression

Our findings provide strong support for long-distance trans-Mediterranean and trans-Saharan migrations during the southward segment of the annual cycle (Figure 3.3H). These extensive migrations likely occur at high altitudes (Stefanescu et al., 2013) and resemble the long-distance autumn migrations of the overwintering generation of monarch butterflies. In contrast, during the spring, monarchs are known to gradually recolonize the USA and Canada in a northward progression over several generations, each covering short distances (Flockhart et al., 2013). Interestingly, our findings suggest a similar trend

in painted ladies, with most spring migrants in our study journeying shorter distances from northern Africa or the Arabian Peninsula (Figure 3.3E-G). This finding reinforces the importance of North Africa as the primary source for spring migrants to Western and Central Europe (Stefanescu et al., 2011), and suggests that the Arabian Peninsula may be an important source for Eastern Europe. However, our sampling was not sufficient to identify definitive trans-Saharan migrants or fully reconstruct the migratory connectivity across the Sahara on the northward segment of the annual cycle. We suspect that most painted ladies migrating north from sub-Saharan Africa undertake shorter journeys to breed in northern Africa or the Arabian Peninsula in late winter, with their offspring subsequently moving into Europe in a gradual northward progression. Painted ladies migrating northwards across the western Sahara must do so against the prevailing northeasterly winds, known as the Harmattan, which may make journeys more energetically costly and, therefore, shorter. Additionally, the similarities in seasonal differences in migratory patterns between painted ladies and monarch butterflies (i.e., long-distance migrations in the autumn and a northward progression in the spring) suggest the presence of comparable environmental cues, such as temperature, photoperiod, and host plant development (Goehring & Oberhauser, 2002), influencing the behaviour of both species. Furthermore, the gradual northward progressions in the spring suggest an adherence to the green wave hypothesis, a phenomenon observed in migratory ungulates (Aikens et al., 2020), bats (Hurme et al., 2022), and birds (Wang et al., 2019), wherein migration closely follows seasonal vegetation growth.

Seasonal leapfrog migration

Leapfrog migration is used to describe a migration pattern commonly found in vertebrates wherein individuals that breed further north migrate beyond other groups to locations further south. Here, we describe a leapfrog migration for one of the segments of the annual migratory cycle of painted lady butterflies. Isotope-based geographic assignment has helped identify similar leapfrog migration patterns in birds (e.g., Nelson et al., 2015). Notably, this study presents some of the first compelling evidence of a

leapfrog migration in insects (but see Hobson et al., 2021). We identified the presence of many long-distance migrants, up to over 3,500 km, from northern and central Europe to West Africa from Aug. through to Nov. (Figure 3.3A-C). In Oct. and Nov., other painted ladies migrate shorter distances from central and southern Europe to the circum-Mediterranean region (Chapter 4). In other words, in autumn, butterflies bred in northern Europe migrate further south than butterflies bred in southern Europe, suggesting a leapfrog migration pattern in the western Afro-Palearctic (Figure 3.4A).

Temporal migration patterns are likely to be the primary driver of the leapfrog migration in painted ladies. We detect a temporal shift in origin in the long-distance migrants from temperate Europe to sub-Saharan Africa, with δ^2H values, a rough proxy for latitude of origin, showing an increase over time; thus, the earliest arrivals to West Africa seem to originate from more northern latitudes (Figure 3.4B). No genetic differentiation has been found between the painted ladies involved in this generational leapfrog migration in the western Afro-Palearctic, pointing to behavioural plasticity as the main mechanism by which painted ladies are cued to fly short or long distances (Chapter 4). Environmental cues in northern Europe (e.g., Scandinavia), such as photoperiod, temperature, and host plant phenology, change earlier in the autumn (i.e., Sep.), and could prompt migratory behaviour (Ethier & Mitchell, 2023; Guerra & Reppert, 2013; Goehring & Oberhauser, 2002). However, the circum-Mediterranean region is not a suitable breeding habitat in Sep. (Talavera et al., 2023), so painted ladies reaching this region must continue further south to suitable breeding grounds in sub-Saharan Africa (Figure 3.3A; Figure 3.4A). In Oct. and Nov., areas in both the circum-Mediterranean region and sub-Saharan Africa contain highly suitable breeding habitat, and so painted ladies of progressively more southern origin can migrate either short or long distances (Figure 3.3B-C; Figure 3.4A). Similar temporal shifts in δ^2H were recently detected in *D. gilippus* and attributed to a leapfrog migration pattern, although a short-distance migratory group was not identified in the study (Hobson et al., 2021). While there are expected additional costs associated with the long-distance migration from northern Europe

to sub-Saharan Africa, such as decreased survival during migration (Newton, 2007), these drawbacks may be outweighed by the advantages of being early arrivals to the region, as has been proposed in the context of birds (Morrison et al., 2019). This advantageous position may bring benefits such as a release from parasites, access to a high abundance of larval host plants, and reduced competition.

The broad spatiotemporal coverage of our sampling on the western side of the range, particularly for the early autumn, facilitated the identification of this leapfrog migration. In contrast, we only have samples from Nov. and Dec. for the easternmost samples, limiting our ability to identify early autumn long-distance movements in that part of the range (Figure 3.3C-D). However, even with these limitations, we were able to detect long-distance migrations from the Eastern Mediterranean to Kenya in Nov. and Dec., providing the first empirical evidence of direct migration from the eastern Palearctic to eastern tropical Africa (Figure 3.3C-D). Additional studies with higher spatiotemporal sampling in central and eastern Africa, as well as in the Arabian Peninsula, will be required to test the possibility of leapfrog migration in the east.

Limitations of the study

While isotope-based estimates of natal origin allowed us to explore the trans-Saharan migratory patterns and migratory connectivity of painted lady butterflies in remarkable detail, some caveats remain. The combination of δ^2H and $^{87}Sr/^{86}Sr$ for geographic assignment provided more specific estimates of natal origin than using a single isotope. However, some individuals exhibited particularly broad estimated areas of natal origin (4 million km^2 on average), often from fragmented and distant areas, due to the redundancy of certain isotopic signatures across the landscape. These nonspecific estimates of natal origin can potentially introduce inaccuracies in downstream metrics, such as estimates of migration distance (Chapter 4; Hallworth et al., 2018). In order to overcome this limitation, we mainly interpreted our results at the population level by overlaying the posterior probability surfaces of multiple individuals and presenting a conservative estimate of migration distance (i.e., minimum

distance) for many individuals. Additionally, in contrast to the findings of Talavera et al. (2018), which relied solely on δ^2H, our approach combining δ^2H and $^{87}Sr/^{86}Sr$ was unable to detect definitive trans-Saharan migrants northwest of the Sahara. Nevertheless, we propose that northward movements from sub-Saharan Africa are still likely to occur, given the large number of painted ladies present in sub-Saharan Africa, compared to North Africa, from Dec. to Feb. (Talavera et al., 2023). To complete the northward migration and connectivity model of painted ladies across the Sahara, future research should concentrate on sampling during late winter (e.g., Feb.) and in locations closer to the northern edge of the Sahara (e.g., Tunisia, Libya), or in the Sahara, to capture northward trans-Saharan migrants.

Methods

Painted lady sample collection

Painted ladies are thought to cross the Sahara twice each year, with one group migrating south in the autumn and the another migrating north in the late winter and early spring (Talavera et al., 2018; Stefanescu et al., 2016; Talavera & Vila, 2016). However, painted ladies have overlapping generations, and thus trans-Saharan migrants do not necessarily migrate at the same time; instead, painted ladies arrive on the far side of the Sahara over a period of weeks or months, the local-scale destinations of which vary between years (García-Berro et al., 2023). To investigate the migratory connectivity of painted lady butterflies, 118 samples were opportunistically collected by the Painted Lady Migration Network, a global citizen science effort, from sites located both south and north of the Sahara from a range of dates to give us the best chance of collecting trans-Saharan migrants (Figure 3.1; Table S3.2).

Hydrogen isotope analysis

Of the 118 samples, the δ^2H of 69 samples have already been reported in the literature (Chapter 4; Talavera et al., 2018; Stefanescu et al., 2016). However, some of these samples were analysed using older standard δ^2H values (ORX: -35.4‰, DS: -172.7‰ and KHS: -54.1‰, CBS: -197‰, respectively). To ensure that these measurements were compatible with the hydrogen isoscape (Ghouri et al., 2023) and with the other samples analysed in this study, the δ^2H values were converted back to the international

standard scale, Vienna Standard Mean Ocean Water - Standard Light Antarctic Precipitation (VSMOW-SLAP), using the *reftrans* function in the *assignR* package in R (Magozzi et al., 2021; Ma et al., 2020).

The non-exchangeable δ^2H of the remaining 49 samples were measured at the Ján Veizer Stable Isotope Laboratory at the University of Ottawa, Canada. Prior to δ^2H analysis, a forewing from each butterfly was soaked, with agitation, in three successive baths (1 h, 30 min., 10 min.) of 2:1 chloroform:methanol solution to remove surficial dust and lipids, which are known to introduce error into δ^2H measurements (Hobson et al., 2017; Paritte & Kelly, 2009), and then dried in the laboratory oven at 50 °C for over 24 h. Samples were carefully cut from the wing to reduce intra-individual variation from differing pigmentation (Hobson et al., 2017) and the presence of wing veins (Lindroos et al., 2023). Samples were then weighed (0.150 ± 0.010 mg) into silver capsules and loaded into a zero-blank autosampler (Thermo, Germany). All measurements were taken using high temperature (1,400 °C) flash pyrolysis (TCEA, Thermo Finnigan, Germany) with a helium carrier passed through a chromium-filled reactor and, after separation, introduced via a Conflow IV interface (Thermo Finnigan, Germany) into a Delta V Plus IRMS (Thermo Finnigan, Germany).

Two different analytical methods were used. The first 41 samples were subjected to the equilibration with dual waters approach, following the methodology outlined in Meier-Augenstein et al. (2011). The non-exchangeable δ^2H of the final 8 samples were determined using the comparative equilibrium approach, as in Bataille et al. (2022). To maintain uniformity and ensure consistency across these analytical protocols, we selected 20 insect samples for duplicate analysis using both protocols (i.e., comparative equilibrium and equilibration with dual waters). Through this comparative analysis, a calibration equation was developed between the two methods (Figure S3.7) and used to ensure all δ^2H values were on the same scale. All new sample δ^2H are reported based on a three-point calibration using: CBS (caribou hoof; -157 ± 0.9‰; Soto et al., 2017), KHS (kudu horn; -35.3 ± 1.1‰; Soto et al., 2017), and USGS43 (human hair; -44.4 ± 2.0‰; Coplen & Qi, 2012). To assess the quality of the

measurements, one keratin reference standard, USGS42 (human hair; measured: -75.3 ± 0.5‰, n=4; standard: -72.9 ± 2.2‰ (Coplen & Qi, 2012)), as well as two in-house chitin standards, ground and homogenised *Lymantria dispar dispar* (measured: -64.4 ± 1.8‰, n = 6; long-term average: -64 ± 0.8‰) and Alfa Aesar chitin (measured: -22.8 ± 0.7‰, n = 4; long-term average: -22 ± 1.2‰), were measured as internal standards. Based on within-run replicates of the internal standards and repeated sample measurements, the precision of all measurements is estimated to be about ± 2‰. All reported δ^2H values are normalised to the VSMOW-SLAP standard scale.

Strontium isotope analysis

Of the 118 samples, the $^{87}Sr/^{86}Sr$ of 18 samples have already been reported (Chapter 4). The $^{87}Sr/^{86}Sr$ analyses for the remaining samples were performed in three analytical batches at different facilities. To prepare the first batch of 25 samples, a single forewing was washed in a 2:1 v/v chloroform:methanol solution in two successive washes. This solution-based cleaning protocol removes surficial dust similarly to cleaning with pressurized nitrogen gas (Chapter 2) but has a higher risk of Sr contamination (Chapter 1). Therefore, the nitrogen gas protocol was chosen for future batches. Three of these samples were digested in 4 mL of 16 M HNO_3 using a MARS 6 microwave digestion system (CEM Corporation, USA). The rest of the samples were digested at 100 °C for 48 h on a hot plate using 1 mL HNO_3. All samples had 1 mL H_2O_2 added to complete digestion. The separation of Sr was performed in microcolumns loaded with 125 µL of Dowex AG50W-X8 cation resin. The matrix was rinsed out using 7 M HNO_3 and Sr was collected with H_2O. The first batch was measured at the Queen's Facility for Isotope Research at Queen's University, Canada, in Jan. 2019 using a NeptuneTM multi-collector inductively coupled plasma mass spectrometer (MC-ICP-MS; ThermoScientific, Bremen, Germany) coupled to a Micro-FAST syringe injection system. The reproducibility of the $^{87}Sr/^{86}Sr$ measurement was 0.71020 ± 0.00006 (1 SD, n = 29) for 1 ppb NIST SRM987.

To prepare the second and third batch for $^{87}Sr/^{86}Sr$ analysis, a single forewing from each butterfly was cleaned using pressurized nitrogen gas for 2 min. at 10 psi to remove any surface contaminants (e.g., dust; Chapter 2). The wings were then digested using microwave digestion (Anton Paar Multiwave 7000; Austria) in 1 mL HNO_3 (16 M; distilled TraceMetal^{TM} Grade; Fisher Chemical, Canada). The separation of Sr was processed using a protocol described in L. Hu et al. (2020a). The remaining steps, including temperature adjustment and duration, aliquot preparation, and analysis for Sr content via inductively coupled plasma mass spectrometry (ICP-MS; Agilent 8800 ICP-QQQ, Agilent Technologies Inc., CA, USA), were consistent with the procedures outlined in Chapter 4. Calibration standards were prepared using single-element certified standards obtained from SCP Science (Montreal, Canada). After separation, eluates were dried and re-dissolved in 200 µL 2% v/v HNO_3 for $^{87}Sr/^{86}Sr$ analysis. The second batch (n = 16) was measured at GEOTOP-UQAM in Montreal, Canada in Jul. 2021 with a Nu-Plasma II MC-ICP-MS (Nu Instruments) coupled to a desolvating nebulizer (Aridus II, CETAC Technologies). The reproducibility of the $^{87}Sr/^{86}Sr$ measurement was 0.71022 ± 0.00006 (n = 6) for 5 ppb NIST SRM987 and 0.71022 ± 0.00002 (n = 14) for 25 ppb NIST SRM987. The reproducibility of an in-house pure Sr standard was 0.70815 ± 0.00002 (n = 4). The third batch (n = 59 plus the 18 samples presented in Chapter 4) was measured at the Pacific Centre for Isotopic and Geochemical Research at the University of British Columbia, Canada, in Dec. 2021 using a Nu-Plasma II MC-ICP-MS (Nu Instruments) coupled to a desolvating nebulizer (Aridus II, CETAC Technologies). The reproducibility of the $^{87}Sr/^{86}Sr$ measurement for 5 ppb NIST SRM987 was 0.71025 ± 0.00009 (n = 138) and 0.71019 ± 0.00011 (n = 48) for 1.4 ppb NIST SRM987. A matrix-matched chitin internal standard, 5 ppb Alfa Aesar chitin, was also used (0.713959 ± 0.00009; n = 3). Procedural blanks were negligible.

Instrumental mass fractionation was corrected by normalizing $^{86}Sr/^{88}Sr$ to 0.1194 using the exponential law (Moore et al., 1982). The isotopes ^{84}Sr, ^{86}Sr, and ^{87}Sr have isobaric interferences from ^{84}Kr, ^{86}Kr, and ^{87}Rb, respectively, and, in all cases, were corrected for using the ^{85}Rb and ^{83}Kr signals.

Bioavailable strontium isoscape for the Afro-Palearctic

Strontium isotope compilation for the Afro-Palearctic region

All statistical analyses were performed in R v4.3.2 (R Core Team, 2021). We compiled 8,755 bioavailable $^{87}Sr/^{86}Sr$ measurements from Europe, the Middle East, and Africa from 308 literature studies (see Data Availability Table). Our literature compilation encompasses 35 more studies specific to the Afro-Palearctic range compared to Bataille et al. (2020). In the majority of cases, geographic coordinates were reported by the authors in the publication. When geographic coordinates were not included, we used Google Earth to georeference geographic information for each sample by using locality names and maps. The method of georeferencing and its associated uncertainty are reported in our metadata. When needed, authors were contacted for clarification purposes regarding sample locality. We converted all data to decimal degrees for consistency.

We contributed an additional 45 plant $^{87}Sr/^{86}Sr$ measurements from Africa to the literature compilation. Using the compilation from the literature, we identified critical spatial data gaps and filled them by procuring plant samples from the collection of the Institut Botànic de Barcelona (IBB, CSIC) with precise georeferencing and metadata (Figure S3.1). Plant samples were selected to maximise geological variability over the study area. The selected plants are from various taxa (mostly the Asteraceae family with some Malvaceae and Urticaceae) and were sampled from 12 countries in Africa between 2014 and 2021. We subsampled ~1 g of plant tissue per sample location, pooling 2 to 5 plants for each location. We cleaned the plants to remove all surface mineral dust by placing the cut sample in distilled deionized (DDI) water in the ultrasonic bath for 15 min. The plants were then rinsed another 2 times with DDI water and with ultrapure deionized H_2O (18.2 MΩ·cm @ 25 °C). Plant samples were then dried in the oven at 70 °C. We digested the plant samples using microwave digestion, analysed their Sr concentrations, isolated their Sr, and determined their $^{87}Sr/^{86}Sr$ using preparation protocols and analytical approaches identical to those described for the painted lady butterfly samples. All our plant

samples underwent $^{87}Sr/^{86}Sr$ analysis at the Pacific Centre for Isotopic and Geochemical Research at the University of British Columbia.

Altogether, the dataset greatly improves the number of samples available for Africa, relative to Bataille et al. (2020) (n = 1820 vs n = 939). While the coverage is greatly improved, the sampling density varies across the study area with a higher density of bioavailable $^{87}Sr/^{86}Sr$ data in Europe (Figure S3.1). The dataset displayed a wide range of $^{87}Sr/^{86}Sr$ spanning from 0.70250 to 0.82636 with bioavailable $^{87}Sr/^{86}Sr$ ranging between 0.70403 and 0.78848 in Africa.

Auxiliary variables for the regression models

We assembled a catalog of 28 environmental and climatic geospatial data known to influence bioavailable $^{87}Sr/^{86}Sr$ variation according to Capo et al. (1998) and Bataille et al. (2020) (Table S3.1). We used the same ensemble of variables as in Bataille et al. (2020) to represent geology, soil properties, relief, climate, and agricultural activity and introduced new atmospheric deposition variables, including volcanic ash (Serna et al., 2020), aerosols (Chien et al., 2016), and anthropogenic deposition (Capo et al., 1998). We reprojected and resampled each of these variables into WGS84-Eckert IV at 1 km resolution. Using the sample locations from our $^{87}Sr/^{86}Sr$ metadata compilation, we extracted the local pixel values for each of these 28 tested predictors.

We used the *VSURF* package (Variable Selection Using Random Forest) to optimise and identify the most important predictors of bioavailable $^{87}Sr/^{86}Sr$ from the 28 variables (Genuer et al., 2015). Fourteen dominant variables were identified to predict bioavailable $^{87}Sr/^{86}Sr$ across the Afro-Palearctic range (Figure S3.2; Figure S3.3A). These predictors are similar to those selected in previous efforts to map bioavailable $^{87}Sr/^{86}Sr$ in other study areas (e.g., Chapter 2; Kramer et al., 2022; Janzen et al., 2020; Bataille et al., 2020, 2018). As in many other regions, geological variables, including the age of the underlying terranes or geological units and the predicted bedrock $^{87}Sr/^{86}Sr$, dominate, reflecting the influence of age and lithology (Bataille & Bowen, 2012), with younger and more mafic geological units

transmitting lower ratios to ecosystems than older more felsic units (Figure S3.2B; Figure S3.2I). Soil properties, notably pH and clay content, show strong relationships with bioavailable $^{87}Sr/^{86}Sr$ with higher soil pH and lower clay content usually corresponding with lower bioavailable $^{87}Sr/^{86}Sr$ because more alkaline soils often reflect carbonate-dominated underlying bedrock with lower $^{87}Sr/^{86}Sr$ (Capo et al., 1998; Figure S3.2F; Figure S3.2H). As expected for this desert-dominated region, the deposition of dust aerosols is an important contributor to bioavailable $^{87}Sr/^{86}Sr$ with higher dust inputs corresponding to high bioavailable $^{87}Sr/^{86}Sr$ (Bataille et al., 2020; Janzen et al., 2020; Figure S3.2G). Higher sea salt aerosol deposition leads bioavailable $^{87}Sr/^{86}Sr$ to converge toward the seawater ratios of 0.7092 (Bataille et al., 2020; Figure S3.2C). Interestingly, several of the newly incorporated atmospheric deposition variables were selected as important predictors of bioavailable $^{87}Sr/^{86}Sr$ and reflect the key inputs of black carbon (Hartman & Richards, 2014; Capo et al., 1998; Figure S3.2D) and volcanic ash (Serna et al., 2020; Figure S3.2A) on soils.

Machine-learning regressions

We first predicted bioavailable $^{87}Sr/^{86}Sr$ data across the Afro-Palearctic region using random forest regression (RF) through the *caret* package (Kuhn, 2008) using the framework of Bataille et al. (2020). This framework used the bioavailable $^{87}Sr/^{86}Sr$ compilation and the 14 dominant predictors identified by *VSURF* to predict bioavailable $^{87}Sr/^{86}Sr$ across the Afro-Palearctic. One of the known issues with RF is the absence of consideration of spatial dependence structure in the data. Several approaches have been proposed to solve this issue including adding "geographical features," such as buffer or oblique distances (Hengl et al., 2018), or combining multi-scale RF models (Georganos et al., 2021). Bataille et al. (2020) demonstrated how RF produces overly confident predictions and extrapolation in data-poor regions.

To address some of these challenges, we use a novel framework for modelling bioavailable $^{87}Sr/^{86}Sr$ (Le Corre et al., *in review*) by applying a spatial interpolation ensemble machine-learning

regression (EML) approach through the *landmap* package (Hengl et al., 2021). The *landmap* framework accounts for spatial dependency by incorporating buffer distances around each point as covariates in the regression while keeping computational needs limited by using oblique distances and PCA to summarise those spatial dependencies. To further account for spatial dependency and geographic sampling biases, the modelling framework applies a spatial cross-validation approach. Additionally, EML combines a series of machine-learning algorithms, or learners, through the use of a meta learner. This combination improves the performance and robustness of the model by limiting the biases of using a single algorithm (e.g., RF). Following Le Corre et al. (*in review*), we used the training dataset and the predictors selected by the RF regression analysis to apply the spatial interpolation EML. We used the default setting to make predictions where the meta-learner is generated from the linear model from five independently-fitted learners including RF, optimised distributed gradient boosting, support vector machines, neural network, and lasso and elastic-net regularized generalised linear models. The *landmap* framework generates mean prediction maps, which represent the best estimate of bioavailable $^{87}Sr/^{86}Sr$, as well as prediction errors. These prediction errors were obtained through quantile forest regression, implemented in *landmap* via the *forestError* package (Lu & Hardin, 2021), and estimated from the lower and upper 67% quantile (~1 standard deviation on the Gaussian distribution). To ensure that the uncertainty estimates were conservative, we added an estimate of intra-site variation (i.e., 0.001) to the prediction errors.

The n-fold cross validation of the spatial interpolation EML demonstrated slightly superior performance to the RF framework (RSME = 0.0029, R2 = 0.74 (Figure S3.3C) vs. RMSE = 0.0031, R2 = 0.73 (Figure S3.3B)). The EML isoscape algorithm incorporates spatial dependencies and uses an unbiased spatial cross-validation approach leading to more robust uncertainty estimates (Le Corre et al., *in review*; Hengl et al., 2021). However, this approach is best applied for local to regional bioavailable

$^{87}Sr/^{86}Sr$ predictions as computational time becomes prohibitive for large datasets (Le Corre et al., *in review*; Hengl et al., 2021).

Isotope-based geographic assignment

The natal origin of each of the painted lady samples was estimated using continuous-surface isotope-based geographic assignment via the *assignR* package (Ma et al., 2020) in R v4.3.2 (R Core Team, 2021). First, a growing-season amount-weighted precipitation isoscape, sourced from waterisotopes.org, using the OIPC v3.2 from Bowen et al. (2005), was calibrated to butterfly wing tissue using the linear relationship between precipitation and a calibration dataset of residential butterflies from across Europe and Africa (Ghouri et al., 2023), resulting in a wing chitin hydrogen isoscape ($\delta^2H_{wing} = 0.80\ (\delta^2H_{GSP}) - 39.80$, $r^2 = 0.53$). The isotopic signature of each unknown-origin painted lady was then compared, using a normal probability density function, to the butterfly wing tissue hydrogen isoscape and the aforementioned bioavailable strontium isoscape to estimate the probability that each pixel of the isoscapes was the natal origin. The resulting posterior probability surfaces were summarised into binary surfaces using a 2:1 odds ratio, where the top third of the probability distribution was re-coded as highly probable (i.e., 1) and the remaining pixels were re-coded as low probability (i.e., 0). A conservative estimate of migration distance, minimum distance, was measured as the shortest distance from the capture location to the highly probable area of natal origin. Next, we screened for butterflies that had a high probability of originating from their capture location or had a minimum distance of less than 100 km. These butterflies are either (1) local or regional butterflies that have developed in the capture area, or (2) migrants from a far-off location that has the same isotopic signature as the capture. After filtering out the putative locals, the migratory trajectories of 59 migrants were assessed. Binary surfaces were summed and then normalised by the number of individuals, resulting in maps representing the proportion of individuals with a high probability of originating from each pixel. Finally, a modification of

the *wDist* function of the *assignR* package was used to estimate the direction that was travelled using a distance-weighted probability density function.

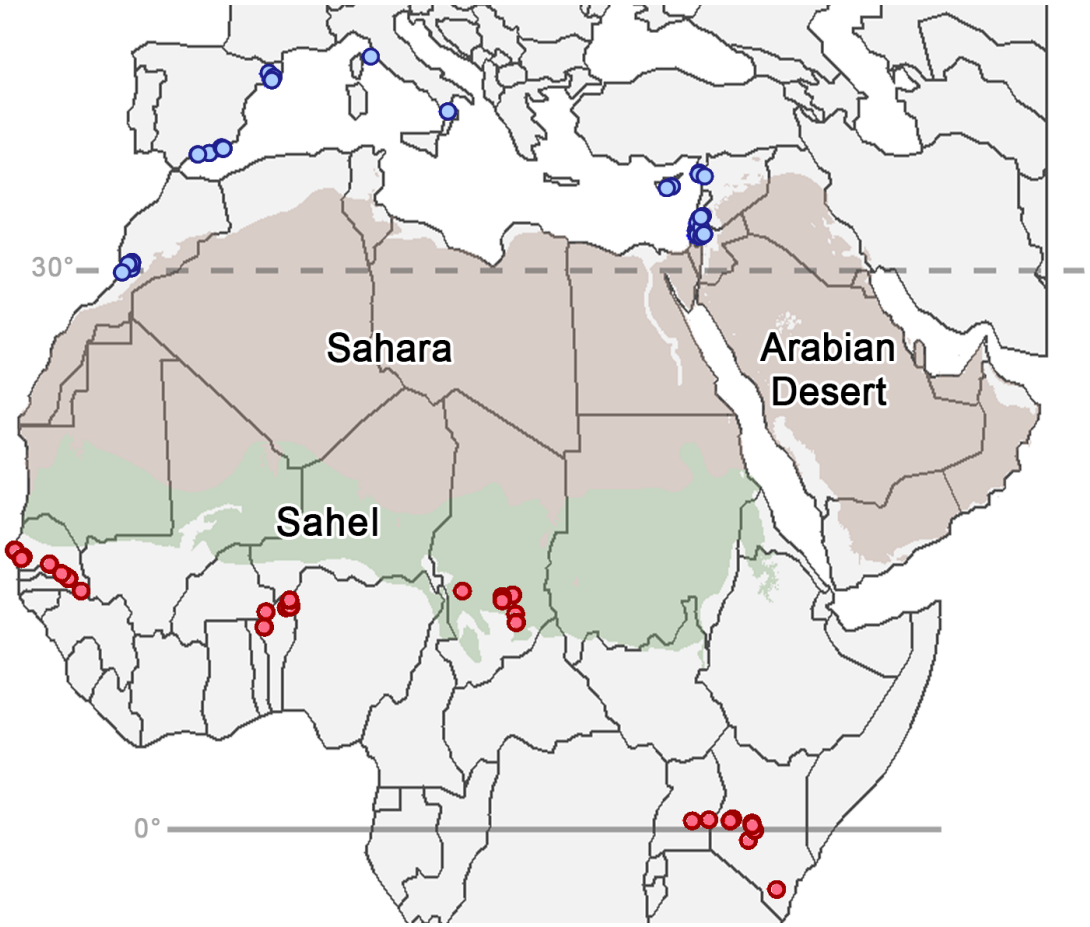

Figure 3.1 Collection sites for painted lady butterflies (n = 118). Butterflies were collected north of the Sahara, encompassing regions in Morocco, Spain, Cyprus, Italy, Israel, Jordan, and Syria, from Jan. to Apr. in 2012, 2016, 2017, and 2019 (blue dots). These butterflies represent northward-migrating painted ladies, based on our current understanding of seasonal patterns of suitable habitat (Talavera et al., 2018, 2023; Menchetti et al., 2019). To portray southward-migrating butterflies, samples were collected south of the Sahara at multiple sites in Senegal, Benin, Chad, Uganda, and Kenya, spanning the months of Aug. through Dec. in 2014, 2017, 2018, and 2019 (red dots; see details in Table S3.2). Desert outlines were sourced from Dinerstein et al. (2017).

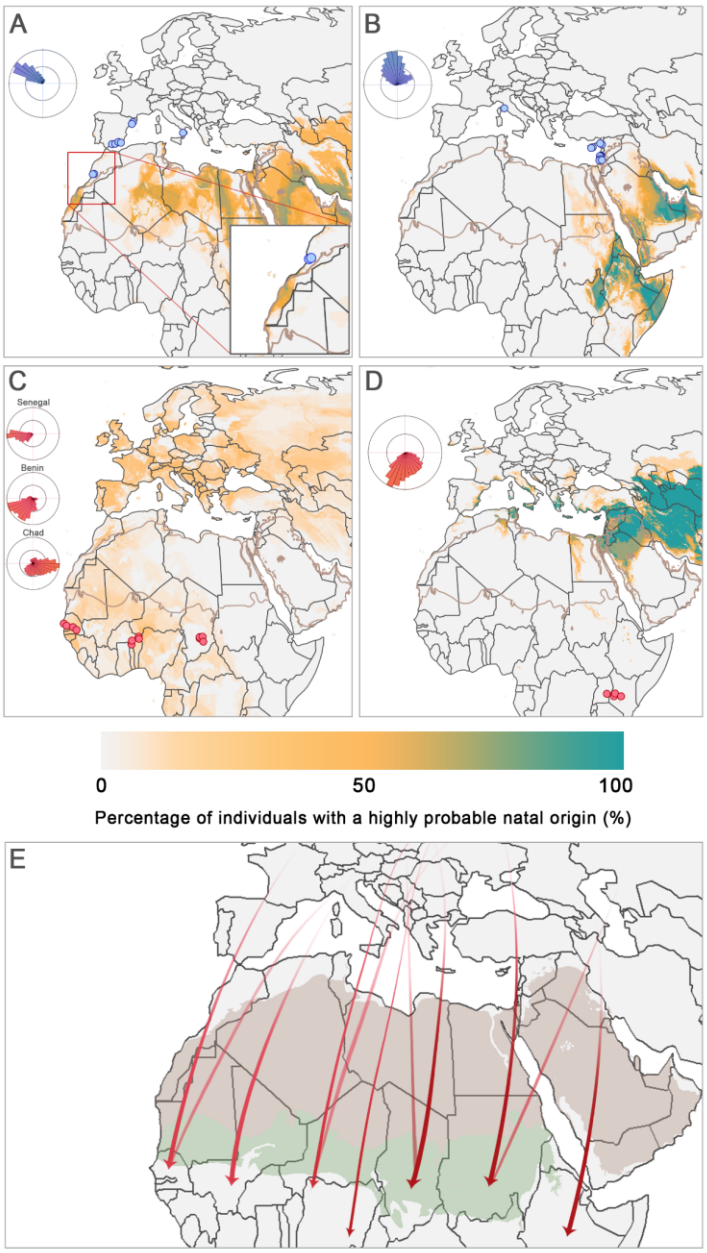

Figure 3.2 Summarised posterior probability surfaces from the δ^2H and $^{87}Sr/^{86}Sr$-based geographic assignment, illustrating the proportion of migratory individuals with a high probable natal origin at a given location, as defined by the 2:1 odds ratio. Teal areas indicate high cohesion in the estimated area of natal origin. The inset rose plots depict the combined probability-weighted estimates of the direction from the estimated natal origin (centre) to the capture location. Red (south of the Sahara) and blue (north of the Sahara) circles represent butterflies that were captured from **(A)** northwest of the Sahara in late winter/early spring (n = 17). The inset map highlights the high probability area of estimated natal origin in the Canary Islands and Western Sahara; **(B)** northeast of the Sahara in late winter/spring. Included is a long-distance migrant from Italy that clustered with the northeast captures (n = 13); **(C)** southwest of the Sahara in the late summer/early autumn (n = 24), and **(D)** southeast of the Sahara in late autumn (n = 5). **(E)** An illustration of the hypothesised broad-front migration pattern with moderate migratory connectivity across the Sahara.

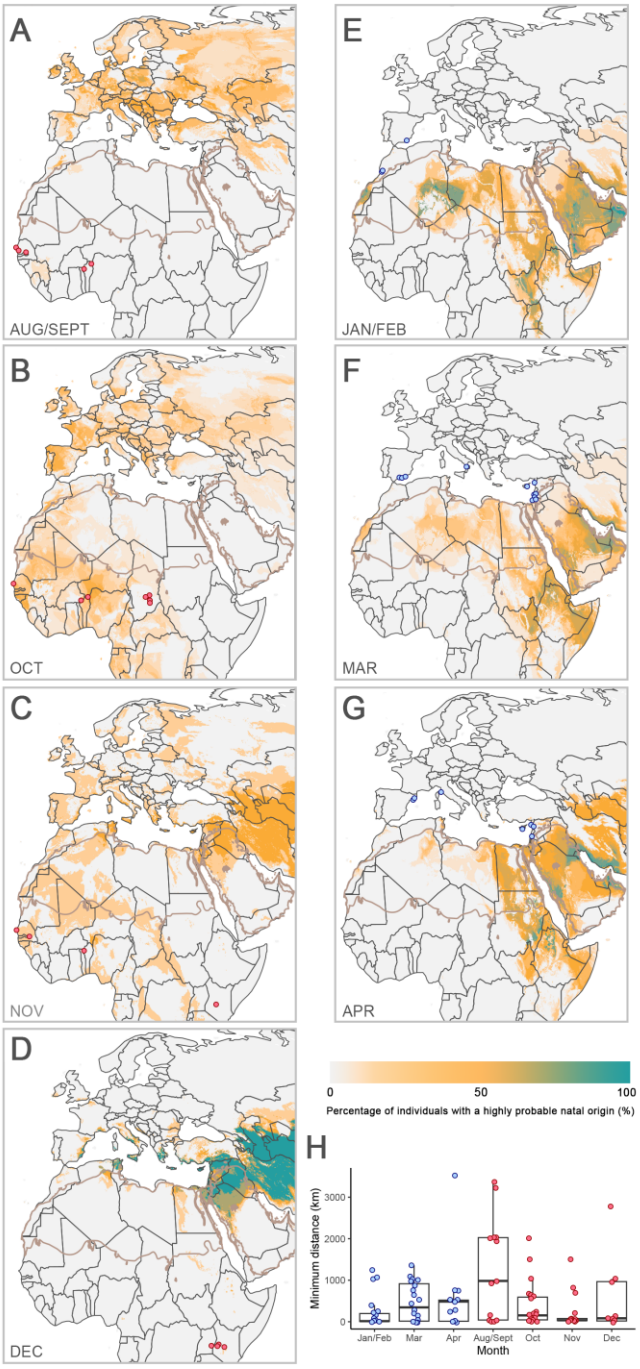

Figure 3.3 Summarised posterior probability surfaces from δ^2H and $^{87}Sr/^{86}Sr$-based geographic assignment, illustrating the proportion of migratory individuals with a high probable natal origin at a given location, as defined by the 2:1 odds ratio, organised by month. Red (south of the Sahara) and blue (north of the Sahara) circles represent individuals captured during **(A)** Sep. (n = 8) from Benin and Senegal, **(B)** Oct. from Senegal, Benin and Chad (n = 13), **(C)** Nov. from Senegal, Benin, and Kenya (n = 4), and **(D)** Dec. captured in Uganda and Kenya (n = 4), **(E)** Jan. (n = 1) and Feb. (n = 6) from Spain and Morocco, **(F)** Mar. from Spain, Italy, Cyprus, Israel, Jordan, and Syria (n = 13), and **(G)** Apr. from Spain, Italy, Cyprus, Israel and Syria (n = 10). **(H)** Minimum migration distance (km) estimates for all painted lady samples (n = 118).

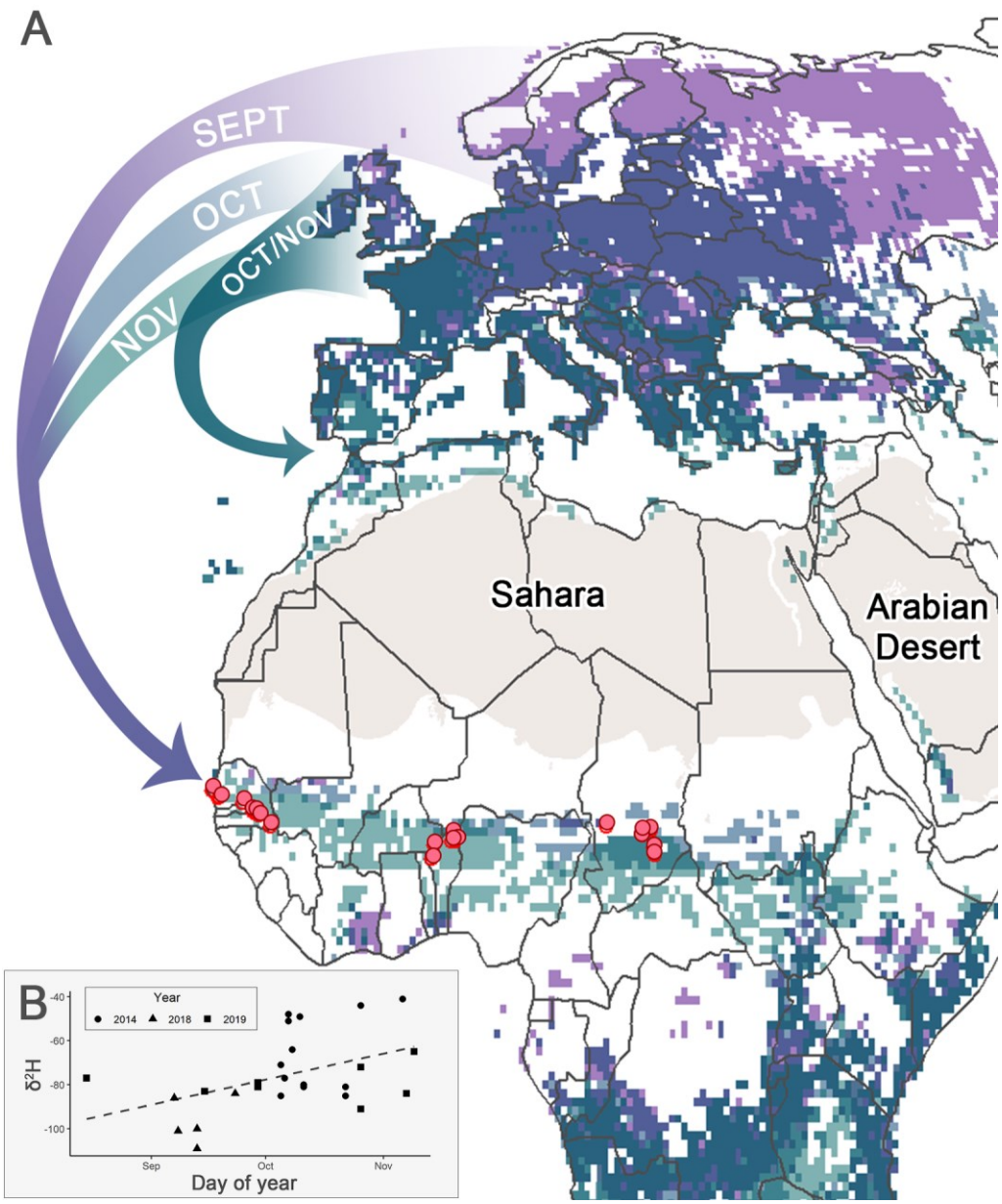

Figure 3.4 Leapfrog migration pattern in the southward trans-Saharan segment of the annual migratory cycle in the Afro-Palearctic. **(A)** Conceptual model illustrating the proposed southward leapfrog migration. The map presents overlapping monthly representations of suitable breeding habitats (P > 95%) sourced from Talavera et al. (2023). In Sept., painted ladies originating from suitable habitats (indicated in purple) migrate to sub-Saharan Africa. In Oct. (suitable habitat indicated by blue) and Nov. (turquoise), painted ladies from progressively southern locations migrate to either the circum-Mediterranean region or sub-Saharan Africa. **(B)** Hydrogen isotope values (‰) of migrants captured in Senegal, Benin, and Chad (red circles in Figure 3.4A) during the autumn (n = 44; $\delta^2H = 0.38(DOY) - 7600$; $R^2 = 0.24$; $p < 0.001$;). Symbols indicate the sampling year.

Chapter 4: Intercontinental panmixia despite distinct migration distances in the trans-Saharan butterfly migrant *Vanessa cardui*

Megan S. Reich*, Daria Shipilina*, Venkat Talla, Farid Bahleman, Khadim Kébé, Johanna L. Berger, Niclas Backström, Gerard Talavera, Clément P. Bataille

*co-first authors

Note: This manuscript is in preparation for submission and has been formatted accordingly

Contribution

I led the writing of the manuscript with substantial contributions from DS and input from all co-authors. CB and GT conceived the idea for the study and organized the sample collection. GT, FB, KK, and I collected the samples. I led the isotope analysis component with input from CB. DS led the genomic analysis component with my help (I did the PCA and admixture analysis) and additional input from GT, VT, and NB. JB did the landmarking for the geometrics morphometrics analysis, and I did the data analysis component.

Abstract

The painted lady butterfly *Vanessa cardui* is renowned for its virtually cosmopolitan distribution and the remarkable long-distance migrations that are part of its annual, multigenerational migratory cycle. In the autumn, *V. cardui* individuals are found north and south of the Sahara, suggesting distinct migratory behaviours within the species. However, the evolutionary and ecological factors shaping these differences in migratory behaviour remain largely unexplored. Here, we performed whole-genome resequencing and analysed the hydrogen and strontium isotopic signatures of 40 *V. cardui* individuals simultaneously collected in the autumn from regions both north and south of the Sahara. Our investigation revealed two main migratory groups: (i) short-distance migrants, journeying from

temperate Europe to the circum-Mediterranean region and (ii) long-distance migrants, originating from temperate Europe, crossing the Mediterranean Sea and Sahara, and reaching West Africa, covering a distance of up to over 4,000 km. Despite these stark differences in migration distance, a genome-wide analysis of 813,810 single nucleotide polymorphisms (SNPs) revealed that both short- and long-distance migrants belong to a single intercontinental panmictic population extending from northern Europe to sub-Saharan Africa. Contrary to common biogeographic patterns, the Sahara is not a catalyst for population substructuring in this species. No significant genetic differentiation or signs of adaptation and selection were observed between the two migratory phenotypes (pairwise F_{ST} = 0.001 ± 0.006). Nonetheless, two individuals, belonging to the early arrivals to the Afrotropical region and covering longer migration distances, exhibited some genetic differentiation. The lack of genetic structure between short- and long-distance migrants suggests that migration distance in *V. cardui* is a plastic response to environmental conditions.

Introduction

Migration has evolved several times in insects (Dingle & Drake, 2007) and is often viewed as an advantageous adaptation, as insects move to favourable environmental conditions, exploit seasonal resources, and escape parasites and predators (J. W. Chapman et al., 2015). Many migratory animals show variation in migratory behaviour that results in distinctive spatiotemporal movement patterns. As an innate behaviour in insects, the proximate mechanisms for migration are likely held in the genome (Merlin & Liedvogel, 2019; Dingle, 2014b), but the environmental and genetic factors driving intraspecific variation in insect migratory behaviour are only beginning to be understood (A. K. Shaw, 2020).

The painted lady butterfly *Vanessa cardui* is renowned for its obligate, annual, multi-generational migratory cycles throughout Africa, Asia, Europe, and North America (Shields, 1992; Williams, 1970). As part of a migratory cycle covering between 8 and 10 generations and involving both

the Palearctic and Afrotropical regions, late summer and autumn generations migrate southward from temperate Europe towards more suitable breeding grounds. While a substantial portion of these southward migrating butterflies journey across the Mediterranean Sea and Sahara to subsequently breed in sub-Saharan Africa (Talavera et al., 2023; Stefanescu et al., 2016; Talavera & Vila, 2016), others migrate to the circum-Mediterranean region (Menchetti et al., 2019; Stefanescu et al., 2013). The factors driving these differences in migratory behaviour, resulting in the disjunct winter distribution of *V. cardui* across the Sahara (Talavera et al., 2023), remain unknown.

Migratory phenotypes include observable characteristics such as migratory propensity, timing, orientation, and wing morphology (Turbek et al., 2018). However, migratory behaviours are complex traits and are therefore difficult to quantify, especially in insects. The distance an individual butterfly covers during migration is a consequence of this complex phenotype, which creates a distribution of migration distances across individuals, reflecting the extent of the species' ecological niche. In cases where the suitable niche is geographically continuous, it is expected that individuals at the extremes of the migration distance distribution (i.e., those who migrate the shortest or longest possible distances) are selected against due to the inherent risks associated with extremes. In such scenarios, stabilising selection may favour migrants that cover intermediate distances. Conversely, when the suitable niche is fragmented by large biogeographic barriers, such as the Sahara, extreme migration distances may be favoured by disruptive selection. Selection for specific migration distances can have important repercussions for survival and growth. For example, pronounced climatic differences between regions north and south of the Sahara influence the composition and quantity of host plant species, predators, parasitoids, and weather events, as well as influencing development time (Talavera et al., 2023). Altogether, this scenario leads us to ask: can we detect the action of adaptive evolutionary forces acting on the extremes of the migration distance distribution and effectively disentangle their action from neutral evolutionary processes?

Differences in migratory routes, distances, and orientation have led to genetic differentiation and subsequent divergent selection in multiple bird species, such as the European blackcap *Sylvia atricapilla,* Swainson's thrush *Catharus ustulatus,* and willow warbler *Phylloscopus trochilus* (Sokolovskis et al., 2023; Delmore et al., 2020, 2012; Mueller et al., 2011). Likewise, differences in migration distance could lead to similar spatiotemporal separation of *V. cardui* lineages, resulting in reduced genetic exchange between *V. cardui* that migrate across the Sahara and those that remain in the circum-Mediterranean region, thus leading to genetic differentiation. However, exploring the genetic underpinnings of natural variation in migratory behaviour requires not only whole-genome sequencing data, but also accurate migratory phenotyping (Merlin & Liedvogel, 2019). Studies on insect migration have lagged behind those of birds and mammals because identifying migratory phenotypes in insects is challenging (Liedvogel et al., 2011). Extrinsic markers such as biologgers commonly record migratory trajectories for birds and mammals, but few studies have used these techniques on insects (but see Menz et al., 2022; S. M. Knight et al., 2019; Wikelski et al., 2006) because insects are generally too small, short-lived, and numerous for these techniques to be applied on a large scale. Instead, studies on insects have mainly relied on observations of physiological state (e.g., wing wear scores), behaviour (e.g., insect-monitoring radar), or regional field monitoring (e.g., spatiotemporal location).

Fortunately, naturally-occurring isotopes are intrinsic markers that have proven increasingly useful for estimating the geographic origin of wild-caught insect migrants and have the potential to identify migratory phenotypes. Isotope geolocation relies on the observation that insect larvae ingest local environmental isotopic signatures through their diet and incorporate these isotopic signatures into their developing tissues (Flockhart et al., 2015; Hobson et al., 1999). Insect wings are relatively inactive tissues and largely preserve the isotopic signature of the natal environment (Chapter 1; Lindroos et al., 2023). Thus, the isotopic signature of the wing of a wild-caught insect can be measured and then compared to a spatial model of isotopic variation (i.e., an isoscape) to estimate the insect's natal origin,

a process known as geographic assignment. However, single isotope-based geographic assignment generally yields broad and unspecific regions of natal origin, making it challenging to calculate downstream estimates, such as migration distance. More spatially-constrained estimates of natal origin can be obtained by combining multiple isotopes with complementary patterns (Chapter 2). Dual isotope-based geographic assignment combining hydrogen isotope values (δ^2H), driven by climatic variables (e.g., precipitation; Hobson et al., 1999; Wassenaar & Hobson, 1998), and strontium isotope ratios ($^{87}Sr/^{86}Sr$), primarily driven by geological processes (e.g., bedrock type and age; Bataille et al., 2020), have previously been used to classify migratory behaviours in birds and bats (e.g., Crowley et al., 2021; Kruszynski et al., 2021). However, isotopes have not often been leveraged to phenotype migratory behaviour and investigate the potential genomic drivers of variation in insect migratory behaviour.

Here, we combined isotope-based phenotyping of migration distance with whole-genome resequencing data to investigate the mechanisms driving variation in migratory behaviour for *V. cardui* individuals. By coupling δ^2H and $^{87}Sr/^{86}Sr$ into a dual geographic assignment framework, we estimated the natal origin and migration distance of 40 adult *V. cardui* synchronously collected from north and south of the Sahara in the autumn. A genome-wide population resequencing approach was used to investigate potential genetic structuring associated with contrasting migratory phenotypes. This study endeavours to shed light on the underlying factors shaping the remarkable trans-Saharan migratory journeys of *V. cardui*.

Results

Isotope-based phenotyping reveals differences in migration distance

We estimated the natal origins of 40 *V. cardui* of unknown-origin captured during the autumn southward migration from both north (i.e., Morocco, Spain, Portugal, Malta) and south (i.e., Benin, Senegal) of the Sahara using δ^2H and $^{87}Sr/^{86}Sr$ following Chapter 2's geographic assignment framework

(Figure 4.1D; Table S4.1). From the posterior probability surfaces, we then calculated a conservative estimate of migration distance (i.e., minimum distance).

Based on migration distance, all individuals were grouped into three categories: (i) long-distance migrants (n = 13, 33%; with minimum migration distances ranging from over 500 to over 4,000 km), (ii) short-distance migrants (n = 3, 7%; with minimum migration distances ranging from over 140 to over 240 km), and (iii) individuals of putatively local origin (n = 24, 60%; having potentially travelled less than 100 km) (Figure 4.1C). Isotopic signatures corresponding to long-distance migrations were found exclusively in individuals captured south of the Sahara, specifically in Senegal and Benin. Based on the summarised posterior probability surfaces, these individuals seemed to originate either from northwestern Africa or Europe, notably from Portugal, Spain, France, or Sweden (Figure 4.1B). However, some of the individuals (n = 6, representing 32% of the south of the Saharan sample; Figure 4.1E) had a high probability of originating from areas near their capture points (< 100 km) and were designated as "putative locals." Notably, no individuals from south of the Sahara were classified in the short-distance migration category.

Among the samples collected north of the Sahara, some belonged to the short-distance migration category (n = 3, 14%; Figure 4.1A). However, the majority of these samples exhibited isotopic signatures consistent with putatively local origin (n = 18, 86%; Figure 4.1E). The isotope-based analysis doesn't clarify whether this local signature indicates (i) pre-migratory, locally-sourced offspring of early immigrants to the region or (ii) immigrants from a distant region with an isotopic signature similar to their capture location. We also considered natural history observations to interpret these patterns. The majority of individuals collected in the circum-Mediterranean region during Oct. and Nov. are likely the descendants of earlier arrivals to the collection area. This inference is substantiated by the favourable breeding conditions in the region during late Sep. and Oct. (Talavera et al., 2023; Menchetti et al., 2019), as well as the observed presence of eggs, larvae, and recently-emerged adults (i.e., expelling meconium)

at the time of collection in Morocco, Malta, and Portugal. Thus, we categorize any samples with a high probability of originating near their capture location as putative locals.

To assess the genomic differentiation between migratory phenotypes, it is crucial to integrate the isotopic signature data with spatiotemporal information from individual samples. Consequently, for subsequent analysis, we grouped individuals that travelled long distances from Senegal and Benin, explicitly excluding individuals with putatively local origins, into the "long-distance" group. To balance sample sizes, we grouped individuals from north of the Sahara, encompassing both the short-distance (n = 3) and putatively local categories (n = 18), into the "short-distance" group, operating under the assumption that these putative locals are the next-generation offspring of short-distance migrants.

Wing morphology and wear are uncorrelated with migration distance

Wing wear scores, a metric scaled from 1 (fresh) to 5 (extremely worn), are often used as a proxy for butterfly age and migratory status (Stefanescu et al., 2016; Flockhart et al., 2013; Miller et al., 2012). The wing wear scores in our study ranged from 2 (few scales lost) to 5 (extremely worn); samples with wing wear scores of 1 were initially screened out of our study as they are expected to be recently-emerged, pre-migratory individuals. These wing wear scores showed no correlation with migration distance (Spearman rank correlation, rho = -0.06, p = 0.70).

Butterfly wing size and shape are sometimes correlated with migratory ability (e.g., Altizer & Davis, 2010). Here, wing shape was uncorrelated with migration distance (p = 0.2) or the country where the sample was collected (p = 0.1). There was a near-significant relationship between wing shape and wing size (R^2 = 0.30; F(1,27) = 1.8, p = 0.07). Wing shape differed between the sexes (F(1,27) = 3.4, p = 0.0002), with the wings of females being more disparate in shape than those of males (Figure S4.1; pairwise comparison, p = 0.03). Despite the differences in wing shape between males and females, we did not detect any difference in migration distance by sex (Wilcoxon test; W = 127, p = 0.47).

Additionally, wing shape was influenced by the date of collection, with earlier captures having smaller and more elongated wings ($F(1,27) = 3.0$, $p = 0.001$; Figure S4.1).

Lack of population structure across the Sahara

We explored if the distinct differences in migration distances, coupled with the evident spatiotemporal separation of short- and long-distance migrants, might be reflected in genetic evidence of early separation. This could manifest as population structure driven by neutral processes or as early signs of adaptive divergence among migratory phenotypes. We assessed these patterns at the whole-genome level, employing a comprehensive approach that integrated summary statistics, principal component analysis (PCA), and ancestry proportion inference analysis. Remarkably, all approaches yielded consistent results: a lack of detectable population structure within the dataset and negligible differentiation between groups classified as short- and long-distance migrants.

First, using 13,215,545 high-quality callable sites from both coding and non-coding regions (38 individuals, two removed due to quality issues), we summarised levels of nucleotide diversity (π) within groups and genetic divergence (d_{XY}) between groups of *V. cardui* individuals with distinct migratory behaviour (short-distance migrants: n = 21, long-distance migrants: n = 13), and calculated the fixation index (F_{st}) as a measure of differentiation (Table S4.2). We observed relatively high mean values of nucleotide diversity in both short- and long-distance migrants ($\pi_{autosome} = 0.012 \pm 0.003$) compared to other Lepidoptera (Mackintosh et al., 2019). Levels of the pairwise nucleotide divergence ($d_{XYautosome} = 0.012 \pm 0.003$) between two phenotypes were elevated, reflecting the effect of high levels of diversity within samples and stochasticity of the estimates. The level of genetic differentiation between autosomes was low but significant (pairwise $F_{ST} = 0.001 \pm 0.006$, $p < 0.001$). A slightly higher fixation index was observed for the Z-chromosome (pairwise $F_{ST} = 0.009 \pm 0.016$), which is expected given that the smaller effective population size makes the Z-chromosome more susceptible to the effects of genetic drift. We repeated this analysis using groups based on capture location (i.e., north vs. south of

the Sahara), but found no substantial differences between summary statistics (Table S4.2). These findings indicate that *V. cardui* that migrate short- versus long-distances have limited genetic differences and share similar allele frequencies, and that the effective population size in general is large.

Secondly, we used PCA to investigate potential genetic structuring. After additional filtering steps, we narrowed down our dataset to 813,810 high-quality single nucleotide polymorphisms (SNPs). This analysis revealed that the majority of samples clustered together with no separation between short- and long-distance migrants (Figure 4.2A), suggesting an overall absence of genetic structure. However, within this general pattern, two individuals stood out as outliers in the PCA; one showed differentiation primarily along the first principal component (i.e., Sample ID: 19H128) and the other exhibited differentiation along the second principal component (i.e., Sample ID: 19H115). Both of these outlier samples were collected in Sep. and were among the earliest arrivals to sub-Saharan Africa (Talavera et al., 2023; Table S4.1). Moreover, these individuals had undertaken particularly long migratory journeys, with one covering over 2,000 km across the Sahara from northwest Africa or Europe (19H115) and the other over 1,000 km from Portugal, France, Sweden, or Finland (19H128) (Figure S4.5). The clear separation of these individuals in the PCA biplot could be indicative of population structuring. We explored the contribution of specific SNPs to the first two principal components with *pcadapt* and identified 924 outlier SNPs that made significant contributions to the observed segregation of individuals. However, it is essential to note that drawing conclusions about the potential processes underlying the observed differences based on data from just two individuals is inherently limited. Nevertheless, we have provided a list of candidate SNPs that may serve as a valuable starting point for future investigations (see Data Availability Table).

Finally, we tested for population structure in our dataset using two different software implementations to infer individual ancestry proportions (admixture analysis). Specifically, we employed the sparse non-negative matrix factorization clustering algorithm (SNMF) and fastSTRUCTURE to test

models assuming 1 to 5 subpopulations. In both cases, the best model was K = 1, indicating that the data are best described by a single panmictic population (Figure 4.2B).

No islands of genetic differentiation between short- and long-distance migrants

The assessment of genetic structure using markers distributed across the entire genome may obscure regional differences in genetic differentiation. We therefore used window-based analysis of genetic differentiation between populations (i.e., F_{ST} scans) to quantify genetic differentiation across the genome and search for potential signatures of selection. Our analyses were based on two sample groupings: (i) migratory phenotype (i.e., short- and long-distance migrants) and (ii) capture location (i.e., north and south of the Sahara). Both comparisons revealed uniform differentiation landscapes characterized by a low average pairwise F_{ST} (Figure 4.2C; Figure S4.4). For autosomal regions, the average F_{ST} was 0.001 and regional peaks had a maximum F_{ST} of 0.113 (Table S4.2). For the Z-chromosome, the average pairwise F_{ST} was 0.009 with a maximum peak of 0.072. This level of variation is consistent with stochasticity of the normalisation and/or neutral variation, as has previously been demonstrated in simulation studies (Lohse, 2017) following simulation regimes applicable to our system. Additionally, none of the local F_{ST} peaks were accompanied by a simultaneous elevation of the genetic divergence and drop in diversity within each population extended over a substantial region, therefore not meeting the expectations for signatures of divergent selection.

Discussion

Contemporary evidence of variation in migratory behaviour

We used isotope-based estimates of migration distance to quantify the natural variation in migration distance exhibited by *V. cardui*. Our findings reveal that butterflies captured in Senegal and Benin during the autumn likely embarked on long migratory journeys, covering up to over 4,000 km as they crossed the Mediterranean Sea and Sahara from Europe. In contrast, *V. cardui* individuals captured in the circum-Mediterranean region in the same season had either undertaken shorter migrations or had

isotopic signatures compatible with their capture area (Figure 4.1). Despite the increasing evidence that *V. cardui* was involved in regular trans-Saharan crossings as part of its annual migratory cycle, this evidence was limited to the monitoring of migratory arrivals in the sub-Sahara (Talavera et al., 2023; Talavera & Vila, 2016) and δ^2H-based geolocation (Talavera et al., 2018; Stefanescu et al., 2016). We have expanded this isotope-based evidence with the addition of $^{87}Sr/^{86}Sr$, narrowing down the potential geographical sources of these long-distance migrants and confirming that distinctive migration strategies are displayed by *V. cardui* found north and south of the Sahara during the autumn months.

In our study, we found no significant association between estimates of migration distance and wing size, wing shape, or sex. In this regard, *V. cardui* differs from North American monarch butterflies *Danaus plexippus*, which show strong associations between migratory ability and wing morphology in that larger and elongated wings are associated with the increased flight potential of the "super generation" during autumn migration (Flockhart et al., 2017a; Y. Li et al., 2016; Altizer & Davis, 2010). The variation in migration distance detected in our study appears to have a basis in behaviour rather than wing morphology, which may indicate limited selection on migration distance, as behaviour is thought to be more plastic than morphology (West-Eberhard, 1989).

We additionally found no significant association between wing wear score and migration distance. Although wing wear scores have long been used as a proxy for butterfly age and migratory status, with high wing wear scores corresponding to older butterflies that have completed their migratory journeys (e.g., Chapter 2; Stefanescu et al., 2017; Flockhart et al., 2013), our results further illustrate that this proxy is highly unreliable (Flockhart et al., 2017a). For example, the butterfly with the highest estimated migration distance, up to over 4,000 km (i.e., 18B721), had a low wing wear score of 2 (i.e., "few scales lost"; Miller et al., 2012), which is often interpreted as belonging to a recently-emerged adult. This finding is in agreement with Korkmaz et al. (2022), who conjecture that high-altitude, gliding flight during migration results in less wing damage than low-altitude foraging and breeding behaviour.

Trans-Saharan panmixia

Our genome-wide analysis revealed no evidence of genetic divergence between *V. cardui* individuals migrating to north or south of the Sahara during autumn (Figure 4.2). Consequently, the *V. cardui* population stretching from Northern Europe to the equatorial regions of sub-Saharan Africa can be characterised as regionally panmictic, confirming the spatial extent of the Afro-Palearctic migratory range. Our findings align well with previous studies using mitochondrial DNA markers (Dapporto et al., 2019; Pfeiler & Markow, 2017; Vodă et al., 2016). Given that large biogeographic barriers, such as the Mediterranean Sea and Sahara, do not seem to lead to population substructuring, it is likely that panmixia will be found at even larger scales. However, *V. cardui* migration seems to generally follow latitudinal trajectories, and extending to larger geographical scales might reveal longitudinal structure and population differentiation (e.g., Singh et al., 2021). Future studies will need to assess the extent to which global panmixia occurs across the entire distributional range of *V. cardui*, preferably by including genome-wide genetic markers from around the world, including remote islands which sometimes host isolated populations that are phenotypically and genetically differentiated (e.g., Alvial et al., 2019).

Special attention should be given to understanding how selection and local adaptation act on migratory behaviour in insects, as well as the methods for detecting them. In our study, although we did not detect clear signatures of selection or adaptation, we did detect two outlier samples in the PCA. There could be multiple explanations for the patterns we detected. First, unlike migratory vertebrates that complete round-trip migrations within a single generation, insect migratory cycles are multi-generational. Multi-generational migratory insects exhibit a complex reticular movement pattern driven by the drastic changes in the location and size of the suitable breeding habitat over the annual migratory cycle (Talavera et al., 2023; Menchetti et al., 2019). Therefore, polygenic within-generation selection due to spatially- and temporally-varying selection pressures could lead to allele frequency changes for a portion of the population (Ehrlich et al., 2021). However, the same alleles selected for in one generation

are unlikely to be favoured by selection pressures in the subsequent generation because of spatiotemporal differences in abiotic and biotic conditions during the migratory journey and in the novel breeding habitat, thus diluting the effect of within-generation local selection. Similar frameworks have been proposed for some fish species which show signs of within-generation local selection within panmictic populations (Ehrlich et al., 2021; Pujolar et al., 2014; Als et al., 2011). A similar scenario has been outlined for *D. plexippus*, which experiences selection pressures on wing shape and wing size during long-distance autumn migrations, only to have these pressures released in subsequent generations (Flockhart et al., 2017a).

Second, it is important to recognize that the exceptionally large effective population size of *V. cardui* (García-Berro et al., 2023) and, consequently, weak genetic drift could impede our ability to detect early, or complete, reproductive isolation between short- and long-distance migrants. In these circumstances, many thousands of generations of reproductive isolation would need to elapse before our analysis would be able to detect significant allele frequency shifts. Therefore, it is possible that reproductive isolation has indeed occurred, but remains undetected. Third, it is conceivable that our sampling strategy was unable to detect genetic differentiation between groups of migrants. Notably, the most genetically differentiated migrants (Figure 4.2A) were on the leading edge of arrivals to West Africa (Sep. 2019) (Talavera et al., 2023) and likely originated in temperate Europe (Figure S4.5). These early arrivals may have been exposed to strong environmental cues in temperate Europe, where seasonal changes occur earlier than in regions closer to the equator, prompting the butterflies to initiate their migrations earlier in the season. Early migrants of *D. plexippus* have been shown to have advantages over their later counterparts, such as enhanced immune defences (Satterfield et al., 2013). Consequently, it is possible that *V. cardui* segregates temporally, rather than by distance. However, it is more plausible that this temporal pattern results from within-generation selection, which is likely to be diluted in the subsequent generation. Despite any ephemeral within-generation local selection, we

anticipate that the capacity to tolerate heterogeneous environments relies primarily on phenotypic plasticity (Enbody et al., 2021). Ultimately, interpreting our results as indicative of regional panmixia remains the most parsimonious approach.

Panmixia across an Afro-Palearctic distributional range and regular trans-Saharan crossings are exceptional phenomena for insects, as evidenced by the fact that the Palearctic and Afrotropical regions are distinct biogeographic realms with unique faunal compositions, sharing only a relatively small number of species. We found that neither differences in migration distance nor the potential biogeographic barrier led to isolation, selection, or significant allele frequency shifts in any genomic region (Figure 4.2C). This finding is in contrast to numerous examples in vertebrate species (e.g., Sokolovskis et al., 2023; Gu et al., 2021; Delmore et al., 2020; Thompson et al., 2020) and a few instances in insect species (e.g., Niitepõld et al., 2009). Some of the species of insects shared between the Palearctic and the Afrotropical regions are suspected to be migratory, particularly among the Lepidoptera, Odonata, and Orthoptera (Chelli & Moulaï, 2019; Pedgley et al., 1995), and thus it is likely that trans-Saharan gene flow occurs in some of these other species as well. Continental-scale panmixia has been demonstrated in other long-distance migratory insect species, suggesting that panmixia is a prevalent feature among migratory species (but see Zhang et al., 2023). For example, whole-genome resequencing of *D. plexippus* revealed high gene flow and low genetic differentiation between butterflies located east and west of the Rocky Mountains, despite following geographically separated migration routes (Talla et al., 2020). Regional panmixia has also been suggested through microsatellite-based population genetics for the green darner dragonfly *Anax junius* in eastern North America (May & Matthews, 2008; Matthews, 2007) and global panmixia has been inferred through mitochondrial DNA analysis for the wandering glider dragonfly *Pantala flavescens* (Ware et al., 2022; Troast et al., 2016).

The widespread panmixia observed in many migratory insects raises questions about the life history strategies promoting panmixia. First, most insect migrations are multi-generational, featuring

complex movement patterns driven by dynamic changes in breeding habitat, promoting intra-population mixing. Additionally, the tendency of long-distance migratory insects to engage in multiple matings, their lack of courtship behaviour, and their practice of laying numerous eggs (e.g., Wiklund & Friberg, 2022; Koch & Suhling, 2005; Pliske, 1975) hints at an eponymous, yet underexplored, link between panmictic tendencies and mating strategies in migratory insects. Large census population sizes in migratory insects, accompanied by intermittent outbreaks, further drive them towards panmixia. Outbreaks increase the number of successful migrants, potentially eroding local adaptation (Chapuis et al., 2009). Outbreaks of *V. cardui* from regions with anomalously high vegetation growth (López-Mañas et al., 2022) may contribute to the observed lack of genetic structure. Similar population dynamics observed in species like *Libytheana carinenta* (Neck, 1983), *A. junius* (Russell et al., 1998), and some hoverflies (Menz et al., 2019) hint at outbreaks being pivotal in shaping the population structure of many migratory insects.

The same life-history factors of migratory insects that appear to promote panmixia among migratory insects (i.e., multi-generational migrations, an absence of assortative mating, and large census population sizes with outbreak dynamics) are also associated with large effective population sizes and high genetic diversity. The multi-generational annual migratory cycle results in a greater number of mutations occurring within the population per unit time, compared to species with longer generation times, and large census population sizes are less susceptible to genetic drift, both of which encourage genetic diversity (Buffalo, 2021). Indeed, our samples showed relatively high genetic diversity ($\pi_{autosome}$ = 0.012) compared to other butterfly species (Mackintosh et al., 2019). This observation aligns with the general trend that migratory butterflies tend to possess higher levels of heterozygosity than sedentary species (García-Berro et al., 2023). Consequently, this abundant genetic variation provides opportunities for at least some individuals to acclimatise to the heterogeneous environmental conditions that are encountered during their multi-generational migrations, thereby facilitating survival.

Due to the obligate, multi-generational migrations with low philopatry, random mating, and large, outbreaking populations, local adaptation is implausible within the Afro-Palearctic population of *V. cardui*. We suggest that rather than adapting to short or long-distance migration, a plastic response to the environment determines the differences we observe in migratory phenotype. It is also possible that the differences in migration distance observed here could also be explained, in whole or in part, by extrinsic mechanisms, including differences in parasite load (Altizer et al., 2015), energy storage and metabolism (Du et al., 2022), wind-assistance and weather events (Gatehouse, 1994), or even personality (B. B. Chapman et al., 2011). However, studies on *D. plexippus* suggest that while migratory state (i.e. resident vs migratory) is genetically determined (Zhan et al., 2014), variation in migration distance is more likely to be due to many loci of small effect or differential gene expression (Talla et al., 2020), likely controlled by epigenetic mechanisms (Merlin & Liedvogel, 2019; Van Petegem et al., 2015; Liedvogel et al., 2011). Variation in migratory behaviour is likely a response to multiple environmental cues such as resource availability, photoperiod, temperature, humidity, and host plant quality. Recent experiments have demonstrated differences in *V. cardui* gene expression, methylation, and gene regulation due to the density of larval conspecifics, larval food availability, and host plant availability for oviposition (Shipilina et al., *in prep.*; Näsvall et al., 2023; Boman et al., 2023), suggesting a strong response to environmental cues. The transcriptional basis of differences in migration distance has been explored in the moth *Helicoverpa armigera* and in *D. plexippus*, yielding promising candidate genes (Talla et al., 2020; Jones et al., 2015). Future controlled laboratory studies with *V. cardui* are needed to disentangle the environmental triggers and molecular pathways of phenotypic plasticity in migration distance.

Conclusion

Here, the combination of isotope-based phenotyping of migration distance and comprehensive whole-genome resequencing provided a unique opportunity to investigate phenotype-genotype associations of migratory behaviour in insects, a challenging endeavour until now. We found distinct differences in migration distance, with most individuals captured in Benin and Senegal exhibiting long-distance migrations of up to 4,000 km, traversing the Mediterranean Sea and Sahara from temperate Europe. In contrast, *V. cardui* captured in the circum-Mediterranean region at the same time either undertook short-distance migrations or displayed isotopic signatures indicative of local origins. These differences in migratory behaviour did not have a clear association with wing morphology or wing wear. Genome-wide comparisons between these migratory groups found negligible genetic differentiation, leading us to conclude that the Afro-Palearctic population of *V. cardui* is panmictic, with regular bidirectional trans-Saharan crossings during the annual migratory cycle. Given the life history traits of *V. cardui*, namely multi-generational migration, their mating strategy, and large population sizes, local adaptation appears implausible within this population. Consequently, future research should explore the role of environmental cues and differential gene expression in shaping the diversity in migration distance.

Materials and Methods

Sample collection

Wild, adult *V. cardui* were captured from six countries located both north and south of the Sahara (Table S4.1). South of the Sahara, butterflies were captured in Senegal and Benin from Aug. to Nov. of 2018 and 2019 (n = 19). North of the Sahara, butterflies were captured from Morocco, Malta, Portugal, and Spain in Nov. 2019 (n = 21). We used behavioural, demographic, and timing evidence to maximize the probability of targeting migratory individuals at these locations. First, we preferentially sampled butterflies with worn wings (i.e., higher wing wear scores) and showing reproductive behaviour (i.e., hilltopping or oviposition) because *V. cardui* typically delay their reproductive behaviour until migration

has been completed (Stefanescu et al., 2021). Second, demographic data in some of the sampling locations supported the arrival of migrants. A monitoring station in Senegal saw a rising number of *V. cardui* adults in the autumn (Aug. through Oct.) during 2018 and 2019, followed, but not preceded, by a peak in larval counts, suggesting that the sudden spike in adults in the autumn is a result of immigration to the region (Talavera et al., 2023). Similarly, a monitoring station in Benin saw high numbers of adults in Sep. and Oct., followed, but not preceded, by high larval counts in Oct. and Nov. (Talavera et al., 2023). Besides this demographic evidence, the time of the year when these adult butterflies were collected matches the first estimated arrival of migrants at the sampled locations. South of the Sahara, monitoring data does not indicate the presence of *V. cardui* year-round (Talavera et al., 2023). North of the Sahara, much of the circum-Mediterranean region is unsuitable for *V. cardui* development in Jul., Aug., and Sep. (Morocco) due to high temperatures and low host plant availability (Stefanescu et al., 2017), suggesting that these individuals represent the first arrival of migrants in the region (Talavera et al., 2023).

Isotopic analysis

Hydrogen isotope values

Prior to δ^2H analysis, a forewing from each *V. cardui* butterfly was soaked, with agitation, in three successive baths (1 h, 30 min., 10 min.) of 2:1 chloroform:methanol solution to remove surficial dust and lipids, which are known to introduce error into δ^2H measurements (Hobson et al., 2017; Paritte & Kelly, 2009). Samples were cut from the same membranous region of the forewing to reduce intra-individual variation from pigmentation (Hobson et al., 2017) and wing veins (Lindroos et al., 2023). Samples were then weighed (0.162 mg ± 0.009 mg) into silver capsules and dried in a 40 °C oven. Non-exchangeable δ^2H values were determined at the Ján Veizer Stable Isotope Laboratory (University of Ottawa, ON, Canada) using a comparative equilibrium approach (Wassenaar & Hobson, 2003). All measurements were taken using high temperature (1,400°C) flash pyrolysis (TCEA, Thermo Finnigan, Germany) with a

helium carrier passed through a chromium-filled reactor and, after separation, introduced to a Delta V Plus IRMS (Thermo Finnigan, Germany) via a Conflow IV interface (Thermo Finnigan, Germany). A three-point calibration was used to calibrate the sample δ^2H values: CBS (caribou hoof; -157 ± 0.9‰; Soto et al., 2017), KHS (kudu horn; -35.3 ± 1.1‰; Soto et al., 2017), and USGS43 (human hair; -44.4 ± 2.0‰; Coplen & Qi, 2012). Internal standards were measured to assess the quality of the measurements, including one keratin reference standard, USGS42 (human hair; measured: -75.3 ± 0.5‰, n = 4; standard: -72.9 ± 2.2‰; Coplen & Qi, 2012), and two in-house chitin standards, ground and homogenised *Lymantria dispar dispar* (measured: -64.4 ± 1.8‰, n = 6; long-term average: -64 ± 0.8‰) and Alfa Aesar chitin (measured: -22.8 ± 0.7‰, n = 4; long-term average: -22 ± 1.2‰). Based on within-run replicates of the internal standards and repeated sample measurements, precision is estimated to be about ± 2‰. All reported δ^2H values are normalized to the Vienna Standard Mean Ocean Water - Standard Light Antarctic Precipitation (VSMOW-SLAP) standard scale.

Strontium isotope ratios

To prepare for $^{87}Sr/^{86}Sr$ analysis, a single forewing from each butterfly was cleaned using pressurized nitrogen gas for 2 min. at 10 psi to remove any surface contaminants (e.g., dust; Chapter 2). The wings were then digested in 1 mL HNO_3 (16 M; distilled TraceMetal™ Grade; Fisher Chemical, Canada) using microwave digestion (Anton Paar Multiwave 7000; Austria). The samples were heated from ambient temperature to 250 °C at a steady rate over 20 min. and then left at 250 °C for 15 min. in a pressurized chamber. An aliquot of 200 µL from each sample was separated and diluted to 2 mL of 2% v/v HNO_3 and analyzed for Sr content via inductively coupled plasma mass spectrometry (ICP-MS; Agilent 8800 ICP-QQQ, Agilent Technologies Inc., CA, USA) at the Department of Earth and Environmental Science (University of Ottawa, Canada). Calibration standards were prepared using single element certified standards purchased from SCP Science (Montreal, Canada). Samples had an average of 3.1 ± 1.7 ng Sr per mg of wing tissue (n = 40).

The remaining aliquot of sample digest was dried down and re-dissolved in 0.5 mL 6 M HNO_3. The separation of Sr was processed in a 100 µL microcolumn loaded with Sr-spec Resin (100 - 150 µm; Eichrom Technologies, LLC). The matrix was rinsed out using 6 M HNO_3, and Sr was collected with 0.05 M HNO_3. To ensure complete separation, the microcolumn process was repeated. After separation, eluates were dried and re-dissolved in 200 µL 2% v/v HNO_3 for $^{87}Sr/^{86}Sr$ analysis.

The $^{87}Sr/^{86}Sr$ analysis was performed at the Pacific Centre for Isotopic and Geochemical Research (University of British Columbia, Canada) using a Nu-Plasma II high-resolution multi-collector inductively coupled plasma mass spectrometer (MC-ICP-MS; Nu Instruments) coupled to a desolvating nebulizer (Aridus II, CETAC Technologies). The isotopes ^{84}Sr, ^{86}Sr, and ^{87}Sr have isobaric interferences from ^{84}Kr, ^{86}Kr, and ^{87}Rb respectively, and were corrected for using the ^{85}Rb and ^{83}Kr signals. Instrumental mass fractionation was corrected by normalizing $^{86}Sr/^{88}Sr$ to 0.1194 using the exponential law (Moore et al., 1982). Procedural blanks were negligible. The reproducibility of the $^{87}Sr/^{86}Sr$ measurement for 5 ppb NIST SRM987 is 0.71025 ± 0.00009 (1 SD, n = 138) and for 1.4 ppb NIST SRM987, 0.71019 ± 0.00011 (n = 48). A matrix-matched chitin internal standard, 5 ppb Alfa Aesar chitin, was also used (0.713959 ± 0.00009; n = 3).

Geographic assignment

Continuous-surface isotope-based geographic assignment was performed via the *assignR* package (Ma et al., 2020) in R v4.1.0 (R Core Team, 2021). The origins of the unknown-origin *V. cardui* were estimated through a probabilistic framework using previously-calibrated isoscapes: (i) a hydrogen isoscape calibrated with residential butterfly samples from across the Palearctic and Afrotropical regions (Ghouri et al., 2023), and (ii) a regional bioavailable strontium isoscape (Chapter 3). The most likely natal origin of each individual was estimated using δ^2H alone, $^{87}Sr/^{86}Sr$ alone, and using both isotopes together (see Data Availability Table). The 2:1 odds ratio was chosen, in keeping with previous studies (e.g. Flockhart et al., 2013), to create binary surfaces from the posterior probability surfaces of the dual δ^2H - $^{87}Sr/^{86}Sr$

geographic assignment, representing the top third of the probability distribution as high probability of natal origin (i.e., "1") and everything else as low probability of natal origin (i.e., "0"). Individual binary surfaces were then summed for each capture location, and divided by the number of individuals, to summarise the results of the geographic assignment into maps of the proportion of individuals with a high probability of natal origin at a given raster cell.

Distance metric

A consensus has not been reached on the optimal method by which to estimate the distance a migratory individual has travelled from posterior probability surfaces (Vander Zanden et al., 2018). We assessed the ability of seven different metrics to accurately estimate the migration distance of aerial migrants in our study area using synthetic data generated in R v4.1.0 (R Core Team, 2021). We generated isotopic signatures for 250 synthetic migrants and then performed dual δ^2H and $^{87}Sr/^{86}Sr$ geographic assignment for each migrant using the *pdRaster* function in the *assignR* package (Ma et al., 2020). Each of the seven metrics was then calculated using the resultant posterior probability surfaces. Most metrics were highly inaccurate, and could under- or over-estimate the actual great circle distance by thousands of kilometres (Figure S4.2). However, the "minimum distance" metric consistently underestimated migration distance for our study area and, therefore, acts as conservative estimate of migration distance (Figure S4.2). Therefore, in this study, we used the minimum distance metric to estimate the distance travelled. This metric measures the shortest distance between the capture location and an isopleth threshold, here defined as the top third of the probability distribution (0.3 isopleth; e.g., Hallworth et al., 2018; Katzner et al., 2017).

Many butterflies had an isotopic signature similar to the local isotopic signature of their capture location. We interpreted individuals with a highly probable natal origin at the capture location (as defined by the 2:1 odds ratio) and/or that had a minimum distance of less than 100 km as "putative locals." These individuals are likely either the locally-sourced offspring of the previous migratory

generation or were immigrants from a far-off region with a similar isotopic signature to that of their capture location. Our interpretation of these samples as putative locals is the more parsimonious approach.

Geometric morphometric analysis

Differences in migration distance or trajectories could potentially be explained by intrinsic factors such as sex, body size, or wing shape. To test for differences in wing shape, photographs of each sample's forewing were taken and used for morphometrics analysis. Since we preferentially chose samples that had higher wing wear scores, extensive damage to the wings made landmarking of many samples impossible. Therefore, only 28 of the 40 samples were landmarked using TPSDig2 v.2.32 (Rohlf, 2016) using 12 conventional landmarks for Nymphalid butterflies (e.g., Escobar-Suárez et al., 2023; Soule et al., 2020). Using the R package *geomorph* (Adams & Otárola-Castillo, 2013), a generalized procrustes analysis removed the translational, rotational, and scaling variation of the shape. A procrustes regression was used to test the effects on wing shape of sex, the month of collection, estimated migration distance, and butterfly wing size.

Genomic analysis and genotyping

Whole genome resequencing

Library preparation for all 40 samples was done using TruSeq PCR-free kits (Illumina, San Diego, USA) at the Institut Botànic de Barcelona (IBB - CSIC, Barcelona, Spain). Whole-genome resequencing was performed with paired-end 2x151 bp reads on one Illumina NovaSeq 6000 S4 lane at the National Genomics Infrastructure (NGI; Stockholm, Sweden) to generate a mean depth of coverage per individual of about 48 reads.

SNP calling

A modified Sarek Nextflow pipeline (Garcia et al., 2020) was used for preprocessing the whole genome resequencing data and for detecting single-nucleotide polymorphisms (SNPs). At the first step of the

Sarek pipeline, we evaluated the quality of the raw reads with FastQC (version 0.11.9; Andrews, 2010). Reads were stringently trimmed using *fastp* (Chen, 2023; Chen et al., 2018) to remove (i) sequences from the 5` end (12 bp) and 3` end (3 bp) of each read, (ii) adaptor sequences, (iii) low quality reads (overall Phred score < 30), and (iv) short reads (< 30 bp). Read quality after trimming was re-evaluated using FastQC. At the next step, reads were mapped to the reference genome (Lohse et al., 2021) using BWA-MEM (version 0.7.17; H. Li, 2013) and then sorted and indexed using SAMtools (version 1.9; H. Li et al., 2009). A mean of 96.6% of the reads were mapped to the reference genome. Optical and PCR duplicates were marked using GATK MarkDuplicates (version 4.1.4.1; DePristo et al., 2011). These duplicates, as well as sequences with low mapping quality (MAPQ < 30), were removed using SAMtools. Since prior SNP data for *V. cardui* were unavailable, the base calibration (BQSR) step module in the Sarek pipeline was skipped.

The first steps of variant calling were performed using GATK Best Practices (Van Der Auwera et al., 2013), as implemented through the Sarek pipeline. To decrease computational time, the Sarek pipeline calls each chromosome separately. MultiQC (version 1.8) was used to assess the quality of the output from all steps of the pipeline. The resulting per chromosome vcf files included from 1.3 to 3 million unfiltered SNPs (78.9 million SNPs total). The last step of variant calling was performed outside of the pipeline to accommodate for invariant site calling (-all-sites option in GenotypeGVCFs), which is necessary for reliable downstream estimation of population genetic summary statistics, such as π and d_{XY}. This variant filtering included multiple steps: (i) hard filtering, (ii) removing SNPs overlapping with TE annotation, (iii) separate quality and coverage filtering for variant and invariant sites, (iv) merging of variant and invariant site vcfs for the F_{ST} estimation. Hard filtering was performed on raw vcf files, which included both variant and invariant sites. Hard filtering is meant to substitute for the variant quality score recalibration (VQSR) step in GATK Best Practices (Van Der Auwera et al., 2013). Using bcftools v1.15 (H. Li, 2011), we filtered for variant quality by depth (QD < 2.0), Fisher strand bias (FS > 60.0), root

mean square mapping quality (MQ < 40.0), u-based z-approximation from the Rank Sum Test for mapping qualities (MQRankSum < -12.5), and u-based z-approximation from the Rank Sum Test for site position (ReadPosRankSum < -8.0). We proceeded to remove indels and multivariate sites (--exclude-types indels, other --max-alleles 2) and reindexed the resulting vcf file. Next, the coordinates of transposable elements and simple repeats were obtained with a custom bash script from a previously published annotation of transposable elements (Shipilina et al., 2022), and used to remove SNPs appearing in these regions.

The quality of the resulting files (one vcf file per chromosome) was evaluated using summary statistics implemented with vcftools (i.e., allele frequency (--freq2), mean depth (-- depth), mean per site depth (--site-mean-depth), per site quality (--site-quality), per sample missingness (--missing-indv), per site missingness (--missing-indv), heterozygosity estimation (--het; Danecek et al., 2011). The obtained values were plotted with custom python scripts for further evaluation. Two individuals were removed due to quality issues (Sample ID: 19H137 and 19H114). Variant and invariant sites were split into two files for downstream analysis. Informed by the summary statistics, we applied filters for quality and depth to the variant sites vcf file (i.e., minor allele frequency (--max-maf 0), mean depth value (--min-meanDP 30), mean depth value (--max-meanDP 80)). We also applied additional filters to the invariant sites vcf file (i.e., quality value (--minQ 30), mean depth value (--min-meanDP 30)). Separate files with both variant and invariant calls were kept as separate chromosomes to decrease computational time. The W chromosome was also removed from the analysis. A region with divergent values of populational statistics was detected in the first third of chromosome 10 corresponding to a large area of transposable element proliferation (Figure 4.2C; Shipilina et al., 2022). Since this region likely does not carry information about genetic structure it was also filtered from the population structure analyses. On a technical note, it is important to mention that this region was retained after

stringent SNP filtration, and future research on V. cardui should be aware that this region may necessitate special treatment (e.g., manual filtering).

Population genetic analysis

For PCA and admixture analysis, variant files per chromosome were concatenated. To investigate genetic variation between individuals, a PCA was performed using PLINK v1.90 b 4.9 (Figure 4.2A). For this analysis, we additionally filtered out singleton SNP sites (i.e., MAF = 0.03), and SNPs that were in linkage (i.e., SNPs with r^2 values > 0.1 using sliding windows of 50 SNPs with a step size of 10 SNPs); a total of 813,810 high quality variants remained after filtering. Outliers in the first two principal components were detected using the R package *pcadapt* (Privé et al., 2020) using Bonferroni-corrected p-values ($\alpha = 0.05$). The PCA was repeated excluding the two outliers, but no additional structure was detected (Figure S4.3B).

Reverse migrations from sub-Saharan Africa to the Maghreb are thought to occur in the autumn, even while southwards trans-Saharan migrations are still underway (Gorki et al., *in review*; Stefanescu et al., 2016). All of the samples captured in Morocco were designated as putative locals, but the posterior probability surfaces of some showed a possibility of originating south of the Sahara (see Data Availability Table). To test whether these samples could have biased our results, we repeated the PCA without samples collected in Morocco (Figure S4.3A). The resulting PCA was based on 647,906 SNPs and showed a single cluster with the same outlier individuals as the original PCA.

After excluding SNPs on the Z chromosome and in coding sequences, genetic structure was also assessed with a likelihood method, the sparse non-negative matrix factorization clustering algorithm, SNMF, in the R package *LEA* v3.6.0 (Frichot et al., 2014). Each number of population clusters (K) from 1 to 5 was run independently with 5 repetitions with the regularisation parameter set to 100, after which cross-validation errors calculated using the cross-entropy criterion were compared. This process was repeated using a Bayesian framework via fastSTRUCTURE (Raj et al., 2014) using the simple allele

frequency prior with 5 repetitions. The number of population clusters from 1 to 5 that best explained the observed structure was chosen with the *chooseK.py* tool.

Genomic scan for selection

To detect any fine-scale regions of differentiation along the genome, a genome scan was performed on groupings based on capture location (i.e., north vs. south of the Sahara) and migratory phenotype (i.e., long vs. short migration distance). For the grouping based on migratory phenotype, individuals from south of the Sahara that were putative locals (n = 6) were removed, while putative locals from north of the Sahara (n = 19) were included with the short-distance migrants (n = 3) to balance the sample size. For genome scans, we retained SNPs falling into coding regions and having minor allele frequencies. We used pixy v1.2.7 (Samuk et al., 2022; Korunes & Samuk, 2021) to calculate nucleotide diversity (π), absolute divergence (d_{XY}), and genetic differentiation (F_{ST}; Hudson method, -hudson) in 20 kb non-overlapping windows using all sites. Windows with less than 10% of sites represented (i.e., < 2,000 bp) were removed from the analysis. Resulting per window statistics were summarized using custom python scripts. For low levels of F_{ST}, we tested if the index significantly differed from 0 using a t-test in the python *scipy* package (p-value: 1.3e-216)

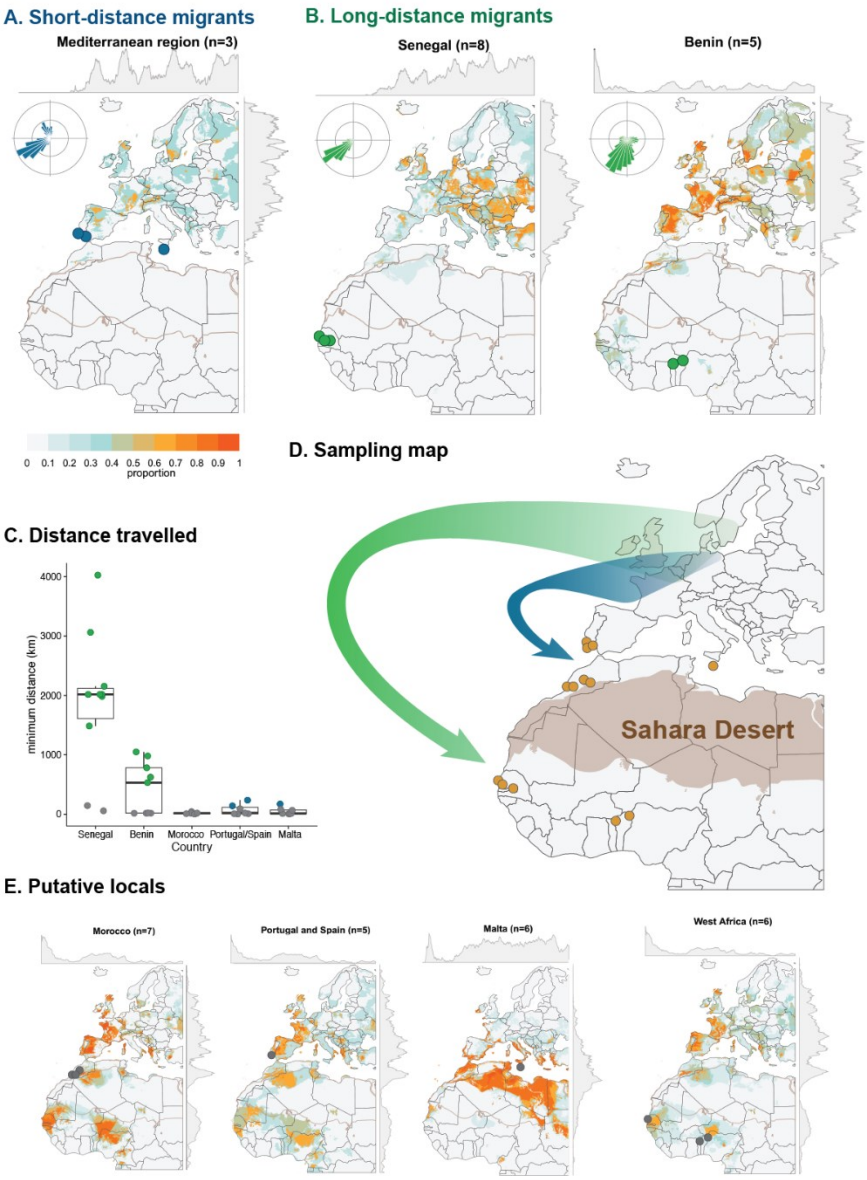

Figure 4.1 Summarised posterior probability surfaces and subsequent estimates of migration distance (i.e., minimum distance) and direction based on dual δ^2H - $^{87}Sr/^{86}Sr$ geographic assignment. **(A, B, E)** Summary maps depict the proportion of individuals with a high probability of natal origin in a given area, as defined by the 2:1 odds ratio. The side margins display the mean proportion by latitude and longitude and only one circle per capture location is shown. The inset rose plot illustrates the average probability-weighted bearing from the estimated natal origin (centre of the plot) to the capture locations. Maps summarise the results for **(A)** short-distance migrants, **(B)** long-distance migrants, and **(E)** putative locals captured in the circum-Mediterranean region and West Africa. **(C)** Boxplot displaying the estimated migration distance (km) categorized by the country of capture. Individuals with a minimum distance of less than 100 km were considered putative locals. **(D)** Map indicating the capture locations both north (Morocco, Malta, and Portugal and Spain) and south (Senegal and Benin) of the Sahara. Butterflies captured south of the Sahara generally migrated longer distances (green arrow) compared to those captured north of the Sahara (blue arrow).

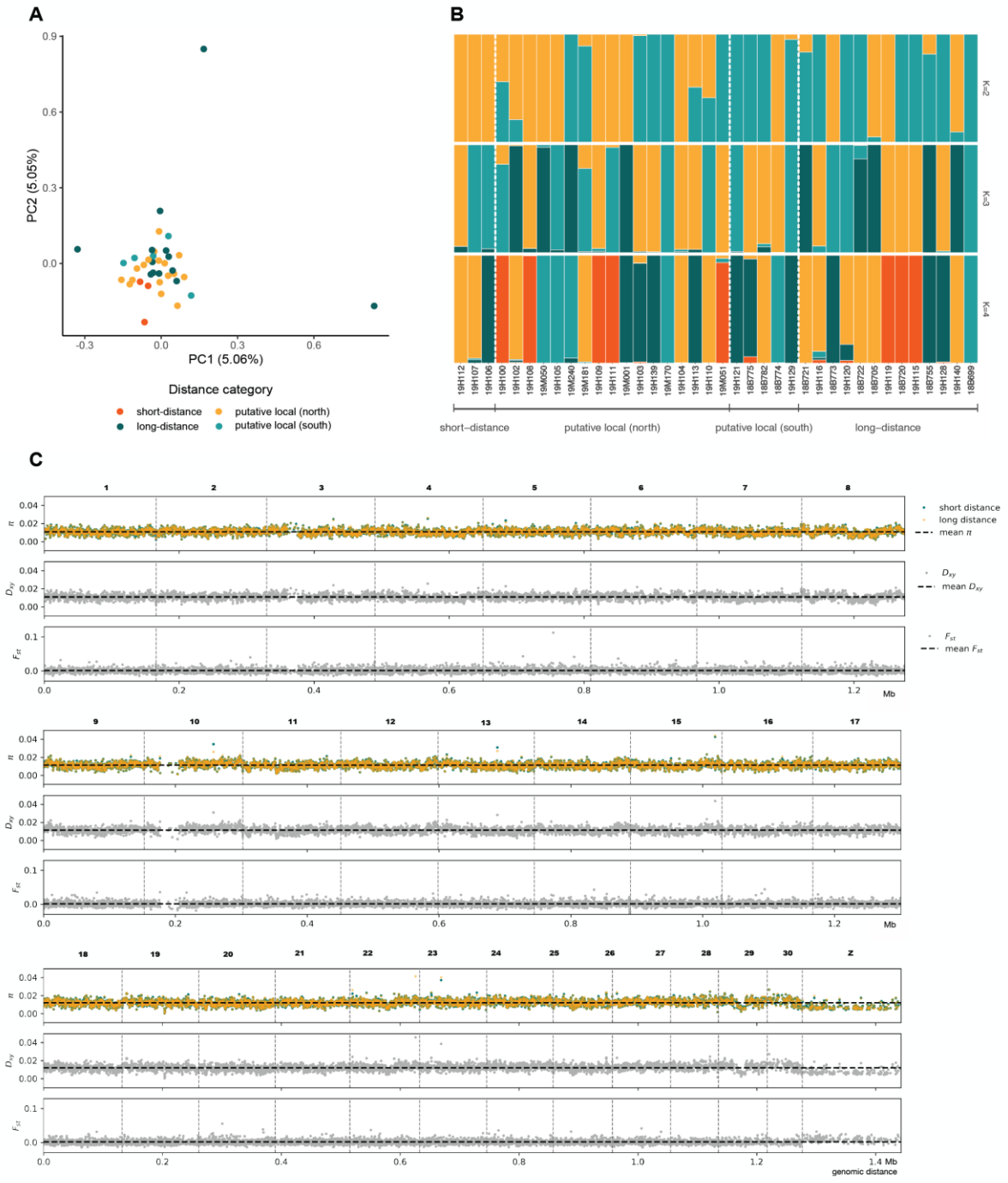

Figure 4.2 Lack of population structure and genetic differentiation between short- and long-distance migrants. **(A)** Principal component analysis (PCA) biplot illustrating the genetic variation in the samples; **(B)** Genomic admixture patterns based on assumptions of 2 to 4 ancestral populations (K = 2 to 4). No discernable structure was observed, with the optimal model demonstrating K = 1 (not visually depicted); **(C)** Genome scans showing within population diversity (π), genetic differentiation (d_{XY}) and fixation index (F_{ST}) between individuals categorized as short- and long-distance migrants. The analysis was performed with sliding, non-overlapping windows of 20 kb. Mean values are indicated by a black dashed line.

General Thesis Conclusions

Summary of main findings

Global ecosystems are experiencing escalating perturbations due to anthropogenic climate change and habitat degradation. In this context, understanding insect migration is vital for the security of insect-mediated ecosystem services and the effective management of pests, invasive species, and vectors of plant and animal disease. However, the study of insect migration has historically been impeded by methodological challenges. This thesis constitutes a substantial contribution to our understanding of insect migration, mainly through the development and application of metals and metal isotopic tools tailored for insect migration research. Using the monarch butterfly and painted lady butterfly as model systems, I developed these isotopic tools through controlled laboratory experiments (Chapter 1) and by applying them to investigate insect migration at scales of increasing complexity: on a single generational segment of the annual migratory cycle (Chapter 2), on multiple generations of the annual migratory cycle (Chapter 3), and to phenotype a complex migratory behaviour (Chapter 4).

In the first chapter, I investigated the pathways of metal incorporation into butterfly wings to test one of the primary assumptions of isotope-based geographic assignment: that the natal isotopic signature is preserved in wing tissue throughout the life of the adult butterfly. I conducted an 8-week diet-switching experiment on monarch butterflies to understand the potential sources of 23 metals and metalloids, $^{87}Sr/^{86}Sr$, and lead isotopes to wing tissue. I validated that the $^{87}Sr/^{86}Sr$ remains indicative of the larval diet, at least in males, although a potential contamination source to the females requires further study. Additionally, a caveat to the use of $^{87}Sr/^{86}Sr$ for geolocation was found in the potential for Sr contamination by wetting. Finally, this study noted that (1) lead accumulates on butterfly wings, likely from dust aerosols, and (2) concentrations of lead exceeding food safety guidelines can be found in the wings of wild monarchs. These results point to possible toxicological consequences and the potential for

lead isotopes to be used to quantify the exposure of monarchs to metal pollution along migration routes.

In the second chapter, I outlined the steps needed to calibrate a regional strontium isoscape for $^{87}Sr/^{86}Sr$-based geographic assignment using random forest regression. I applied these steps to monarch butterflies from a single generation in eastern North America to show that combining δ^2H and $^{87}Sr/^{86}Sr$ into a dual assignment framework provides the most spatially constrained estimates of natal origin, compared to using either isotope alone.

In the third chapter, I applied the framework of the second chapter to investigate the migratory patterns of multiple generations of painted lady butterflies crossing the Sahara. This study advanced on the previous framework by using ensemble machine learning to calibrate a regional strontium isoscape for Europe and Africa. The southward autumnal migration across the Sahara was characterized using δ^2H and $^{87}Sr/^{86}Sr$-based geographic assignment as a broad-front, parallel migration with moderate migratory connectivity. Additionally, a leapfrog migration pattern, characterized by long-distance migrants from northern Europe journeying further south to sub-Saharan Africa than butterflies migrating to the circum-Mediterranean region, was proposed in the westernmost region. However, spatiotemporal sampling limitations prevented a thorough characterization of the northward vernal migration, which likely consists of a gradual, northward progression. This work constitutes the most advanced understanding of trans-Saharan migratory patterns for any insect thus far.

The leapfrog migration pattern detected in the third chapter results in a disjunct distribution of painted lady butterflies in the western Afro-Palearctic region in the autumn, with some painted ladies journeying short distances from Europe to the circum-Mediterranean region while others journey long distances to sub-Saharan Africa. In the fourth chapter, I combined δ^2H and $^{87}Sr/^{86}Sr$-based geographic assignment with whole-genome resequencing to investigate the ecological and evolutionary factors influencing migration behaviour. Although isotope-based estimates of migration distance were able to

categorize individuals into distinctive groups, genome-wide analysis found no signals of selection, and all specimens belonged to a panmictic population. Given the lack of adaptive variation detected between short- and long-distance migrants, it is likely that migration distance is a plastic response to environmental conditions in painted lady butterflies.

Future directions

Ecosystems worldwide face the growing impact of anthropogenic climate change and habitat degradation, creating an urgency for the scientific community to intensify efforts to unravel the migratory patterns of insect species, understand their impacts on ecosystems, and predict future changes (Satterfield et al., 2020). While it is estimated that thousands of insect species engage in migration, baseline information regarding the migratory strategies of the majority of these species remains unexplored (Satterfield et al., 2020). In fact, even the identity of many of these putative migratory species is unknown, and there is a paucity of empirical evidence to support the migratory behaviour of many taxa (Chowdhury et al., 2021a). Relying on monarch and painted lady butterflies as model species for other migratory insects relies on the assumption of shared life history traits. Comparative studies are needed to validate this assumption, but it is improbable that this premise holds true in all cases (e.g., Segre et al., 2023; Van Klink et al., 2022). Nonetheless, the increased understanding of monarch and painted lady butterfly migration presented in this thesis can be used to inform our understanding of lesser-studied insect migrants and jumpstart research with evidence-based hypotheses.

The isotopic geolocation tools developed in this thesis offer the potential to fill in gaps in our fundamental understanding of insect migration (Hobson, 2023). For example, isotope geolocation can verify instances of long-distance movement (e.g., Dargent et al., 2023), helping identify insect species engaged in migratory behaviour. Isotope geolocation could also be used to quantify the distances individual insects are capable of traveling, a parameter with implications for predicting range

expansions, genetic structure, and population dynamics. Furthermore, these isotopic geolocation tools can help address biosecurity concerns by estimating the origin of intercepted exotic pests (e.g., Holder et al., 2019, 2014). This method is also valuable for studying the movements of species of conservation concern because it does not interfere with migratory behaviour, and isotopic signatures can be measured from the tissues of insects that have died of natural causes (Hobson et al., 2021).

In addition to providing fundamental information on insect movements, metals and metal isotopic tools can also deepen our understanding of the spatiotemporal migration patterns of well-known insects. Numerous studies employing δ^2H-based geographic assignment in insect research may benefit from the higher spatial precision achievable through the combination of δ^2H and $^{87}Sr/^{86}Sr$ (Chapter 2). For example, future research can expand on the work presented in this thesis by applying $^{87}Sr/^{86}Sr$ to investigate migratory patterns throughout each generation of the annual migration cycle of monarch butterflies and painted lady butterflies (e.g., Flockhart et al., 2013). Similar extensions could be applied to other migratory insects with established δ^2H data, including dragonflies (e.g., Hallworth et al., 2018), hoverflies (e.g., Clem et al., 2023), moths (e.g., Torniainen & Mikonranta, 2018), and beetles (e.g., Palmu et al., 2017). Additionally, isotopes offer migration ecologists a unique opportunity to go back in time and assess the presence of changes to migration patterns. Future research could also temporally expand by using archived specimens to detect shifts in migratory connectivity over time (e.g., Flockhart et al., 2017b).

A simultaneous expansion in the development of isotopic tools and technologies could facilitate a broader application of isotope geolocation to study insect migration. Improvements could be made to various aspects of the isotope-based geographic assignment framework. First, the field would benefit from a decrease in the throughput time of isotopic measurements, a standardization of methodologies, reduced costs, and an improved ability to measure metal isotopes on small masses of organic tissue. Second, isotope-based geographic assignment relies on the robustness and accuracy of the underlying

isoscapes. These spatial models could be further improved through the collection of targeted calibration data, as well as through an increase in the mechanistic understanding of isotopic variation across the landscape. Third, additional statistical tools are needed to harmoniously combine isotopes with alternate geolocation tools, such as wind trajectory modelling and the results of pollen metabarcoding analysis. Finally, insect migration research would benefit from the further development of other isotopic systems that have the potential to provide information on geolocation and insect physiology and diet, such as lead, calcium, zinc, and sulphur isotopes.

The findings of this thesis not only advanced our understanding of insect migration but also hold the potential for applications in other fields. Chapter 1 investigated the sources of metals and metalloids in the wing tissues of butterflies with implications for physiology, diet, and toxicology. Future studies in these areas should consider whether metal isotopes can provide novel insights into complex biological processes. Additionally, geolocation using $^{87}Sr/^{86}Sr$ is not restricted to insects; it is a well-established technique in diverse disciplines such as archaeology, forensic science, palaeoecology, and food sciences. The regional strontium isoscapes, machine learning frameworks, and calibration data generated in this thesis will be a valuable asset for these diverse fields.

Overall conclusion

In conclusion, this thesis substantially advances our understanding of insect migration. The development of metals and metal isotopic tools within this work expanded our ability to decipher the complexities of multigenerational migration patterns, characterize migratory behaviour, and explore the underlying basis of the migratory syndrome. Such knowledge is imperative for conserving vital ecosystem services in a changing world and navigating the challenges posed by migratory insect pests and invasive species. I anticipate that this thesis marks the beginning of a rapid advancement in methodologies and mindset that will propel future studies toward new discoveries regarding the nature of insect migration.

Data Availability Table

Chapter	DOI	Link
Chapter 1	10.3389/fevo.2023.1085903	https://osf.io/n4pvm/
Chapter 2	10.17605/OSF.IO/8WZAM	https://osf.io/8wzam/
Chapter 3	view only	https://osf.io/6vny3/?view_only=2bb199d2d891474ebfaffb462b003640
Chapter 4	view only	https://osf.io/dzh2g/?view_only=6dc9f9bd496f4b538b0708d5f13cfce8

Appendix A: Supplementary Material for Chapter 1

Natural metal concentrations in ashed milkweed and monarch wings

Elemental analysis of ashed milkweed samples

To estimate the elemental concentrations of wild milkweed plants of different species (*Asclepias* spp.) in eastern North America, 85 milkweed samples were analyzed for a suite of 12 elements (i.e., Al, Ba, Cd, Co, Cr, Cu, Mg, Mn, Ni, Pb, Sr, and Zn). The milkweed samples were collected and analyzed as part of a recent study (Chapter 2). Milkweed samples were cleaned by rinsing with DDI and the use of an ultrasonic bath (~10 min.), then dry ashed at 600 °C for 4 h to assist digestion. Samples were digested in 16 M HNO_3 (TraceMetal™ Grade; Fisher Chemical, Canada) for 16 h at 120 °C. Ultraclean hydrogen peroxide was added to some samples to complete the digestion. After digestion, the samples were dried on a hot plate at 90 °C then re-dissolved in 1 mL of 2% v/v HNO_3. One-tenth of the sample was separated out and diluted to 3 mL 2% v/v HNO_3 for trace element analysis using the ICP-MS at the University of Ottawa.

Element concentrations were prepared by bracketing each set of samples with calibration standards prepared using single element certified standards purchased from SCP Science Inc. (Montreal, QC, Canada). Detection limits were conservatively estimated as three times the standard deviation of the blanks; 28 Cd and 5 Ni were below the calculated detection limit and were thus removed from further analysis. Some remaining Cd and Ni were near the detection limit; otherwise, procedural blanks were negligible (< 5%). Additionally, Mg were ~150 times higher than the calibration points and Cd were ~100 times lower than the calibration points; therefore, the absolute concentrations of these elements are uncertain, but the relative values are likely meaningful. Due to differences between the set-up of five analytical runs, the number of milkweed samples analyzed for each element differ (Table S1.4). Intra-run precision of standards was acceptable (RSD < 10%) for all elements except Mg (20%) and Al (15%). Between-run precision of peach leaves (n = 3; SRM 1547 Peach Leaves, National Institute of

Standards and Technology) was found to be poor for all elements except Pb, Mn, and Al (Table S1.1). The sample concentrations are calculated based on the mass of the sample after it is dry ashed, a process which removes carbon, hydrogen, nitrogen, and some oxygen and volatile elements (e.g., Cl, Br, S) from the sample. Therefore, the milkweed concentrations cannot be directly compared to toxicological limits and the accuracy of the peach leaves standard measurements cannot be assessed. However, the relative concentrations are meaningful, allowing for the detection of relationships between milkweed and possible explanatory variables.

Of the 12 elements measured in the ashed milkweed leaves, Mg is the most abundant followed by Mn (Table S1.4). Milkweed leaves show broad ranges of elemental concentrations (Table S1.4). Strontium and Cd have the largest ranges with a ~70-fold difference between the minimum and maximum values; Mg has the smallest range with a substantial 5-fold difference. All elements show a positively skewed distribution.

Elemental analysis of wild monarch wings

To estimate the natural exposure of wild monarch butterflies to metals in eastern North America, the wings of 100 monarch butterflies were tested for a suite of 12 elements (i.e., Al, Ba, Cd, Co, Cr, Cu, Mg, Mn, Ni, Pb, Sr, and Zn). The butterflies were captured in the spring of 2011 from sites in Texas, Oklahoma, and Missouri as part of a previous study (Flockhart et al., 2013). These butterflies are assumed to be members of the overwintering generation captured during their return migration from the overwintering sites in central Mexico. Therefore, the natal origins of these monarchs could be anywhere in the USA or Canada, although recent isotope-based geographic assignment using hydrogen and strontium isotopes found that most of these individuals likely originated in Texas (Chapter 2).

To prepare the samples, a single forewing was dry-cleaned using pressurized nitrogen gas (~10 psi for 2 min.) then digested in 16 M HNO_3 (TraceMetal™ Grade; Fisher Chemical, Canada) for 16 h at 120 °C. Ultraclean hydrogen peroxide was added to some samples to complete the digestion. After digestion,

the samples were dried on a hot plate at 90 °C then re-dissolved in 1 mL of 2% v/v HNO_3. One-tenth of the sample was separated out and diluted to 3 mL 2% v/v HNO_3 for trace element analysis using the ICP-MS at the University of Ottawa.

Element concentrations were prepared by bracketing each set of samples with calibration standards prepared using single element certified standards purchased from SCP Science Inc. (Montreal, QC, Canada). Detection limits were conservatively estimated as three times the standard deviation of the blanks; measurements of 3 Cd, 63 Cr, 1 Co, and 63 Ni measurements were below the calculated detection limit and were thus removed from further analysis. Some remaining Cd, Co, and Ni measurements were near the detection limit; otherwise, procedural blanks were negligible (< 5%). Additionally, Cd were ~100 times lower than the calibration points; therefore, the absolute values of Cd are uncertain, but the relative values are likely meaningful. Intra-run precision of standards was acceptable (RSD < 10%) for all elements except Mg and Cr, which should be interpreted with caution.

Magnesium was the most abundant element detected followed by Al (i.e., over 100 ng/mg). All other elements had mean concentrations below 20 ng/mg.

Comparison to permissible limits/toxicological studies

To test if the wild monarchs had metal concentrations that could indicate possible toxicological effects, the metal concentrations of the toxic metals As, Cd, Mn, Pb, and Tl measured in the monarch wings were compared to international permissible limits and toxicological studies on insects (Table S1.4). However, most of the studies looked at the concentrations of metals in food that produce adverse effects, rather than the concentrations of metals in insect tissue at which adverse effects occur. Regardless, examples of insect consumption thresholds are listed in Table S1.4. Few studies have tested the effects of metal exposure to monarch butterflies specifically, although notable exceptions have found negative impacts on monarch survival at doses of Zn as low as 344 ng/mg (Shephard et al., 2020)

and high Na has been associated with decreased survival (Snell-Rood et al., 2014). However, a more recent study found no effects on monarch survival at Na concentrations of 2090 ng/mg and Zn of 555 ng/mg (Shephard et al., 2021). For Pb and Cd, international permissible limits as set by the World Health Organization (WHO) and the United Nation's Food and Agriculture Organization (FAO) for human food (Codex Alimentarius: International Food Standards, 2019) were used. Human-derived limits are non-protective for insects and adverse physiological and behavioural effects can be detected well below set permissible limits (Monchanin et al., 2021; Hopkin, 1990); thus, these limits should be considered to be overestimates. Few studies have investigated the toxicological effects on Mn on insects (Ben-Shahar, 2018) but it is clear that effects are highly species-specific. For example, foraging behaviour of the European honeybee is impacted at Mn concentrations of 2750 ng/mg, the forest cockchafer (*Melolontha hippocastani*) exhibits reduced fitness at 1805 ng/mg, *Cabera pusaria* (L.) caterpillars were negatively affected at 695 ng/mg (Martinek et al., 2020), and *Lymantria dispar* (L.) moths were detected to have reduced survival at 4,087 ng/mg (Kula et al., 2014). A study on *Spodoptera exigua* (Hübner) moths found minimum sublethal (i.e., larval weight loss) concentrations of Co, Ni, and Cu to be 15 ng/mg, 140 ng/mg, and 140 ng/mg, respectively (Cheruiyot et al., 2013).

Predictors of milkweed elemental composition

To identify factors that are potentially predictive of ashed milkweed element concentrations, the top-down linear mixed model selection approach suggested by Zuur et al. (2009) was followed for each element, excluding Ba due to low sample size. Previous studies have found that element concentrations in the soil and degree of urbanization can strongly influence milkweed elemental concentrations (Mitchell et al., 2020). Therefore, spatial geochemical soil data from three soil horizons (i.e., top 0-5 cm, A horizon, and C horizon) were downloaded from the USGS (D. B. Smith et al., 2013). Point data were interpolated for each of the elements and soil horizons using inverse distance weighting using ArcGIS Pro (Esri, Redlands, California, USA). Element concentrations in the three soil horizons were highly

correlated, so the A horizon was chosen as a potential explanatory variable as this horizon is most likely to be accessed by the roots of milkweed and likely integrates both residual and transported (e.g., aeolian, anthropogenic) soils. Additionally, land use classifications from the National Land Cover Database (NLCD) were gathered (Dewitz & U.S. Geological Survey, 2021; Homer et al., 2020; S. Jin et al., 2019; Yang et al., 2018). Classifications were simplified into four categories: natural, agricultural, wetland, and urban. Soil element concentrations and land use classifications were extracted from the spatial surfaces at the location of the milkweed collection sites. Linear mixed models were fit using the *nlme* package (Pinheiro et al., 2020) in R (R Core Team, 2013) and final models were selected using AICs. Fixed effects included land use, soil elemental concentration and their interaction; random effects included ICP-MS analytical run, sampling year, sampling month, and milkweed species. Models including spatial autocorrelation structures (gaussian, spherical, and exponential) were also compared. Distributions of the response (i.e., ashed milkweed elemental concentration) and explanatory variables were inspected for normality and all milkweed elements and the soil concentrations of some elements (i.e., Cd, Cu, Co, Ni, Pb) were natural log-transformed.

Final models of ashed milkweed element concentrations show high variability in the explanatory variables selected for each element (Table S1.5). All final models except those for Mg and Sr include concentration in soil as an explanatory variable; however, this effect is only significant for Ni and Al. There is a negative relationship between the concentration of Cu and Cd in soil and in milkweed (Table S1.5); the concentration in milkweed of all other elements increases with higher concentration in soil. Landuse is only implicated as a relevant factor for Mg, Sr, Cd and Pb; this influence is mainly driven by the wetland category. A temporal variable (i.e., capture month or year) is included in the final model of Mn, Ni, Pb, Zn, Mg, and Sr. Overall, the linear mixed models have poor goodness-of-fit and exhibit considerable model uncertainty via intermediate models with similar AICs.

We expected to find strong relationships between the element concentrations in soil and milkweed; strong relationships would suggest that current maps of metal concentrations in soil (USGS) could be used like an isoscape for geographic assignment (i.e., a "metalscape"). However, we found weak and non-significant relationships between the soil and biosphere for 7 of the 11 elements (e.g., Figure S1.6). Both Sr and Mg were suggested as geolocation tools that should be further explored (Table 1.1), but concentration in soil was not chosen by the model selection procedure as an important predictor for either of these metals (Table S1.5; Figure S1.6). This suggests that more research is needed to understand the spatial patterns of metals in insect tissue before single metals can be used for geolocation purposes. Previous studies have also found similarly weak correlations in both natural (Wieringa et al., 2020) and controlled laboratory (Lin et al., 2021) conditions. Weak correlations are likely influenced by the fact that the elemental soil concentrations used in this study are interpolated from samples of the total soil and may not reflect the bioavailable component of soil elements accessible to the plants (Tibbett et al., 2021). Soil samples that are processed to represent the bioavailable portion of soil elements may yield stronger relationships (Peijnenburg & Jager, 2003). Many of the final linear models included milkweed species as a random effect and indicate substantial differences between species (Table S1.5). The inclusion of this term suggests that there may be inter-specific differences in metal uptake, regulatory, or storage mechanisms even among milkweed species. Alternatively, milkweed species are known to occupy distinct ecosystems (Pocius et al., 2018) and thus this variable could be selected by the model as a proxy for ecological and environmental conditions at a higher resolution than the landuse variable. The poor fit of the linear mixed models indicates that explanatory variables not included in the full model are likely important in determining the concentration of elements in milkweed. Elemental concentrations in milkweed may also be influenced by factors such as distance to anthropogenic sources of metals (Fritsch et al., 2011), developmental stage of the plant, and soil type. Nevertheless, previous studies have found that the weak relationships

found between single elements does not necessarily preclude the geolocation ability of trace elements when combined into a chemoprint (Wieringa et al., 2020).

Table S1.1 The mean, standard deviation, and relative standard deviation (calculated as sd/mean*100) as calculated for SRM 1547 Peach Leaves (National Institute of Standards and Technology) subjected to the same preparation procedure as the milkweed samples (i.e., ashed, digested). The samples (n = 3) were analyzed during three ICP-MS runs. Sample concentrations cannot be directly compared to reference values because the sample concentrations are calculated based on the mass of the sample after it is dry ashed, a process which removes carbon, hydrogen, nitrogen, and some oxygen and volatile elements (e.g., Cl, Br, S) from the sample.

Element	mean (ng/mg)	SD	n	RSD (%)
Mg	46156	5560	3	12
Al	2343	86	3	4
Cr	10	3	3	32
Mn	993	78	3	8
Co	0.84	0.13	3	15
Ni	12	7	3	56
Cu	53	23	3	44
Zn	236	61	3	26
Sr	608	158	3	26
Cd	0.24	0.05	3	21
Pb	7.6	0.4	3	6
Ba	NA	NA	0	*NA*

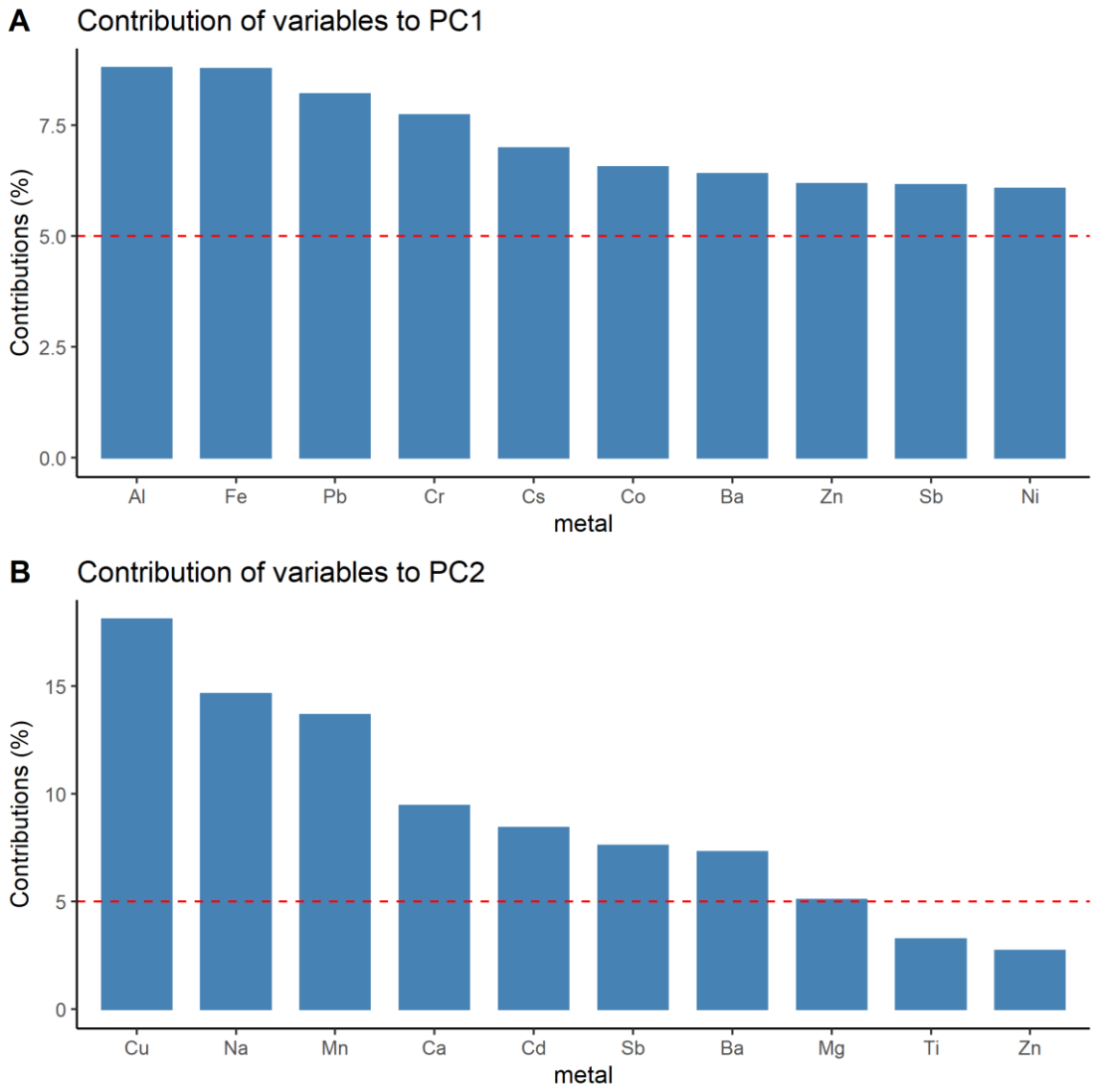

Figure S1.1 Contribution of metals in the wings of monarch butterflies from the diet-switching experiment to **(A)** PC1 and **(B)** PC2. Produced using the *factoextract* package in R (Kassambara & Mundt, 2020)

Table S1.2 Metal concentrations (1 ng of metal per 1 mg of sample material = 1 ppm (mean ± SD (n)) of the larval diet, adult diet, and monarch butterfly wings at different weeks of the diet-switching experiment.

metal	larval diet (n=3)	Monarch wings separated by week of sampling									adult diet (n=4)
		0	1	2	3	4	5	6	7	8	
Al	50±5	3.9±0.5 (4)	13±3 (2)	17±4 (2)	14 (1)	17±11 (2)	11±1 (2)	12 (1)	22±9 (2)	27±6 (2)	0.2±0.03
As	*NA*	bdl	0.17±0.08 (2)	0.11±0.03 (2)	0.13 (1)	0.10±0.10 (2)	0.04±0.01 (2)	0.05 (1)	0.04±0.01 (2)	0.06±0.03 (2)	*NA*
Ba	25±5	0.6±0.1 (4)	5.0±2.5 (2)	4.7±0.8 (2)	5.1 (1)	7.8±6.2 (2)	3.0±1.3 (2)	2.1 (1)	3.3±0.5 (2)	4.4±2.2 (2)	5.4±0.6
Ca	18477 ±1802	718±26 (4)	546±198 (2)	558±226 (2)	521 (1)	622±194 (2)	807±44 (2)	880 (1)	603±168 (2)	457±89 (2)	191±37
Cd	0.01±0.002	0.003±0.001 (4)	0.011±0.002 (2)	0.016±0.002 (2)	0.008 (1)	0.012±0.008 (2)	0.025±0.002 (2)	0.011 (1)	0.036±0.027 (2)	0.028±0.006 (2)	0.0004±0.0001
Co	0.14±0.02	0.011±0.005 (4)	0.042±0.007 (2)	0.081±0.024 (2)	0.073 (1)	0.052±0.011 (2)	0.046±0.005 (2)	0.038 (1)	0.085±0.030 (2)	0.041±0.008 (2)	0.013±0.001
Cr	0.5±0.2	0.7±0.1 (4)	1.2±0.4 (2)	0.9±0.2 (2)	0.9 (1)	1.2±0.3 (2)	1.0±0.2 (2)	1.1 (1)	1.2±0.1 (2)	1.1±0.05 (2)	0.033±0.002
Cs	*NA*	0.0018±0.0008 (4)	0.0035±0.0009 (2)	0.0053±0.0003 (2)	0.0045 (1)	0.006±0.0002 (2)	0.0041±0.0004 (2)	0.005 (1)	0.0041±0.0003 (2)	0.0039±0.0005 (2)	0.011±0.001
Cu	7.7±0.3	4.9±0.8 (4)	4.2±0.1 (2)	5.4±0.3 (2)	5.1 (1)	5.1±0.3 (2)	7.2±0.3 (2)	5.4 (1)	7.0±0.5 (2)	6.5±0.8 (2)	0.02±0.03
Fe	112±6	45±8 (4)	79±8 (2)	97±9 (2)	93 (1)	92±59 (2)	83±25 (2)	84 (1)	147±2 (2)	108±17 (2)	*NA*
Mg	4168±330	529±261 (4)	160±9 (2)	190±34 (2)	193 (1)	199±1 (2)	260±2 (2)	263 (1)	292±56 (2)	205±28 (2)	73±5
Mn	79±20	5.1±0.6 (4)	5.4±0.4 (2)	4.5±0.4 (2)	5.5 (1)	4.4±1.2 (2)	3.5±0.4 (2)	3.0 (1)	4.3±0.6 (2)	3.9±0.7 (2)	1.7±0.2
Mo	*NA*	0.36±0.06 (4)	0.34±0.07 (2)	0.32±0 (2)	0.25 (1)	0.37±0.05 (2)	0.37±0.05 (2)	0.4 (1)	0.38±0.06 (2)	0.34±0.08 (2)	0.0038±0.0003
Na	*NA*	60±16 (4)	46±24 (2)	60±10 (2)	60 (1)	60±4 (2)	106±42 (2)	43 (1)	79±17 (2)	69±18 (2)	0.46±0.03
Ni	1.11±0.06	1.2±0.5 (4)	1.6±0.1 (2)	1.8±0.7 (2)	1.9 (1)	2.3±0.1 (2)	1.5±0.2 (2)	2.6 (1)	3.0±0.7 (2)	2.4±0.1 (2)	0.25±0.02
Pb	0.22±0.06	0.03±0.03 (4)	0.18±0.05 (2)	0.37±0.05 (2)	0.31 (1)	0.32±0.08 (2)	0.41±0.15 (2)	0.26 (1)	0.49±0.09 (2)	0.58±0.17 (2)	0.0011±0.0006
Rb	*NA*	0.2±0.1 (4)	0.8±0.3 (2)	1.1±0.1 (2)	1 (1)	2.1±0.4 (2)	0.8±0.3 (2)	1.2 (1)	0.9±0.2 (2)	1.1±0.1 (2)	5.8±0.3
Sb	*NA*	0.06±0.02 (4)	1.48±0.17 (2)	2.15±0.44 (2)	1.65 (1)	2.19±1.11 (2)	1.07±0.02 (2)	0.49 (1)	1.06±0.69 (2)	1.4±0.07 (2)	0.004±0.001
Sr	189±21	5.4±1.0 (4)	5.6±0.7 (2)	8.5±4.1 (2)	6.6 (1)	6.3±2.6 (2)	7.7±0.7 (2)	7.1 (1)	8.1±0.8 (2)	3.4±0.7 (2)	3.7±0.4
Ti	10.2±0.3	7.1±2.1 (4)	3.0±0.02 (2)	4.2±1.2 (2)	2.9 (1)	3.4±0.6 (2)	3.8±0.2 (2)	3.1 (1)	4.4±0.3 (2)	4.2±0.6 (2)	0.06±0.01
Tl	*NA*	0.0039±0.0026 (3)	0.0045±0.0031 (2)	0.0033±0.0004 (2)	0.0042 (1)	0.0025±0.0012 (2)	0.0051±0.0012 (2)	bdl	0.0023±0.0002 (2)	0.0023±0.0004 (2)	0.001±0.0001
U	*NA*	bdl	0.0008±0.0001 (2)	0.0011±0.0009 (2)	0.0010 (1)	0.0012 (1)	bdl	bdl	0.0008±0.0003 (2)	0.0013±0.0003 (2)	*NA*
Zn	18±4	19±5 (4)	25±8 (2)	22±2 (2)	26 (1)	35±18 (2)	40±1 (2)	22 (1)	37.5±0.2 (2)	34.1±0.7 (2)	1.84±0.07

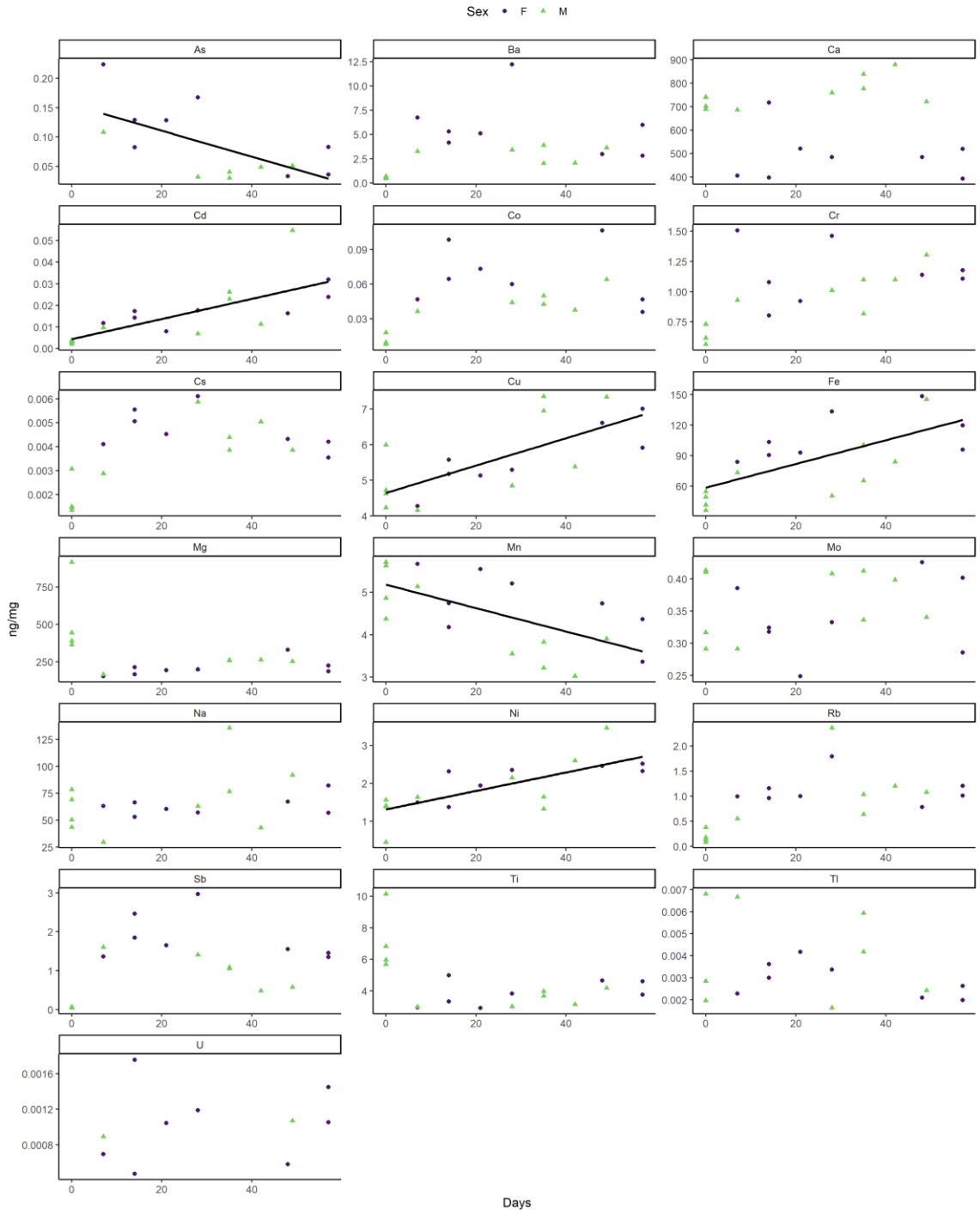

Figure S1.2 Metal concentrations (ng/mg) in monarch wings over 8 weeks from the diet-switching experiment. Males are indicated by green triangles and females by purple dots. Missing metals can be found in the main text (Zn, Al: Figure 1.2; Sr: Figure 1.3; Pb: Figure 1.4).

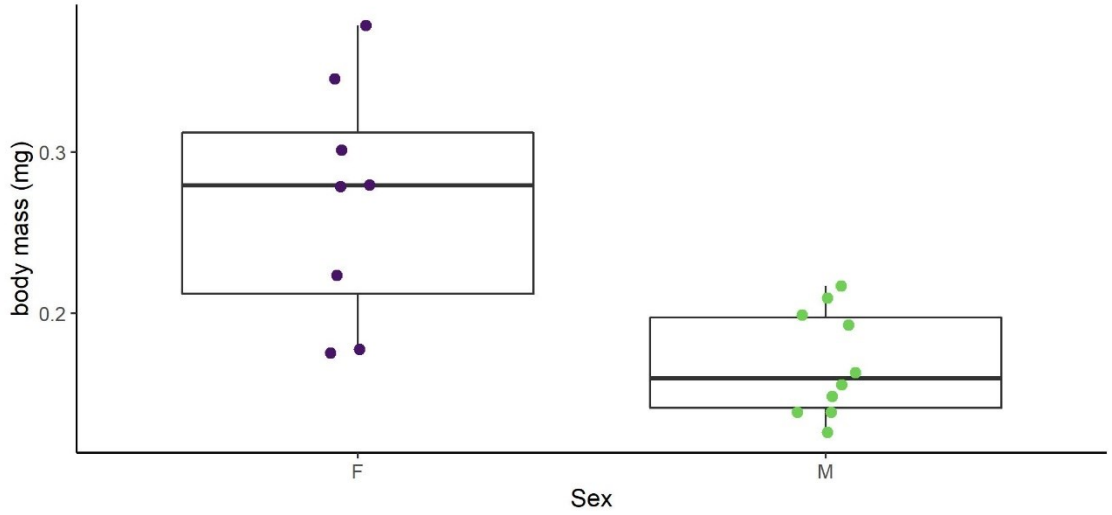

Figure S1.3 Boxplot demonstrating the confounding relationship between monarch body mass (mg) and sex (point-biserial correlation = -0 .70) for the diet-switching experiment.

Table S1.3 A repeat of the multivariate multiple regression (Table 1.1) was performed for each metal in the wings of the monarchs from the diet-switching experiment. To test for model sensitivity to the confounding relationship between body mass and sex (Figure S1.3), sex was excluded from the regression, leaving time (days) and body mass (mg) as explanatory variables. Model fit is given as adjusted R^2 and non-standardized (ng/mg) effect sizes are reported for each predictor (β ± SE, t-value); significant relationships are starred and in bold (α = 0.05). The sample size is 18 for all metals except As (n = 14), Tl (n = 16), and U (n = 10). Only a few regression results were sensitive to the removal of the sex variable: (1) for Ca and Sb, significant effects that were previously attributed to sex were now attributed to body mass, (2) the effect of body mass on Ba and Mn changed to statistically significant, and (3) the effect of days on Cr, Cs, and Rb became statistically significant.

Metal	Adj. R^2	Time (days)	Body mass (mg)
Category 1: intrinsic factors			
As	**0.60***	**-0.0018±0.0006, -2.9***	0.0003±0.0001, 2.8
Ca	**0.57***	-1.3±1.2, -1.1	**-1.6±0.34, -4.8***
Co	0.15	0.00061±0.00031, 2.0	-0.00009±0.00008, -1.1
Mn	**0.57***	**-0.030±0.007, -3.9***	**0.006±0.002, 2.9***
Mo	**0.25***	0.0004±0.0006, 0.7	**-0.0004±0.0002, -2.7***
Sb	**0.29***	0.011±0.008, 1.4	**0.006±0.002, 2.7***
Category 2: exogenous bioaccumulation			
Al	**0.68***	**0.30±0.06, 5.4***	0.05±0.02, 3.1
Cr	**0.28***	**0.007±0.003, 2.6***	0.001±0.0007, 1.4
Cd	**0.49***	**0.0005 ± 0.0001, 4.2***	-0.00002±0.00003, -0.7
Cu	**0.50***	**0.038±0.009, 4.2***	-0.002±0.003, -1.0
Fe	**0.50***	**1.2±0.3, 4.1***	-0.13±0.08, -1.6
Pb	**0.77***	**0.008±0.001, 7.4***	0.0007±0.0003, 2.3
Category 3: dietary bioaccumulation			
Ni	**0.47***	**0.024±0.006, 4.2***	-0.0002±0.0016, -0.1
Zn	**0.38***	**0.31±0.09, 3.5***	0.01±0.02, 0.5
Category 4: geolocation			
Ba	**0.39***	0.04±0.03, 1.4	**0.024±0.007, 3.4***
Cs	0.20	**0.00003±0.00002, 2.2***	0.000006±0.000004, 1.3
Mg	0.21	-3.4±1.9, -1.8	-0.95±0.52,-1.8
Na	0.13	0.37±.26, 1.4	-0.11±0.07, -1.5
Rb	0.20	**0.014±0.006, 2.3***	0.002±0.002, 1.0
Sr	-0.02	0.0005±0.0245, -0.02	-0.008±0.007, -1.2
Ti	0.16	-0.04±0.02, -1.9	-0.007±0.005, -1.3
Tl	0.05	-0.00003±0.00002, -1.4	-0.000006±0.000006, -1.0
U	-0.18	0.000004±0.000007, 0.6	0.000001±0.000002, 0.6

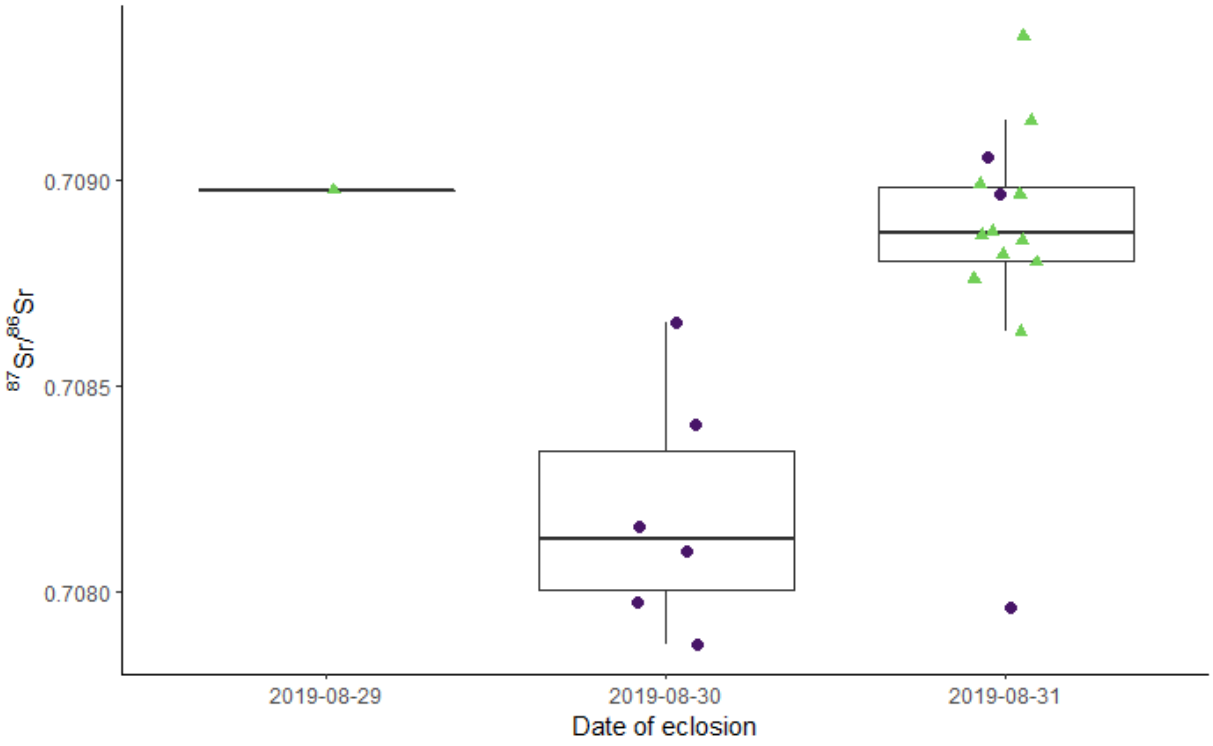

Figure S1.4 Boxplot of $^{87}Sr/^{86}Sr$ by date of eclosion for the diet-switching experiment. Most male monarchs (green triangles) emerged from their chrysalises one day after the females (purple dots).

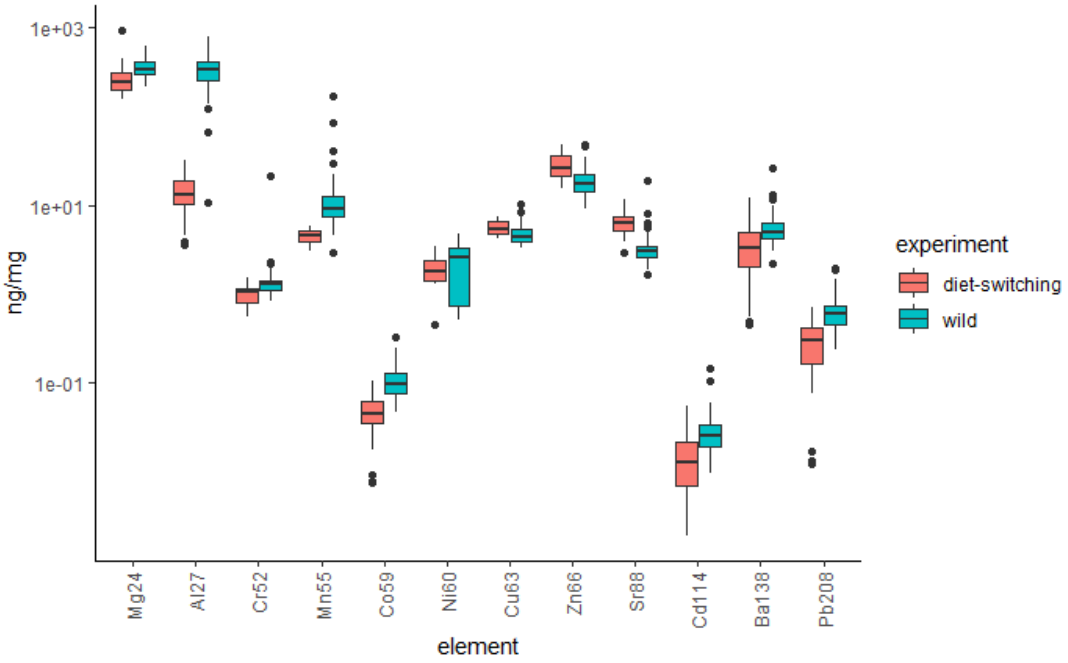

Figure S1.5 Boxplot comparing the concentrations of metals found in the forewings of wild monarch butterflies (blue; n = 100 except for Cr (n = 37), Co (n = 99), Ni (n = 37), and Cd (n = 97)) to those found in the diet-switching experiment (red; n = 18). Note the logarithmic scale on the y-axis. Wild monarchs tend to have higher metal concentrations than experimental monarchs, except for Cu, Zn, and Sr, which have lower concentrations.

Table S1.4 Mean, standard deviation, and maximum concentration of the 12 metals measured in wild ashed milkweed and wild monarch butterflies across the eastern USA. Permissible limits of certain toxic elements are listed and occurrences above these limits are marked in bold text.

metal	ashed milkweed (ng/mg)		monarch (ng/mg; n=100)		consumption threshold (ng/mg)	reference
	mean ± SD (n)	range	mean ± SD	maximum		
Al	431±509 (85)	71-3847	**333±122**	**777**	160	(Kijak et al., 2014)
Cd	0.11±0.10 (57)	0.03-0.52	0.03±0.02	**0.15**	0.05-2	(Codex Alimentarius: International Food Standards, 2019)
Cr	1.84±1.07 (85)	0.42-5.57	1.2±2.1	22		
Cu	172±104 (85)	51-472	4.7±1.3	10	140	(Cheruiyot et al., 2013)
Mn	880±980 (85)	188-8114	12.9±18.0	167	695-4087	(Martinek et al., 2020, 2018; Søvik et al., 2015; Kula et al., 2014)
Ni	15.8±14.1 (80)	1.4-74.1	0.9±1.3	4.8	140	(Cheruiyot et al., 2013)
Pb	1.38±1.01 (85)	0.31-6.78	**0.6±0.3**	**2**	0.01-1	(Codex Alimentarius: International Food Standards, 2019)
Zn	460±299 (85)	75-1688	19.1±6.9	48	344	(Shephard et al., 2020)
Co	0.96±1.03 (85)	0.27-6.58	0.11±0.05	0.32	15	(Cheruiyot et al., 2013)
Mg	51932±17697 (85)	26398-139666	354±86	618		
Ba	309±286 (10)	62-820	5.8±2.9	26		
Sr	399±410 (85)	37-2605	3.3±1.8	19	NA	NA

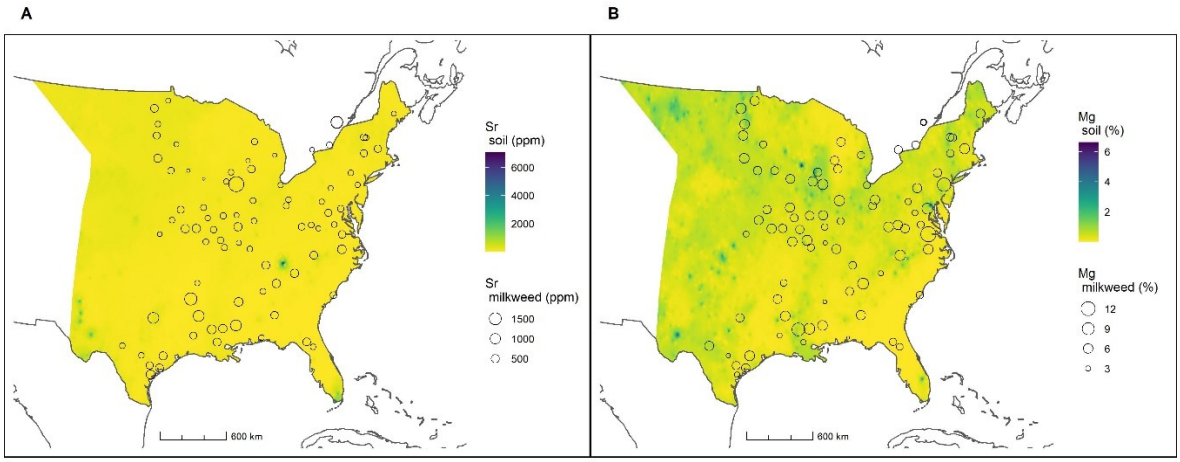

Figure S1.6 Maps demonstrating the weak correlations between metal concentrations in ashed milkweed samples and soil in the eastern USA. Metal concentrations in soil were interpolated from USGS soil samples (A horizon) (D. B. Smith et al., 2013). **(A)** Strontium concentration in the soil and milkweed are weakly correlated. The concentration in soil was not highlighted as an important variable by the model selection process (Table S1.5). **(B)** Likewise, Mg concentrations in the soil and the milkweed are weakly correlated and Mg concentration in the soil was not selected as an important predictor by the model selection procedure (Table S1.5).

Table S1.5 Final models for the concentration of each metal in ashed milkweed following the model selection procedure outlined in Zuur et al. (2009). Dashes indicate that the variable was not selected for the final model. All response variables and the soil concentrations of Cd, Cu, Co, Ni, and Pb were natural log-transformed to meet the assumption of normality. Pseudo R^2 was calculated based on Nakagawa et al. (2017). *p < 0.05

metal	model fit		fixed effect			random effect				spatial autocorrelation structure
	AIC	Pseudo R^2	soil (β±SE, df, t)	landuse (Wald test; df, F)	soil * landuse (Wald test; df, F)	species (SD)	analytical run (SD)	Year	Month	
Al	212	0.30	0.13±0.07, 72, 2.0*	-	-	0.42	-	-	-	-
Cd	127	-	-0.71±0.47, 55, -1.5	3,0.4	3, 3.6*	-	-			gaussian
Cr	127	0.51	0.0025±0.0014, 79, 1.8	-	-	-	0.43			-
Cu	92	-	-.065±0.080, 61, -0.8	-	-	0.053	0.51	-	-	-
Mn	172	-	0.00015±0.00017, 64, 0.9	-	-	0.63	-	-	0.0005	exponential
Ni	176	-	0.25±0.10, 48, 2.4*	-	-	0.73	0.34	-	0.31	-
Pb	165	0.32	0.59±0.42, 72, 1.4	3, 5.9*	3, 2.8*	-	-	-	0.20	-
Zn	142	-	0.0015±0.0021, 66, 0.72	-	-	0.66	-	0.00004	-	-
Co	177	0.42	0.075±0.078, 79, 1.0			-	0.53	-	-	gaussian
Mg	48	-	-	3, 1.72	-	0.22	-	0.00002	0.000003	-
Sr	191	-	-	3, 4.1*	-	0.39	-	0.44	-	exponential

Appendix B: Supplementary Material for Chapter 2

Unknown-origin monarch butterflies

Unknown-origin monarch butterflies were captured in the USA in spring 2011 as part of a previous study (Flockhart et al., 2013). Wing wear scores were assigned to each of the unknown-origin monarchs upon capture. Wing wear scores allow researchers to estimate the age of a butterfly as more worn/tattered butterflies (score = 5) are likely to be older than fresh, unmarked butterflies (score = 1). For this study, we used 100 butterflies that received high wing wear scores and were captured in Apr. (score ≥ 3) or May (score ≥ 4), and are therefore likely to represent overwintering individuals (Figure S2.1). These monarchs were captured between Apr. 13 and May 8, 2011. Monarchs were sighted in the South Central USA well before sampling began (i.e., first sightings in late Feb.), and the northward migration was well-advanced by May 8 (Figure S2.2). The pace of the northward migration in spring 2011 was reported to be unusually rapid, likely due to unfavourable conditions in Texas (O. R. Taylor, 2011).

Monarch δ^2H isoscape

We constructed a new monarch δ^2H isoscape using the *assignR* package (Ma et al., 2020). The unknown-origin monarchs used in this study were previously assigned using δ^2H and $\delta^{13}C$ (Flockhart et al., 2013). The δ^2H assignments were made using a δ^2H isoscape calibrated using known-origin monarch δ^2H from Hobson et al. (1999). Since then, the precipitation δ^2H isoscape and known-origin monarch calibration dataset have both been updated, prompting us to revise the assignments. The known-origin calibration dataset we used here (i.e., Hobson et al., 2019) uses samples taken from the same locations and at the same time as Hobson et al. (1999), but was analyzed using a modern method (Figure S2.3). We tested the effect of analytical run between Hobson et al. (2019) and Hobson et al. (1999) using a linear mixed model with precipitation δ^2H and reference (i.e., 2019 or 1999) as fixed effects and sample site as random intercept and reference as random slope. We found that the δ^2H measured using the analytical

techniques of Hobson et al. (2019) differ significantly from the δ^2H reported in 1999 (lmm: β = -8.41 ± 0.90, df = 26.72, t = -9.39, $p < 0.001$).

As the analytical methods and standards used in Flockhart et al. (2013) and Hobson et al. (2019) are identical, the δ^2H used in both of these papers can be directly compared without transformation. Despite this compatibility, we revised the δ^2H of both the known-origin monarch calibration dataset (Hobson et al., 2019) and the unknown-origin monarch butterflies (Flockhart et al., 2013) to the most up-to-date reference scale of Soto et al. (2017). We applied this correction to facilitate the comparison of δ^2H and isoscapes developed in this study with future studies and reduce end-user confusion. To standardize δ^2H in both, we used the following equation provided by Soto et al. (2017):

$$(revised\ \delta^2H) = 10.774 + 0.852 * (reported\ \delta^2H) \quad \text{Eqn. S2.1}$$

To facilitate the comparison and combination of the $^{87}Sr/^{86}Sr$ and δ^2H geographic assignments, the precipitation δ^2H isoscape was first modified to be the same resolution and projection as the $^{87}Sr/^{86}Sr$ isoscape (1 km²) using the *raster* package (Hijmans, 2020). Using the *assignR* package's *calRaster* function, we fit a linear regression model between the adjusted mean known-origin monarch δ^2H and the growing season precipitation δ^2H isoscape (Bowen, 2018; IAEA/WMO, 2018; Bowen et al., 2005) and applied the linear relationship to the precipitation δ^2H isoscape (Figure S2.4). We found a positive relationship between growing season precipitation and known-origin monarch δ^2H (y = 0.78(x) - 51.35, R^2 = 0.73, $p < 0.001$). The predicted monarch δ^2H isoscape (Figure 2.4A) and its associated standard deviation for eastern North America (Figure 2.4B) can be found in the main text. The monarch δ^2H isoscape shows broad latitudinal bands with more depleted δ^2H towards the northwest (Figure 2.4A).

Plant $^{87}Sr/^{86}Sr$ isoscape

Previous works have primarily used mechanistic approaches to predict $^{87}Sr/^{86}Sr$ in rocks and ecosystems across the USA (e.g., Bataille & Bowen, 2012). This mechanistic isoscape was tested against the $^{87}Sr/^{86}Sr$ of local animal tissues and, while promising, did not reach sufficient accuracy to apply continuous-

surface assignments (Crowley et al., 2017). Poor accuracy stems, partly, from not incorporating multiple factors that could influence $^{87}Sr/^{86}Sr$ across the landscape (Bataille et al., 2020). To address this issue, Bataille et al. (2018) proposed a novel approach using random forest regression, a decision-tree-based machine learning algorithm that integrates both empirical data of $^{87}Sr/^{86}Sr$ in ecosystems (i.e., $^{87}Sr/^{86}Sr$ of georeferenced biological samples) and geospatial data products (e.g., raster files depicting environmental variables) (Bataille et al., 2020, 2018). This approach provided an accurate, high-resolution $^{87}Sr/^{86}Sr$ isoscape for Western Europe (Bataille et al., 2018) and was then extended to the global scale using a large compilation of $^{87}Sr/^{86}Sr$ from multiple substrates including plants, local animals, soils, and water (Bataille et al., 2020). The resulting $^{87}Sr/^{86}Sr$ isoscape showed excellent predictive power with the promising possibility of applying continuous-surface geographic assignment using $^{87}Sr/^{86}Sr$ in a range of fields, including ecology. However, Bataille et al. (2020) also cautioned that, while accurate, their global $^{87}Sr/^{86}Sr$ isoscape should be recalibrated for tissue-specific and regional studies. Regional recalibration offers several advantages, including: (i) removing geographic sampling biases, (ii) targeting substrates specific to one application (e.g., plants), and (iii) the possibility to use regional geospatial data.

We used an empirical dataset of plant $^{87}Sr/^{86}Sr$ and explanatory variables to train a random forest regression model and create a plant $^{87}Sr/^{86}Sr$ isoscape. Prior to fieldwork collecting plant samples, we carefully selected the general sampling areas to supplement gaps in the spatial distribution of data from the literature and obtain a dataset representative of geological regions across eastern North America. Factors considered when selecting the sampling sites included major geological units, presence of surficial geology, climate region, distance to the coast, and anthropogenic influences. Once at the collection area, we selected a location where the possible factors influencing intra-site $^{87}Sr/^{86}Sr$ variability were minimized; samples were collected from parks, forests, and minimally-disturbed areas. At each selected site, five leaves were collected from each of 3 to 4 milkweed plants growing at least 10

meters apart to avoid sampling microhabitats. We also recorded metadata at each location (e.g., photo, location, species, distance from infrastructure). Leaf samples were placed into a plant press, dried, and stored in plastic bags for long-term storage.

Plants primarily uptake their strontium from local soils through their roots, and, in most cases, different plants at a given location show very similar $^{87}Sr/^{86}Sr$. However, in some cases, plants with different rooting depths (e.g., trees vs. grasses) might show significant differences in $^{87}Sr/^{86}Sr$ (Poszwa et al., 2002). Differences in $^{87}Sr/^{86}Sr$ between plants at a single location usually occur in areas where the topsoil mineralogical composition differs substantially from that at depth (Capo et al., 1998). Local $^{87}Sr/^{86}Sr$ variability is also influenced by the presence of fertilizers in the topsoil (e.g., Thomsen & Andreasen, 2019), atmospheric sources (Serna et al., 2020; Hartman & Richards, 2014), thin surficial deposits (Snoeck et al., 2020), high heterogeneity of bedrock geology, and rapid erosion rates leading to local soil movements (Snoeck et al., 2020). In an attempt to control for these factors, we exclusively sampled and analyzed herbaceous plants of similar root depth (i.e., no shrubs or trees) and all the plant data compiled from the literature were from species with similar rooting depth to *Asclepias* spp. (e.g., grasses) which was approximately 1 m (Schenk & Jackson, 2002).

After sample collection, the leaves of the 144 new plant samples were used for $^{87}Sr/^{86}Sr$ analysis. Before analysis, samples were cleaned of any surface dust by rinsing with double-deionized water in an ultrasonic bath for 10 min. Samples were then digested and solubilized. To facilitate digestion, we first ashed the plant samples at 600 °C for 4 h. The ashed samples were then digested in perfluoroalkoxy alkanes (PFA) vials (Savillex, LLC., Eden Prairie, MN, USA) using concentrated nitric acid (16 M; TraceMetal™ Grade; Fisher Chemical, Mississauga, ON, Canada) for 16 h at 120°C. After digestion, the samples were dried on a hot plate at 90°C. The dried samples were re-dissolved in 1 mL of 2% v/v HNO_3 (double distilled). A 100 µL aliquot of each solution was taken and diluted to 3 mL 2% v/v HNO_3 to measure the Sr concentration. We measured Sr concentration via inductively coupled plasma mass

spectrometry (ICP-MS; Agilent 8800 ICP-QQQ, Agilent Technologies Inc., Santa Clara, CA, USA) at the Department of Earth and Environmental Sciences, University of Ottawa. Calibration standards were prepared using single element certified standards purchased from SCP Science Inc. (Montreal, QC, Canada). Another aliquot with 100 ng of Sr from the remaining 900 µL of each sample digest was subset into PFA vials. The solutions were dried down, re-dissolved in 0.5 mL 6 M HNO_3, and loaded on chromatography columns with *Sr-spec Resin™* (50 – 100 µL; Eichrom Technologies LLC, Lisle, IL, USA) to separate Sr from the matrix. The eluate with Sr fraction of each sample was prepared into 2 mL 0.05 M HNO_3, ready for Sr isotope analysis. The $^{87}Sr/^{86}Sr$ analysis was performed at the Isotope Geochemistry and Geochronology Research Centre**,** Carleton University, using a Thermo Scientific™ Neptune™ high-resolution multi-collector inductively coupled plasma mass spectrometer (MC-ICP-MS; Thermo Fisher Scientific, Bremen, Germany). Because the Sr concentration is high in plant samples, we used the traditional self-aspiration system with an uptake rate of 100 µL/min following the method in Hu et al. (2020a). Instrumental mass fractionation was corrected by normalizing $^{86}Sr/^{88}Sr$ to 0.1194 using the exponential law. Reference material SRM® 987 (0.71034 ± 0.00026 [95% CI]; National Institute of Standards and Technology, Gaithersburg, MD, USA) and a pure Sr in-house standard (both at 100 ng/g Sr concentration) were analyzed together with plant samples to monitor the status of the instrument. During the analysis of plant samples, the measured $^{87}Sr/^{86}Sr$ of the two standards were 0.71027 (± 0.00002, n = 17) for SRM® 987 and 0.70824 (± 0.00007, n = 7) for the in-house standard. The final dataset of plant $^{87}Sr/^{86}Sr$ (i.e., both new and from the literature) had a right-skewed distribution with a median ratio of 0.7102 and an interquartile range of 0.7094 to 0.7113 (n = 398).

We assembled a portfolio of 29 geospatial data products selected as potential explanatory variables because they represent potential factors influencing $^{87}Sr/^{86}Sr$ variation on the landscape (Bataille et al., 2020, 2018; Table S2.2). Each of the potential explanatory variables was previously projected into WGS84-Eckert IV and resampled to 1 km^2 resolution (Bataille et al., 2018). Here, we re-

projected each of the rasters into an appropriate equal-area projection for North America: North America Albers equal-area conic.

We used the location of each plant sample in the plant $^{87}Sr/^{86}Sr$ dataset to extract the local pixel values of each of these explanatory variables. We used the *VSURF* package (Variable Selection Using Random Forest) to optimize our model and select the geospatial data products that best predict the $^{87}Sr/^{86}Sr$ variations in plants, based on out-of-bag error decrease (Genuer et al., 2015).

The *VSURF* variable selection procedure identified six explanatory variables that were dominant predictors of $^{87}Sr/^{86}Sr$ in plants across eastern North America (i.e., r.srsrq3, r.srsrq1, r.m1, r.ph, r.maxage_geol, r.phkcl; Table S2.2). We removed soil pH in KCl solution (r.phkcl), the least important variable suggested by *VSURF*, from consideration because of its similarity to soil pH in H_2O solution (x10) (r.ph). The five most dominant predictors were geological variables, including bedrock model products (Bataille et al., 2018), geological age of rock units from the GLiM (Hartmann & Moosdorf, 2012), and soil pH in H_2O solution (x10) (Hengl et al., 2017; Figure 2.3A). Maps of these predictors have been plotted to show the spatial patterns that influence the resultant $^{87}Sr/^{86}Sr$ isoscape (Figure S2.6). The top predictors of the plant $^{87}Sr/^{86}Sr$ were comparable to those found in previous studies to be important for a $^{87}Sr/^{86}Sr$ isoscape of Western Europe, including GLiM age (maximum) and the bedrock model outputs (Bataille et al., 2018). Plant $^{87}Sr/^{86}Sr$ decreased with soil pH; this is likely due to the preferential weathering of carbonates with $^{87}Sr/^{86}Sr$ converging towards 0.708 in alkaline soils (Figure S2.5). As expected, $^{87}Sr/^{86}Sr$ increased with rock age and with increasing $^{87}Sr/^{86}Sr$ in bedrock (Figure S2.5). Higher $^{87}Sr/^{86}Sr$ observed in plants collected in older geological regions, such as the Canadian Shield, and lower $^{87}Sr/^{86}Sr$ were observed in plants collected on young carbonate units (Bataille et al., 2020, 2018; Figure S2.6). However, these geological variables were unable to inform plant $^{87}Sr/^{86}Sr$ at higher ratios (Figure S2.5). The positive correlation between plant $^{87}Sr/^{86}Sr$ and model residuals has been observed before and reflects

the higher $^{87}Sr/^{86}Sr$ variability in older rock units (Bataille et al., 2018). Except for these regions with higher $^{87}Sr/^{86}Sr$, most of the study area had plant $^{87}Sr/^{86}Sr$ that could be predicted within ± 0.001.

Cleaning butterfly wings for $^{87}Sr/^{86}Sr$ analysis

Butterfly wings undergoing $\delta^{2}H$ and $\delta^{13}C$ isotopic analysis are traditionally cleaned with a 2:1 chloroform-methanol solution to remove surface oils and pigments (Hobson et al., 1999). This cleaning step is important because lipids, pigmentation, and differences in scaling (e.g., as a result of wing wear) can increase within-wing variation in these isotopes (Hobson et al., 2017). Cleaning is even more critical for trace-metal isotopes like strontium because airborne dust particles or clay sticking to the wings might contain significant amounts of strontium. However, when analyzing trace metals, solvent washing can also lead to contamination and metal exchange between the solvent and wing tissues, as has been shown for human hair (Kempson & Skinner, 2012). Therefore, alternate cleaning methods need to be considered. A study performed on feathers demonstrated that dry-cleaning with pressurized dry nitrogen gas was an effective cleaning method to remove waxy deposits and particulates (Font et al., 2007), and this technique was successfully applied and validated on *Helicoverpa armigera* moths (Holder, 2012). This method limits the risk of solvent contamination while effectively removing dust particles.

We cleaned the monarch wing samples (one forewing per individual) using dry-cleaning with pressurized nitrogen gas (~10 psi) for 2 min. This technique has already been used on moths (Holder et al., 2014; Holder, 2012), but here we verified the validity of this dry-cleaning protocol for monarch butterflies by analyzing butterfly wings under scanning electron microscopy to assess the presence of dust on the wing surface. Butterfly wings were purposefully dusted and then subjected to one of two treatment methods: cleaning with 2:1 chloroform-methanol or pressurized nitrogen gas. The amount of dust present after treatment was assessed visually.

Both cleaning methods showed a marked decrease in the number of particles attached to the wing compared to the control (Figure S2.7). Given the equal performance of the surface cleaning and the additional advantages of the dry-cleaning method, such as removing the risk of Sr leaching into the washing solution, we chose to continue using pressurized nitrogen gas to remove surface contamination from the monarch wing samples.

Bayesian probabilistic geographic assignment

The $^{87}Sr/^{86}Sr$ of the unknown-origin monarch butterflies were moderately right-skewed and had a median of 0.7087 and interquartile range from 0.7084 to 0.7092 (n = 100). The δ^2H of the same monarchs had a mean (± SD) of -77.7‰ (± 11.3).

Geographic assignment of the 100 unknown-origin monarch butterflies was performed in three ways: (i) δ^2H assignment, (ii) $^{87}Sr/^{86}Sr$ assignment, and (iii) dual δ^2H and $^{87}Sr/^{86}Sr$ assignment. The single-isotope assignment method is integrated into the *assignR* package (Ma et al., 2020). The geographic assignment method uses a continuous-surface assignment framework to estimate the most likely natal origin of each individual with an unknown origin (z^*) using the observed δ^2H or $^{87}Sr/^{86}Sr$ (x^*). The probability that any given cell of the isoscape *(c)* represents a potential origin for a wing [$f(z^*|c)$] was then evaluated using a normal probability density function:

$$f(z^*|c) = \left(\frac{1}{\sigma\sqrt{2\pi}}\right) exp\left[-\frac{{z^*}^2}{2}\right] \qquad \text{with } z^* = \frac{x^*-\mu_C}{\sigma} \qquad \text{Eqn. S2}$$

Where μ_c and σ represent the mean prediction and its uncertainty over the entire study area. This equation is valid when using a single isotope system for assignment. The dual-isotope assignment method is not built into the current version of the *assignR* package but operates similarly. Under the assumption of independence between the two variables, the combined probability density for δ^2H and $^{87}Sr/^{86}Sr$ dual assignment is:

$$f(z_H^*, z_{Sr}^*|c) = \left(\frac{1}{\sigma\sqrt{2\pi}}\right) exp\left[-\frac{{z_H^*}^2+{z_{Sr}^*}^2}{2}\right] \qquad \text{Eqn. S3}$$

where z_H^* and z_{Sr}^* are the observed values for each wing. This joint function is the product of the marginal functions of each isotope system and yields high likelihood estimates when both marginal probability densities are also high. The probability of origin is normalized by dividing by the highest probability cell and converted to a percentile scale by multiplying by 100.

Nominal assignment

To further investigate differences in the individual assignment maps, a nominal approach was taken to assign individuals to large zones of probable origin. These zones were defined by Flockhart et al. (2017b) and are based on the known spatiotemporal distribution of monarchs during the breeding season. The maximum dual δ^2H and $^{87}Sr/^{86}Sr$ assignment probability of origin was calculated for each zone, and the individual was assigned to the zone with the highest probability of origin. Nominal assignment to zones found that 35% of the 100 monarch butterflies were found to originate from northern Mexico (i.e., "south"), 25% from the southwest, 21% from the southeast, 6% from Florida, and the remaining 13% from more northernly zones (Figure S2.9).

Summed binary maps

We summarized the individual assignment maps in an alternate way to the averaged assignments described in the main text (Figure 2.6). As described previously, the top 33% of the probability distribution for each individual was defined as high probability for this study. Areas of high probability were coded with a '1' and low probability areas with a '0'. These binary surfaces were then summed for all individuals (Figure S2.10A) and the three clusters (Figure S2.10B-D). Therefore, the scale of these maps is the number of individuals that have a high probability of originating from a given location. This method of summarizing individual assignment maps is common in ecology (e.g., Flockhart et al., 2013). The large-scale patterns of these binary stack maps (Figure S2.10) agree with those displayed by the averaged assignment maps (Figure 2.6).

Table S2.1: List of considerations when planning an animal mobility study using $^{87}Sr/^{86}Sr$-based geographic assignment. See Figure 2.1 for a corresponding flowchart to guide you through the process.

Step	Considerations
1a) Is $^{87}Sr/^{86}Sr$ assignment a suitable technique for your study organism?	What is the turnover time of Sr in the tissue of interest (e.g., Anders et al., 2019)?
	What are the possible sources of Sr to the animal during tissue formation (e.g., different foods, water sources, dust; see Lengfelder et al., 2019)?
	What is the home range of the study species? Animals with large home ranges may integrate Sr from more disparate sources.
	What are the possible sources of Sr contamination (e.g., hair submerged in water; see L. Hu et al., 2018)?
1b) Is $^{87}Sr/^{86}Sr$ assignment a suitable technique for your study area?	What is the range of $^{87}Sr/^{86}Sr$ in your study area? Estimate the range using a global $^{87}Sr/^{86}Sr$ isoscape (e.g., Bataille et al., 2020).
	Check the accompanying uncertainty raster; is your study area in an area of high or low uncertainty?
TIP: Will $^{87}Sr/^{86}Sr$ be able to help you answer your study question? For example, can $^{87}Sr/^{86}Sr$ assignment differentiate between two breeding areas? To test the resolution of potential $^{87}Sr/^{86}Sr$ assignments before starting your study, try simulating an unknown-origin $^{87}Sr/^{86}Sr$ dataset and performing assignments with an existing isoscape (e.g., Bataille et al., 2020).	
1c) Is there an existing regional $^{87}Sr/^{86}Sr$ isoscape for your study area?	Using a regional $^{87}Sr/^{86}Sr$ isoscape fitted with ecologically relevant known-origin training data is highly recommended (Bataille et al., 2020).
2a) Do you have sufficient known-origin $^{87}Sr/^{86}Sr$ samples?	Are there any relevant $^{87}Sr/^{86}Sr$ from the tissue of interest reported in the literature (see Bataille et al. (2020) for a list of studies)?
	Will any other tissues/species give an appropriate estimate of the $^{87}Sr/^{86}Sr$ of your tissue (e.g., can you use local plant $^{87}Sr/^{86}Sr$ as a proxy for butterfly $^{87}Sr/^{86}Sr$?)
	Do you have enough known-origin samples to produce a high-quality regional isoscape?
	Do you have the budget to supplement the literature records with your own samples?
	How much sample mass do you need to collect?
2b) What species/tissue should you collect?	What species should you sample (e.g., herbaceous plants, shrubs, trees, your study animal, residential animals)?
	What tissue should you sample (e.g., stem, leaf, insect wing, feather, bone, horn, teeth)?
2c) Where should you collect known-origin samples (landscape scale)?	Do your known-origin samples cover the spatial extent of your study area?
	Have you sampled across the range of potential $^{87}Sr/^{86}Sr$? Are there any unique bedrock units you should sample?
2d) Where should you collect samples (local scale)?	What are the potential sources of site contamination (e.g., mixing of non-local sources of Sr via flooding, pesticides, fertilizer)?
	Have you tried to account for intrasite variability and the nugget effect (e.g., pooling samples from a site or collecting multiple samples per site)?
3) Measure the $^{87}Sr/^{86}Sr$ of your samples	How will you clean the samples of possible environmental $^{87}Sr/^{86}Sr$ contamination (e.g., Figure S2.7)?
	After measuring the mass of Sr in your samples, work with your technician to determine the best concentration of Sr to submit for $^{87}Sr/^{86}Sr$ analysis (e.g., the MC-ICP-MS at Carleton University gives ~5V for 100 ppb of Sr and samples were prepared to this concentration).
TIP: How much does each $^{87}Sr/^{86}Sr$ sample cost for analysis? Each sample can cost as little as $50USD and be run on as little as 1 ng of Sr. Contact your preferred isotope analysis laboratory for a quote and ask for the precision of their instrument for the mass of sample that you have available.	
4) Make a regional $^{87}Sr/^{86}Sr$ isoscape using random forest regression	Are there any regional, high-resolution geospatial data specific to your study area that you could use to improve upon global datasets?
	How will you create a spatial depiction of the isoscape uncertainty?
	How will you test the validity and strength of your regional isoscape model?
5) Geographic assignment using the *assignR* package	What is the best way to summarize the information contained in the individual assignment maps (Campbell et al., 2020; Ma et al., 2020)?

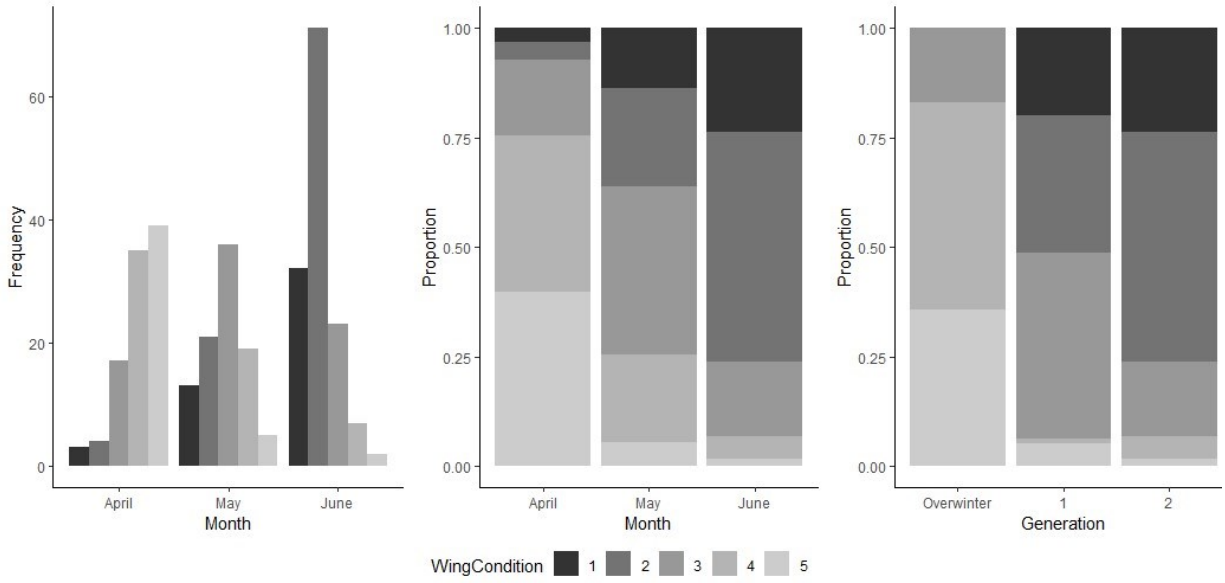

Figure S2.1 Wing wear scores of the unknown-origin monarch butterflies from which the butterflies used in this study were selected. Data are reproduced from Flockhart et al. (2013). Wing wear was scored on a scale from 1 (fresh) to 5 (extremely worn). The left-most bar plot shows the frequency of each wing wear score by month. The center figure shows the proportion of captured monarchs assigned to each wing wear score for each month of capture. Worn monarchs (wing wear ≥ 3) were more frequently captured in Apr. and make up a large proportion of the Apr. captures; these monarchs are assumed to be returning from the overwintering grounds in Mexico. The right-most plot shows the proportion of captured individuals with each wing wear score assigned to each generation. As in Flockhart et al. (2013), monarchs captured with high wing wear scores in Apr. (wing wear ≥ 3) and May (wing wear ≥ 4) were assigned as overwintering butterflies, whereas monarchs captured with low wing wear scores in Apr. (wing wear < 3) and May (wing wear < 4) were assigned as first-generation and monarchs captured in Jun. were assigned as second-generation. This study only used monarchs classified as overwintering butterflies.

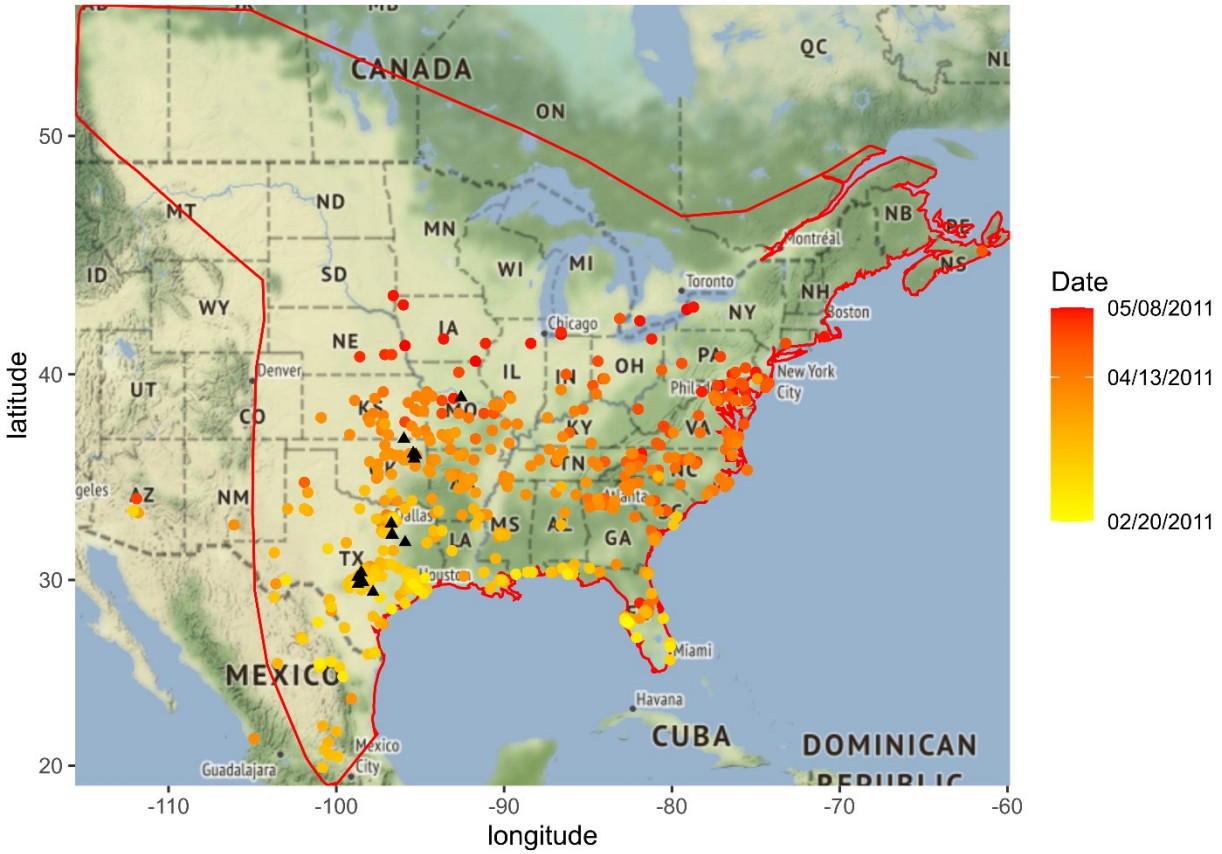

Figure S2.2 Map of first sightings of adult monarchs during the spring northward migration from the first sighting of 2011 up to May 8, as recorded with Journey North (https://maps.journeynorth.org/map/?year=2021&map=monarch-adult-first). Monarchs classified as overwintering and used in this study were collected between Apr. 13 and May 8, 2011. The coloured circles represent Journey North records, and the black triangles are the capture locations of the monarchs used in this study. The base map is a Google Map terrain created using *ggmap* (Kahle & Wickham, 2013).

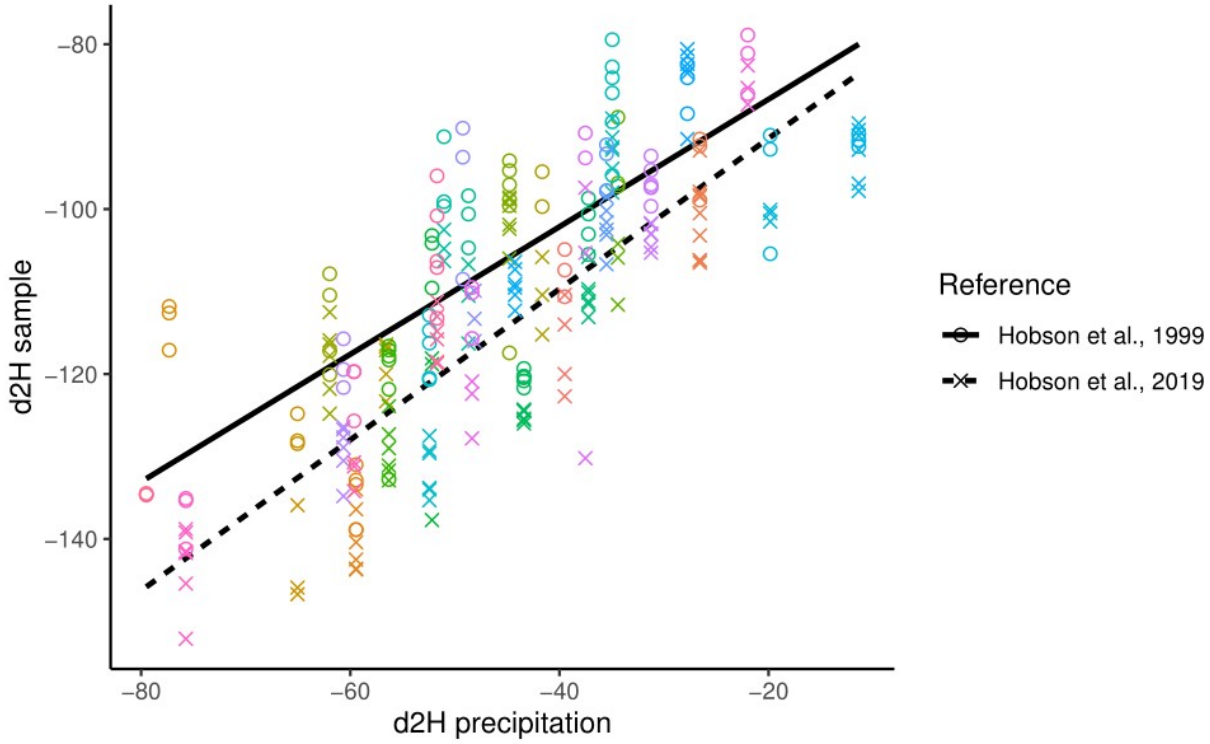

Figure S2.3 A scatterplot of the untransformed δ^2H of precipitation at a given site. Sample δ^2H of monarchs were extracted from Hobson et al. (2019) and (1999) and δ^2H precipitation from a long-term growing season precipitation isoscape (Bowen, 2018; IAEA/WMO, 2018; Bowen et al., 2005). Colours indicate the collection site of the samples, circles are the 1999 untransformed sample δ^2H, and crosses are the 2019 untransformed sample δ^2H. A linear model between precipitation and sample δ^2H was fit for each of the references.

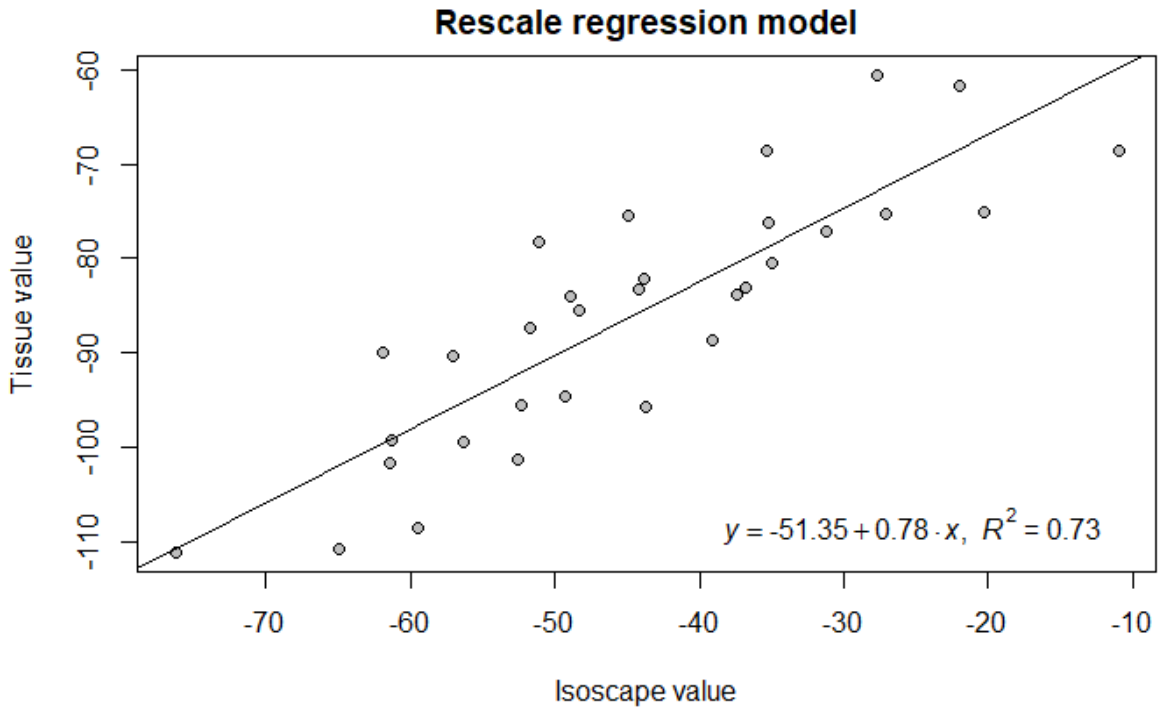

Figure S2.4 Linear regression model used for monarch δ^2H isoscape calibration. The relationship between the growing season precipitation δ^2H isoscape (i.e., isoscape value) and known-origin monarch δ^2H (i.e., tissue value) is shown.

Table S2.2 List of 29 geological, climatic, environmental, and anthropogenic explanatory variables used in the multivariate regression.

Variable	Description	Initial Resolution	Source
r.age	Terrane age attribute	1km	(Mooney et al., 1998)
r.ai	Global Aridity Index	30-arc sec	(Zomer et al., 2008)
r.bulk	Bulk density of the fine earth fraction (kg/m^3)	250 m	(Hengl et al., 2017)
r.cec	Cation Exchange Capacity (cmol+ /kg)	250 m	(Hengl et al., 2017)
r.clay	Clay (weight %)	250 m	(Hengl et al., 2017)
r.dust	Multi-models average of dust deposition ($g/m^2/year$)	1°	(Mahowald et al., 2006a)
r.elevation	Hole-filled Digital Elevation Model	90 m	(Jarvis et al., 2008)
r.GUM	Unconsolidated sediment	categorical	(Börker et al., 2018)
r.lc	Global Land Cover (2009)	300 m	(Arino et al., 2012)
r.litho	GLiM 2nd lithological class attribute	1km	(Hartmann & Moosdorf, 2012)
r.m1	Median bedrock model ($^{87}Sr/^{86}Sr$)	1km	(Bataille et al., 2018)
r.map	Mean annual precipitation (mm/yr)	30-arc sec	(Hijmans et al., 2005)
r.maxage_geol	GLiM age attribute – maximum (Myrs)	1km	(Hartmann & Moosdorf, 2012)
r.meanage_geol	GLiM age attribute – mean (Myrs)	1km	(Hartmann & Moosdorf, 2012)
r.minage_geol	GLiM age attribute – minimum (Myrs)	1km	(Hartmann & Moosdorf, 2012)
r.nfert	Global Nitrogen Fertilization (Kg per ha)	30-arc sec	(Potter et al., 2010)
r.orc	Soil organic carbon (g/kg)	250 m	(Hengl et al., 2017)
r.pet	Global Potential Evapo-Transpiration	30-arc sec	(Zomer et al., 2008)
r.ph	Soil pH in H_2O solution (x10)	250 m	(Hengl et al., 2017)
r.phkcl	Soil pH in KCl solution	250 m	(Hengl et al., 2017)
r.salt	CCSM.3 simulation of salt deposition ($g/m^2/year$)	1.4°	(Mahowald et al., 2006b)
r.sand	Sand (weight %)	250 m	(Hengl et al., 2017)
r.silt	Silt (weight %)	250 m	(Hengl et al., 2017)
r.soilthick	Soil thickness (m)	1km	(Pelletier et al., 2016)
r.srsrq1	Quartile 1 bedrock model ($^{87}Sr/^{86}Sr$)	1km	(Bataille et al., 2018)
r.srsrq3	Quartile 3 bedrock model ($^{87}Sr/^{86}Sr$)	1km	(Bataille et al., 2018)
r.ssa	Multi-model average sea salt wet+dry deposition (kg/ha/yr)	1°	(Vet et al., 2014)
r.ssaw	Multi-model average sea salt wet deposition (kg/ha/yr)	1°	(Vet et al., 2014)
r.xx	GLiM 1st lithological class attribute	1km	(Hartmann & Moosdorf, 2012)

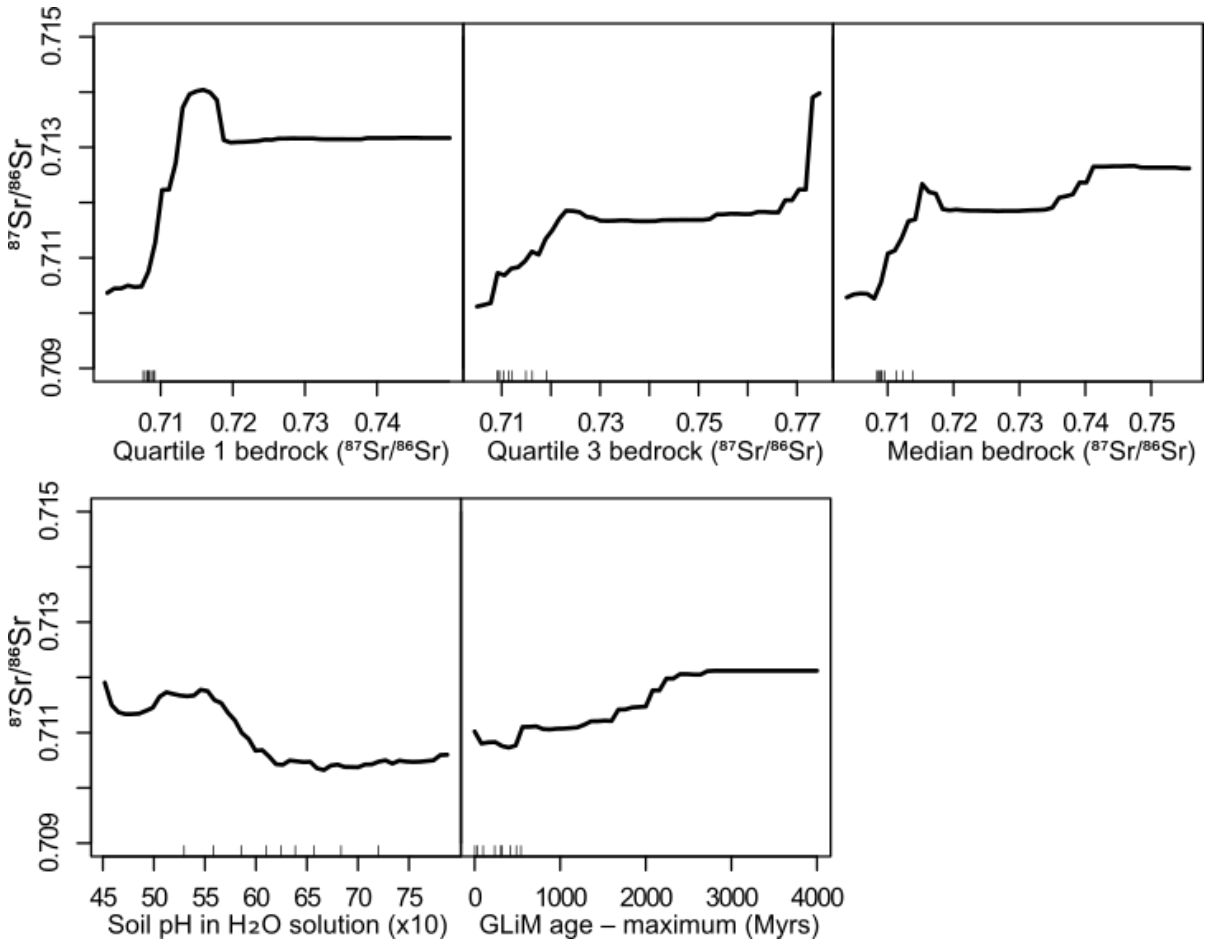

Figure S2.5 Partial dependence plots for the explanatory variables selected by *VSURF*. Small ticks on the x-axis represent deciles. Refer to Table S2.2 for the description and source of each variable.

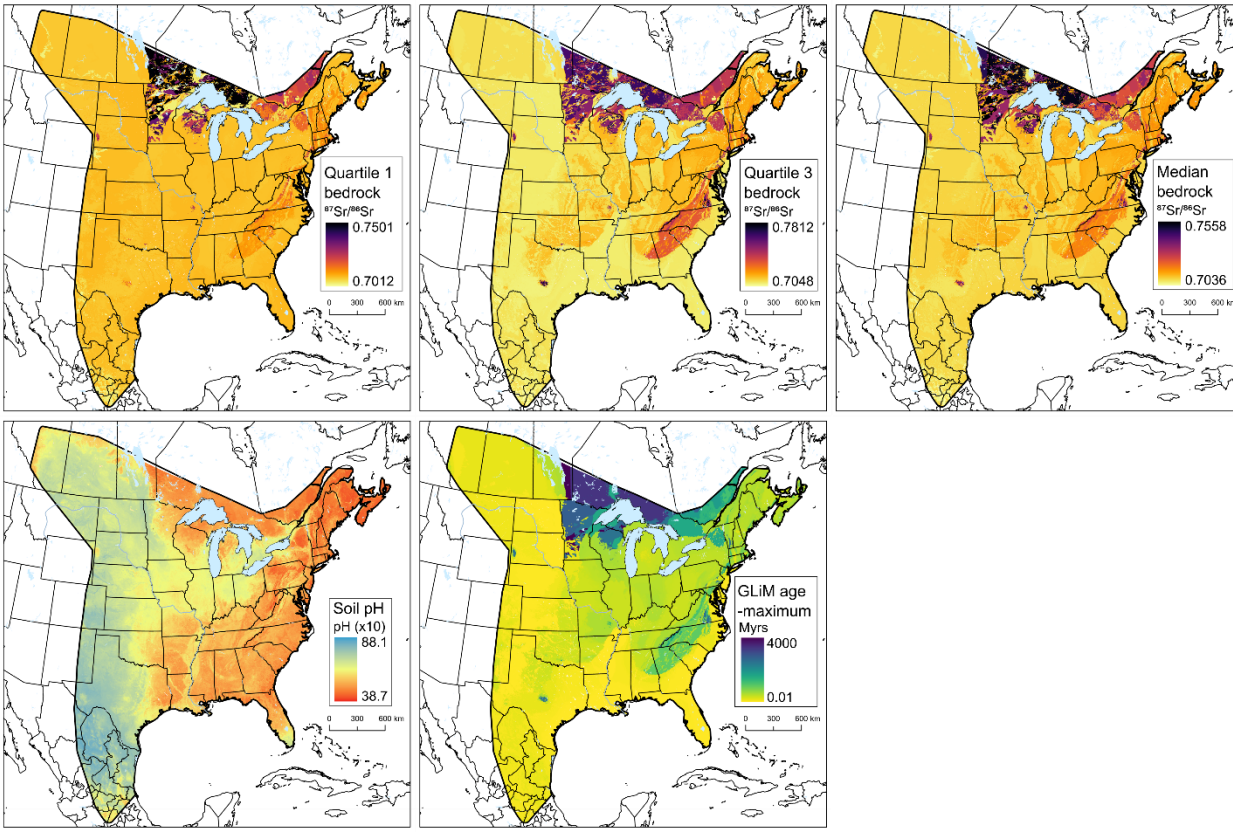

Figure S2.6 Spatial plots of the five explanatory variables selected as predictors by *VSURF* and used in the random forest regression model. Refer to Table S2.2 for the description and source of each variable.

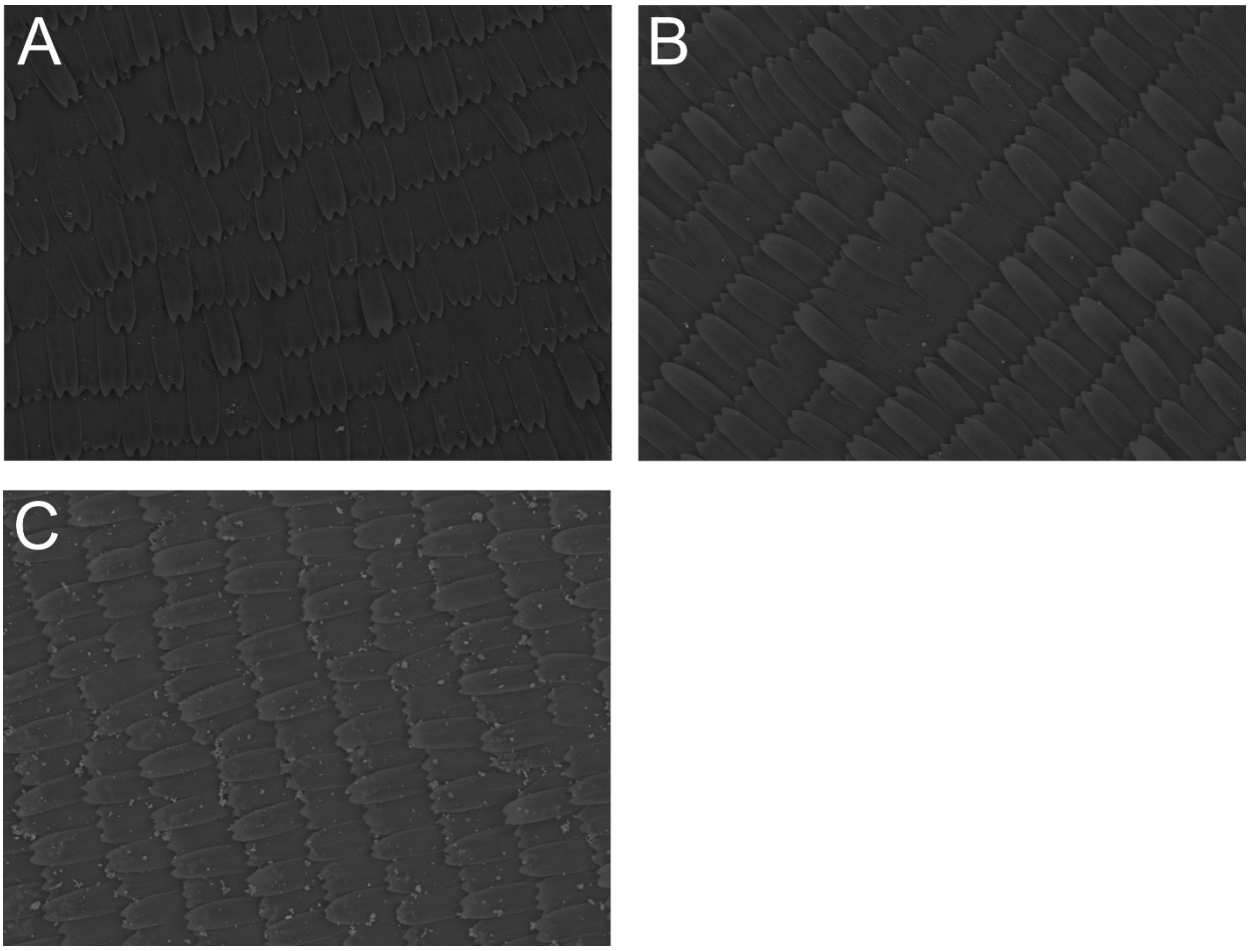

Figure S2.7 Scanning electron microscope (SEM) images of monarch wings. The magnification is x130. Light grey spots are external particulate matter. **(A)** After cleaning with 2:1 chloroform:methanol, **(B)** after cleaning with pressurized N_2 gas at ~10 psi for 2 min. per side, **(C)** control image of a pre-cleaned butterfly wing.

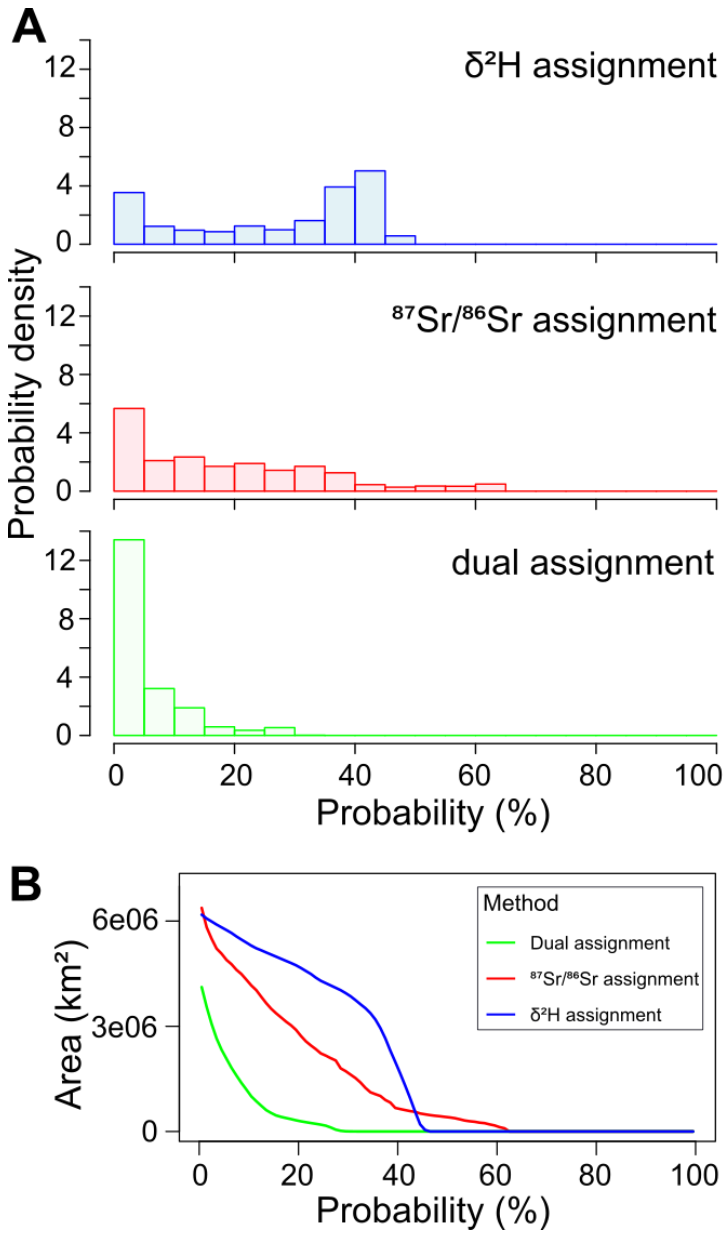

Figure S2.8 Quantitative analysis of the averaged probabilistic assignment maps (n = 100). **(A)** Density of assignment probabilities for each type of assignment. Increased probability densities at higher assignment probability indicate higher confidence; **(B)** Comparison of the precision performance of the three assignment averages. The graph shows the area with an assignment probability greater than or equal to a given assignment probability. When the assignment probability is 0%, the entire study area is a possible region of natal origin. When the assignment probability increases (i.e., only regions closely matching the isotopic signature are considered), the potential region of natal origin becomes more and more constrained. When the assignment probability is 100% (i.e., only pixels with exact isotopic matches are considered or an assignment without isoscape uncertainty), the potential region of natal origin is limited to a few pixels. Dual δ^2H and $^{87}Sr/^{86}Sr$ assignment has the highest precision, followed by $^{87}Sr/^{86}Sr$ assignment, then δ^2H assignment.

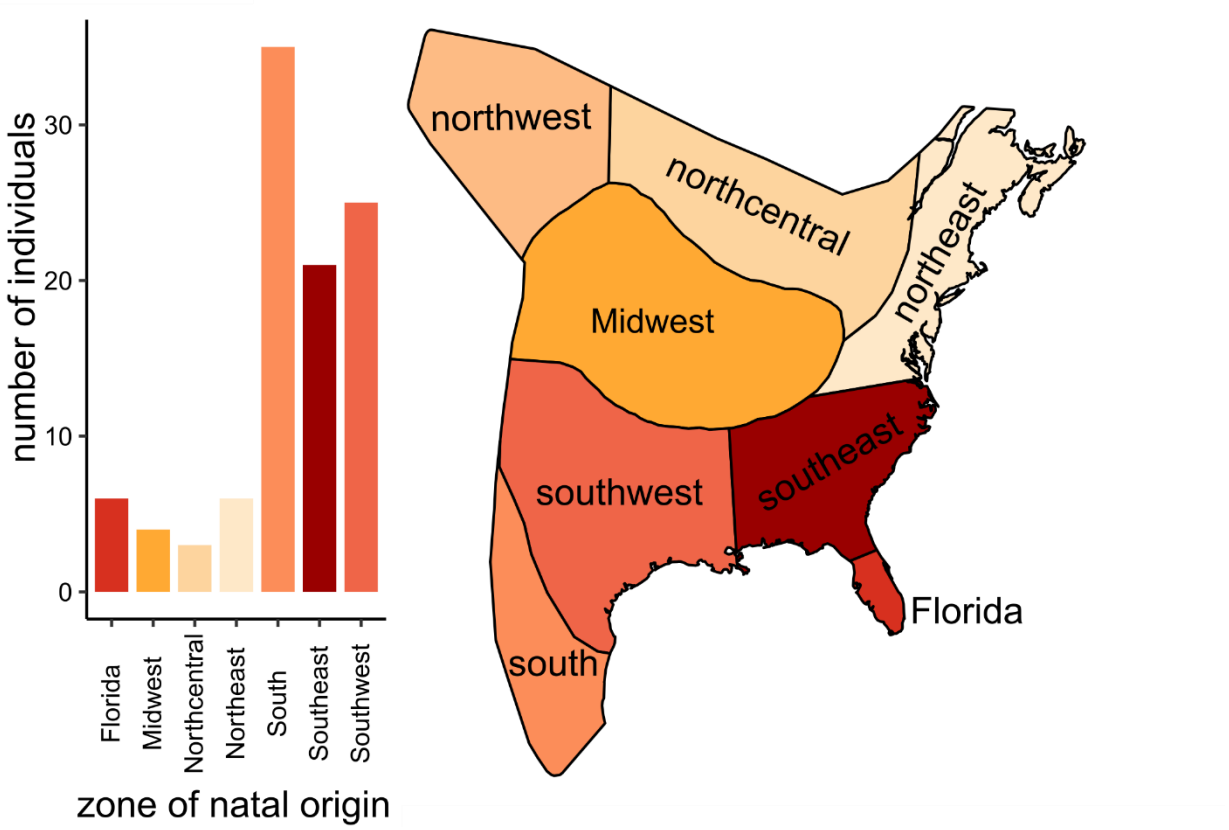

Figure S2.9 Nominal assignment of the 100 monarch butterflies. The monarchs were assigned to zones (Flockhart et al., 2017b) by finding the maximum dual δ^2H and $^{87}Sr/^{86}Sr$ assignment probability of origin and assigning individuals to the zone with the highest probability of origin.

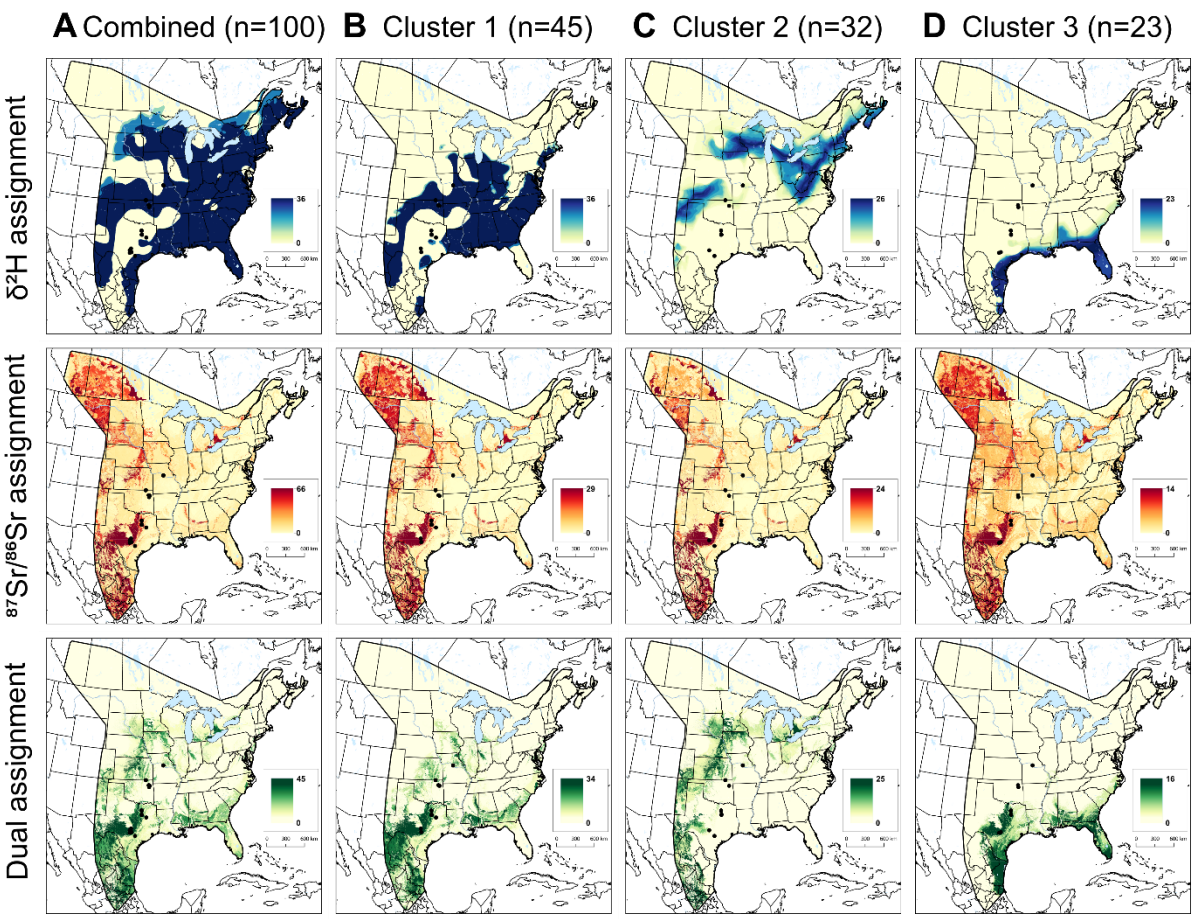

Figure S2.10: Summed binary maps of the highly probable natal origin. The scale of each map is the sum of the binary maps of the individuals using a 2:1 odds ratio and has a maximum equal to n.

Appendix C: Supplementary Material for Chapter 3

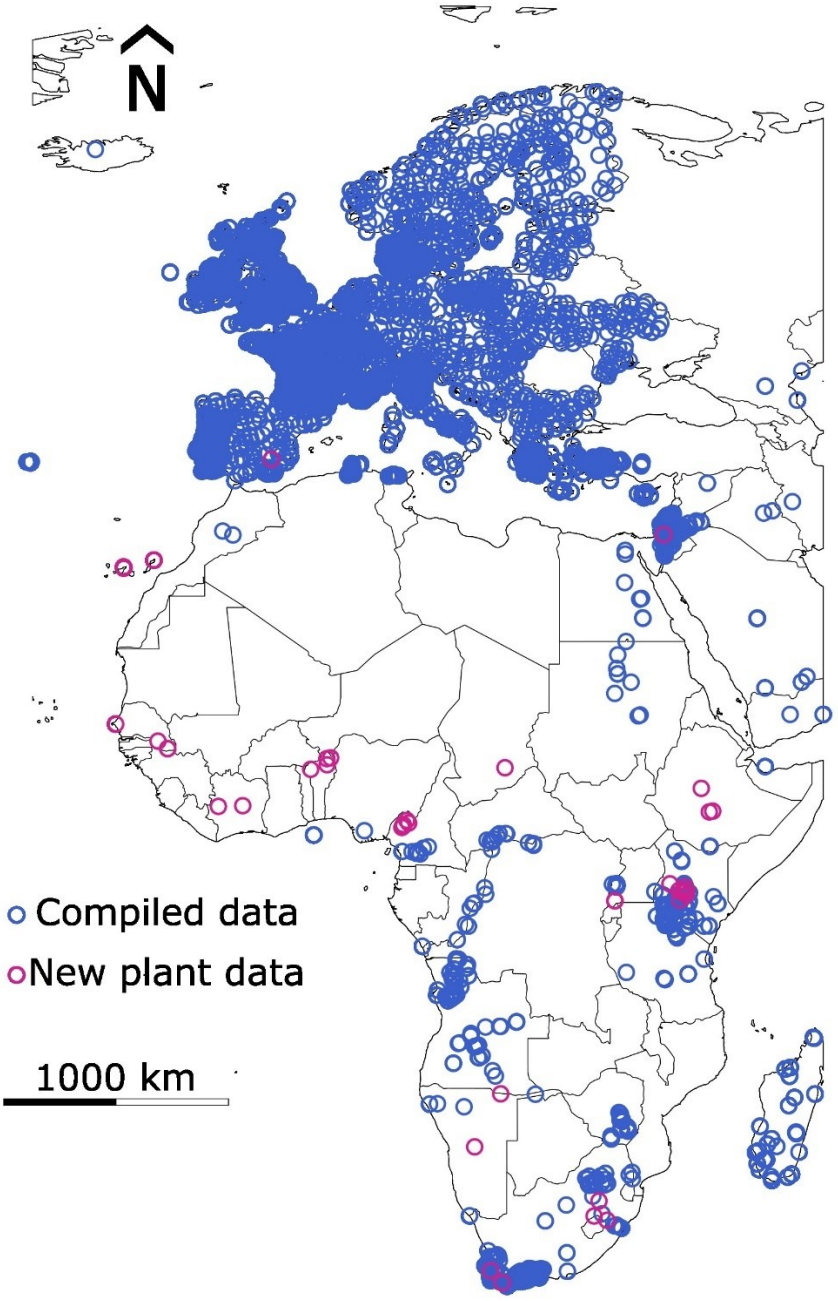

Figure S3.1 Geographic distribution of bioavailable $^{87}Sr/^{86}Sr$ data compilation across the Afro-Palearctic range. Compiled data from the literature is depicted in blue, while pink represents newly collected plant sample data from this study (see Data Availability Table). The shapefile for country boundaries was obtained from the *rnaturalearth* package (Massicotte & South, 2023).

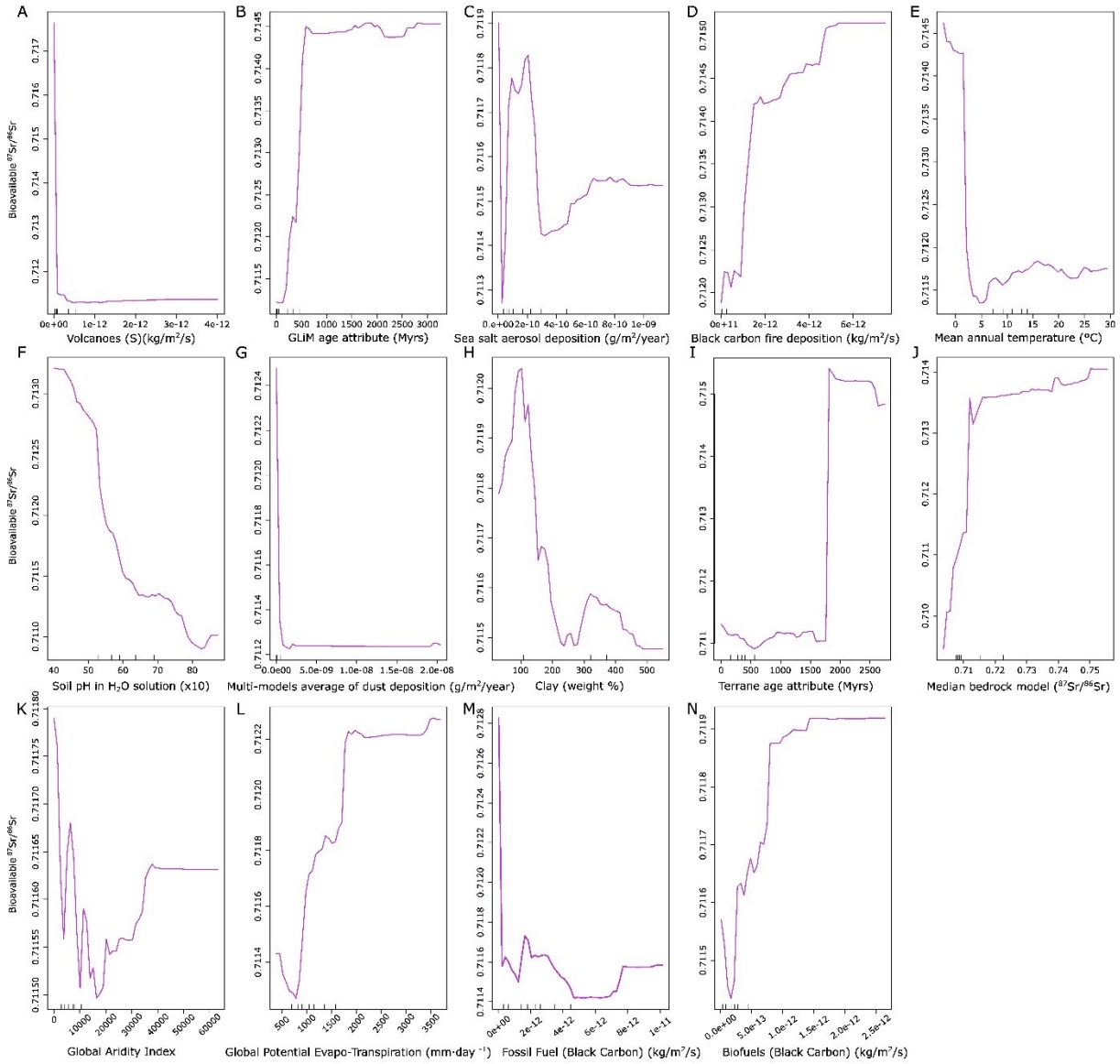

Figure S3.2 Partial dependence plots between each predictor (x-axis) and the predicted bioavailable $^{87}Sr/^{86}Sr$ (y-axis) from the random forest regression. Hash marks along the x-axis show sample decile values. Refer to Table S3.1 for the source of each variable: **(A)** volcanoes, **(B)** GLiM age attribute - mean, **(C)** sea salt aerosol deposition, **(D)** black carbon - fire deposition, **(E)** mean annual temperature, **(F)** soil pH in H_2O solution (x10), **(G)** multi-model average of dust deposition, **(H)** clay, **(I)** terrane age attribute, **(J)** median bedrock model, **(K)** global aridity index, **(L)** global potential evapotranspiration, **(M)** fossil fuel (black carbon), and **(N)** biofuels (black carbon).

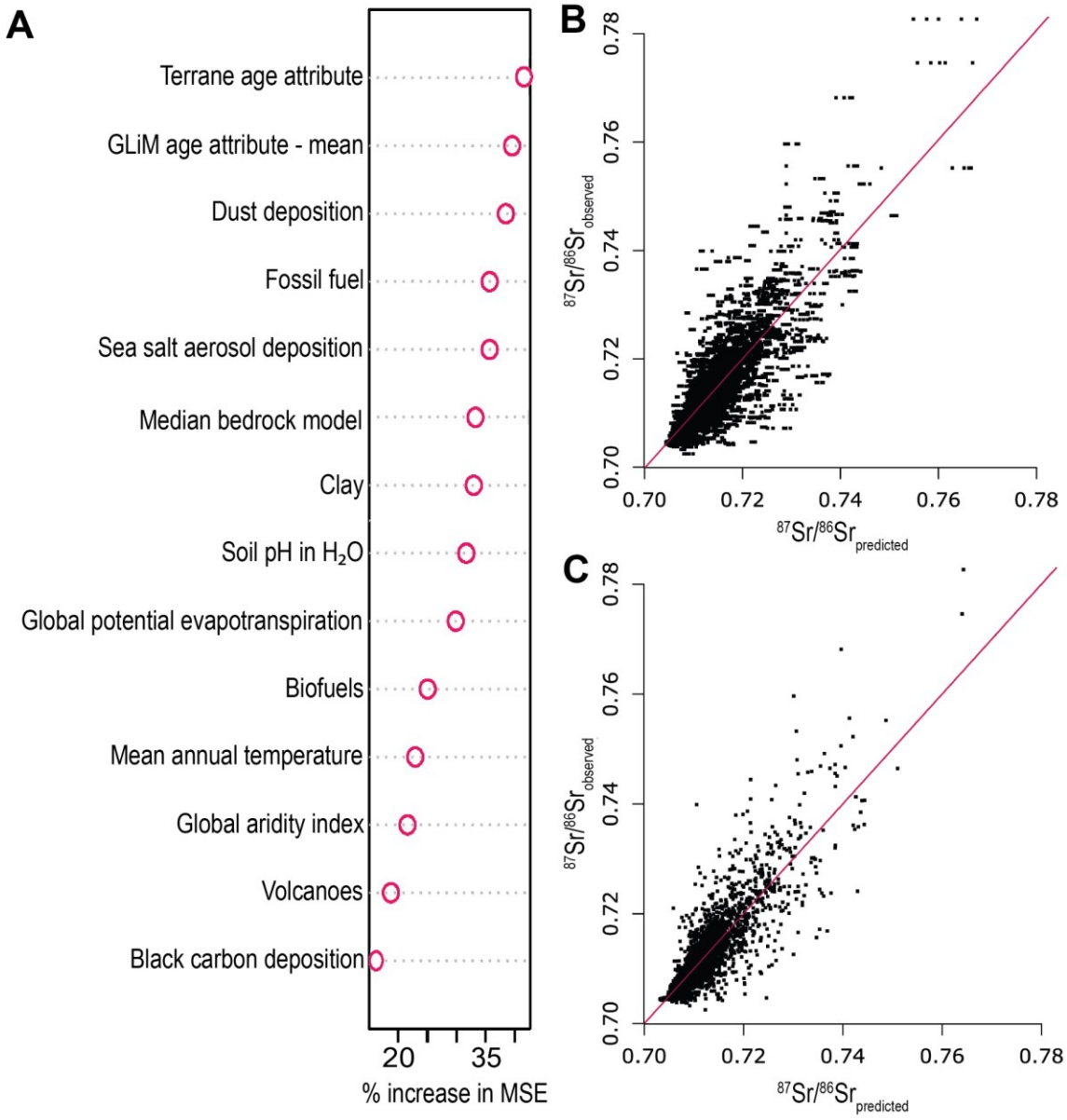

Figure S3.3 Machine learning model performance. **(A)** Variable importance plot after selection of predictors by *VSURF* with % increase in MSE (percent increase in mean squared error) as the evaluation standard. If a variable is important, then the model's mean squared error of prediction will increase when the variable is taken out of the model. **(B)** N-fold cross-validation results between observed and predicted bioavailable $^{87}Sr/^{86}Sr$ with the best fit linear model (pink line) for the random forest regression model using the framework of Bataille et al. (2020); **(C)** N-fold cross-validation results for the spatial interpolation ensemble machine learning model using the *landmap* package (Hengl et al. 2021). The pink line represents the best-fit linear model.

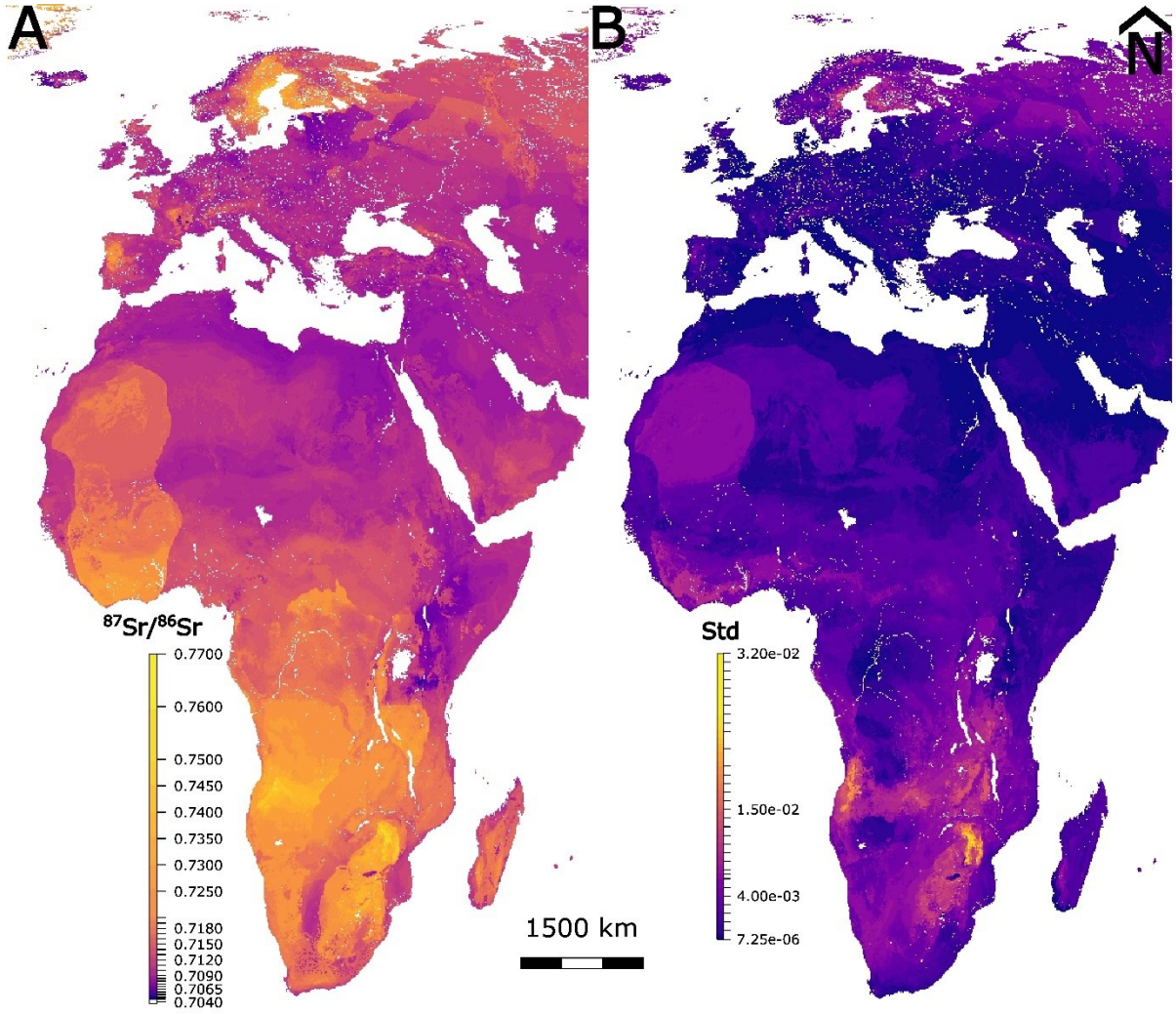

Figure S3.4 Predicted bioavailable strontium isoscape across the Afro-Palearctic and its associated uncertainty generated using random forest regression. **(A)** Mean bioavailable $^{87}Sr/^{86}Sr$ predictions; **(B)** Standard deviation of bioavailable $^{87}Sr/^{86}Sr$ predictions. Colour scale breakpoints were selected to improve visualisation and increase contrast.

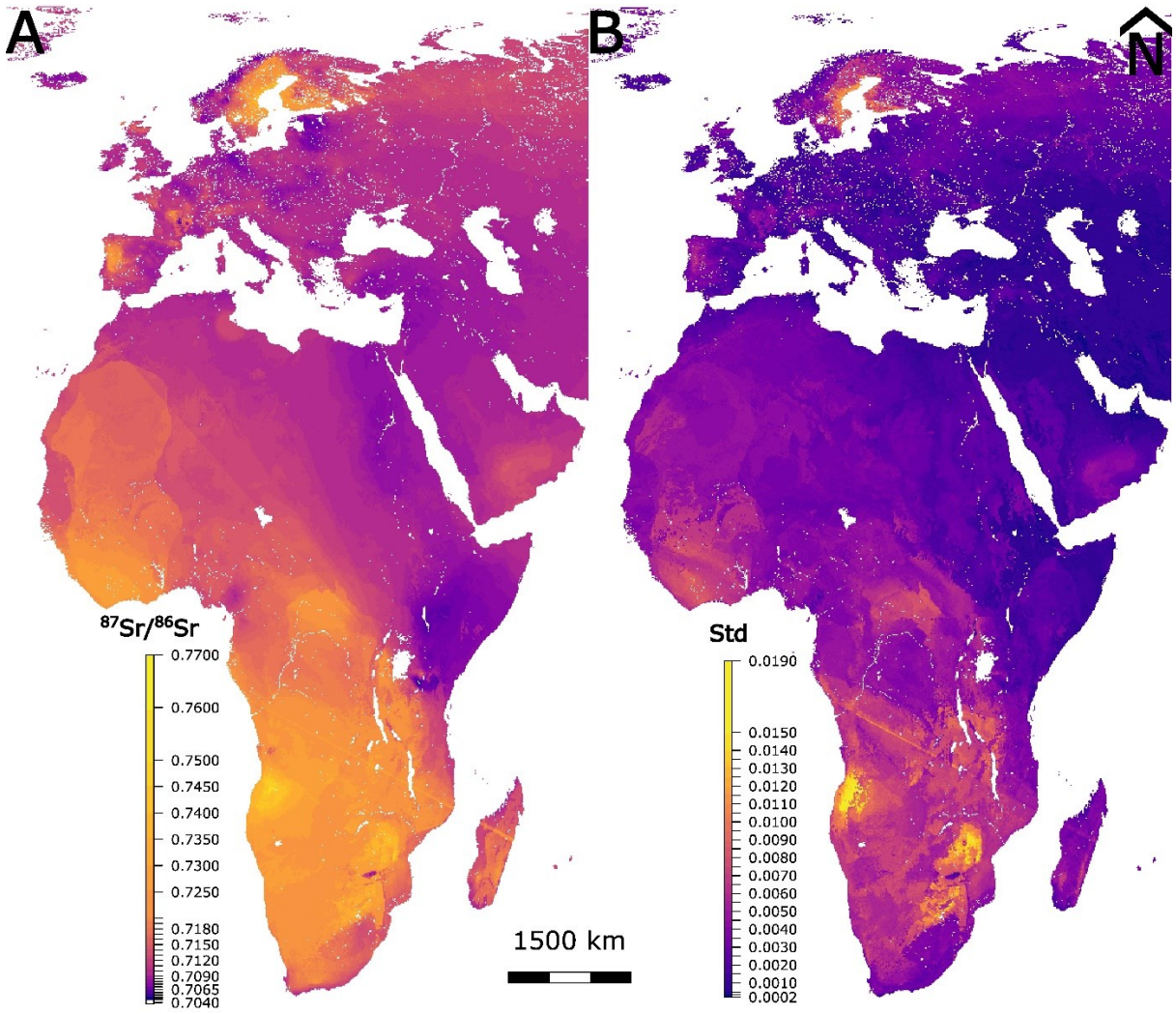

Figure S3.5 Predicted bioavailable strontium isoscape across the Afro-Palearctic and its associated uncertainty generated using ensemble machine learning. **(A)** Mean bioavailable $^{87}Sr/^{86}Sr$ predictions; **(B)** Standard deviation of bioavailable $^{87}Sr/^{86}Sr$ predictions.

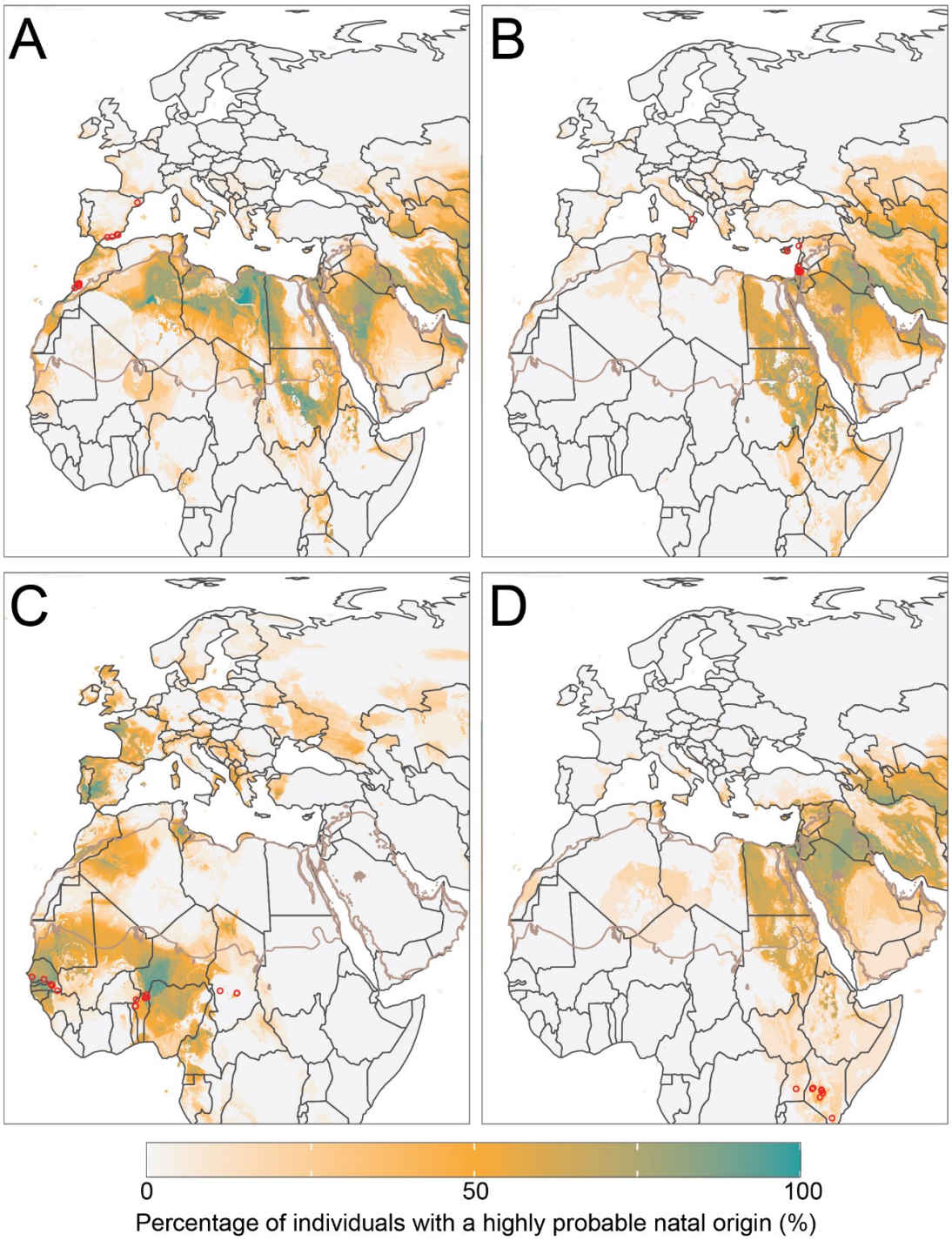

Figure S3.6 Estimated natal origins of painted ladies categorised as putative locals. (A) Captures from northwest of the Sahara in the late winter/early spring (n =18); **(B)** captures from northeast of the Sahara in the late winter/spring (n = 10); **(C)** captures from southwest of the Sahara in the autumn (n =20); **(D)** captures from southeast of the Sahara in the late autumn (n =11).

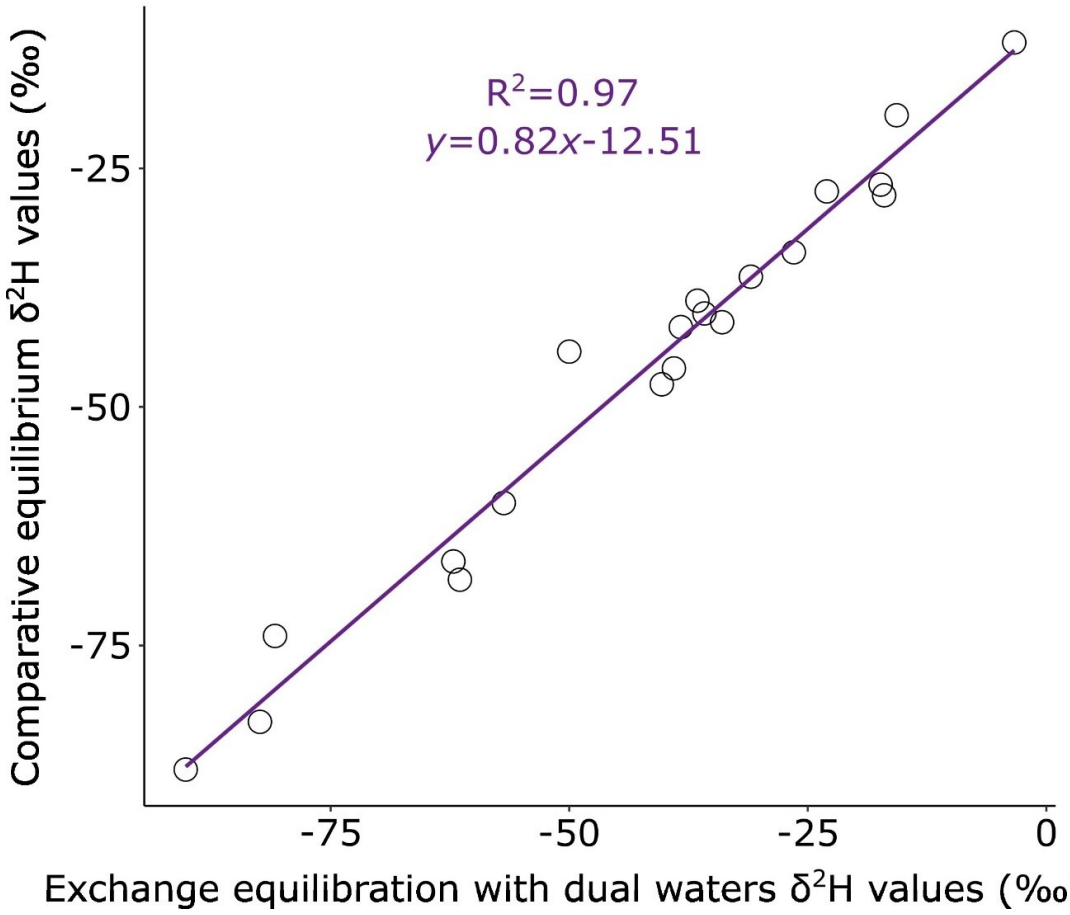

Figure S3.7 Scatterplot of wing samples (n = 20) from a given site used for duplicate analysis using both the exchange equilibration with dual waters (%) and comparative equilibrium protocols (%). The linear relationship was used to transform the δ²H values of samples analysed with the exchange equilibration with dual waters protocol to align with values measured using the comparative equilibrium protocol.

Table S3.1 List of 28 geological, climatic, environmental, and anthropogenic geospatial data used as auxiliary variables in the random forest regression and in the spatial interpolation ensemble machine learning to create our regional bioavailable strontium isoscape for the Afro-Palearctic range based on Bataille et al. (2020). The important variables selected by *VSURF* are in bold.

Variable ID	Description	Source of data
r.age	**Terrane age attribute (Myrs)**	**(Mooney et al., 1998)**
r.ai	**Global Aridity Index**	**(Trabucco & Zomer, 2019)**
r.bulk	Bulk density of the fine earth fraction (kg/m^3)	(Hengl et al., 2021)
r.cec	Cation exchange capacity (cmol(+)/kg)	(Hengl et al., 2021)
r.clay	**Clay content (%)**	**(Hengl et al., 2021)**
r.biof	**Biofuels (black carbon) (kg/m^2/s)**	**(Chien et al., 2016)**
r.biog	Primary biogenic deposition (kg/m^2/s)	(Chien et al., 2016)
r.wet	Wet dust deposition (kg/m^2/s)	(Chien et al., 2016)
r.foss	**Fossil Fuel (black carbon) (kg/m^2/s)**	**(Chien et al., 2016)**
r.dry	Dry dust deposition (kg/m^2/s)	(Chien et al., 2016)
r.dust	**Multi-models average of dust deposition (g/m^2/year)**	**(Chien et al., 2016)**
r.dust20	Dust deposition (kg/m^2/s)	(Chien et al., 2016)
r.fire	**Black carbon deposition (kg/m^2/s)**	**(Chien et al., 2016)**
r.volc	**Volcanos (S) (kg/m^2/s)**	**(Brahney et al., 2015)**
r.elevation	Hole-filled Digital Elevation Model	(Jarvis et al., 2008)
r.GUM	Unconsolidated sediment map	(Börker et al., 2018)
r.bouger	WGM2012_Bouguer Mean	(Balmino et al., 2012)
r.m1	**Median bedrock model (^{87}Sr/^{86}Sr)**	**(Bataille et al., 2018)**
r.mat	**Mean annual temperature (°C)**	**(Harris et al., 2020)**
r.map	Mean annual precipitation (mm/yr)	(Harris et al., 2020)
r.maxage_geol	GLiM age attribute – maximum (Myrs)	(Hartmann & Moosdorf, 2012; Bataille et al., 2020)
r.meanage_geol	**GLiM age attribute – mean (Myrs)**	**(Hartmann & Moosdorf, 2012; Bataille et al., 2020)**
r.minage_geol	GLiM age attribute – minimum (Myrs)	(Hartmann & Moosdorf, 2012; Bataille et al., 2020)
r.pet	**Global Potential Evapo-Transpiration (mm day^{-1})**	**(Trabucco & Zomer, 2019)**
r.ph	**Soil pH in H_2O solution (x10)**	**(Hengl et al., 2021)**
r.salt	**Simulation of sea salt aerosol deposition (g/m^2/year)**	**(Chien et al., 2016)**
r.srsrq1	Quartile 1 bedrock model (^{87}Sr/^{86}Sr)	(Bataille et al., 2018)
r.srsrq3	Quartile 3 bedrock model (^{87}Sr/^{86}Sr)	(Bataille et al., 2018)

Table S3.2 Capture date and location of each painted lady sample (n = 118) and the hydrogen isotope value (δ^2H) and strontium isotope ratio ($^{87}Sr/^{86}Sr$) measured in the wing tissue. For additional metadata, see Data Availability Table.

ID	Date	Country	δ^2H	δ^2H publication	$^{87}Sr/^{86}Sr$	$^{87}Sr/^{86}Sr$ publication
GTcoll19B405	22.III.2019	Cyprus	-46	this study	0.70840	this study
GTcoll19B407	22.III.2019	Cyprus	-34	this study	0.70887	this study
GTcoll19B408	22.III.2019	Cyprus	-41	this study	0.70846	this study
GTcoll19B412	5.IV.2019	Cyprus	-27	this study	0.70949	this study
GTcoll19D088	19.III.2019	Italy	-40	this study	0.71094	this study
GTcoll19D089	19.III.2019	Italy	-43	this study	0.71102	this study
GTcoll19D125	23.III.2019	Israel	-33	this study	0.70826	this study
GTcoll19D178	20.III.2019	Israel	-24	this study	0.70897	this study
GTcoll19D209	21.III.2019	Israel	-27	this study	0.70852	this study
GTcoll19D268	11.III.2019	Israel	-30	this study	0.70891	this study
GTcoll19D270	5.IV.2019	Israel	-40	this study	0.70879	this study
GTcoll19D274	7.IV.2019	Israel	-69	this study	0.70858	this study
GTcoll19D309	3.III.2019	Israel	-53	this study	0.70924	this study
GTcoll19D311	8.III.2019	Israel	-16	this study	0.70854	this study
GTcoll19D347	6.I.2019	Spain	-55	this study	0.70996	this study
GTcoll19D358	9.I.2019	Spain	-43	this study	0.71072	this study
GTcoll19D366	14.III.2019	Spain	-39	this study	0.71020	this study
GTcoll19D421	26.IV.2019	Spain	-55	this study	0.71149	this study
GTcoll19D505	12.III.2019	Jordan	-17	this study	0.70879	this study
GTcoll19D509	12.III.2019	Jordan	-40	this study	0.70934	this study
GTcoll19D635	20.III.2019	Jordan	-32	this study	0.70898	this study
GTcoll19D639	20.III.2019	Jordan	-19	this study	0.70933	this study
GTcoll19D727	28.III.2019	Syria	-12	this study	0.70860	this study
GTcoll19D729	4.IV.2019	Syria	-36	this study	0.70853	this study
GTcoll19D737	4.IV.2019	Syria	-47	this study	0.70858	this study
GTcoll19D742	12.IV.2019	Syria	-30	this study	0.70903	this study
GTcoll19D757	18.IV.2019	Italy	-68	this study	0.70990	this study
GTcoll19D784	8.IV.2019	Italy	-16	this study	0.70973	this study
GTcoll19D858	27.IV.2019	Spain	-48	this study	0.70989	this study
GTcoll19F038	9.III.2019	Spain	-36	this study	0.71327	this study
GTcoll19F064	9.III.2019	Spain	-50	this study	0.70933	this study
GTcoll19F065	9.III.2019	Spain	-64	this study	0.71141	this study
GTcoll19F156	11.IV.2019	Israel	-28	this study	0.70875	this study
GTcoll19F216	6.XII.2018	Kenya	-26	this study	0.70785	this study

RVcoll17G997	28.XI.2017	Kenya	-60	this study	0.70790	this study
RVcoll17H061	29.XI.2017	Kenya	-67	this study	0.70712	this study
RVcoll17H062	29.XI.2017	Kenya	-51	this study	0.70710	this study
RVcoll17H084	29.XI.2017	Kenya	-59	this study	0.70843	this study
RVcoll17H159	30.XI.2017	Kenya	-47	this study	0.70694	this study
RVcoll17H163	30.XI.2017	Kenya	-51	this study	0.70830	this study
RVcoll17H173	30.XI.2017	Kenya	-49	this study	0.70782	this study
RVcoll17H244	1.XII.2017	Kenya	-57	this study	0.70876	this study
RVcoll17H335	4.XII.2017	Kenya	-65	this study	0.70707	this study
RVcoll17H342	4.XII.2017	Kenya	-56	this study	0.70699	this study
RVcoll17H357	4.XII.2017	Kenya	-50	this study	0.70818	this study
RVcoll17H360	4.XII.2017	Kenya	-69	this study	0.70896	this study
RVcoll17H384	5.XII.2017	Uganda	-61	this study	0.70834	this study
RVcoll17H397	6.XII.2017	Uganda	-32	this study	0.71214	this study
RVcoll17H760	18.XII.2017	Kenya	-40	this study	0.70992	this study
RVcoll14M265	27.IV.2012	Spain	-49	Talavera et al. (2018)	0.70915	this study
RVcoll14M274	28.IV.2012	Spain	-51	Talavera et al. (2018)	0.70920	this study
RVcoll14M281	28.IV.2012	Spain	-48	Talavera et al. (2018)	0.70834	this study
RVcoll14M282	28.IV.2012	Spain	-49	Talavera et al. (2018)	0.70896	this study
RVcoll16C403	24.II.2016	Spain	-57	Talavera et al. (2018)	0.71086	this study
RVcoll16C407	23.II.2016	Spain	-58	Talavera et al. (2018)	0.71088	this study
RVcoll16C409	25.II.2016	Spain	-38	Talavera et al. (2018)	0.71036	this study
RVcoll16C413	16.II.2016	Spain	-25	Talavera et al. (2018)	0.71066	this study
RVcoll16C416	25.II.2016	Spain	-47	Talavera et al. (2018)	0.70982	this study
RVcoll16C425	16.II.2016	Spain	-35	Talavera et al. (2018)	0.71210	this study
RVcoll17A040	24.II.2017	Morocco	-38	Talavera et al. (2018)	0.70994	this study
RVcoll17A094	27.II.2017	Morocco	-46	Talavera et al. (2018)	0.71234	this study
RVcoll17A114	27.II.2017	Morocco	-53	Talavera et al. (2018)	0.71015	this study
RVcoll17A139	28.II.2017	Morocco	-52	Talavera et al. (2018)	0.70962	this study
RVcoll17A157	28.II.2017	Morocco	-48	Talavera et al. (2018)	0.71042	this study
RVcoll17A159	28.II.2017	Morocco	-43	Talavera et al. (2018)	0.70932	this study
RVcoll17A162	28.II.2017	Morocco	-25	Talavera et al. (2018)	0.71187	this study
RVcoll17A167	28.II.2017	Morocco	-39	Talavera et al. (2018)	0.70978	this study
RVcoll17A173	28.II.2017	Morocco	-49	Talavera et al. (2018)	0.71063	this study
RVcoll17A174	28.II.2017	Morocco	-53	Talavera et al. (2018)	0.71000	this study
RVcoll17A175	28.II.2017	Morocco	-48	Talavera et al. (2018)	0.70976	this study
RVcoll17A179	28.II.2017	Morocco	-48	Talavera et al. (2018)	0.71033	this study
RVcoll17A184	28.II.2017	Morocco	-35	Talavera et al. (2018)	0.71083	this study
RVcoll17A187	28.II.2017	Morocco	-34	Talavera et al. (2018)	0.71013	this study

RVcoll17A209	24.II.2017	Morocco	-45	Talavera et al. (2018)	0.71047	this study
Rvcoll14T075	3.X.2014	Chad	-71	Stefanescu et al. (2016)	0.71419	this study
Rvcoll14T186	5.X.2014	Chad	-85	Stefanescu et al. (2016)	0.71659	this study
Rvcoll14T192	5.X.2014	Chad	-71	Stefanescu et al. (2016)	0.71578	this study
Rvcoll14T202	6.X.2014	Chad	-58	Stefanescu et al. (2016)	0.71525	this study
Rvcoll14T240	6.X.2014	Chad	-77	Stefanescu et al. (2016)	0.71722	this study
Rvcoll14T273	7.X.2014	Chad	-48	Stefanescu et al. (2016)	0.72377	this study
Rvcoll14T280	7.X.2014	Chad	-51	Stefanescu et al. (2016)	0.71731	this study
Rvcoll14T305	8.X.2014	Chad	-64	Stefanescu et al. (2016)	0.71616	this study
Rvcoll14T339	10.X.2014	Chad	-49	Stefanescu et al. (2016)	0.72095	this study
Rvcoll14T366	11.X.2014	Chad	-81	Stefanescu et al. (2016)	0.71591	this study
Rvcoll14T378	11.X.2014	Chad	-80	Stefanescu et al. (2016)	0.71393	this study
Rvcoll14T597	21.X.2014	Benin	-71	Stefanescu et al. (2016)	0.71210	this study
Rvcoll14T630	21.X.2014	Benin	-56	Stefanescu et al. (2016)	0.71374	this study
Rvcoll14T645	22.X.2014	Benin	-81	Stefanescu et al. (2016)	0.71092	this study
Rvcoll14T653	22.X.2014	Benin	-78	Stefanescu et al. (2016)	0.71322	this study
Rvcoll14T715	22.X.2014	Benin	-85	Stefanescu et al. (2016)	0.71427	this study
Rvcoll14T867	26.X.2014	Benin	-44	Stefanescu et al. (2016)	0.71420	this study
Rvcoll14T876	26.X.2014	Benin	-55	Stefanescu et al. (2016)	0.71434	this study
Rvcoll14T967	2.XI.2014	Senegal	-70	Stefanescu et al. (2016)	0.71295	this study
Rvcoll14U004	4.XI.2014	Senegal	-66	Stefanescu et al. (2016)	0.71394	this study
Rvcoll14U014	4.XI.2014	Senegal	-68	Stefanescu et al. (2016)	0.71433	this study
Rvcoll14U016	4.XI.2014	Senegal	-65	Stefanescu et al. (2016)	0.71515	this study
Rvcoll14U018	4.XI.2014	Senegal	-64	Stefanescu et al. (2016)	0.71369	this study
Rvcoll14U050	5.XI.2014	Senegal	-59	Stefanescu et al. (2016)	0.71562	this study
Rvcoll14U061	5.XI.2014	Senegal	-45	Stefanescu et al. (2016)	0.71502	this study
Rvcoll14U074	6.XI.2014	Senegal	-41	Stefanescu et al. (2016)	0.71619	this study
GTcoll18B699	8.IX.2018	Senegal	-101	Chapter 4	0.71063	Chapter 4
GTcoll18B705	7.IX.2018	Senegal	-86	Chapter 4	0.71021	Chapter 4
GTcoll18B720	13.IX.2018	Senegal	-100	Chapter 4	0.71438	Chapter 4
GTcoll18B721	13.IX.2018	Senegal	-109	Chapter 4	0.71522	Chapter 4
GTcoll18B722	13.IX.2018	Senegal	-69	Chapter 4	0.71543	Chapter 4
GTcoll18B773	23.IX.2018	Benin	-84	Chapter 4	0.71298	Chapter 4
GTcoll18B774	23.IX.2018	Benin	-81	Chapter 4	0.71516	Chapter 4
GTcoll18B775	23.IX.2018	Benin	-76	Chapter 4	0.71327	Chapter 4
GTcoll18B782	22.IX.2018	Benin	-79	Chapter 4	0.71367	Chapter 4
GTcoll19H115	29.IX.2019	Senegal	-79	Chapter 4	0.71013	Chapter 4
GTcoll19H116	29.IX.2019	Senegal	-81	Chapter 4	0.70971	Chapter 4
GTcoll19H119	26.X.2019	Senegal	-91	Chapter 4	0.70980	Chapter 4

GTcoll19H120	26.X.2019	Senegal	-72	Chapter 4	0.71019	Chapter 4
GTcoll19H121	9.XI.2019	Senegal	-65	Chapter 4	0.70997	Chapter 4
GTcoll19H128	15.IX.2019	Benin	-83	Chapter 4	0.72613	Chapter 4
GTcoll19H129	15.VIII.2019	Benin	-77	Chapter 4	0.72074	Chapter 4
GTcoll19H137	9.X.2019	Benin	-83	Chapter 4	0.71756	Chapter 4
GTcoll19H140	7.XI.2019	Benin	-84	Chapter 4	0.71525	Chapter 4

Appendix D: Supplementary Material for Chapter 4

Table S4.1 Sample metadata. Capture date and location of each *V. cardui* sample and the hydrogen isotope value (δ^2H) and strontium isotope ratio ($^{87}Sr/^{86}Sr$) measured in the wing tissue.

Sample	Capture Date	Latitude	Longitude	Country	δ^2H (± SD)	$^{87}Sr/^{86}Sr$ (± SD)
18B755	22.IX.2018	11.70681	3.216345	Benin	-81 ± 2	0.71318 ± 0.00003
18B782	22.IX.2018	11.70681	3.216345	Benin	-79 ± 2	0.71367 ± 0.00006
18B773	23.IX.2018	11.74402	3.276339	Benin	-84 ± 2	0.71298 ± 0.00009
18B774	23.IX.2018	11.74402	3.276339	Benin	-81 ± 2	0.71516 ± 0.00004
18B775	23.IX.2018	11.74402	3.276339	Benin	-76 ± 2	0.71327 ± 0.00005
19H129	15.VIII.2019	10.7275	1.380323	Benin	-77 ± 2	0.72074 ± 0.00006
19H128	15.IX.2019	10.7275	1.380323	Benin	-83 ± 2	0.72613 ± 0.00006
19H137	9.X.2019	10.7275	1.380323	Benin	-83 ± 2	0.71756 ± 0.00004
19H140	7.XI.2019	10.7275	1.380323	Benin	-84 ± 2	0.71525 ± 0.00005
19M240	6.XI.2019	30.33404	-9.4085	Morocco	-68 ± 2	0.71288 ± 0.00004
19M001	31.X.2019	30.4975	-8.82024	Morocco	-74 ± 2	0.71375 ± 0.00002
19M002	31.X.2019	30.4975	-8.82024	Morocco	-87 ± 2	0.71353 ± 0.00004
19M170	4.XI.2019	31.38014	-5.99294	Morocco	-64 ± 2	0.71362 ± 0.00003
19M181	4.XI.2019	31.38014	-5.99294	Morocco	-72 ± 2	0.71473 ± 0.00002
19M050	1.XI.2019	31.73267	-7.2829	Morocco	-75 ± 2	0.71655 ± 0.00003
19M051	1.XI.2019	31.73267	-7.2829	Morocco	-79 ± 2	0.71451 ± 0.00002
18B720	13.IX.2018	13.97696	-14.5436	Senegal	-100 ± 2	0.71438 ± 0.00009
18B721	13.IX.2018	13.97696	-14.5436	Senegal	-109 ± 2	0.71522 ± 0.00005
18B722	13.IX.2018	13.97696	-14.5436	Senegal	-69 ± 2	0.71543 ± 0.00003
18B699	08.IX.2018	14.35961	-16.4946	Senegal	-101 ± 2	0.71063 ± 0.00011
18B705	07.IX.2018	14.71873	-17.1292	Senegal	-86 ± 2	0.71021 ± 0.00002
19H115	29.IX.2019	14.70977	-17.1248	Senegal	-79 ± 2	0.71013 ± 0.00002
19H116	29.IX.2019	14.70977	-17.1248	Senegal	-81 ± 2	0.70971 ± 0.00002
19H119	26.X.2019	14.70977	-17.1248	Senegal	-91 ± 2	0.70980 ± 0.00001

19H120	26.X.2019	14.70977	-17.1248	Senegal	-72 ± 2	0.71020 ± 0.00001
19H121	9.XI.2019	14.70977	-17.1248	Senegal	-65 ± 2	0.70997 ± 0.00002
19H104	18.XI.2019	35.90683	14.39475	Malta	-57 ± 2	0.70992 ± 0.00002
19H100	18.XI.2019	35.93002	14.40412	Malta	-57 ± 2	0.71090 ± 0.00002
19H139	18.XI.2019	35.93002	14.40412	Malta	-73 ± 2	0.71022 ± 0.00002
19H102	20.XI.2019	35.94727	14.35173	Malta	-59 ± 2	0.70997 ± 0.00002
19H103	20.XI.2019	35.94727	14.35173	Malta	-57 ± 2	0.71007 ± 0.00003
19H105	22.XI.2019	36.06184	14.28611	Malta	-49 ± 2	0.70954 ± 0.00001
19H106	22.XI.2019	36.06184	14.28611	Malta	-77 ± 2	0.71151 ± 0.00004
19H108	24.XI.2019	37.09005	-8.16606	Portugal	-69 ± 2	0.71025 ± 0.00004
19H109	24.XI.2019	37.24111	-8.35311	Portugal	-70 ± 2	0.71397 ± 0.00004
19H110	25.XI.2019	37.26194	-8.5447	Portugal	-71 ± 2	0.71369 ± 0.00004
19H111	25.XI.2019	37.26194	-8.5447	Portugal	-85 ± 2	0.71439 ± 0.00003
19H112	27.XI.2019	37.26194	-8.5447	Portugal	-90 ± 2	0.71779 ± 0.00004
19H113	27.XI.2019	37.26194	-8.5447	Portugal	-57 ± 2	0.71817 ± 0.00002
19H107	23.XI.2019	37.20373	-7.26035	Spain	-87 ± 2	0.71279 ± 0.00003

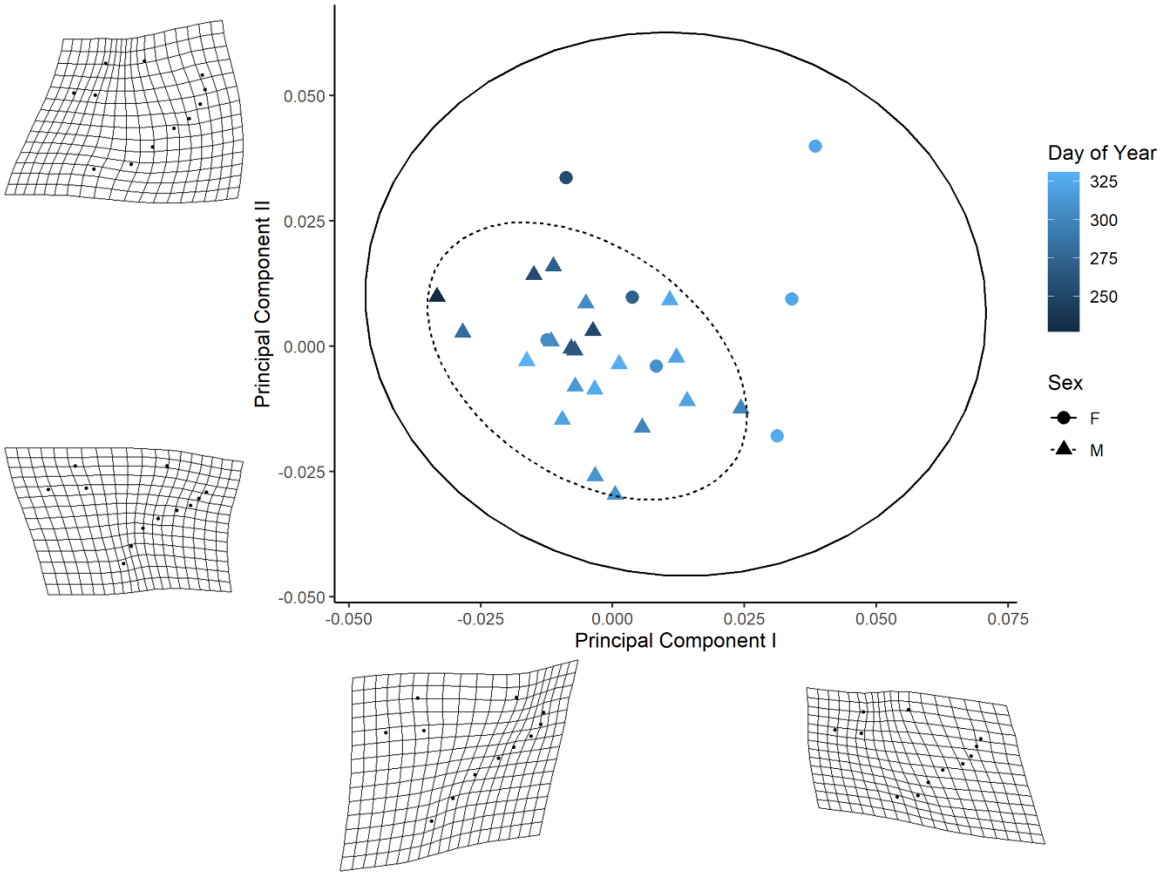

Figure S4.1 Wing geometric morphometric analysis. Principal components biplot of *V. cardui* wing shape (n = 28). The shade indicates the day of the year that the sample was captured and shape indicates males (triangles) and females (circles). Females have greater variation in shape, as indicated by the larger 95% confidence ellipse for females (solid) compared to males (dashed). Shape differences between the extremes of the first principal component range from a subtly narrowed wing to a round wing (shape differences from the mean magnified by 5).

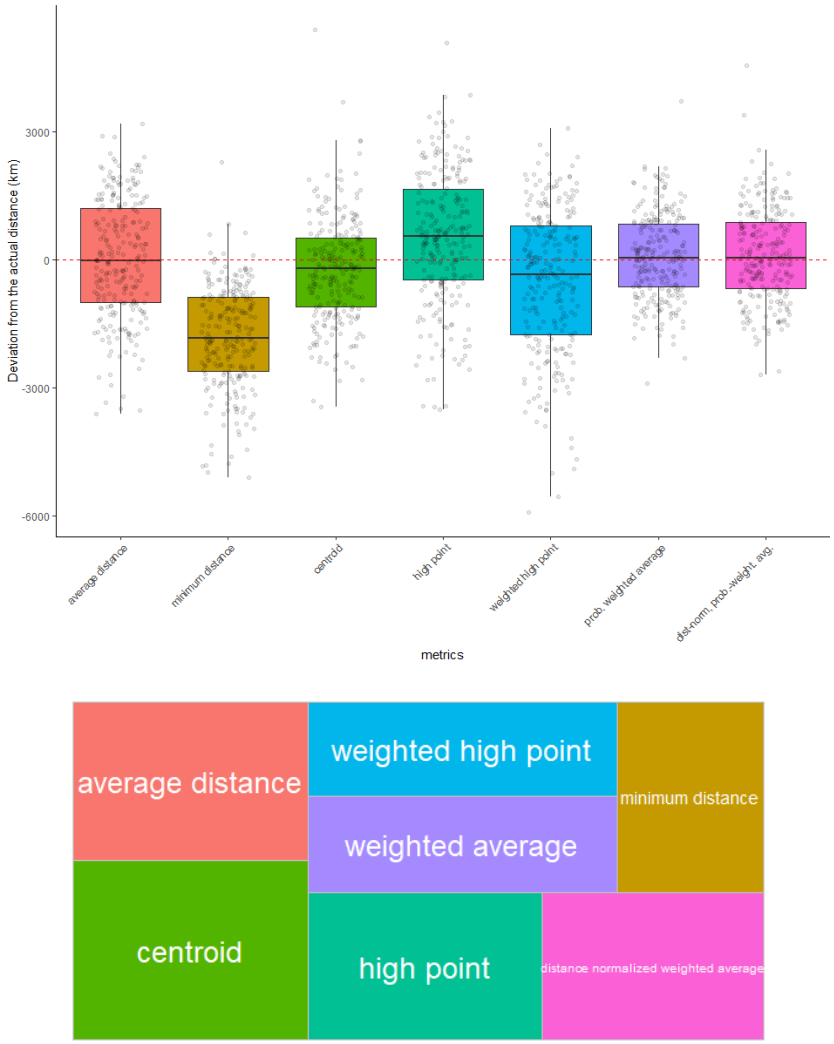

Figure S4.2 Performance of seven metrics estimating the distance travelled by 250 synthetic migrants. Metrics include: (i) the average distance metric, which acts as the null model as it is determined mainly by geography, (ii) the minimum distance method, calculating the shortest distance to an isopleth threshold value (e.g., Katzner et al., 2017). (iii) the centroid method, calculating the distance to the centre of the highly probable area of natal origin, usually defined by the 2:1 odds ratio (e.g., Flockhart et al., 2017b), (iv) the high point method, calculating the distance to the raster cell with the highest probability (e.g., Vander Zanden et al., 2018), (v) the weighted high point, calculating the probability-weighted distance to the raster cell with the highest probability, (vi) the probability-weighted average distance, calculating the probability-weighted average distance (*assignR* package: Ma et al. (2020)), and (vii) the distance-normalised probability-weighted average distance, calculating the probability-weighted average distance, while normalising for the number of cells at each distance. **(A)** Deviations from the actual distance (km) for each estimate of migration distance. Values below the red dashed line indicate under-estimates of the actual distance. **(B)** Treemap showing the proportion of synthetic migrants for which each metric was the best at estimating the actual migration distance. The average distance metric was the best at estimating migration distance for 16% of the individuals, demonstrating the inaccuracy of these metrics.

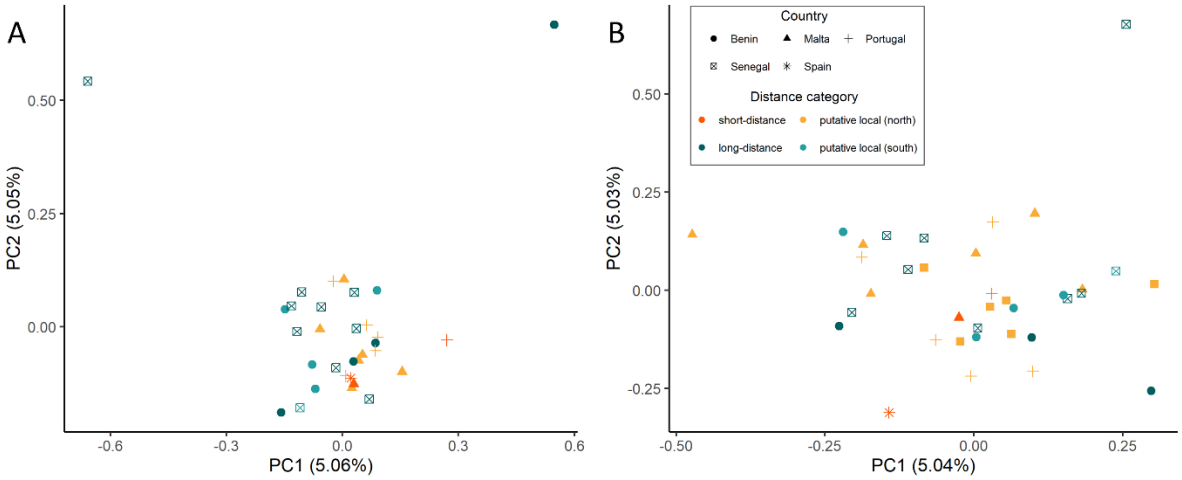

Figure S4.3 Principal component analysis (PCA) biplot illustrating the genetic variation in samples, **(A)** excluding samples from Morocco, and **(B)** excluding two outliers (19H128 and 19H115).

Table S4.2 Population genetic summary statistics. Within-group nucleotide diversity (π) and between-group absolute divergence (d_{XY}) and genetic differentiation (F_{ST}) calculated separately for the autosomes and the Z chromosome (mean ± sd, maximum). Summary statistics are obtained from window-based values (20 kb) calculated in pixy. Samples are grouped by migration distance (i.e., short distance and Mediterranean putative locals vs long distance) and capture location (north vs south of the Sahara).

	Migration distance		Capture location	
	Autosomes	Z chromosome	Autosome	Z chromosome
π (short/north)	0.012 ± 0.003, < 0.070	0.008 ± 0.003, < 0.020	0.012 ± 0.003, < 0.070	0.008 ± 0.003, < 0.018
π (long/south)	0.012 ± 0.003, < 0.067	0.008 ± 0.003, < 0.022	0.012 ± 0.003, < 0.067	0.008 ± 0.003, < 0.020
d_{XY}	0.012 ± 0.003, < 0.069	0.008 ± 0.003, < 0.023	0.012 ± 0.003, < 0.069	0.008 ± 0.003, < 0.020
F_{ST}	0.001± 0.006, < 0.113	0.009 ± 0.016, < 0.072	0.001 ± 0.005, < 0.048	0.007 ± 0.005, < 0.019

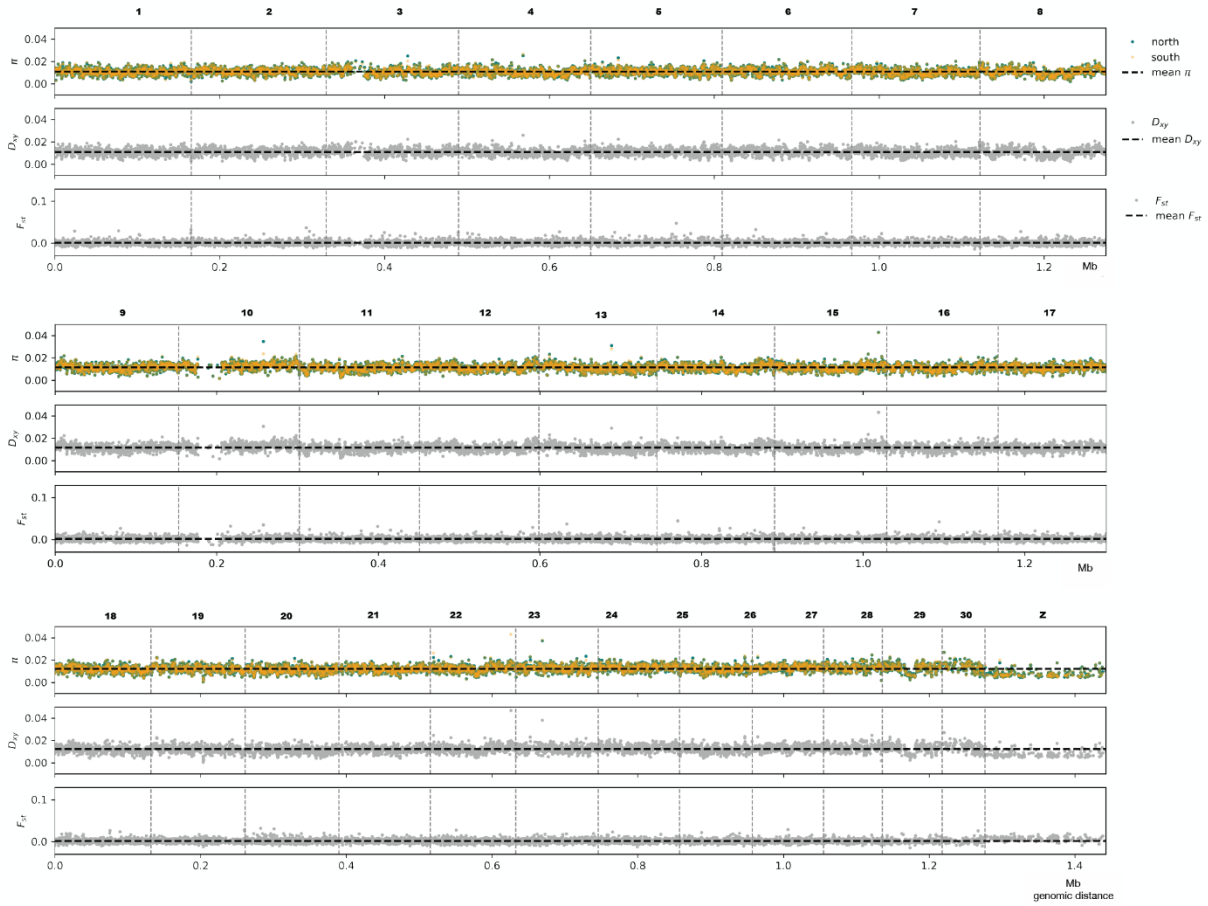

Figure S4.4 Genome scans showing within population diversity (π), genetic differentiation (d_{XY}) and fixation index (F_{ST}) between individuals captured north and south of the Sahara. The analysis was performed with sliding, non-overlapping windows of 20 kb. Mean values are indicated by a black dashed line.

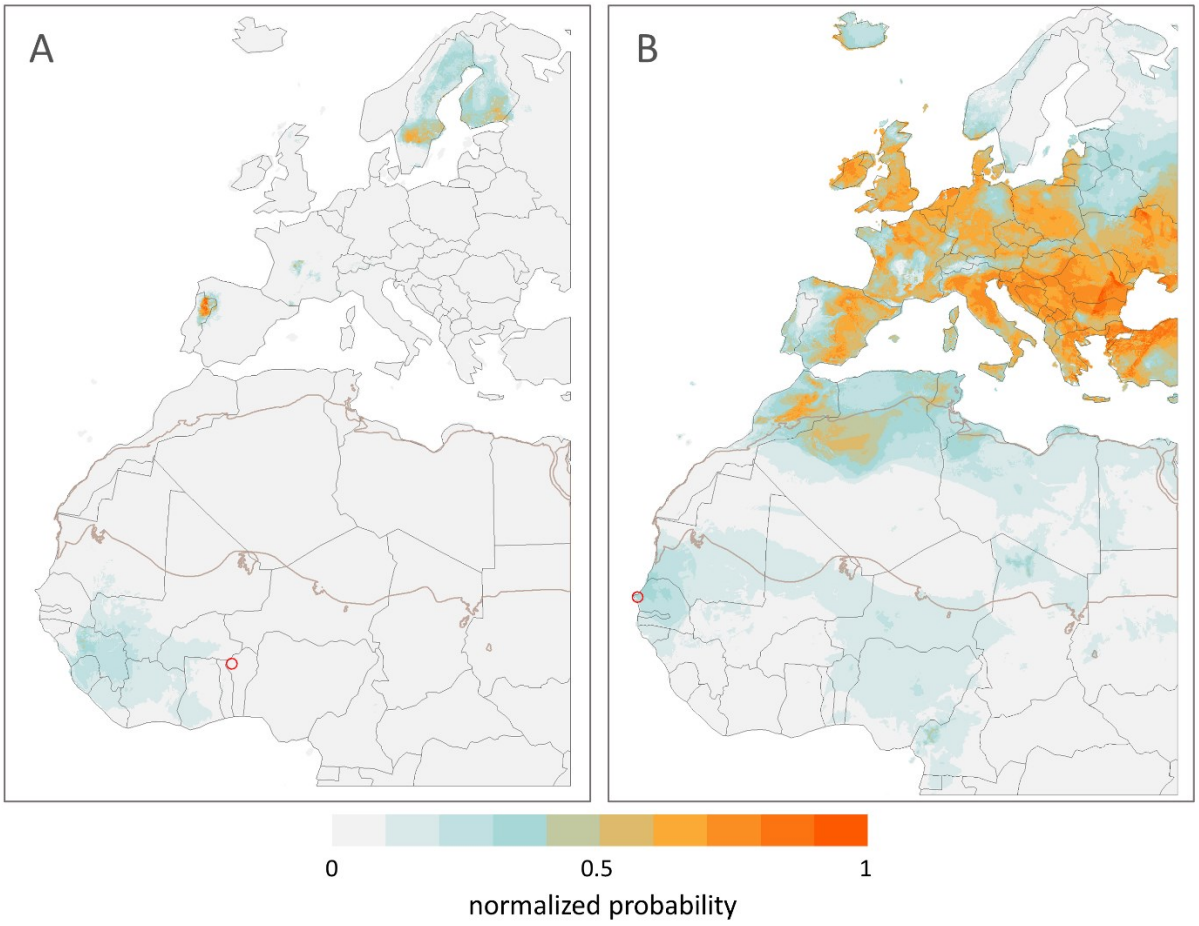

Figure S4.5 Examples of normalized posterior probability surfaces. Samples **(A)** 19H128 and **(B)** 19H115 were collected at the red circles in Sep. 2019.

References

Adams, D. C., & Otárola-Castillo, E. (2013). *geomorph*: An R package for the collection and analysis of geometric morphometric shape data. *Methods in Ecology and Evolution*, *4*(4), 393–399. https://doi.org/10.1111/2041-210X.12035

Agrawal, A. A., & Inamine, H. (2018). Mechanisms behind the monarch's decline. *Science*, *360*(6395), 1294–1296. https://doi.org/10.1126/science.aat5066

Aikens, E. O., Mysterud, A., Merkle, J. A., Cagnacci, F., Rivrud, I. M., Hebblewhite, M., Hurley, M. A., Peters, W., Bergen, S., De Groeve, J., Dwinnell, S. P. H., Gehr, B., Heurich, M., Hewison, A. J. M., Jarnemo, A., Kjellander, P., Kröschel, M., Licoppe, A., Linnell, J. D. C., … Kauffman, M. J. (2020). Wave-like patterns of plant phenology determine ungulate movement tactics. *Current Biology*, 30(17), 3444-3449.e4. https://doi.org/10.1016/j.cub.2020.06.032

Åkesson, S., Bianco, G., & Hedenström, A. (2016). Negotiating an ecological barrier: Crossing the Sahara in relation to winds by common swifts. *Philosophical Transactions of the Royal Society B*, *371*(1704). https://doi.org/10.1098/rstb.2015.0393

Als, T. D., Hansen, M. M., Maes, G. E., Castonguay, M., Riemann, L., Aarestrup, K., Munk, P., Sparholt, H., Hanel, R., & Bernatchez, L. (2011). All roads lead to home: Panmixia of European eel in the Sargasso Sea. *Molecular Ecology*, *20*(7), 1333–1346. https://doi.org/10.1111/j.1365-294X.2011.05011.x

Altizer, S., & Davis, A. (2010). Populations of monarch butterflies with different migratory behaviors show divergence in wing morphology. *Evolution*, *64*(4), 1018–1028. https://doi.org/10.1111/j.1558-5646.20

Altizer, S., Bartel, R., & Han, B. A. (2011). Animal migration and infectious disease risk. *Science*, *331*(6015), 296–302. https://doi.org/10.1126/science.1194694

Altizer, S., Hobson, K. A., Davis, A. K., De Roode, J. C., & Wassenaar, L. I. (2015). Do healthy monarchs migrate farther? Tracking natal origins of parasitized vs. uninfected monarch butterflies overwintering in Mexico. *PLOS ONE*, *10*(11), e0141371. https://doi.org/10.1371/journal.pone.0141371

Alvial, I. E., Vargas, H. A., Marinov, M., Esquivel, C., Araya, J., Araya-Donoso, R., Vila, I., & Véliz, D. (2019). Isolation on a remote island: Genetic and morphological differentiation of a cosmopolitan odonate. *Heredity*, *122*(6), 893–905. https://doi.org/10.1038/s41437-018-0165-z

Anastopoulos, I., Bhatnagar, A., Bikiaris, D., & Kyzas, G. (2017). Chitin adsorbents for toxic metals: A review. *International Journal of Molecular Sciences*, *18*(1), 114. https://doi.org/10.3390/ijms18010114

Anders, D., Osmanovic, A., & Vohberger, M. (2019). Intra- and inter-individual variability of stable strontium isotope ratios in hard and soft body tissues of pigs. *Rapid Communications in Mass Spectrometry*, *33*(3), 281–290. https://doi.org/10.1002/rcm.8350

Andreani, G., Ferlizza, E., Cabbri, R., Fabbri, M., Bellei, E., & Isani, G. (2021). Essential (Mg, Fe, Zn and Cu) and non-essential (Cd and Pb) elements in predatory insects (*Vespa crabro* and *Vespa velutina*): A molecular perspective. *International Journal of Molecular Sciences*, *22*(228). https://doi.org/10.3390/ijms22010228

Andrews, S. (2010). *FastQC: a quality control tool for high throughput sequence data* [Computer software].

Aptekmann, A. A., Buongiorno, J., Giovannelli, D., Glamoclija, M., Ferreiro, D. U., & Bromberg, Y. (2022). mebipred: Identifying metal-binding potential in protein sequence. *Bioinformatics*, *38*(14), 3532–3540. https://doi.org/10.1093/bioinformatics/btac358

Arino, O., Perez, R., Julio, J., Kalogirou, V., Bontemps, S., & Defourny, Pierre Van Bogaert, E. (2012). *Global Land Cover Map for 2009 (GlobCover 2009)*. European Space Agency (ESA) & Université catholique de Louvain (UCL). https://doi.org/10.1594/PANGAEA.787668

Balmino, G., Vales, N., Bonvalot, S., & Briais, A. (2012). Spherical harmonic modelling to ultra-high degree of Bouguer and isostatic anomalies. *Journal of Geodesy*, *86*(7), 499–520. https://doi.org/10.1007/s00190-011-0533-4

Bataille, C. P., & Bowen, G. J. (2012). Mapping 87Sr/86Sr variations in bedrock and water for large scale provenance studies. *Chemical Geology*, *304–305*, 39–52. https://doi.org/10.1016/J.CHEMGEO.2012.01.028

Bataille, C. P., Von Holstein, I. C. C., Laffoon, J. E., Willmes, M., Liu, X.-M., & Davies, G. R. (2018). A bioavailable strontium isoscape for Western Europe: A machine learning approach. *PLOS ONE*, *13*(5), 27. https://doi.org/10.1371/journal.pone.0197386

Bataille, C. P., Crowley, B. E., Wooller, M. J., & Bowen, G. J. (2020). Advances in global bioavailable strontium isoscapes. *Palaeogeography, Palaeoclimatology, Palaeoecology*, *555*, 109849. https://doi.org/10.1016/j.palaeo.2020.109849

Bataille, C. P., Jaouen, K., Milano, S., Trost, M., Steinbrenner, S., Crubézy, É., & Colleter, R. (2021). Triple sulfur-oxygen-strontium isotopes probabilistic geographic assignment of archaeological remains using a novel sulfur isoscape of western Europe. PLOS ONE, 16(5), e0250383. https://doi.org/10.1371/journal.pone.0250383

Bataille, C. P., Ammer, S. T. M., Bhuiyan, S., Chartrand, M. M. G., St-Jean, G., & Bowen, G. J. (2022). Multi-isotopes in human hair: A tool to initiate cross-border collaboration in international cold-cases. *PLOS ONE*, *17*(10), e0275902. https://doi.org/10.1371/journal.pone.0275902

Batalden, R. V., Oberhauser, K., & Peterson, A. T. (2008). Ecological niches in sequential generations of eastern North American monarch butterflies (Lepidoptera: Danaidae): The ecology of migration

and likely climate change implications. *Environmental Entomology*, *36*(6), 1365–1373. https://doi.org/10.1603/0046-225x(2007)36[1365:enisgo]2.0.co;2

Ben-Shahar, Y. (2018). The impact of environmental Mn exposure on insect biology. *Frontiers in Genetics*, *9*(70), 1–7. https://doi.org/10.3389/fgene.2018.00070

Boman, J., Zhu, Y., Höök, L., Vila, R., Talavera, G., & Backström, N. (2023). Environmental stress during larval development induces DNA methylation shifts in the migratory painted lady butterfly (*Vanessa cardui*). *Molecular Ecology*, mec.16957. https://doi.org/10.1111/mec.16957

Borisov, S. N., Iakovlev, I. K., Borisov, A. S., Zuev, A. G., & Tiunov, A. V. (2020). Isotope evidence for latitudinal migrations of the dragonfly *Sympetrum fonscolombii* (Odonata: Libellulidae) in Middle Asia. *Ecological Entomology*. https://doi.org/10.1111/een.12930

Börker, J., Hartmann, J., Amann, T., & Romero-Mujalli, G. (2018). Terrestrial sediments of the earth: Development of a global unconsolidated sediments map database (GUM). *Geochemistry, Geophysics, Geosystems*, *19*, 997–1024. https://doi.org/10.1002/2017GC007273

Bowden, J., Digby, P. G. N., & Sherlock, P. L. (1984). Studies of elemental composition as a biological marker in insects. I. The influence of soil type and host-plant on elemental composition of Noctua pronuba (Lepidoptera: Noctuidae). *Bulletin of Entomological Research*, *75*, 207–225. https://doi.org/10.1017/S0007485300015947

Bowen, G. J., Wassenaar, L. I., & Hobson, K. A. (2005). Global application of stable hydrogen and oxygen isotopes to wildlife forensics. *Oecologia*, *143*(3), 337–348. https://doi.org/10.1007/s00442-004-1813-y

Bowen, G. J. (2018). *Gridded maps of the isotopic composition of meteoric waters.* [Computer software]. http://www.waterisotopes.org.

Brahney, J., Ballantyne, A. P., Kociolek, P., Leavitt, P. R., Farmer, G. L., & Neff, J. C. (2015). Ecological changes in two contrasting lakes associated with human activity and dust transport in western

Wyoming: Dust-P controls on alpine lake ecology. *Limnology and Oceanography*, *60*, 678–695. https://doi.org/10.1002/lno.10050

Briedis, M., Bauer, S., Adamík, P., Alves, J. A., Costa, J. S., Emmenegger, T., Gustafsson, L., Koleček, J., Krist, M., Liechti, F., Lisovski, S., Meier, C. M., Procházka, P., & Hahn, S. (2020). Broad-scale patterns of the Afro-Palaearctic landbird migration. *Global Ecology and Biogeography*, *29*(4), 722–735. https://doi.org/10.1111/geb.13063

Brower, L. P. (1995). Understanding and misunderstanding the migration of the monarch butterfly (Nymphalidae) in North America: 1857-1995. *Journal of the Lepidopterists' Society*, *49*(4), 304–385.

Brower, L. P., Taylor, O. R., William, E. H., Slayback, D. A., Zubieta, R. R., & Ramírez, M. I. (2012). Decline of monarch butterflies overwintering in Mexico: Is the migratory phenomenon at risk? *Insect Conservation and Diversity*, *5*(2), 95–100. https://doi.org/10.1111/j.1752-4598.2011.00142.x

Buffalo, V. (2021). Quantifying the relationship between genetic diversity and population size suggests natural selection cannot explain Lewontin's Paradox. *eLife*, *10*, e67509. https://doi.org/10.7554/eLife.67509

Butt, A., Qurat-ul-Ain, Rehman, K., Khan, M. X., & Hesselberg, T. (2018). Bioaccumulation of cadmium, lead, and zinc in agriculture-based insect food chains. *Environmental Monitoring and Assessment*, *190*(12). https://doi.org/10.1007/s10661-018-7051-2

Calvert, W. H. (1999). Patterns in the spatial and temporal use of Texas milkweeds (Asclepiadaceae) by the monarch butterfly (*Danaus plexippus* L.) during fall, 1996. *Journal of the Lepidopterists' Society*, *53*(1), 37–44.

Campbell, C. J., Fitzpatrick, M. C., Vander Zanden, H. B., & Nelson, D. M. (2020). Advancing interpretation of stable isotope assignment maps: Comparing and summarizing origins of

known-provenance migratory bats. *Animal Migration*, *7*(1), 27–41. https://doi.org/10.1515/ami-2020-0004

Capo, R. C., Stewart, B. W., & Chadwick, O. A. (1998). Strontium isotopes as tracers of ecosystem processes: Theory and methods. *Geoderma*, *82*, 197–225. https://doi.org/10.1016/S0016-7061(97)00102-X

Cardoso-Jaime, V., Broderick, N. A., & Maya-Maldonado, K. (2022). Metal ions in insect reproduction: A crosstalk between reproductive physiology and immunity. *Current Opinion in Insect Science*, *52*, 100924. https://doi.org/10.1016/j.cois.2022.100924

Celorio-Mancera, M. D. L. P., Wheat, C. W., Huss, M., Vezzi, F., Neethiraj, R., Reimegård, J., Nylin, S., & Janz, N. (2016). Evolutionary history of host use, rather than plant phylogeny, determines gene expression in a generalist butterfly. *BMC Evolutionary Biology*, *16*(1). https://doi.org/10.1186/s12862-016-0627-y

Chamberlain, C. P., Blum, J. D., Holmes, T. R. H., Feng, X., Sherry, T. W., & Graves, G. R. (1997). The use of isotope tracers for identifying populations of migratory birds. *Oecologia*, *109*(1), 132–141.

Chapman, B. B., Hulthén, K., Blomqvist, D. R., Hansson, L.-A., Nilsson, J.-Å., Brodersen, J., Anders Nilsson, P., Skov, C., & Brönmark, C. (2011). To boldly go: Individual differences in boldness influence migratory tendency. *Ecology Letters*, *14*(9), 871–876. https://doi.org/10.1111/j.1461-0248.2011.01648.x

Chapman, J. W., Drake, V. A., & Reynolds, D. R. (2011). Recent insights from radar studies of insect flight. *Annual Review of Entomology*, *56*, 337–356. https://doi.org/10.1146/annurev-ento-120709-144820

Chapman, J. W., Reynolds, D. R., & Wilson, K. (2015). Long-range seasonal migration in insects: Mechanisms, evolutionary drivers and ecological consequences. *Ecology Letters*, *18*(3), 287–302. https://doi.org/10.1111/ele.12407

Chapuis, M.-P., Loiseau, A., Michalakis, Y., Lecoq, M., Franc, A., & Estoup, A. (2009). Outbreaks, gene flow and effective population size in the migratory locust, *Locusta migratoria*: A regional-scale comparative survey. *Molecular Ecology*, *18*(5), 792–800. https://doi.org/10.1111/j.1365-294X.2008.04072.x

Chelli, A., & Moulaï, R. (2019). Ecological characterization of the odonatofauna in lotic and lentic waters of northeast Algeria. *Annales de La Société Entomologique de France*, 55(5), 430–445. https://doi.org/10.1080/00379271.2019.1660215

Chen, S., Zhou, Y., Chen, Y., & Gu, J. (2018). fastp: An ultra-fast all-in-one FASTQ preprocessor. *Bioinformatics*, *34*(17), i884–i890. https://doi.org/10.1093/bioinformatics/bty560

Chen, S. (2023). Ultrafast one-pass FASTQ data preprocessing, quality control, and deduplication using fastp. *iMeta*, *2*(2), e107. https://doi.org/10.1002/imt2.107

Cheruiyot, D. J., Boyd, R. S., & Moar, W. J. (2013). Exploring lower limits of plant elemental defense by cobalt, copper, nickel, and zinc. *Journal of Chemical Ecology*, *39*(5), 666–674. https://doi.org/10.1007/s10886-013-0279-y

Chien, C., Mackey, K. R. M., Dutkiewicz, S., Mahowald, N. M., Prospero, J. M., & Paytan, A. (2016). Effects of African dust deposition on phytoplankton in the western tropical Atlantic Ocean off Barbados. *Global Biogeochemical Cycles*, *30*(5), 716–734. https://doi.org/10.1002/2015GB005334

Chowdhury, S., Fuller, R. A., Dingle, H., Chapman, J. W., & Zalucki, M. P. (2021a). Migration in butterflies: A global overview. *Biological Reviews*, *61*, brv.12714. https://doi.org/10.1111/brv.12714

Chowdhury, S., Zalucki, M. P., Amano, T., Woodworth, B. K., Venegas-Li, R., & Fuller, R. A. (2021b). Seasonal spatial dynamics of butterfly migration. *Ecology Letters*, *24*(9), 1814–1823. https://doi.org/10.1111/ele.13787

Chowdhury, S., Zalucki, M. P., Amano, T., Poch, T. J., Lin, M., Ohwaki, A., Lin, D., Yang, L., Choi, S., Jennions, M. D., & Fuller, R. A. (2022). Trends and progress in studying butterfly migration. *Integrative Conservation*, *1*, 8–24. https://doi.org/10.1002/inc3.13

Clark, E. W. (1958). A review of literature on calcium and magnesium in insects. *Annals of the Entomological Society of America*, *51*, 142–154.

Clem, C. S., Hobson, K. A., & Harmon-Threatt, A. N. (2023). Insights into natal origins of migratory Nearctic hover flies (Diptera: Syrphidae): new evidence from stable isotope (δ^2H) assignment analyses. *Ecography*, *2023*(2), e06465. https://doi.org/10.1111/ecog.06465

Clobert, J., Le Galliard, J. F., Cote, J., Meylan, S., & Massot, M. (2009). Informed dispersal, heterogeneity in animal dispersal syndromes and the dynamics of spatially structured populations. *Ecology Letters*, *12*(3), 197–209. https://doi.org/10.1111/j.1461-0248.2008.01267.x

Codex alimentarius: International food standards, 1 (2019).

Cohen, E. B., & Satterfield, D. A. (2020). 'Chancing on a spectacle:' Co-occurring animal migrations and interspecific interactions. *Ecography*, *43*, 1–15. https://doi.org/10.1111/ecog.04958

Commission for Environmental Cooperation. (2007). *North America Elevation 1-Kilometer Resolution*. Commission for Environmental Cooperation. http://www.cec.org/naatlas/

Consuegra, J., Grenier, T., Baa-Puyoulet, P., Rahioui, I., Akherraz, H., Gervais, H., Parisot, N., Da Silva, P., Charles, H., Calevro, F., & Leulier, F. (2020). Drosophila-associated bacteria differentially shape the nutritional requirements of their host during juvenile growth. *PLoS Biology,* 18(3). https://doi.org/10.1371/journal.pbio.3000681

Copeland, S. R., Sponheimer, M., de Ruiter, D. J., Lee-Thorp, J. A., Codron, D., le Roux, P. J., Grimes, V., & Richards, M. P. (2011). Strontium isotope evidence for landscape use by early hominins. *Nature*, *474*(7349), 76–78. https://doi.org/10.1038/nature10149

Coplen, T. B., & Qi, H. (2012). USGS42 and USGS43: Human-hair stable hydrogen and oxygen isotopic reference materials and analytical methods for forensic science and implications for published measurement results. *Forensic Science International*, *214*(1–3), 135–141. https://doi.org/10.1016/j.forsciint.2011.07.035

Coutu, A. N., Lee-Thorp, J., Collins, M. J., & Lane, P. J. (2016). Mapping the elephants of the 19th century East African ivory trade with a multi-isotope approach. *PLoS ONE*, *11*(10), 1–23. https://doi.org/10.1371/journal.pone.0163606

Crowley, B. E., Miller, J. H., & Bataille, C. P. (2017). Strontium isotopes ($^{87}Sr/^{86}Sr$) in terrestrial ecological and palaeoecological research: Empirical efforts and recent advances in continental-scale models. *Biological Reviews*, *92*, 43–59. https://doi.org/10.1111/brv.12217

Crowley, B. E., Bataille, C. P., Haak, B. A., & Sommer, K. M. (2021). Identifying nesting grounds for juvenile migratory birds with dual isotope: An initial test using North American raptors. *Ecosphere*, *12*(10), 0–21. https://doi.org/10.1002/ecs2.3765

Danecek, P., Auton, A., Abecasis, G., Albers, C. A., Banks, E., DePristo, M. A., Handsaker, R. E., Lunter, G., Marth, G. T., Sherry, S. T., McVean, G., Durbin, R., & 1000 Genomes Project Analysis Group. (2011). The variant call format and VCFtools. *Bioinformatics*, *27*(15), 2156–2158. https://doi.org/10.1093/bioinformatics/btr330

Dapporto, L., Cini, A., Vodă, R., Dincă, V., Wiemers, M., Menchetti, M., Magini, G., Talavera, G., Shreeve, T., Bonelli, S., Casacci, L. P., Balletto, E., Scalercio, S., & Vila, R. (2019). Integrating three comprehensive data sets shows that mitochondrial DNA variation is linked to species traits and paleogeographic events in European butterflies. *Molecular Ecology Resources*, *19*(6), 1623–1636. https://doi.org/10.1111/1755-0998.13059

Dargent, F., Gilmour, S. M., Brown, E. A., Kassen, R., & Kharouba, H. M. (2021). Low prevalence of the parasite *Ophryocystis elektroscirrha* at the range edge of the eastern North American monarch

(*Danaus plexippus*) butterfly population. *Canadian Journal of Zoology*, *99*(5), 409–413. https://doi.org/10.1139/cjz-2020-0175

Dargent, F., Candau, J.-N., Studens, K., Perrault, K. H., Reich, M. S., & Bataille, C. P. (2023). Characterizing eastern spruce budworm's large-scale dispersal events through flight behavior and stable isotope analyses. *Frontiers in Ecology and Evolution*, *11*, 1060982. https://doi.org/10.3389/fevo.2023.1060982

Davis, A. K., & Holden, M. T. (2015). Measuring intraspecific variation in flight-related morphology of monarch butterflies (*Danaus plexippus*): Which sex has the best flying gear? *Journal of Insects*, *2015*, 1–6. https://doi.org/10.1155/2015/591705

Degryse, P., De Muynck, D., Delporte, S., Boyen, S., Jadoul, L., De Winne, J., Ivaneanu, T., & Vanhaecke, F. (2012). Strontium isotopic analysis as an experimental auxiliary technique in forensic identification of human remains. *Analytical Methods*, *4*, 2674. https://doi.org/10.1039/c2ay25035g

Delmore, K., Fox, J. W., & Irwin, D. E. (2012). Dramatic intraspecific differences in migratory routes, stopover sites and wintering areas, revealed using light-level geolocators. *Proceedings of the Royal Society B: Biological Sciences*, *279*(1747), 4582–4589. https://doi.org/10.1098/rspb.2012.1229

Delmore, K., Illera, J. C., Pérez-Tris, J., Segelbacher, G., Lugo Ramos, J. S., Durieux, G., Ishigohoka, J., & Liedvogel, M. (2020). The evolutionary history and genomics of European blackcap migration. *eLife*, *9*, e54462. https://doi.org/10.7554/eLife.54462

Dempster, J. P., Lakhani, K. H., & Coward, P. A. (1986). The use of chemical composition as a population marker in insects: A study of the Brimstone butterfly. *Ecological Entomology*, *11*, 51–65. https://doi.org/10.1111/j.1365-2311.1986.tb00279.x

DePristo, M. A., Banks, E., Poplin, R., Garimella, K. V., Maguire, J. R., Hartl, C., Philippakis, A. A., Del Angel, G., Rivas, M. A., Hanna, M., McKenna, A., Fennell, T. J., Kernytsky, A. M., Sivachenko, A. Y., Cibulskis, K., Gabriel, S. B., Altshuler, D., & Daly, M. J. (2011). A framework for variation discovery and genotyping using next-generation DNA sequencing data. *Nature Genetics*, *43*(5), 491–498. https://doi.org/10.1038/ng.806

Dewitz, J., & U.S. Geological Survey. (2021). National Land Cover Database (NLCD) 2019 Products (ver. 2.0, June 2021). *U.S. Geological Survey Data Release*. https://doi.org/10.5066/P9KZCM54

Di, N., Hladun, K. R., Zhang, K., Liu, T. X., & Trumble, J. T. (2016). Laboratory bioassays on the impact of cadmium, copper and lead on the development and survival of honeybee (*Apis mellifera* L.) larvae and foragers. *Chemosphere*, *152*, 530–538. https://doi.org/10.1016/j.chemosphere.2016.03.033

Diffendorfer, J. E., Drum, R. G., Mitchell, G. W., Rendón-Salinas, E., Sánchez-Cordero, V., Semmens, D. J., Thogmartin, W. E., & March, I. J. (2023). The benefits of big-team science for conservation: Lessons learned from trinational monarch butterfly collaborations. *Frontiers in Environmental Science*, *11*, 1079025. https://doi.org/10.3389/fenvs.2023.1079025

Dinerstein, E., Olson, D., Joshi, A., Vynne, C., Burgess, N. D., Wikramanayake, E., Hahn, N., Palminteri, S., Hedao, P., Noss, R., Hansen, M., Locke, H., Ellis, E. C., Jones, B., Barber, C. V., Hayes, R., Kormos, C., Martin, V., Crist, E., … Saleem, M. (2017). An ecoregion-based approach to protecting half the terrestrial realm. *BioScience*, *67*(6), 534–545. https://doi.org/10.1093/biosci/bix014

Dingle, H., & Drake, V. A. (2007). What is migration? *BioScience*, *57*(2), 113–121. https://doi.org/10.1641/B570206

Dingle, H. (2014a). Evolutionary genetics of migration. In *Migration* (pp. 248–268). Oxford University Press. https://doi.org/10.1093/acprof:oso/9780199640386.003.0014

Dingle, H. (2014b). *Migration: The biology of life on the move* (2nd ed.). Oxford University Press.

Dockx, C., Brower, L. P., Wassenaar, L. I., & Hobson, K. A. (2004). Do North American monarch butterflies travel to Cuba? Stable isotope and chemical tracer techniques. *Ecological Applications*, *14*(4), 1106–1114.

Dow, J. A. (2017). The essential roles of metal ions in insect homeostasis and physiology. *Current Opinion in Insect Science*, *23*, 43–50. https://doi.org/10.1016/j.cois.2017.07.001

Du, B., Ding, D., Ma, C., Guo, W., & Kang, L. (2022). Locust density shapes energy metabolism and oxidative stress resulting in divergence of flight traits. *Proceedings of the National Academy of Sciences*, *119*(1), e2115753118. https://doi.org/10.1073/pnas.2115753118

Ehrlich, M. A., Wagner, D. N., Oleksiak, M. F., & Crawford, D. L. (2021). Polygenic selection within a single generation leads to subtle divergence among ecological niches. *Genome Biology and Evolution*, *13*(2), evaa257. https://doi.org/10.1093/gbe/evaa257

Enbody, E. D., Pettersson, M. E., Sprehn, C. G., Palm, S., Wickström, H., & Andersson, L. (2021). Ecological adaptation in European eels is based on phenotypic plasticity. *Proceedings of the National Academy of Sciences*, *118*(4), e2022620118. https://doi.org/10.1073/pnas.2022620118

Escobar-Suárez, S., Villalobos-Leiva, A., Fabres, A., Órdenes-Clavería, R., Cruz-Jofré, F., Laroze, D., Correa, M., Valladares, M. A., Cáceres, J. S. D., & Benítez, H. A. (2023). A geometric morphometrics and genetics characterization of *Vanessa carye* in an extreme elevational gradient in the Chilean Altiplano. *Zoologischer Anzeiger*, *304*, 105–112. https://doi.org/10.1016/j.jcz.2023.04.001

Esker, D., Forman, S. L., Widga, C., Walker, J. D., & Andrew, J. E. (2019). Home range of the Columbian mammoths (*Mammuthus columbi*) and grazing herbivores from the Waco Mammoth National Monument, (Texas, USA) based on strontium isotope ratios from tooth enamel bioapatite. *Palaeogeography, Palaeoclimatology, Palaeoecology*, *534*(109291). https://doi.org/10.1016/j.palaeo.2019.109291

Espeset, A., Kobiela, M. E., Sikkink, K. L., Pan, T., Roy, C., & Snell-Rood, E. C. (2019). Anthropogenic increases in nutrients alter sexual selection dynamics: A case study in butterflies. *Behavioral Ecology*, *30*(3), 598–608. https://doi.org/10.1093/beheco/arz004

Ethier, D. M., & Mitchell, G. W. (2023). Effects of climate on fall migration phenology of monarch butterflies departing the northeastern breeding grounds in Canada. *Global Change Biology*, *29*(8), 2122–2131. https://doi.org/10.1111/gcb.16579

Evans, R. D., Wang, W., Evans, H. E., & Georg, R. B. (2017). Variation in Zn, C, and N isotope ratios in three stream insects. *Facets*, *1*, 205–216. https://doi.org/10.1139/facets-2016-0023

Fattorini, N., Costanzo, A., Romano, A., Rubolini, D., Baillie, S., Bairlein, F., Spina, F., & Ambrosini, R. (2023). Eco-evolutionary drivers of avian migratory connectivity. *Ecology Letters*, *26*(7), 1095–1107. https://doi.org/10.1111/ele.14223

Fauberteau, A. E., Chartrand, M. M. G., Hu, L., St-Jean, G., & Bataille, C. P. (2021). Investigating a cold case using high-resolution multi-isotope profiles in human hair. *Forensic Chemistry*, *22*. https://doi.org/10.1016/j.forc.2020.100300

Feindt, W., Oppenheim, S. J., DeSalle, R., Goldstein, P. Z., & Hadrys, H. (2018). Transcriptome profiling with focus on potential key genes for wing development and evolution in *Megaloprepus caerulatus*, the damselfly species with the world's largest wings. *PLoS ONE*, *13*(1), 1–17. https://doi.org/10.1371/journal.pone.0189898

Filipiak, M., Woyciechowski, M., & Czarnoleski, M. (2021). Stoichiometric niche, nutrient partitioning and resource allocation in a solitary bee are sex-specific and phosphorous is allocated mainly to the cocoon. *Scientific Reports*, *11*(1), 652. https://doi.org/10.1038/s41598-020-79647-7

Filipiak, M., & Filipiak, Z. M. (2022). Application of ionomics and ecological stoichiometry in conservation biology: Nutrient demand and supply in a changing environment. *Biological Conservation*, *272*, 109622. https://doi.org/10.1016/j.biocon.2022.109622

Finch, T., Saunders, P., Avilés, J. M., Bermejo, A., Catry, I., De La Puente, J., Emmenegger, T., Mardega, I., Mayet, P., Parejo, D., Račinskis, E., Rodríguez-Ruiz, J., Sackl, P., Schwartz, T., Tiefenbach, M., Valera, F., Hewson, C., Franco, A., & Butler, S. J. (2015). A pan-European, multipopulation assessment of migratory connectivity in a near-threatened migrant bird. *Diversity and Distributions*, *21*(9), 1051–1062. https://doi.org/10.1111/ddi.12345

Flockhart, D. T. T., Wassenaar, L. I., Martin, T. G., Hobson, K. A., Wunder, M. B., & Norris, D. R. (2013). Tracking multi-generational colonization of the breeding grounds by monarch butterflies in eastern North America. *Proceedings of the Royal Society B*, *280*(20131087). https://doi.org/10.1098/rspb.2013.1087

Flockhart, D. T. T., Kyser, T. K., Chipley, D., Miller, N. G., & Norris, D. R. (2015). Experimental evidence shows no fractionation of strontium isotopes ($^{87}Sr/^{86}Sr$) among soil, plants, and herbivores: Implications for tracking wildlife and forensic science. *Isotopes in Environmental and Health Studies*, *51*(3), 372–381. https://doi.org/10.1080/10256016.2015.1021345

Flockhart, D. T. T., Fitz-gerald, B., Brower, L. P., Derbyshire, R., Altizer, S., Hobson, K. A., Wassenaar, L. I., & Norris, D. R. (2017a). Migration distance as a selective episode for wing morphology in a migratory insect. *Movement Ecology, 5(7), 1-9*. https://doi.org/10.1186/s40462-017-0098-9

Flockhart, D. T. T., Brower, L. P., Ramirez, M. I., Hobson, K. A., Wassenaar, L. I., Altizer, S., & Norris, D. R. (2017b). Regional climate on the breeding grounds predicts variation in the natal origin of monarch butterflies overwintering in Mexico over 38 years. *Global Change Biology*, *23*(7), 2565–2576. https://doi.org/10.1111/gcb.13589

Flockhart, D. T. T., Dabydeen, A., Satterfield, D. A., Hobson, K. A., Wassenaar, L. I., & Norris, D. R. (2018). Patterns of parasitism in monarch butterflies during the breeding season in eastern North America. *Ecological Entomology*, *43*(1), 28–36. https://doi.org/10.1111/een.12460

Flores-Martínez, J. J., Martínez-Pacheco, A., Rendón-Salinas, E., Rickards, J., Sarkar, S., & Sánchez-Cordero, V. (2019). Recent Forest Cover Loss in the Core Zones of the Monarch Butterfly Biosphere Reserve in Mexico. *Frontiers in Environmental Science*, *7*(11), 1–8. https://doi.org/10.3389/fenvs.2019.00167

Font, L., Nowell, G. M., Graham Pearson, D., Ottley, C. J., & Willis, S. G. (2007). Sr isotope analysis of bird feathers by TIMS: A tool to trace bird migration paths and breeding sites. *Journal of Analytical Atomic Spectrometry*, *22*(5), 513–522. https://doi.org/10.1039/b616328a

Fox, E. W., Ver Hoef, J. M., & Olsen, A. R. (2020). Comparing spatial regression to random forests for large environmental data sets. *PLoS ONE*, *15*(3), 1–22. https://doi.org/10.1371/journal.pone.0229509

Frichot, E., Mathieu, F., Trouillon, T., Bouchard, G., & François, O. (2014). Fast and Efficient Estimation of Individual Ancestry Coefficients. *Genetics*, *196*(4), 973–983. https://doi.org/10.1534/genetics.113.160572

Fritsch, C., Cœurdassier, M., Giraudoux, P., Raoul, F., Douay, F., Rieffel, D., de Vaufleury, A., & Scheifler, R. (2011). Spatially explicit analysis of metal transfer to biota: Influence of soil contamination and landscape. *PLoS ONE*, *6*(5), 26–29. https://doi.org/10.1371/journal.pone.0020682

Fukano, Y., & Soga, M. (2021). Why do so many modern people hate insects? The urbanization–disgust hypothesis. *Science of The Total Environment*, *777*, 146229. https://doi.org/10.1016/j.scitotenv.2021.146229

Funck, J., Bataille, C., Rasic, J., & Wooller, M. (2021). A bio-available strontium isoscape for eastern Beringia: A tool for tracking landscape use of Pleistocene megafauna. *Journal of Quaternary Science*, *36*(1), 76–90. https://doi.org/10.1002/jqs.3262

Gao, B., Hedlund, J., Reynolds, D. R., Zhai, B., Hu, G., & Chapman, J. W. (2020). The 'migratory connectivity' concept, and its applicability to insect migrants. *Movement Ecology*, *8*(1), 1–13. https://doi.org/10.1186/s40462-020-00235-5

Garcia, M., Juhos, S., Larsson, M., Olason, P. I., Martin, M., Eisfeldt, J., DiLorenzo, S., Sandgren, J., Díaz De Ståhl, T., Ewels, P., Wirta, V., Nistér, M., Käller, M., & Nystedt, B. (2020). Sarek: A portable workflow for whole-genome sequencing analysis of germline and somatic variants. *F1000Research*, *9*, 63. https://doi.org/10.12688/f1000research.16665.2

García-Berro, A., Talla, V., Vila, R., Wai, H. K., Shipilina, D., Chan, K. G., Pierce, N. E., Backström, N., & Talavera, G. (2023). Migratory behaviour is positively associated with genetic diversity in butterflies. *Molecular Ecology*, *32*(3), 560–574. https://doi.org/10.1111/mec.16770

Gatehouse, A. G. (1994). Insect migration: Variability and success in a capricious environment. *Population Ecology*, *36*(2), 165–171. https://doi.org/10.1007/BF02514932

Genuer, R., Poggi, J.-M., & Tuleau-Malot, C. (2015). VSURF: An R Package for Variable Selection Using Random Forests. *The R Journal*, *7*(2). http://cran.r-project.org/package=VSURF.

Georganos, S., Grippa, T., Niang Gadiaga, A., Linard, C., Lennert, M., Vanhuysse, S., Mboga, N., Wolff, E., & Kalogirou, S. (2021). Geographical random forests: A spatial extension of the random forest algorithm to address spatial heterogeneity in remote sensing and population modelling. *Geocarto International*, *36*(2), 121–136. https://doi.org/10.1080/10106049.2019.1595177

Ghouri, S., Reich, M. S., Lopez-Mañas, R., Talavera, G., Bowen, G. J., Vila, R., Talla, V. N. K., Collins, S. C., Martins, D. J., & Bataille, C. P. (2024). A hydrogen isoscape for tracing the migration of herbivorous lepidopterans across the Afro-Palearctic range. Rapid Communications in Mass Spectrometry, 38(3), e9675. https://doi.org/10.1002/rcm.9675

Gilroy, J. J., Gill, J. A., Butchart, S. H. M., Jones, V. R., & Franco, A. M. A. (2016). Migratory diversity predicts population declines in birds. *Ecology Letters*, *19*(3), 308–317. https://doi.org/10.1111/ele.12569

Goehring, L., & Oberhauser, K. S. (2002). Effects of photoperiod, temperature, and host plant age on induction of reproductive diapause and development time in *Danaus plexippus*. *Ecological Entomology*, *27*(6), 674–685. https://doi.org/10.1046/j.1365-2311.2002.00454.x

Gorki, J. L., Sáez, L., López-Mañas, R., Menchetti, M., Shapoval, N., Andersen, A., Benyamini, D., Daniels, S., García-Berro, A., Reich, M. S., Scalercio, S., Toro-Delgado, E., Bataille, C. P., Domingo-Marimon, C., Vila, R., Suchan, T., Talavera, G. (*in review*). Pollen metabarcoding reveals the origin and multigenerational migratory pathway of an intercontinental-scale butterfly outbreak.

Greenberg, R., & Marra, P. P. (2005). *Birds of two worlds: The ecology and evolution of migration*. JHU Press.

Gu, Z., Pan, S., Lin, Z., Hu, L., Dai, X., Chang, J., Xue, Y., Su, H., Long, J., Sun, M., Ganusevich, S., Sokolov, V., Sokolov, A., Pokrovsky, I., Ji, F., Bruford, M. W., Dixon, A., & Zhan, X. (2021). Climate-driven flyway changes and memory-based long-distance migration. *Nature*, *591*, 259-564. https://doi.org/10.1038/s41586-021-03265-0

Guerra, P. A., & Reppert, S. M. (2013). Coldness triggers northward flight in remigrant monarch butterflies. *Current Biology*, *23*(5), 419–423. https://doi.org/10.1016/j.cub.2013.01.052

Guilherme, J. L., Jones, V. R., Catry, I., Beal, M., Dias, M. P., Oppel, S., Vickery, J. A., Hewson, C. M., Butchart, S. H. M., & Rodrigues, A. S. L. (2023). Connectivity between countries established by landbirds and raptors migrating along the African–Eurasian flyway. *Conservation Biology*, *37*(1), e14002. https://doi.org/10.1111/cobi.14002

Guo, J., Fu, X., Zhao, S., Shen, X., Wyckhuys, K. A. G., & Wu, K. (2020). Long-term shifts in abundance of (migratory) crop-feeding and beneficial insect species in northeastern Asia. *Journal of Pest Science*, *93*(2), 583–594. https://doi.org/10.1007/s10340-019-01191-9

Hallworth, M. T., Marra, P. P., McFarland, K. P., Zahendra, S., & Studds, C. E. (2018). Tracking dragons: Stable isotopes reveal the annual cycle of a long-distance migratory insect. *Biology Letters*, *14*(12). https://doi.org/10.1098/rsbl.2018.0741

Hammad, S. M., El-Minshawy, A. M., & Raafat, A. M. (1973). Biology of the painted lady Vanessa (*Pyrameis cardui* L. Lepidoptera, Nymphalidae) on artichoke in A.R. of Egypt. *Atti del 2 Congresso Internazionale sul Carciofo, Bari. Italy*, 929–935.

Harris, I., Osborn, T. J., Jones, P., & Lister, D. (2020). Version 4 of the CRU TS monthly high-resolution gridded multivariate climate dataset. *Scientific Data*, *7*(1), 109. https://doi.org/10.1038/s41597-020-0453-3

Hartman, G., & Richards, M. (2014). Mapping and defining sources of variability in bioavailable strontium isotope ratios in the Eastern Mediterranean. *Geochimica et Cosmochimica Acta*, *126*, 250–264. https://doi.org/10.1016/j.gca.2013.11.015

Hartmann, J., & Moosdorf, N. (2012). The new global lithological map database GLiM: A representation of rock properties at the Earth surface. *Geochemistry, Geophysics, Geosystems*, *13*(12). https://doi.org/10.1029/2012GC004370

Hawkes, W. L., Walliker, E., Gao, B., Forster, O., Lacey, K., Doyle, T., Massy, R., Roberts, N. W., Reynolds, D. R., Özden, Ö., Chapman, J. W., & Wotton, K. R. (2022). Huge spring migrations of insects from the Middle East to Europe: Quantifying the migratory assemblage and ecosystem services. *Ecography*, *2022:e06288.* https://doi.org/10.1111/ecog.06288

Hawkes, W. L., Davies, K., Weston, S., Moyes, K., Chapman, J. W., & Wotton, K. R. (2023). Bat activity correlated with migratory insect bioflows in the Pyrenees. *Royal Society Open Science*, *10*(8), 230151. https://doi.org/10.1098/rsos.230151

Heinrich, K., & Collins, L. (2017). Determining the geographical origin of Asian longhorn beetle (*Anoplophora glabripennis*) specimens using stable isotope and trace element analyses. *Pest Management Science*, *73*(5), 967–975. https://doi.org/10.1002/ps.4408

Hengl, T., Mendes de Jesus, J., Heuvelink, G. B. M., Ruiperez Gonzalez, M., Kilibarda, M., Blagotić, A., Shangguan, W., Wright, M. N., Geng, X., Bauer-Marschallinger, B., Guevara, M. A., Vargas, R., MacMillan, R. A., Batjes, N. H., Leenaars, J. G. B., Ribeiro, E., Wheeler, I., Mantel, S., & Kempen, B. (2017). SoilGrids250m: Global gridded soil information based on machine learning. *PLoS ONE*, *12*(2), e0169748. https://doi.org/10.1371/journal.pone.0169748

Hengl, T., Nussbaum, M., Wright, M. N., Heuvelink, G. B. M., & Gräler, B. (2018). Random forest as a generic framework for predictive modeling of spatial and spatio-temporal variables. *PeerJ*, *6*(e5518). https://doi.org/10.7717/peerj.5518

Hengl, T., Miller, M. A. E., Križan, J., Shepherd, K. D., Sila, A., Kilibarda, M., Antonijević, O., Glušica, L., Dobermann, A., Haefele, S. M., McGrath, S. P., Acquah, G. E., Collinson, J., Parente, L., Sheykhmousa, M., Saito, K., Johnson, J. M., Chamberlin, J., Silatsa, F. B. T., … Crouch, J. (2021). African soil properties and nutrients mapped at 30 m spatial resolution using two-scale ensemble machine learning. *Scientific Reports*, *11*(1), 1–18. https://doi.org/10.1038/s41598-021-85639-y

Hijmans, R. J., Cameron, S. E., Parra, J. L., Jones, P. G., & Jarvis, A. (2005). Very high resolution interpolated climate surfaces for global land areas. *International Journal of Climatology*, *25*, 1965–1978. https://doi.org/10.1002/joc.1276

Hijmans, R. J. (2020). *raster: Geographic Data Analysis and Modeling* (R package version 3.3-13). https://doi.org/R package version 3.3-13, https://cran.r-project.org/package=raster

Hirsch, H. V. B., Mercer, J., Sambaziotis, H., Huber, M., Stark, D. T., Torno-Morley, T., Hollocher, K., Ghiradella, H., & Ruden, D. M. (2003). Behavioral effects of chronic exposure to low levels of lead in *Drosophila melanogaster*. *NeuroToxicology*, *24*(3), 435–442. https://doi.org/10.1016/S0161-813X(03)00021-4

Hobson, K. A., Wassenaar, L. I., & Taylor, O. R. (1999). Stable isotopes (δD and $\delta^{13}C$) are geographic indicators of natal origins of monarch butterflies in eastern North America. *Oecologia*, *120*(3), 397–404.

Hobson, K. A., Barnett-Johnson, R., & Cerling, T. (2010). Chapter 13: Using isoscapes to track animal migration. In J. B. West (Ed.), *Isoscapes: Understanding Movement, Pattern, and Process on Earth Through Isotope Mapping* (pp. 273–298). Springer Netherlands. https://doi.org/10.1007/978-90-481-3354-3_13

Hobson, K. A., Plint, T., Serrano, E. G., Alvarez, X. M., Ramirez, I., & Longstaffe, F. J. (2017). Within-wing isotopic ($\delta^{2}H$, $\delta^{13}C$, $\delta^{15}N$) variation of monarch butterflies: Implications for studies of migratory origins and diet. *Animal Migration*, *4*(1), 8–14. https://doi.org/10.1515/ami-2017-0002

Hobson, K. A., Kardynal, K. J., & Koehler, G. (2019). Expanding the isotopic toolbox to track monarch butterfly (*Danaus plexippus*) origins and migration: On the utility of stable oxygen isotope ($\delta^{18}O$) measurements. *Frontiers in Ecology and Evolution*, *7*(224). https://doi.org/10.3389/fevo.2019.00224

Hobson, K. A., & Wassenaar, L. I. (2019). *Tracking animal migration with stable isotopes*. Elsevier. https://doi.org/10.1016/B978-0-12-814723-8.00001-5

Hobson, K. A., Kusack, J. W., & Mora-Alvarez, B. X. (2021). Origins of six species of butterflies migrating through northeastern Mexico: New insights from stable isotope (δ^2H) analyses and a call for documenting butterfly migrations. *Diversity*, *13*(102), 1–12. https://doi.org/10.3390/d13030102

Hobson, K. A. (2023). Stable isotopes and a changing world. *Oecologia*. https://doi.org/10.1007/s00442-023-05387-w

Holder, P. W. (2012). *Isotopes and trace elements as geographic origin markers for biosecurity pests* [Lincoln University]. https://researcharchive.lincoln.ac.nz/handle/10182/5249

Holder, P. W., Armstrong, K., Van Hale, R., Millet, M.-A., Frew, R., Clough, T. J., & Baker, J. A. (2014). Isotopes and trace elements as natal origin markers of *Helicoverpa armigera* - An experimental model for biosecurity pests. *PLoS ONE*, *9*(3), e92384. https://doi.org/10.1371/journal.pone.0092384

Holder, P. W., Van Hale, R. J., Frew, R., George, S., & Armstrong, K. F. (2019). Natal origin of the invasive biosecurity pest, brown marmorated stink bug *(Halyomorpha halys*: Penatomidae), determined by dual-element stable isotope-ratio mass spectrometry. *Pest Management Science*, *76*(4), 1456–1463. https://doi.org/10.1002/ps.5659

Homer, C., Dewitz, J., Jin, S., Xian, G., Costello, C., Danielson, P., Gass, L., Funk, M., Wickham, J., Stehman, S., Auch, R., & Riitters, K. (2020). Conterminous United States land cover change patterns 2001–2016 from the 2016 National Land Cover Database. *ISPRS Journal of Photogrammetry and Remote Sensing*, *162*, 184–199. https://doi.org/10.1016/j.isprsjprs.2020.02.019

Honegger, H. W., Dewey, E. M., & Ewer, J. (2008). Bursicon, the tanning hormone of insects: Recent advances following the discovery of its molecular identity. *Journal of Comparative Physiology A: Neuroethology, Sensory, Neural, and Behavioral Physiology*, *194*, 989–1005. https://doi.org/10.1007/s00359-008-0386-3

Hopkin, S. P. (1990). Critical Concentrations, Pathways of Detoxification and Cellular Ecotoxicology of Metals in Terrestrial Arthropods. *Functional Ecology*, *4*(3), 321. https://doi.org/10.2307/2389593

Hoppe, K. A., Koch, P. L., Carlson, R. W., & Webb, S. D. (1999). Tracking mammoths and mastodons: Reconstruction of migratory behavior using strontium isotope ratios. *Geology*, *27*(5), 439. https://doi.org/10.1130/0091-7613(1999)027<0439:TMAMRO>2.3.CO;2

Hu, G., Lim, K. S., Horvitz, N., Clark, S. J., Reynolds, D. R., Sapir, N., & Chapman, J. W. (2016). Mass seasonal bioflows of high-flying insect migrants. *Science*, *354*(6319), 420–424. https://doi.org/10.1126/science.aah4379 BRAIN

Hu, L., Fernandez, D. P., & Cerling, T. E. (2018). Longitudinal and transverse variation of trace element concentrations in elephant and giraffe hair: Implication for endogenous and exogenous contributions. *Environmental Monitoring and Assessment*, *190*(644). https://doi.org/10.1007/s10661-018-7038-z

Hu, L., Fernandez, D. P., & Cerling, T. E. (2019). Trace element concentrations in horn: Endogenous levels in keratin and susceptibility to exogenous contamination. *Chemosphere*, *237*, 124443. https://doi.org/10.1016/j.chemosphere.2019.124443

Hu, L., Chartrand, M. M. G., St-Jean, G., Lopes, M., & Bataille, C. P. (2020a). Assessing the reliability of mobility interpretation from a multi-isotope hair profile on a traveling individual. *Frontiers in Ecology and Evolution*, *8*(568943), 1–17. https://doi.org/10.3389/fevo.2020.568943

Hu, L., Fernandez, D. P., Cerling, T. E., & Tipple, B. J. (2020b). Fast exchange of strontium between hair and ambient water: Implication for isotopic analysis in provenance and forensic studies. *PLoS ONE*, *15*(5), 1–14. https://doi.org/10.1371/journal.pone.0233712

Huang, X. (2020). *Characterization of Drywall Products for Assessing Impacts Associated with End-of-Life Management (EPA/600/R-20/286)*. United States Environmental Protection Agency.

Hurme, E., Fahr, J., Eidolon Monitoring Network, Eric-Moise, B. F., Hash, C. T., O'Mara, M. T., Richter, H., Tanshi, I., Webala, P. W., Weber, N., Wikelski, M., & Dechmann, D. K. N. (2022). Fruit bat migration matches green wave in seasonal landscapes. *Functional Ecology*, 36(8), 2043–2055. https://doi.org/10.1111/1365-2435.14097

IAEA/WMO. (2018). *Global Network of Isotopes in Precipitation*. The GNIP Database. https://doi.org/The GNIP Database, https://nucleus.iaea.org/wiser

Inamine, H., Ellner, S. P., Springer, J. P., & Agrawal, A. A. (2016). Linking the continental migratory cycle of the monarch butterfly to understand its population decline. *Oikos*, *125*(8), 1081–1091. https://doi.org/10.1111/oik.03196

James, D. G., James, T. S., Seymour, L., Kappen, L., Russell, T., Harryman, B., & Bly, C. (2018). Citizen scientist tagging reveals destinations of migrating monarch butterflies, *Danaus plexippus* (L.) from the Pacific Northwest. *Journal of the Lepidopterists' Society*, *72*(2), 127–144. https://doi.org/10.18473/lepi.v72i2.a5

Janzen, A., Bataille, C., Copeland, S. R., Quinn, R. L., Ambrose, S. H., Reed, D., Hamilton, M., Grimes, V., Richards, M. P., le Roux, P., & Roberts, P. (2020). Spatial variation in bioavailable strontium isotope ratios ($^{87}Sr/^{86}Sr$) in Kenya and northern Tanzania: Implications for ecology, paleoanthropology, and archaeology. *Palaeogeography, Palaeoclimatology, Palaeoecology*, *560*, 109957. https://doi.org/10.1016/j.palaeo.2020.109957

Jarvis, A., Reuter, H. I., Nelson, A., & Guevara, E. (2008). *Hole-filled SRTM for the globe Version 4, available from the CGIAR-CSI SRTM 90m Database, http://srtm.csi.cgiar.org*.

Jiguet, F., Burgess, M., Thorup, K., Conway, G., Arroyo Matos, J. L., Barber, L., Black, J., Burton, N., Castelló, J., Clewley, G., Copete, J. L., Czajkowski, M. A., Dale, S., Davis, T., Dombrovski, V., Drew, M., Elts, J., Gilson, V., Grzegorczyk, E., … Hewson, C. (2019). Desert crossing strategies of migrant

songbirds vary between and within species. *Scientific Reports*, *9*(1), 20248. https://doi.org/10.1038/s41598-019-56677-4

Jin, P., Chen, J., Zhan, H., Huang, S., Wang, J., & Shu, Y. (2020). Accumulation and excretion of zinc and their effects on growth and food utilization of *Spodoptera litura* (Lepidoptera: Noctuidae). *Ecotoxicology and Environmental Safety*, *202*(110883). https://doi.org/10.1016/j.ecoenv.2020.110883

Jin, S., Homer, C., Yang, L., Danielson, P., Dewitz, J., Li, C., Zhu, Z., Xian, G., & Howard, D. (2019). Overall methodology design for the United States National Land Cover Database 2016 products. *Remote Sensing*, *11*(24), 2971. https://doi.org/10.3390/rs11242971

Joern, A., Provin, T., & Behmer, S. T. (2012). Not just the usual suspects: Insect herbivore populations and communities are associated with multiple plant nutrients. *Ecology*, *93*(5), 1002–1015. https://doi.org/10.1890/11-1142.1

Johnson, C. G. (1960). A Basis for a General System of Insect Migration and Dispersal by Flight. *Nature*, *186*, 348–350.

Jones, C. M., Papanicolaou, A., Mironidis, G. K., Vontas, J., Yang, Y., Lim, K. S., Oakeshott, J. G., Bass, C., & Chapman, J. W. (2015). Genomewide transcriptional signatures of migratory flight activity in a globally invasive insect pest. *Molecular Ecology*, *24*(19), 4901–4911. https://doi.org/10.1111/mec.13362

Judd, T. M., Magnus, R. M., & Fasnacht, M. P. (2010). A nutritional profile of the social wasp *Polistes metricus*: Differences in nutrient levels between castes and changes within castes during the annual life cycle. *Journal of Insect Physiology*, *56*(1), 42–56. https://doi.org/10.1016/j.jinsphys.2009.09.002

Kabata-Pendias, A., & Mukherjee, A. B. (2007). *Trace Elements from Soil to Human*. Springer Berlin Heidelberg. https://doi.org/10.1007/978-3-540-32714-1

Kahle, D., & Wickham, H. (2013). ggmap: Spatial visualization with ggplot2. *R Journal*, *5*(1), 144–161. https://doi.org/10.32614/rj-2013-014

Kaspari, M. (2020). The seventh macronutrient: How sodium shortfall ramifies through populations, food webs and ecosystems. *Ecology Letters*, *23*(7), 1153–1168. https://doi.org/10.1111/ele.13517

Kaspari, M. (2021). The invisible hand of the periodic table: How micronutrients shape ecology. *Annual Review of Ecology, Evolution, and Systematics*, *52*(1), 199–219. https://doi.org/10.1146/annurev-ecolsys-012021-090118

Kassambara, A., & Mundt, F. (2020). *factoextra: Extract and Visualize the Results of Multivariate Data Analyses* (R package version 1.0.7.).

Katzner, T. E., Nelson, D. M., Braham, M. A., Doyle, J. M., Fernandez, N. B., Duerr, A. E., Bloom, P. H., Fitzpatrick, M. C., Miller, T. A., Culver, R. C. E., Braswell, L., & DeWoody, J. A. (2017). Golden Eagle fatalities and the continental-scale consequences of local wind-energy generation. *Conservation Biology*, *31*(2), 406–415. https://doi.org/10.1111/cobi.12836

Kauffman, M. J., Cagnacci, F., Chamaillé-Jammes, S., Hebblewhite, M., Hopcraft, J. G. C., Merkle, J. A., Mueller, T., Mysterud, A., Peters, W., Roettger, C., Steingisser, A., Meacham, J. E., Abera, K., Adamczewski, J., Aikens, E. O., Bartlam-Brooks, H., Bennitt, E., Berger, J., Boyd, C., … Zuther, S. (2021). Mapping out a future for ungulate migrations. *Science*, *372*(6542), 566–569. https://doi.org/10.1126/science.abf0998

Kempson, I. M., Skinner, W. M., & Kirkbride, K. P. (2006). Advanced analysis of metal distributions in human hair. *Environmental Science and Technology*, *40*(10), 3423–3428. https://doi.org/10.1021/es052158v

Kempson, I. M., & Skinner, W. M. (2012). A comparison of washing methods for hair mineral analysis: Internal versus external effects. *Biological Trace Element Research*, *150*, 10–14. https://doi.org/10.1007/s12011-012-9456-z

Kennedy, J. S. (1985). Migration, Behavioural and Ecological. In University of Texas Marine Science Institute (Ed.), *Migration: Mechanisms and Adaptive Significance* (pp. 1–868).

Kijak, E., Rosato, E., Knapczyk, K., & Pyza, E. (2014). *Drosophila melanogaster* as a model system of aluminum toxicity and aging. *Insect Science*, *21*, 189–202. https://doi.org/10.1111/1744-7917.12017

Klaassen, R. H. G., Hake, M., Strandberg, R., Koks, B. J., Trierweiler, C., Exo, K.-M., Bairlein, F., & Alerstam, T. (2014). When and where does mortality occur in migratory birds? Direct evidence from long-term satellite tracking of raptors. *Journal of Animal Ecology*, *83*(1), 176–184. https://doi.org/10.1111/1365-2656.12135

Knight, E. C., Harrison, A., Scarpignato, A. L., Van Wilgenburg, S. L., Bayne, E. M., Ng, J. W., Angell, E., Bowman, R., Brigham, R. M., Drolet, B., Easton, W. E., Forrester, T. R., Foster, J. T., Haché, S., Hannah, K. C., Hick, K. G., Ibarzabal, J., Imlay, T. L., Mackenzie, S. A., … Marra, P. P. (2021). Comprehensive estimation of spatial and temporal migratory connectivity across the annual cycle to direct conservation efforts. *Ecography*, *44*, 665–679. https://doi.org/10.1111/ecog.05111

Knight, S. M., Pitman, G. M., Flockhart, D. T. T., & Norris, D. R. (2019). Radio-tracking reveals how wind and temperature influence the pace of daytime insect migration. *Biology Letters*, *15*(7). https://doi.org/10.1098/rsbl.2019.0327

Kobiela, M. E., & Snell-rood, E. C. (2018). Integrative and comparative biology nickel exposure has complex transgenerational effects in a butterfly. *Integrative and Comparative Biology*, *58*(5), 1008–1017. https://doi.org/10.1093/icb/icy096

Koch, K., & Suhling, F. (2005). Do behavioural and life-history traits vary with mate-guarding intensity in libellulid odonates? *Canadian Journal of Zoology*, *83*(12), 1631–1637. https://doi.org/10.1139/z05-163

Koleček, J., Procházka, P., El-Arabany, N., Tarka, M., Ilieva, M., Hahn, S., Honza, M., De La Puente, J., Bermejo, A., Gürsoy, A., Bensch, S., Zehtindjiev, P., Hasselquist, D., & Hansson, B. (2016). Cross-continental migratory connectivity and spatiotemporal migratory patterns in the great reed warbler. *Journal of Avian Biology*, *47*(6), 756–767. https://doi.org/10.1111/jav.00929

Korkmaz, R., Rajabi, H., Eshghi, S., Gorb, S. N., & Büscher, T. H. (2022). The frequency of wing damage in a migrating butterfly. *Insect Science*, 1744-7917.13153. https://doi.org/10.1111/1744-7917.13153

Korunes, K. L., & Samuk, K. (2021). pixy: Unbiased estimation of nucleotide diversity and divergence in the presence of missing data. *Molecular Ecology Resources*, *21*(4), 1359–1368. https://doi.org/10.1111/1755-0998.13326

Kowalski, R., Davies, S. E., & Hawkes, C. (1989). Metal composition as a natural marker in anthomyiid fly *Delia radicum* (L.). *Journal of Chemical Ecology*, *15*(4), 1231–1239. https://doi.org/10.1007/BF01014825

Kramer, R. T., Kinaston, R. L., Holder, P. W., Armstrong, K. F., King, C. L., Sipple, W. D. K., Martin, A. P., Pradel, G., Turnbull, R. E., Rogers, K. M., Reid, M., Barr, D., Wijenayake, K. G., Buckley, H. R., Stirling, C. H., & Bataille, C. P. (2022). A bioavailable strontium ($^{87}Sr/^{86}Sr$) isoscape for Aotearoa New Zealand: Implications for food forensics and biosecurity. *PLOS ONE*, *17*(3), e0264458. https://doi.org/10.1371/journal.pone.0264458

Kruszynski, C., Bailey, L. D., Courtiol, A., Bach, L., Bach, P., Göttsche, M., Göttsche, M., Hill, R., Lindecke, O., Matthes, H., Pommeranz, H., Popa-Lisseanu, A. G., Seebens-Hoyer, A., Tichomirowa, M., & Voigt, C. C. (2021). Identifying migratory pathways of Nathusius' pipistrelles (*Pipistrellus*

nathusii) using stable hydrogen and strontium isotopes. *Rapid Communications in Mass Spectrometry*, *35*(6), 1–11. https://doi.org/10.1002/rcm.9031

Kuhn, M. (2008). Building Predictive Models in *R* Using the caret Package. *Journal of Statistical Software*, *28*(5). https://doi.org/10.18637/jss.v028.i05

Kula, E., Martinek, P., Chromcová, L., & Hedbávný, J. (2014). Development of *Lymantria dispar* affected by manganese in food. *Environmental Science and Pollution Research*, *21*(20), 11987–11997. https://doi.org/10.1007/s11356-014-3075-5

Landry, J., & Parrott, L. (2016). Could the lateral transfer of nutrients by outbreaking insects lead to consequential landscape-scale effects? *Ecosphere*, *7*(3). https://doi.org/10.1002/ecs2.1265

Larsen, T. B. (1975). Provisional notes of migrant butterflies in Lebanon. *Atalanta*, *6*.

Larsen, T. B. (1982). The importance of migration to the butterfly fauna of Arabia (Lep., Rhopalocera). *Atalanta*, *13*(4).

Larsen, T. B. (1984). The zoogeographical composition and distribution of the Arabian butterflies (Lepidoptera; Rhopalocera). *Journal of Biogeography*, *11*(2), 119. https://doi.org/10.2307/2844685

Le Corre, M., Dargent, F., Grimes, V., Wright, J., Coté, S. D., Candau, J., Reich, M. S., Miller, M., Holmes, B., Bataille, C. P., & Britton, K. (*in review*). An ensemble machine learning bioavailable strontium isoscape for Eastern Canada.

Lengfelder, F., Grupe, G., Stallauer, A., Huth, R., & Söllner, F. (2019). Modelling strontium isotopes in past biospheres – Assessment of bioavailable $^{87}Sr/^{86}Sr$ ratios in local archaeological vertebrates based on environmental signatures. *Science of the Total Environment*, *648*, 236–252. https://doi.org/10.1016/j.scitotenv.2018.08.014

Li, H., Handsaker, B., Wysoker, A., Fennell, T., Ruan, J., Homer, N., Marth, G., Abecasis, G., Durbin, R., & 1000 Genome Project Data Processing Subgroup. (2009). The Sequence Alignment/Map format

and SAMtools. *Bioinformatics*, *25*(16), 2078–2079. https://doi.org/10.1093/bioinformatics/btp352

Li, H. (2011). A statistical framework for SNP calling, mutation discovery, association mapping and population genetical parameter estimation from sequencing data. *Bioinformatics*, *27*(21), 2987–2993. https://doi.org/10.1093/bioinformatics/btr509

Li, H. (2013). *Aligning sequence reads, clone sequences and assembly contigs with BWA-MEM* (arXiv:1303.3997). arXiv. https://doi.org/10.48550/arXiv.1303.3997

Li, Y., Pierce, A. A., & de Roode, J. C. (2016). variation in forewing size linked to migratory status in monarch butterflies. *Animal Migration*, *3*(1), 27–34. https://doi.org/10.1515/ami-2016-0003

Liedvogel, M., Åkesson, S., & Bensch, S. (2011). The genetics of migration on the move. *Trends in Ecology and Evolution*, *26*(11), 561–569. https://doi.org/10.1016/j.tree.2011.07.009

Liedvogel, M., & Lundberg, M. (2014). The genetics of migration. In *Animal Movement Across Scales* (pp. 561–569). https://doi.org/10.1016/j.tree.2011.07.009

Lin, T., Chen, X., Li, B., Chen, P., Guo, M., Zhou, X., Zhong, S., & Cheng, X. (2019). Geographical origin identification of *Spodoptera litura* (Lepidoptera: Noctuidae) based on trace element profiles using tobacco as intermedium planted on soils from five different regions. *Microchemical Journal*, *146*, 49–55. https://doi.org/10.1016/j.microc.2018.12.051

Lin, T., Chen, P., Chen, X., Shen, J., Zhong, S., Sun, Q., Guo, M., & Cheng, X. (2021). Geographical Classification of *Helicoverpa armigera* (Lepidoptera: Noctuidae) through Mineral Component Analysis. *Analytical Letters*, *54*(4), 669–683. https://doi.org/10.1080/00032719.2020.1777560

Lindroos, E. E., Bataille, C. P., Holder, P. W., Talavera, G., & Reich, M. S. (2023). Temporal stability of δ^2H in insect tissues: Implications for isotope-based geographic assignments. *Frontiers in Ecology and Evolution*, *11*, 1060836. https://doi.org/10.3389/fevo.2023.1060836

Lohse, K. (2017). Come on feel the noise – from metaphors to null models. *Journal of Evolutionary Biology*, *30*(8), 1506–1508. https://doi.org/10.1111/jeb.13109

Lohse, K., Wright, C., Talavera, G., & García-Berro, A. (2021). The genome sequence of the painted lady, *Vanessa cardui* Linnaeus 1758. *Wellcome Open Research*, *6*, 324. https://doi.org/10.12688/wellcomeopenres.17358.1

Lok, T., Overdijk, O., & Piersma, T. (2015). The cost of migration: Spoonbills suffer higher mortality during trans-Saharan spring migrations only. *Biology Letters*, *11*, 20140944. https://doi.org/10.1098/rsbl.2014.0944

López-Mañas, R., Pascual-Díaz, J. P., García-Berro, A., Bahleman, F., Reich, M. S., Pokorny, L., Bataille, C. P., Vila, R., Domingo-Marimon, C., & Talavera, G. (2022). Erratic spatiotemporal vegetation growth anomalies drive population outbreaks in a trans-Saharan insect migrant. *Proceedings of the National Academy of Sciences*, *119*(19), 3–5. https://doi.org/10.1073/pnas.2121249119

Lu, B., & Hardin, J. (2021). A unified framework for random forest prediction error estimation. *Journal of Machine Learning Research*, *22*, 1–41.

Lv, H., Zhai, M., Zeng, J., Zhang, Y., Zhu, F., Shen, H., Qiu, K., Gao, B., Reynolds, D. R., Chapman, J. W., & Hu, G. (2023). Changing patterns of the East Asian monsoon drive shifts in migration and abundance of a globally important rice pest. *Global Change Biology*, *29*(10), 2655–2668. https://doi.org/10.1111/gcb.16636

Ma, C., Vander Zanden, H. B., Wunder, M. B., & Bowen, G. J. (2020). assignR: An R package for isotope-based geographic assignment. *Methods in Ecology and Evolution*, *00*, 1–6. https://doi.org/10.1111/2041-210x.13426

Mackintosh, A., Laetsch, D. R., Hayward, A., Charlesworth, B., Waterfall, M., Vila, R., & Lohse, K. (2019). The determinants of genetic diversity in butterflies. *Nature Communications*, *10*(1), 3466. https://doi.org/10.1038/s41467-019-11308-4

Magozzi, S., Bataille, C., Hobson, K., Wunder, W., Howa, J., Contina, A., Vander Zanden, H., & Bowen, G. (2021). Calibration chain transformation improves the comparability of organic hydrogen and oxygen stable isotope data. *Methods in Ecology and Evolution*, 0–3. https://doi.org/10.1111/2041-210x.13556

Mahowald, N. M., Muhs, D. R., Levis, S., Rasch, P. J., Yoshioka, M., Zender, C. S., & Luo, C. (2006a). Change in atmospheric mineral aerosols in response to climate: Last glacial period, preindustrial, modern, and doubled carbon dioxide climates. *Journal of Geophysical Research Atmospheres*, *111*(D10202). https://doi.org/10.1029/2005JD006653

Mahowald, N. M., Lamarque, J. F., Tie, X. X., & Wolff, E. (2006b). Sea-salt aerosol response to climate change: Last Glacial Maximum, preindustrial, and doubled carbon dioxide climates. *Journal of Geophysical Research Atmospheres*, *111*(D05303). https://doi.org/10.1029/2005JD006459

Marcacci, G., Briedis, M., Diop, N., Diallo, A. Y., Kebede, F., & Jacot, A. (2023). A roadmap integrating research, policy, and actions to conserve Afro-Palearctic migratory landbirds at a flyway scale. *Conservation Letters*, *16*(1). https://doi.org/10.1111/conl.12933

Maret, W. (2016). *Metallomics: A primer of integrated biometal sciences*. Imperial College Press. https://doi.org/10.1142/p1044

Marra, P. P., Studds, C. E., & Webster, M. (2010). Migratory Connectivity. In M. D. Breed & J. Moore (Eds.), *Encyclopedia of Animal Behavior* (Vol. 2, pp. 455–461). Academic Press.

Martinek, P., Kula, E., & Hedbávný, J. (2018). Reactions of *Melolontha hippocastani* adults to high manganese content in food. *Ecotoxicology and Environmental Safety*, *148*, 37–43. https://doi.org/10.1016/j.ecoenv.2017.10.020

Martinek, P., Hedbávný, J., Kudláček, T., Šťasta, M., & Kula, E. (2020). Adverse responses of *Cabera pusaria* caterpillars to high dietary manganese concentration. *Entomologia Experimentalis et Applicata*, *168*(8), 635–643. https://doi.org/10.1111/eea.12919

Marx, M., Korner-Nievergelt, F., & Quillfeldt, P. (2016). Analysis of ring recoveries of European Turtle Doves *Streptopelia turtur*—Flyways, migration timing and origin areas of hunted birds. *Acta Ornithologica*, *51*(1), 55–70. https://doi.org/10.3161/00016454AO2016.51.1.005

Massicotte, P., & South, A. (2023). rnaturalearth: World Map Data from Natural Earth. https://github.com/ropensci/rnaturalearth

Matthews, J. H. (2007). *Research in Motion: Patterns of Large-Scale Migration in Dragonflies and Birds*. The University of Texas at Austin.

Max, K. (2008). Building predictive models in R using the caret package. *Journal Of Statistical Software*, *28*(5), 1–26. https://doi.org/10.1053/j.sodo.2009.03.002

May, M. L., & Matthews, J. H. (2008). Chapter 6 Migration in Odonata: A case study of Anax junius. In *Dragonflies and Damselflies: Model Organisms for Ecological and Evolutionary Research* (pp. 63–78). Oxford University Press.

McLean, J. A., Laks, P., & Shore, T. L. (1983). Comparisons of elemental profiles of the western spruce budworm reared on three host foliages and artificial medium. In R. L. Talerico & M. Montgomery (Eds.), *Proceedings, forest defoliator—Host interactions: A comparison between gypsy moth and spruce budworms* (pp. 33–40). U.S. Department of Agriculture. https://www.fs.usda.gov/treesearch/pubs/4109

Meehan, T. D., & Crossley, M. S. (2023). Change in monarch winter abundance over the past decade: A Red List perspective. *Insect Conservation and Diversity*, *16*(5), 566–573. https://doi.org/10.1111/icad.12646

Meier-Augenstein, W., Chartrand, M. M. G., Kemp, H. F., & St-Jean, G. (2011). An inter-laboratory comparative study into sample preparation for both reproducible and repeatable forensic ^{2}H isotope analysis of human hair by continuous flow isotope ratio mass spectrometry: Inter-lab

human hair ^{2}H exchange protocol study. *Rapid Communications in Mass Spectrometry*, *25*(21), 3331–3338. https://doi.org/10.1002/rcm.5235

Menchetti, M., Guéguen, M., & Talavera, G. (2019). Spatio-temporal ecological niche modelling of multigenerational insect migrations. *Proceedings of the Royal Society B: Biological Sciences*, *286*(1910), 20191583. https://doi.org/10.1098/rspb.2019.1583

Menz, M. H. M., Brown, B. V., & Wotton, K. R. (2019). Quantification of migrant hoverfly movements (diptera: Syrphidae) on the west coast of North America. *Royal Society Open Science*, *6*(4). https://doi.org/10.1098/rsos.190153

Menz, M. H. M., Scacco, M., Bürki-Spycher, H.-M., Williams, H. J., Reynolds, D. R., Chapman, J. W., & Wikelski, M. (2022). Individual tracking reveals long-distance flight-path control in a nocturnally migrating moth. *Science*, *377*(6607), 764–768. https://doi.org/10.1126/science.abn1663

Merlin, C., & Liedvogel, M. (2019). The genetics and epigenetics of animal migration and orientation: Birds, butterflies and beyond. *Journal of Experimental Biology*, *222*, 1–12. https://doi.org/10.1242/jeb.191890

Merritt, T. J. S., & Bewick, A. J. (2017). Genetic diversity in insect metal tolerance. *Frontiers in Genetics*, *8*(NOV), 1–6. https://doi.org/10.3389/fgene.2017.00172

Mesjasz-Przybyłowicz, J., Orłowska, E., Augustyniak, M., Nakonieczny, M., Tarnawska, M., Przybyłowicz, W., & Migula, P. (2014). Elemental distribution in reproductive and neural organs of the epilachna nylanderi (Coleoptera: Coccinellidae), a phytophage of nickel hyperaccumulator *Berkheya coddii* (Asterales: Asteraceae) by micro-PIXE. *Journal of Insect Science*, *14*. https://doi.org/10.1093/jisesa/ieu014

Meynard, C. N., Gay, P., Lecoq, M., Foucart, A., Piou, C., & Chapuis, M. (2017). Climate-driven geographic distribution of the desert locust during recession periods: Subspecies' niche differentiation and

relative risks under scenarios of climate change. *Global Change Biology*, *23*(11), 4739–4749. https://doi.org/10.1111/gcb.13739

Miller, N. G., Wassenaar, L. I., Hobson, K. A., & Norris, D. R. (2011). Monarch butterflies cross the Appalachians from the west to recolonize the east coast of North America. *Biology Letters*, *7*, 43–46. https://doi.org/10.1098/rsbl.2010.0525

Miller, N. G., Wassenaar, L. I., Hobson, K. A., & Norris, R. (2012). Migratory connectivity of the monarch butterfly (*Danaus plexippus*): Patterns of spring re-colonization in eastern North America. *PLoS ONE*, *7*(3), e31891. https://doi.org/10.1371/journal.pone.0031891

Mitchell, T. S., Agnew, L., Meyer, R., Sikkink, K. L., Oberhauser, K. S., Borer, E. T., & Snell-Rood, E. C. (2020). Traffic influences nutritional quality of roadside plants for monarch caterpillars. *Science of The Total Environment*, *724*(138045), 138045. https://doi.org/10.1016/j.scitotenv.2020.138045

Mogren, C. L., & Trumble, J. T. (2010). The impacts of metals and metalloids on insect behavior. *Entomologia Experimentalis et Applicata*, *135*(1), 1–17. https://doi.org/10.1111/j.1570-7458.2010.00967.x

Momeni-Dehaghi, I., Bennett, J. R., Mitchell, G. W., Rytwinski, T., & Fahrig, L. (2021). Mapping the premigration distribution of eastern Monarch butterflies using community science data. *Ecology and Evolution*, *00*, 1–7. https://doi.org/10.1002/ece3.7912

Monchanin, C., Devaud, J. M., Barron, A. B., & Lihoreau, M. (2021). Current permissible levels of metal pollutants harm terrestrial invertebrates. *Science of the Total Environment*, *779*, 146398. https://doi.org/10.1016/j.scitotenv.2021.146398

Mooney, W. D., Laske, G., & Masters, T. G. (1998). CRUST 5.1: A global crustal model at 5° × 5°. *Journal of Geophysical Research*, *103*(B1), 727–747. https://doi.org/10.1029/97jb02122

Moore, L. J., Murphy, T. J., Barnes, I. L., & Paulsen, P. J. (1982). Absolute isotopic abundance ratios and atomic weight of a reference sample of strontium. *Journal of Research of the National Bureau of Standards*, *87*(1), 1–8.

Morrison, C. A., Alves, J. A., Gunnarsson, T. G., Þórisson, B., & Gill, J. A. (2019). Why do earlier-arriving migratory birds have better breeding success? *Ecology and Evolution*, *9*(15), 8856–8864. https://doi.org/10.1002/ece3.5441

Mueller, J. C., Pulido, F., & Kempenaers, B. (2011). Identification of a gene associated with avian migratory behaviour. *Proceedings of the Royal Society B: Biological Sciences*, *278*(1719), 2848–2856. https://doi.org/10.1098/rspb.201

Nagoshi, R. N., Fleischer, S., & Meagher, R. L. (2009). Texas is the overwintering source of fall armyworm in central Pennsylvania: Implications for migration into the northeastern United States. *Environmental Entomology*, *38*(6), 1546–1554. https://doi.org/10.1603/022.038.0605

Nakagawa, S., Johnson, P. C. D., & Schielzeth, H. (2017). The coefficient of determination R2 and intra-class correlation coefficient from generalized linear mixed-effects models revisited and expanded. *Journal of the Royal Society Interface*, *14*(134), 20170213. https://doi.org/10.1098/rsif.2017.0213

Nakano, T., Jeon, S.-R., Shindo, J., Fumoto, T., Okada, N., & Shimada, J. (2001). Sr isotopic signature in plant-derived Ca in rain. *Water, Air, and Soil Pollution*, *130*, 769–774. https://doi.org/10.1023/A:1013849905563

Näsvall, K., Shipilina, D., Vila, R., Talavera, G., & Backstrom, N. (2023). *Resource availability affects activity profiles of regulatory elements in a long-distance butterfly migrant* [Preprint]. Authorea. https://doi.org/10.22541/au.167827909.99815237/v1

Neck, R. W. (1983). Causal analysis of a migration of the snout butterfly, *Libytheana bachmanii larvata* (Strecker) (Liibytheidae). *Journal of the Lepidopterists' Society*, *37*(2), 121–128.

Negri, I., Mavris, C., Di Prisco, G., Caprio, E., & Pellecchia, M. (2015). Honey Bees (*Apis mellifera*, L.) as Active Samplers of Airborne Particulate Matter. *PLoS ONE*, *10*(7), e0132491. https://doi.org/10.1371/journal.pone.0132491

Nelson, D. M., Braham, M., Miller, T. A., Duerr, A. E., Cooper, J., Lanzone, M., Lemaître, J., & Katzner, T. (2015). Stable hydrogen isotopes identify leapfrog migration, degree of connectivity, and summer distribution of Golden Eagles in eastern North America. *The Condor*, *117*(3), 414–429. https://doi.org/10.1650/CONDOR-14-209.1

Nessel, M. P., Konnovitch, T., Romero, G. Q., & González, A. L. (2021). Nitrogen and phosphorus enrichment cause declines in invertebrate populations: A global meta-analysis. *Biological Reviews*, *96*(6), 2617–2637. https://doi.org/10.1111/brv.12771

Newton, I. (2007). Weather-related mass-mortality events in migrants. *Ibis*, *149*, 453–467. https://doi.org/10.1111/j.1474-919X.2007.00704.x

Nickles, E. P., Ghiradella, H., Bakhru, H., & Haberl, A. (2002). Egg of the Karner Blue butterfly (*Lycaeides melissa samuelis*): Morphology and elemental analysis. *Journal of Morphology*, *251*, 140–148. https://doi.org/10.1002/jmor.1079

Niitepõld, K., Smith, A. D., Osborne, J. L., Reynolds, D. R., Carreck, L., Martin, A. P., Marden, J. H., Ovaskainen, O., Hanski, I., Niitep, K., Smith, A. D., Osborne, J. L., Reynolds, D. R., Carreck, N. L., Martin, A. P., Marden, J. H., Ovaskainen, O., & Hanski, I. (2009). Flight Metabolic Rate and Pgi Genotype Influence Butterfly Dispersal Rate in the Field. *Ecology*, *90*(8), 2223–2232.

Nitzsche, K. N., Shin, K. C., Kato, Y., Kamauchi, H., Takano, S., & Tayasu, I. (2020). Magnesium and zinc stable isotopes as a new tool to understand Mg and Zn sources in stream food webs. *Ecosphere*, *11*(8). https://doi.org/10.1002/ecs2.3197

Nitzsche, K. N., Wakaki, S., Yamashita, K., Shin, K. C., Kato, Y., Kamauchi, H., & Tayasu, I. (2022). Calcium and strontium stable isotopes reveal similar behaviors of essential Ca and nonessential Sr in stream food webs. *Ecosphere*, *13*(2), 1–19. https://doi.org/10.1002/ecs2.3921

Norris, D. R., Lank, D. B., Pither, J., Chipley, D., Ydenberg, R. C., & Kyser, T. K. (2007). Trace element profiles as unique identifiers of western sandpiper (*Calidris mauri*) populations. *Canadian Journal of Zoology*, *85*, 579–583. https://doi.org/10.1139/Z07-024

Ogra, Y., & Hirata, T. (Eds.). (2017). *Metallomics*. Springer Japan. https://doi.org/10.1007/978-4-431-56463-8

Orłowski, G., Mróz, L., Kadej, M., Smolis, A., Tarnawski, D., Karg, J., Campanaro, A., Bardiani, M., Harvey, D. J., Méndez, M., Thomaes, A., Vrezec, A., Ziomek, K., Rudecki, A. L., & Mader, D. (2020). Breaking down insect stoichiometry into chitin-based and internal elemental traits: Patterns and correlates of continent-wide intraspecific variation in the largest European saproxylic beetle. *Environmental Pollution*, *262*, 114064. https://doi.org/10.1016/j.envpol.2020.114064

Otuka, A., Dudhia, J., Watanabe, T., & Furuno, A. (2005). A new trajectory analysis method for migratory planthoppers, *Sogatella furcifera* (Horváth) (Homoptera: Delphacidae) and *Nilaparvata lugens* (Stål), using an advanced weather forecast model. *Agricultural and Forest Entomology*, *7*, 1–9. https://doi.org/10.1111/j.1461-9555.2005.00236.x

Palmu, E., Birkhofer, K., Hanson, H. I., & Hedlund, K. (2017). Can δD and $\delta^{18}O$ stable isotopes be used to detect long-range dispersal among carabid beetles? *Applied Soil Ecology*, *119*, 99–103. https://doi.org/10.1016/j.apsoil.2017.06.006

Paritte, J. M., & Kelly, J. F. (2009). Effect of cleaning regime on stable-isotope ratios of feathers in Japanese Quail (*Coturnix japonica*). *The Auk*, *126*(1), 165–174. https://doi.org/10.1525/auk.2009.07187

Parmesan, C. (2003). Butterflies as bioindicators for climate change effects. In C. Boggs, W. Watt, & P. Ehrlich (Eds.), *Butterflies: Ecology and Evolution in Flight* (pp. 541–560). University of Chicago Press.

Pass, G. (2018). Beyond aerodynamics: The critical roles of the circulatory and tracheal systems in maintaining insect wing functionality. *Arthropod Structure and Development*, *47*, 391–407. https://doi.org/10.1016/j.asd.2018.05.004

Pedgley, D. E., Reynolds, D. R., & Tatchell, G. M. (1995). Long-range insect migration in relation to climate and weather: Africa and Europe. In *Insect migration: Tracking resources through space and time* (pp. 3–29). Cambridge University Press.

Peijnenburg, W. J. G. M., & Jager, T. (2003). Monitoring approaches to assess bioaccessibility and bioavailability of metals: Matrix issues. *Ecotoxicology and Environmental Safety*, *56*, 63–77. https://doi.org/10.1016/S0147-6513(03)00051-4

Pelletier, J., Broxton, P., Hazenberg, P., Zeng, X., Troch, P., Niu, G., Williams, Z., Brunke, M., & Gochis, D. (2016). A gridded global data set of soil, intact regolith, and sedimentary deposit thicknesses for regional and global land surface modeling. *Journal of Advances in Modeling Earth Systems*, *8*, 41–65. https://doi.org/10.1002/2017MS001065

Pelton, E. M., Schultz, C. B., Jepsen, S. J., Black, S. H., & Crone, E. E. (2019). Western monarch population plummets: status, probable causes, and recommended conservation actions. *Frontiers in Ecology and Evolution*, *7*, 258. https://doi.org/10.3389/fevo.2019.00258

Pfeiler, E., & Markow, T. A. (2017). Population connectivity and genetic diversity in long-distance migrating insects: Divergent patterns in representative butterflies and dragonflies. *Biological Journal of the Linnean Society*, *122*, 479–486.

Phillips, B. B., Bullock, J. M., Gaston, K. J., Hudson-Edwards, K. A., Bamford, M., Cruse, D., Dicks, L. V., Falagan, C., Wallace, C., & Osborne, J. L. (2021). Impacts of multiple pollutants on pollinator

activity in road verges. *Journal of Applied Ecology*, *58*(5), 1017–1029. https://doi.org/10.1111/1365-2664.13844

Pinheiro, J., Bates, D., DebRoy, S., Sarkar, D., EISPACK authors, Heisterkamp, S., Van Willigen, B., Ranke, J & R Core Team (2020). *nlme: Linear and Nonlinear Mixed Effects Models* (R package version 3.1-151).

Pleasants, J. M., & Oberhauser, K. S. (2013). Milkweed loss in agricultural fields because of herbicide use: Effect on the monarch butterfly population. *Insect Conservation and Diversity*, *6*(2), 135–144. https://doi.org/10.1111/j.1752-4598.2012.00196.x

Pliske, T. E. (1975). Courtship behavior of the Monarch Butterfly, *Danaus plexippus* L. *Annals of the Entomological Society of America*, *68*(1), 143–151. https://doi.org/10.1093/aesa/68.1.143

Pocius, V. M., Pleasants, J. M., Debinski, D. M., Bidne, K. G., Hellmich, R. L., Bradbury, S. P., & Blodgett, S. L. (2018). Monarch butterflies show differential utilization of nine midwestern milkweed species. *Frontiers in Ecology and Evolution*, *6*, 169. https://doi.org/10.3389/fevo.2018.00169

Poszwa, A., Dambrine, E., Ferry, B., Pollier, B., & Loubet, M. (2002). Do deep tree roots provide nutrients to the tropical rainforest? *Biogeochemistry*, *60*(1), 97–118. https://doi.org/10.1023/A:1016548113624

Potter, P., Ramankutty, N., Bennett, E. M., & Donner, S. D. (2010). Characterizing the spatial patterns of global fertilizer application and manure production. *Earth Interactions*, *14*(2), 1–22. https://doi.org/10.1175/2009EI288.1

Prather, C. M., Laws, A. N., Cuellar, J. F., Reihart, R. W., Gawkins, K. M., & Pennings, S. C. (2018). Seeking salt: Herbivorous prairie insects can be co-limited by macronutrients and sodium. *Ecology Letters*, *21*, 1467–1476. https://doi.org/10.1111/ele.13127

Privé, F., Luu, K., Vilhjálmsson, B. J., & Blum, M. G. B. (2020). Performing highly efficient genome scans for local adaptation with R Package pcadapt Version 4. *Molecular Biology and Evolution*, *37*(7), 2153–2154. https://doi.org/10.1093/molbev/msaa053

Prudic, K. L., McFarland, K. P., Oliver, J. C., Hutchinson, R. A., Long, E. C., Kerr, J. T., & Larrivée, M. (2017). eButterfly: Leveraging Massive Online Citizen Science for Butterfly Consevation. *Insects*, *8*(2). https://doi.org/10.3390/insects8020053

Pujolar, J. M., Jacobsen, M. W., Als, T. D., Frydenberg, J., Munch, K., Jónsson, B., Jian, J. B., Cheng, L., Maes, G. E., Bernatchez, L., & Hansen, M. M. (2014). Genome-wide single-generation signatures of local selection in the panmictic European eel. *Molecular Ecology*, *23*(10), 2514–2528. https://doi.org/10.1111/mec.12753

Pye, K. (2004). Isotope and trace element analysis of human teeth and bones for forensic purposes. *Geological Society, London, Special Publications*, *232*, 215–236. https://doi.org/10.1144/GSL.SP.2004.232.01.20

R Core Team. (2013). *R: A language and environment for statistical computing* (3.6.3) [Computer software]. R Foundation for Statistical Computing, Vienna, Austria. http://www.r-project.org/

R Core Team. (2021). *R: A language and environment for statistical computing* (4.1.0) [Computer software]. R Foundation for Statistical Computing, Vienna, Austria. https://www.r-project.org/

Raj, A., Stephens, M., & Pritchard, J. K. (2014). fastSTRUCTURE: Variational inference of population structure in large SNP data sets. *Genetics*, *197*(2), 573–589. https://doi.org/10.1534/genetics.114.164350

Ramenofsky, M., & Wingfield, J. C. (2007). Regulation of migration. *BioScience*, *57*(2), 135–143. https://doi.org/10.1641/B570208

Rankin, M. A., & Burchsted, J. C. A. (1992). The cost of migration in insects. *Annual Review Entomology*, *37*, 533–559.

Reihart, R. W., Angelos, K. P., Gawkins, K. M., Hurst, S. E., Montelongo, D. C., Laws, A. N., Pennings, S. C., & Prather, C. M. (2021). Crazy ants craving calcium: Macronutrients and micronutrients can limit and stress an invaded grassland brown food web. *Ecology*, *102*(2). https://doi.org/10.1002/ecy.3263

Reppert, S. M., & de Roode, J. C. (2018). Demystifying monarch butterfly migration. *Current Biology*, *28*(17), R1009–R1022. https://doi.org/10.1016/j.cub.2018.02.067

Reynolds, D. R., Chapman, J. W., & Harrington, R. (2006). The migration of insect vectors of plant and animal viruses. *Advances in Virus Research*, *67*, 453–516. https://doi.org/10.1016/S0065-3527(06)67012-7

Rodiouchkina, K., Rodushkin, I., Goderis, S., & Vanhaecke, F. (2022). Longitudinal isotope ratio variations in human hair and nails. *Science of the Total Environment*, *808*, 152059. https://doi.org/10.1016/j.scitotenv.2021.152059

Roff, D. A., & Fairbairn, D. J. (2007). The evolution and genetics of migration in insects. *BioScience*, *57*(2), 155–164. https://doi.org/10.1641/b570210

Rohlf, F. J. (2016). *tpsDig2 ver. 2.32.* [Computer software].

Rudnick, R. L., & Gao, S. (2014). Composition of the Continental Crust. In *Treatise on Geochemistry* (2nd ed., pp. 1–51). Elsevier Ltd. https://doi.org/10.1016/B978-0-08-095975-7.00301-6

Ruegg, K. C., Anderson, E. C., Harrigan, R. J., Paxton, K. L., Kelly, J. F., Moore, F., & Smith, T. B. (2017). Genetic assignment with isotopes and habitat suitability (GAIAH), a migratory bird case study. *Methods in Ecology and Evolution*, *8*(10), 1241–1252. https://doi.org/10.1111/2041-210X.12800

Rundel, C. W., Wunder, M. B., Alvarado, A. H., Ruegg, K. C., Harrigan, R., Schuh, A., Kelly, J. F., Siegel, R. B., Desante, D. F., Smith, T. B., & Novembre, J. (2013). Novel statistical methods for integrating genetic and stable isotope data to infer individual-level migratory connectivity. *Molecular Ecology*, *22*, 4163–4176. https://doi.org/10.1111/mec.12393

Rushing, C. S., Marra, P. P., & Studds, C. E. (2017). Incorporating breeding abundance into spatial assignments on continuous surfaces. *Ecology and Evolution*, *7*(11), 3847–3855. https://doi.org/10.1002/ece3.2605

Russell, R. W., May, M. L., Soltesz, K. L., & Fitzpatrick, J. W. (1998). Massive swarm migrations of dragonflies (Odonata) in eastern North America. *The American Midland Naturalist*, *140*(2), 325–342. https://doi.org/10.1674/0003-0031(1998)140[0325:MSMODO]2.0.CO;2

Rutz, C., & Hays, G. C. (2009). New frontiers in biologging science. *Biology Letters*, *5*, 289–292. https://doi.org/10.1098/rsbl.2009.0089

Salih, A. A. M., Baraibar, M., Mwangi, K. K., & Artan, G. (2020). Climate change and locust outbreak in East Africa. *Nature Climate Change*, *10*(7), 584–585. https://doi.org/10.1038/s41558-020-0835-8

Samuk, K., Korunes, K., Trevisani, M. D., & Niema Moshiri. (2022). *ksamuk/pixy: Pixy 1.2.7.beta1* (1.2.7.beta1) [Computer software]. Zenodo. https://doi.org/10.5281/ZENODO.6551490

Sanderson, F. J., Donald, P. F., Pain, D. J., Burfield, I. J., & Van Bommel, F. P. J. (2006). Long-term population declines in Afro-Palearctic migrant birds. *Biological Conservation*, 93–105. https://doi.org/10.1016/j.biocon.2006.02.008

Satterfield, D. A., Wright, A. E., & Altizer, S. (2013). Lipid reserves and immune defense in healthy and diseased migrating monarchs Danaus plexippus. *Current Zoology*, *59*(3), 393–402. https://doi.org/10.1093/czoolo/59.3.393

Satterfield, D. A., & Davis, A. K. (2014). Variation in wing characteristics of monarch butterflies during migration: Earlier migrants have redder and more elongated wings. *Animal Migration*, *2*(1), 1–7. https://doi.org/10.2478/ami-2014-0001

Satterfield, D. A., Maerz, J. C., Hunter, M. D., Flockhart, D. T. T., Hobson, K. A., Norris, D. R., Streit, H., de Roode, J. C., & Altizer, S. (2018). Migratory monarchs that encounter resident monarchs show

life-history differences and higher rates of parasite infection. *Ecology Letters*. https://doi.org/10.1111/ele.13144

Satterfield, D. A., Sillett, T. S., Chapman, J. W., Altizer, S., & Marra, P. P. (2020). Seasonal insect migrations: Massive, influential, and overlooked. *Frontiers in Ecology and the Environment*, 1–10. https://doi.org/10.1002/fee.2217

Schenk, H. J., & Jackson, R. B. (2002). Rooting depths, lateral root spreads and below-ground/above-ground allometries of plants in water-limited ecosystems. *Journal of Ecology*, *90*, 480–494. https://doi.org/10.1046/j.1365-2745.2002.00682.x

Seebens, H., Blackburn, T. M., Dyer, E. E., Genovesi, P., Hulme, P. E., Jeschke, J. M., Pagad, S., Pyšek, P., Winter, M., Arianoutsou, M., Bacher, S., Blasius, B., Brundu, G., Capinha, C., Celesti-Grapow, L., Dawson, W., Dullinger, S., Fuentes, N., Jäger, H., … Essl, F. (2017). No saturation in the accumulation of alien species worldwide. *Nature Communications*, *8*(1), 14435. https://doi.org/10.1038/ncomms14435

Seewagen, C. L. (2020). The threat of global mercury pollution to bird migration: Potential mechanisms and current evidence. *Ecotoxicology*, *29*(8), 1254–1267. https://doi.org/10.1007/s10646-018-1971-z

Segre, H., Kleijn, D., Bartomeus, I., WallisDeVries, M. F., De Jong, M., Frank Van Der Schee, M., Román, J., & Fijen, T. P. M. (2023). Butterflies are not a robust bioindicator for assessing pollinator communities, but floral resources offer a promising way forward. *Ecological Indicators*, *154*, 110842. https://doi.org/10.1016/j.ecolind.2023.110842

Sekercioglu, C. H. (2007). Conservation ecology: Area trumps mobility in fragment bird extinctions. *Current Biology*, *17*(8), R283–R286. https://doi.org/10.1016/j.cub.2007.02.019

Sellick, M. J., Kyser, T. K., Wunder, M. B., Chipley, D., & Norris, D. R. (2009). Geographic variation of strontium and hydrogen isotopes in avian tissue: Implications for tracking migration and dispersal. *PLoS ONE*, *4*(3). https://doi.org/10.1371/journal.pone.0004735

Selvey, A. D. (2020). *Transcriptomic Exploration of the Vanessa cardui Immune System*. University of Nevada, Reno.

Serna, A., Prates, L., Mange, E., Salazar-García, D. C., & Bataille, C. P. (2020). Implications for paleomobility studies of the effects of quaternary volcanism on bioavailable strontium: A test case in North Patagonia (Argentina). *Journal of Archaeological Science*, *121*, 105198. https://doi.org/10.1016/J.JAS.2020.105198

Shaw, A. K. (2020). Causes and consequences of individual variation in animal movement. *Movement Ecology*, *8*(1), 1–12. https://doi.org/10.1186/s40462-020-0197-x

Shaw, J. A., Boyd, A., House, M., Cowin, G., & Baer, B. (2018). Multi-modal imaging and analysis in the search for iron-based magnetoreceptors in the honeybee *Apis mellifera*. *Royal Society Open Science*, *5*(9). https://doi.org/10.1098/rsos.181163

Shephard, A. M., Mitchell, T. S., Henry, S. B., Oberhauser, K. S., Kobiela, M. E., & Snell-Rood, E. C. (2020). Assessing zinc tolerance in two butterfly species: Consequences for conservation in polluted environments. *Insect Conservation and Diversity*, *13*(2), 201–210. https://doi.org/10.1111/icad.12404

Shephard, A. M., Mitchell, T. S., & Snell-rood, E. C. (2021). Monarch caterpillars are robust to combined exposure to the roadside micronutrients sodium and zinc. *Conservation Physiology*, *9*, 1–15. https://doi.org/10.1093/conphys/coab061

Shephard, A. M., Brown, N. S., & Snell-Rood, E. C. (2022). Anthropogenic zinc exposure increases mortality and antioxidant gene expression in monarch butterflies with low access to dietary

macronutrients. *Environmental Toxicology and Chemistry*, *41*(5), 1286–1296. https://doi.org/10.1002/etc.5305

Shields, O. (1992). World distribution of the *Vanessa cardui* group (Nymphalidae). *Journal of the Lepidopterists' Society*, *46*(3), 235–238.

Shipilina, D., Nasvall, K., Höök, L., Vila, R., Talavera, G., & Backström, N. (2022). Linkage mapping and genome annotation give novel insights into gene family expansions and regional recombination rate variation in the painted lady (*Vanessa cardui*) butterfly. *Genomics*, 110481. https://doi.org/10.1101/2022.04.14.488360

Shipilina D, Höök L, Talla V, Parkes E, Talavera G, Backström N. (*in prep.*). Transcriptomic analysis reveals pathways underlying environmental stress response in a migratory butterfly.

Simonetti, A., Gariépy, C., & Carignan, J. (2000a). Pb and Sr isotopic compositions of snowpack from Québec, Canada: Inferences on the sources and deposition budgets of atmospheric heavy metals. *Geochimica et Cosmochimica Acta*, *64*(1), 5–20. https://doi.org/0016-7037/00

Simonetti, A., Gariépy, C., & Carignan, J. (2000b). Pb and Sr isotopic evidence for sources of atmospheric heavy metals and their deposition budgets in northeastern North America. *Geochimica et Cosmochimica Acta*, *64*(20), 3439–3452. https://doi.org/0016-7037/00

Singh, V. K., Kumar, S., Awasthi, S., & Gupta, S. K. (2021). Phylogeography and population expansion of Western Himalayan highly-erratically migratory painted lady butterfly (Lepidoptera: Nymphalidae: *Vanessa cardui*). *Journal of Asia-Pacific Entomology*, *24*(4), 1116–1121. https://doi.org/10.1016/j.aspen.2021.10.005

Slobodian, M. R., Petahtegoose, J. D., Wallis, A. L., Levesque, D. C., & Merritt, T. J. S. (2021). The effects of essential and non-essential metal toxicity in the *Drosophila melanogaster* insect model: A review. *Toxics*, *9*(10). https://doi.org/10.3390/toxics9100269

Smith, D. B., Cannon, W. F., Woodruff, L. G., Solano, F., Kilburn, J. E., & Fey, D. L. (2013). Geochemical and mineralogical data for soils of the conterminous United States. *U.S. Geological Survey Data Series*, *801*, 1–26. https://doi.org/10.3133/ds801

Smith, K. E., & Weis, D. (2020). Evaluating spatiotemporal resolution of trace element concentrations and Pb isotopic compositions of honeybees and hive products as biomonitors for urban metal distribution. *GeoHealth*, *4*(7). https://doi.org/10.1029/2020GH000264

Smith, K. E., Weis, D., Scott, S. R., Berg, C. J., Segal, Y., & Claeys, P. (2021). Regional and global perspectives of honey as a record of lead in the environment. *Environmental Research*, *195*(November 2020), 110800. https://doi.org/10.1016/j.envres.2021.110800

Snell-Rood, E. C., Espeset, A., Boser, C. J., White, W. A., & Smykalski, R. (2014). Anthropogenic changes in sodium affect neural and muscle development in butterflies. *PNAS*, *111*(28), 10221–10226. https://doi.org/10.1073/pnas.1323607111

Snell-Rood, E. C., & Steck, M. K. (2019). Behaviour shapes environmental variation and selection on learning and plasticity: Review of mechanisms and implications. *Animal Behaviour*, *147*, 147–156. https://doi.org/10.1016/j.anbehav.2018.08.007

Snoeck, C., Ryan, S., Pouncett, J., Pellegrini, M., Claeys, P., Wainwright, A. N., Mattielli, N., Lee-Thorp, J. A., & Schulting, R. J. (2020). Towards a biologically available strontium isotope baseline for Ireland. *Science of the Total Environment*, *712*, 136248. https://doi.org/10.1016/j.scitotenv.2019.136248

Sokolovskis, K., Lundberg, M., Åkesson, S., Willemoes, M., Zhao, T., Caballero-Lopez, V., & Bensch, S. (2023). Migration direction in a songbird explained by two loci. *Nature Communications*, *14*(1), 165. https://doi.org/10.1038/s41467-023-35788-7

Somveille, M., Manica, A., & Rodrigues, A. S. L. (2019). Where the wild birds go: Explaining the differences in migratory destinations across terrestrial bird species. *Ecography*, *42*(2), 225–236. https://doi.org/10.1111/ecog.03531

Soto, D. X., Koehler, G., Wassenaar, L. I., & Hobson, K. A. (2017). Re-evaluation of the hydrogen stable isotopic composition of keratin calibration standards for wildlife and forensic science applications. *Rapid Communications in Mass Spectrometry*, *31*(14), 1193–1203. https://doi.org/10.1002/rcm.7893

Soule, A. J., Decker, L. E., & Hunter, M. D. (2020). Effects of diet and temperature on monarch butterfly wing morphology and flight ability. *Journal of Insect Conservation*, *24*(6), 961–975. https://doi.org/10.1007/s10841-020-00267-7

Søvik, E., Perry, C. J., LaMora, A., Barron, A. B., & Ben-Shahar, Y. (2015). Negative impact of manganese on honeybee foraging. *Biology Letters*, *11*(3), 1–4. https://doi.org/10.1098/rsbl.2014.0989

Stefanescu, C., Alarcón, M., Izquierdo, R., Páramo, F., & Àvila, A. (2011). Moroccan source areas of the Painted Lady Butterfly *Vanessa cardui* (Nymphalidae: Nymphalinae) migrating into Europe in spring. *Journal of the Lepidopterists' Society*, *65*(1), 15–26. https://doi.org/10.18473/lepi.v65i1.a2

Stefanescu, C., Páramo, F., Åkesson, S., Alarcón, M., Ávila, A., Brereton, T., Carnicer, J., Cassar, L. F., Fox, R., Heliölä, J., Hill, J. K., Hirneisen, N., Kjellén, N., Kühn, E., Kuussaari, M., Leskinen, M., Liechti, F., Musche, M., Regan, E. C., … Chapman, J. W. (2013). Multi-generational long-distance migration of insects: Studying the painted lady butterfly in the Western Palaearctic. *Ecography*, *36*(4), 474–486. https://doi.org/10.1111/j.1600-0587.2012.07738.x

Stefanescu, C., Soto, D. X., Talavera, G., Vila, R., & Hobson, K. A. (2016). Long-distance autumn migration across the Sahara by painted lady butterflies: Exploiting resource pulses in the tropical savannah. *Biology Letters*, *12*, 1–4. https://doi.org/10.1098/rsbl.2016.0561

Stefanescu, C., Puig-Montserrat, X., Samraoui, B., Izquierdo, R., Ubach, A., & Arrizabalaga, A. (2017). Back to Africa: Autumn migration of the painted lady butterfly Vanessa cardui is timed to coincide with an increase in resource availability. *Ecological Entomology*, *42*(6), 737–747. https://doi.org/10.1111/een.12442

Stefanescu, C., Ubach, A., & Wiklund, C. (2021). Timing of mating, reproductive status and resource availability in relation to migration in the painted lady butterfly. *Animal Behaviour*, *172*, 145–153. https://doi.org/10.1016/j.anbehav.2020.12.013

Still, C. J., & Powell, R. L. (2010). Continental-scale distributions of vegetation stable carbon isotope ratios. In *Isoscapes* (pp. 179–193). Springer Netherlands. https://doi.org/10.1007/978-90-481-3354-3_9

Studier, E. H. (1996). Composition of bodies of Cave Crickets (*Hadenoecus subterraneus*), their eggs, and their egg predator, *Neaphaenops tellkampfi*. *American Midland Naturalist*, *136*(1), 101–109.

Stuhr, S., Truong, V. K., Vongsvivut, J., Senkbeil, T., Yang, Y., Al Kobaisi, M., Baulin, V. A., Werner, M., Rubanov, S., Tobin, M. J., Cloetens, P., Rosenhahn, A., Lamb, R. N., Luque, P., Marchant, R., & Ivanova, E. P. (2018). Structure and chemical organization in damselfly *Calopteryx haemorrhoidalis* Wings: A spatially resolved FTIR and XRF analysis with synchrotron radiation. *Scientific Reports*, *8*(1), 1–9. https://doi.org/10.1038/s41598-018-26563-6

Suchan, T., Talavera, G., Sáez, L., Ronikier, M., & Vila, R. (2018). Pollen metabarcoding as a tool for tracking long-distance insect migrations. *Molecular Ecology Resources*, 1–14. https://doi.org/10.1111/1755-0998.12948

Suchan, T., Bataille, C. P., Reich, M. S., Toro-Delgado, E., Vila, R., Pierce, N. E., Talavera, G. (*in review*). A trans-oceanic flight of over 4,200 km by painted lady butterflies.

Sultana, R., Kumar, S., Samejo, A. A., Soomro, S., & Lecoq, M. (2021). The 2019–2020 upsurge of the desert locust and its impact in Pakistan. *Journal of Orthoptera Research*, *30*(2), 145–154. https://doi.org/10.3897/jor.30.65971

Sun, H. X., Tang, W. C., Chen, H., Chen, W., Zhang, M., Liu, X., & Zhang, G. R. (2013). Food utilization and growth of cutworm *Spodoptera litura* Fabricius larvae exposed to nickel, and its effect on reproductive potential. *Chemosphere*, *93*(10), 2319–2326. https://doi.org/10.1016/j.chemosphere.2013.08.025

Sures, B. (2004). Environmental parasitology: Relevancy of parasites in monitoring environmental pollution. *Trends in Parasitology*, *20*(4), 170–177. https://doi.org/10.1016/j.pt.2004.01.014

Tacail, T., Le Houedec, S., & Skulan, J. L. (2020). New frontiers in calcium stable isotope geochemistry: Perspectives in present and past vertebrate biology. *Chemical Geology*, *537*, 119471. https://doi.org/10.1016/j.chemgeo.2020.119471

Talavera, G., & Vila, R. (2016). Discovery of mass migration and breeding of the painted lady butterfly *Vanessa cardui* in the Sub-Sahara: The Europe-Africa migration revisited. *Biological Journal of the Linnean Society*, *120*(2), 274–285. https://doi.org/10.1111/bij.12873

Talavera, G., Bataille, C., Benyamini, D., Gascoigne-Pees, M., & Vila, R. (2018). Round-trip across the Sahara: Afrotropical painted lady butterflies recolonize the Mediterranean in early spring. *Biology Letters*, *14*, 20180274. https://doi.org/10.1098/rsbl.2018.0274

Talavera, G., García-Berro, A., Talla, V. N. K., Ng'iru, I., Bahleman, F., Kébé, K., Nzala, K. M., Plasencia, D., Marafi, M. A. J., Kassie, A., Goudégnon, E. O. A., Kiki, M., Benyamini, D., Reich, M. S., López-Mañas, R., Benetello, F., Collins, S. C., Bataille, C. P., Pierce, N. E., … Vila, R. (2023). The Afrotropical breeding grounds of the Palearctic-African migratory painted lady butterflies (*Vanessa cardui*). *Proceedings of the National Academy of Sciences*, *120*(16), e2218280120. https://doi.org/10.1073/pnas.2218280120

Talla, V., Pierce, A. A., Adams, K. L., de Man, T. J. B., Nallu, S., Villablanca, F. X., Kronforst, M. R., & de Roode, J. C. (2020). Genomic evidence for gene flow between monarchs with divergent migratory phenotypes and flight performance. *Molecular Ecology*, *29*(14), 2567–2582. https://doi.org/10.1111/mec.15508

Tanaka, Y. K., & Hirata, T. (2018). Stable isotope composition of metal elements in biological samples as tracers for element metabolism. *Analytical Sciences*, *34*(6), 645–655. https://doi.org/10.2116/analsci.18SBR02

Taylor, C. M., & Norris, D. R. (2010). Population dynamics in migratory networks. *Theoretical Ecology*, *3*, 65–73. https://doi.org/10.1007/s12080-009-0054-4

Taylor, O. R. (2011). *Monarch Population Status*. Monarch Watch Blog. https://monarchwatch.org/blog/2011/04/26/monarch-population-status-10/

Tessnow, A. E., Nagoshi, R. N., Meagher, R. L., & Fleischer, S. J. (2023). Revisiting fall armyworm population movement in the United States and Canada. *Frontiers in Insect Science*, *3*, 1104793. https://doi.org/10.3389/finsc.2023.1104793

Thompson, N. F., Anderson, E. C., Clemento, A. J., Campbell, M. A., Pearse, D. E., Hearsey, J. W., Kinziger, A. P., & Garza, J. C. (2020). A complex phenotype in salmon controlled by a simple change in migratory timing. *Science*, *370*(6516), 609–613. https://doi.org/10.1126/science.aba9059

Thomsen, E., & Andreasen, R. (2019). Agricultural lime disturbs natural strontium isotope variations: Implications for provenance and migration studies. *Science Advances*, *5*(eaav8083). https://doi.org/10.1126/sciadv.aav8083

Tibbett, M., Green, I., Rate, A., De Oliveira, V. H., & Whitaker, J. (2021). The transfer of trace metals in the soil-plant-arthropod system. *Science of the Total Environment*, *779*. https://doi.org/10.1016/j.scitotenv.2021.146260

Tigar, B. J., & Hursthouse, A. (2016). Applying biogeochemistry to identify the geographic origins of insects - A model using *Prostephanus truncatus*. *Journal of Environmental Studies*, *2*(1). https://doi.org/10.13188/2471-4879.1000004

Todt, W., Cliff, R. A., Hanser, A., & Hofmann, A. W. (1996). Evaluation of a ^{202}Pb–^{205}Pb double spike for high-precision lead isotope analysis. In *Earth Processes: Reading the Isotopic Code* (pp. 429–437). American Geophysical Union (AGU). https://doi.org/10.1029/GM095p0429

Torniainen, J., & Mikonranta, L. (2018). The origins of northern European *Autographa gamma* individuals evaluated using hydrogen stable isotopes. *Ecological Entomology*, *43*(5), 699–702. https://doi.org/10.1111/een.12635

Trabucco, A., & Zomer, R. (2019). *Global Aridity Index and Potential Evapotranspiration (ET0) Climate Database v2*. https://doi.org/10.6084/m9.figshare.7504448.v3

Troast, D., Suhling, F., Jinguji, H., Sahlén, G., & Ware, J. (2016). A global population genetic study of *Pantala flavescens*. *PLOS ONE*, *11*(3), e0148949. https://doi.org/10.1371/journal.pone.0148949

Tsai, C.-C., Childers, R. A., Nan Shi, N., Ren, C., Pelaez, J. N., Bernard, G. D., Pierce, N. E., & Yu, N. (2020). Physical and behavioral adaptations to prevent overheating of the living wings of butterflies. *Nature Communications*, *11*(1), 1–14. https://doi.org/10.1038/s41467-020-14408-8

Turbek, S. P., Scordato, E. S. C., & Safran, R. J. (2018). The role of seasonal migration in population divergence and reproductive isolation. *Trends in Ecology & Evolution*, *33*(3), 164–175. https://doi.org/10.1016/j.tree.2017.11.008

Urquhart, F. A. (1941). A proposed method for marking migrant butterflies. *The Canadian Entomologist*, *73*(2), 21–22. https://doi.org/10.4039/Ent7321-2

Urquhart, F. A., & Urquhart, N. R. (1976). The overwintering site of the eastern population of the monarch butterfly (*Danaus p. Plexippus*; Danaidae) in southern Mexico. *Journal of the Lepidopterists' Society*, *30*(3), 153–158.

Van Der Auwera, G. A., Carneiro, M. O., Hartl, C., Poplin, R., Del Angel, G., Levy-Moonshine, A., Jordan, T., Shakir, K., Roazen, D., Thibault, J., Banks, E., Garimella, K. V., Altshuler, D., Gabriel, S., & DePristo, M. A. (2013). From FastQ data to high-confidence variant calls: The genome analysis toolkit best practices pipeline. *Current Protocols in Bioinformatics*, *43*(1). https://doi.org/10.1002/0471250953.bi1110s43

Van Der Merwe, N. J., Lee-Thorp, J. A., Thackeray, J. F., Hall-Martin, A., Kruger, F. J., Coetzee, H., Bell, R. H. V., & Lindeque, M. (1990). Source-area determination of elephant ivory by isotopic analysis. *Nature*, *346*(6286), 744–746. https://doi.org/10.1038/346744a0

Van Gorkum, R., & Bouwman, E. (2005). The oxidative drying of alkyd paint catalysed by metal complexes. *Coordination Chemistry Reviews*, *249*, 1709–1728. https://doi.org/10.1016/j.ccr.2005.02.002

Van Klink, R., Bowler, D. E., Gongalsky, K. B., & Chase, J. M. (2022). Long-term abundance trends of insect taxa are only weakly correlated. *Biology Letters*, *18*(2), 20210554. https://doi.org/10.1098/rsbl.2021.0554

Van Petegem, K. H. P., Pétillon, J., Renault, D., Wybouw, N., Van Leeuwen, T., Stoks, R., & Bonte, D. (2015). Empirically simulated spatial sorting points at fast epigenetic changes in dispersal behaviour. *Evolutionary Ecology*, *29*(2), 299–310. https://doi.org/10.1007/s10682-015-9756-9

van Swaay, C. A. M., Dennis, E. B., Schmucki, R., Sevilleja, C. G., Aghababyan, K., Åström, S., Balalaikins, M., Bonelli, S., Botham, M., Bourn, N., Brereton, T., Cancela, J. P., Carlisle, B., Chambers, P., Collins, S., Dopagne, C., Dziekanska, I., Escobés, R., Faltynek Fric, Z., … Roy, D. B. (2020). *Assessing Butterflies in Europe—Butterfly Indicators 1990-2018: Technical report*. Butterfly Conservation Europe & ABLE/eBMS (www.butterfly-monitoring.net).

Vandenbosch, R. (2007). What do monarch population time series tell us about eastern and western population mixing? *Journal of the Lepidopterists' Society*, *61*(1).

Vander Zanden, H. B., Nelson, D. M., Wunder, M. B., Conkling, T. J., & Katzner, T. (2018). Application of isoscapes to determine geographic origin of terrestrial wildlife for conservation and management. *Biological Conservation*, *228*(October), 268–280. https://doi.org/10.1016/j.biocon.2018.10.019

Vet, R., Artz, R. S., Carou, S., Shaw, M., Ro, C. U., Aas, W., Baker, A., Bowersox, V. C., Dentener, F., Galy-Lacaux, C., Hou, A., Pienaar, J. J., Gillett, R., Forti, M. C., Gromov, S., Hara, H., Khodzher, T., Mahowald, N. M., Nickovic, S., … Reid, N. W. (2014). A global assessment of precipitation chemistry and deposition of sulfur, nitrogen, sea salt, base cations, organic acids, acidity and pH, and phosphorus. *Atmospheric Environment*, *93*, 3–100. https://doi.org/10.1016/j.atmosenv.2013.10.060

Vickery, J. A., Ewing, S. R., Smith, K. W., Pain, D. J., Bairlein, F., Škorpilová, J., & Gregory, R. D. (2014). The decline of Afro-Palaearctic migrants and an assessment of potential causes. *Ibis*, *156*(1), 1–22. https://doi.org/10.1111/ibi.12118

Vodă, R., Dapporto, L., Dincă, V., Shreeve, T. G., Khaldi, M., Barech, G., Rebbas, K., Sammut, P., Scalercio, S., Hebert, P. D. N., & Vila, R. (2016). Historical and contemporary factors generate unique butterfly communities on islands. *Scientific Reports*, *6*(1), 28828. https://doi.org/10.1038/srep28828

Wagner, D. L., Grames, E. M., Forister, M. L., Berenbaum, M. R., & Stopak, D. (2021). Insect decline in the Anthropocene: Death by a thousand cuts. *Proceedings of the National Academy of Sciences of the United States of America*, *118*(2), 1–10. https://doi.org/10.1073/pnas.2023989118

Wahlberg, N., & Rubinoff, D. (2011). Vagility across *Vanessa* (Lepidoptera: Nymphalidae): mobility in butterfly species does not inhibit the formation and persistence of isolated sister taxa. *Systematic Entomology*, *36*(2), 362–370. https://doi.org/10.1111/j.1365-3113.2010.00566.x

Walker, A., & Coetzer, A. J. (2020) *Vanessa cardui*. *The IUCN Red List of Threatened Species*, e.T174379A161326679. https://dx.doi.org/10.2305/IUCN.UK.2020-3.RLTS.T174379A161326679.en.

Wang, Xin, Cao, L., Fox, A. D., Fuller, R., Griffin, L., Mitchell, C., Zhao, Y., Moon, O.-K., Cabot, D., Xu, Z., Batbayar, N., Kölzsch, A., Van Der Jeugd, H. P., Madsen, J., Chen, L., & Nathan, R. (2019). Stochastic simulations reveal few green wave surfing populations among spring migrating herbivorous waterfowl. Nature Communications, 10(1), 2187. https://doi.org/10.1038/s41467-019-09971-8

Wang, Xueye, Bocksberger, G., Lautenschläger, T., Finckh, M., Meller, P., O'Malley, G. E., & Oelze, V. M. (2023). A bioavailable strontium isoscape of Angola with implications for the archaeology of the transatlantic slave trade. *Journal of Archaeological Science*, *154*, 105775. https://doi.org/10.1016/j.jas.2023.105775

Wanty, R. B., Balistrieri, L. S., Wesner, J. S., Walters, D. M., Schmidt, T. S., Stricker, C. A., Kraus, J. M., & Wolf, R. E. (2017). In vivo isotopic fractionation of zinc and biodynamic modeling yield insights into detoxification mechanisms in the mayfly *Neocloeon triangulifer*. *Science of the Total Environment*, *609*, 1219–1229. https://doi.org/10.1016/j.scitotenv.2017.07.269

Ware, J., Kohli, M. K., Mendoza, C. M., Troast, D., Jinguji, H., Hobson, K. A., Sahlén, G., Anderson, R. C., & Suhling, F. (2022). Evidence for widespread gene flow and migration in the Globe Skimmer dragonfly *Pantala flavescens*. *International Journal of Odonatology*, *25*, 43–55. https://doi.org/10.48156/1388.2022.1917166

Warren, M. S., Maes, D., van Swaay, C. A. M., Goffart, P., Van Dyck, H., Bourn, N. A. D., Wynhoff, I., Hoare, D., & Ellis, S. (2020). The decline of butterflies in Europe: Problems, significance, and possible solutions. *Proceedings of the National Academy of Science*, *118*(2), e2002551117. https://doi.org/10.1073/pnas.2002551117

Wassenaar, L. I., & Hobson, K. A. (1998). Natal origins of migratory monarch butterflies at wintering colonies in Mexico: New isotopic evidence. *Proceedings of the National Academy of Science of the United States of America*, *95*, 15436–15439.

Wassenaar, L. I., & Hobson, K. A. (2003). Comparative equilibration and online technique for determination of non-exchangeable hydrogen of keratins for use in animal migration studies. *Isotopes in Environmental and Health Studies*, *39*(3), 211–217. https://doi.org/10.1080/1025601031000096781

Webster, M. S., Marra, P. P., Haig, S. M., Bensch, S., & Holmes, R. T. (2002). Links between worlds: Unraveling migratory connectivity. *Trends in Ecology & Evolution*, *17*(2), 76–83. https://doi.org/10.1016/S0169-5347(01)02380-1

Welti, E. A. R., Roeder, K. A., de Beurs, K. M., Joern, A., & Kaspari, M. (2020). Nutrient dilution and climate cycles underlie declines in a dominant insect herbivore. *Proceedings of the National Academy of Sciences*, *117*(13), 7271–7275. https://doi.org/10.1073/pnas.1920012117

West, J. B., Bowen, G. J., Dawson, T. E., & Tu, K. P. (2009). *Isoscapes: Understanding movement, pattern, and process on Earth through isotope mapping*. Springer Netherlands. https://doi.org/10.1007/978-90-481-3354-3

West-Eberhard, M. J. (1989). Phenotypic plasticity and the origins of diversity. *Annual Review of Ecology and Systematics*, *20*(1), 249–278. https://doi.org/10.1146/annurev.es.20.110189.001341

Widga, C., Walker, J. D., & Stockli, L. D. (2010). Middle Holocene Bison diet and mobility in the eastern Great Plains (USA) based on $\delta^{13}C$, $\delta^{18}O$, and $^{87}Sr/^{86}Sr$ analyses of tooth enamel carbonate. *Quaternary Research*, *73*(03), 449–463. https://doi.org/10.1016/j.yqres.2009.12.001

Widga, C., Walker, J. D., & Boehm, A. (2017). Variability in bioavailable $^{87}Sr/^{86}Sr$ in the North American Midcontinent. *Open Quaternary*, *3*(4), 1–7. https://doi.org/10.5334/oq.32

Wieringa, J. G., Nagel, J., Nelson, D. M., Carstens, B. C., & Gibbs, H. L. (2020). Using trace elements to identify the geographic origin of migratory bats. *PeerJ*, *8*(2017), 1–23. https://doi.org/10.7717/peerj.10082

Wikelski, M., Moskowitz, D., Adelman, J. S., Cochran, J., Wilcove, D. S., & May, M. L. (2006). Simple rules guide dragonfly migration. *Biology Letters*, *2*, 325–329. https://doi.org/10.1098/rsbl.2006.0487

Wiklund, C., & Friberg, M. (2022). Testing the migration syndrome: Comparative fecundity of migratory and non-migratory nymphaline butterflies. *Ecological Entomology*, *47*(6), 1061–1067. https://doi.org/10.1111/een.13195

Wilcox, A., Flockhart, T., Newman, A., & Norris, R. (2019). An evaluation of studies on the potential threats contributing to the decline of eastern migratory North American monarch butterflies (*Danaus plexippus*). *Frontiers in Ecology and Evolution*, *7*, 1–12. https://doi.org/10.3389/fevo.2019.00099

Williams, C. B. (1930). *The migration of butterflies*. Oliver and Boyd.

Williams, C. B. (1958). *Insect migration*. Collins.

Williams, C. B. (1970). The migrations of the painted lady butterfly, *Vanessa cardui* (Nymphalidae), with special reference to North America. *The Lepidopterists' Society*, *24*(3).

Wotton, K. R., Gao, B., Menz, M. H. M., Morris, R. K. A., Ball, S. G., Lim, K. S., Reynolds, D. R., Hu, G., & Chapman, J. W. (2019). Mass seasonal migrations of hoverflies provide extensive pollination and crop protection services. *Current Biology*, *29*, 2167–2173. https://doi.org/10.1016/j.cub.2019.05.036

Wunder, M. B. (2010). Using isoscapes to model probability surfaces for determining geographic origins. In *Isoscapes* (pp. 251–270). Springer Netherlands. https://doi.org/10.1007/978-90-481-3354-3_12

Wunder, M. B. (2012). Determining geographic patterns of migration and dispersal using stable isotopes in keratins. *Journal of Mammalogy*, *93*(2), 360–367. https://doi.org/10.1644/1

Xiao, G., & Zhou, B. (2016). What can flies tell us about zinc homeostasis? *Archives of Biochemistry and Biophysics*, *611*, 134–141. https://doi.org/10.1016/j.abb.2016.04.016

Yang, L., Jin, S., Danielson, P., Homer, C., Gass, L., Bender, S. M., Case, A., Costello, C., Dewitz, J., Fry, J., Funk, M., Granneman, B., Liknes, G. C., Rigge, M., & Xian, G. (2018). A new generation of the United States National Land Cover Database: Requirements, research priorities, design, and implementation strategies. *ISPRS Journal of Photogrammetry and Remote Sensing*, *146*, 108–123. https://doi.org/10.1016/j.isprsjprs.2018.09.006

Zhan, S., Zhang, W., Niitepõld, K., Hsu, J., Haeger, J. F., Zalucki, M. P., Altizer, S., de Roode, J. C., Reppert, S. M., & Kronforst, M. R. (2014). The genetics of monarch butterfly migration and warning colouration. *Nature*, *514*(7522), 317–321. https://doi.org/10.1038/nature13812

Zhang, L., Li, Z., Peng, Y., Liang, X., Wilson, K., Chipabika, G., Karangwa, P., Uzayisenga, B., Mensah, B. A., Kachigamba, D. L., & Xiao, Y. (2023). Global genomic signature reveals the evolution of fall armyworm in the Eastern hemisphere. *Molecular Ecology*, mec.17117. https://doi.org/10.1111/mec.17117

Zhang, M., Cao, T., Jin, K., Ren, Z., Guo, Y., Shi, J., Zhong, Y., & Ma, E. (2008). Estimating divergence times among subfamilies in Nymphalidae. *Science Bulletin*, *53*(17), 2652–2658. https://doi.org/10.1007/s11434-008-0344-z

Zhang, Y., Ying, H., & Xu, Y. (2019). Comparative genomics and metagenomics of the metallomes. *Metallomics*, *11*(6), 1026–1043. https://doi.org/10.1039/c9mt00023b

Zhou, J., Chen, J., & Shu, Y. (2021). Lead stress affects the reproduction of *Spodoptera litura* but not by regulating the vitellogenin gene promoter. *Ecotoxicology and Environmental Safety*, *208*, 111581. https://doi.org/10.1016/j.ecoenv.2020.111581

Zhou, X., Taylor, M. P., & Davies, P. J. (2018). Tracing natural and industrial contamination and lead isotopic compositions in an Australian native bee species. *Environmental Pollution*, *242*, 54–62. https://doi.org/10.1016/j.envpol.2018.06.063

Zomer, R. J., Trabucco, A., Bossio, D. A., & Verchot, L. V. (2008). Climate change mitigation: A spatial analysis of global land suitability for clean development mechanism afforestation and reforestation. *Agriculture, Ecosystems and Environment*, *126*, 67–80. https://doi.org/10.1016/j.agee.2008.01.014

Zuur, A., Ieno, E. N., Walker, N., Saveliev, A. A., & Smith, G. M. (2009). *Mixed effects models and extensions in ecology with R*. Springer. https://www.taylorfrancis.com/books/9780429576966/chapters/10.4324/9780429201271-2

Zylstra, E. R., Ries, L., Neupane, N., Saunders, S. P., Ramírez, M. I., Rendón-Salinas, E., Oberhauser, K. S., Farr, M. T., & Zipkin, E. F. (2021). Changes in climate drive recent monarch butterfly dynamics. *Nature Ecology & Evolution*, *5*(10), 1441–1452. https://doi.org/10.1038/s41559-021-01504-1